POLITECHNIKA GDAŃSKA

Imię i nazwisko autora rozprawy: mgr inż. Dorota Rogala-Wielgus
Dyscyplina naukowa: Inżynieria Materiałowa

ROZPRAWA DOKTORSKA

Tytuł rozprawy w języku polskim: „Powłoki na osnowie pierwiastkowego węgla przeznaczone na implanty tytanowe”

Tytuł rozprawy w języku angielskim: „Coatings based on elemental carbon for titanium implants”

Promotor *podpis*	Drugi promotor Nie dotyczy *podpis*
prof. dr hab. inż. Andrzej Zieliński	
Promotor pomocniczy *podpis*	Kopromotor Nie dotyczy *podpis*
dr inż. Beata Majkowska-Marzec	

Gdańsk, rok 2023

POLITECHNIKA GDAŃSKA

OŚWIADCZENIE

Autor rozprawy doktorskiej: mgr inż. Dorota Rogala-Wielgus

Ja, niżej podpisany(a), oświadczam, iż jestem świadomy(a), że zgodnie z przepisem art. 27 ust. 1 i 2 ustawy z dnia 4 lutego 1994 r. o prawie autorskim i prawach pokrewnych (t.j. Dz.U. z 2021 poz. 1062), uczelnia może korzystać z mojej rozprawy doktorskiej zatytułowanej:
„Powłoki na osnowie pierwiastkowego węgla przeznaczone na implanty tytanowe"
do prowadzenia badań naukowych lub w celach dydaktycznych.[1]

Świadomy(a) odpowiedzialności karnej z tytułu naruszenia przepisów ustawy z dnia 4 lutego 1994 r. o prawie autorskim i prawach pokrewnych i konsekwencji dyscyplinarnych określonych w ustawie Prawo o szkolnictwie wyższym i nauce (Dz.U.2021.478 t.j.), a także odpowiedzialności cywilno-prawnej oświadczam, że przedkładana rozprawa doktorska została napisana przeze mnie samodzielnie.

Oświadczam, że treść rozprawy opracowana została na podstawie wyników badań prowadzonych pod kierunkiem i w ścisłej współpracy z promotorem prof. dr hab. inż. Andrzejem Zielińskim oraz promotorem pomocniczym dr inż. Beatą Majkowską-Marzec.

Niniejsza rozprawa doktorska nie była wcześniej podstawą żadnej innej urzędowej procedury związanej z nadaniem stopnia doktora.

Wszystkie informacje umieszczone w ww. rozprawie uzyskane ze źródeł pisanych i elektronicznych, zostały udokumentowane w wykazie literatury odpowiednimi odnośnikami, zgodnie z przepisem art. 34 ustawy o prawie autorskim i prawach pokrewnych.

Potwierdzam zgodność niniejszej wersji pracy doktorskiej z załączoną wersją elektroniczną.

Gdańsk, dnia ....

podpis doktoranta

Ja, niżej podpisany(a), wyrażam zgodę/nie wyrażam zgody* na umieszczenie ww. rozprawy doktorskiej w wersji elektronicznej w otwartym, cyfrowym repozytorium instytucjonalnym Politechniki Gdańskiej.

Gdańsk, dnia ....

podpis doktoranta

**niepotrzebne usunąć*

[1] Art. 27. 1. Instytucje oświatowe oraz podmioty, o których mowa w art. 7 ust. 1 pkt 1, 2 i 4–8 ustawy z dnia 20 lipca 2018 r. – Prawo o szkolnictwie wyższym i nauce, mogą na potrzeby zilustrowania treści przekazywanych w celach dydaktycznych lub w celu prowadzenia działalności naukowej korzystać z rozpowszechnionych utworów w oryginale i w tłumaczeniu oraz zwielokrotniać w tym celu rozpowszechnione drobne utwory lub fragmenty większych utworów.
2. W przypadku publicznego udostępniania utworów w taki sposób, aby każdy mógł mieć do nich dostęp w miejscu i czasie przez siebie wybranym korzystanie, o którym mowa w ust. 1, jest dozwolone wyłącznie dla ograniczonego kręgu osób uczących się, nauczających lub prowadzących badania naukowe, zidentyfikowanych przez podmioty wymienione w ust. 1.

OPIS ROZPRAWY DOKTORSKIEJ

Autor rozprawy doktorskiej: mgr inż. Dorota Rogala-Wielgus

Tytuł rozprawy doktorskiej w języku polskim: Powłoki na osnowie pierwiastkowego węgla przeznaczone na implanty tytanowe

Tytuł rozprawy w języku angielskim: Coatings based on elemental carbon for titanium implants

Język rozprawy doktorskiej: polski

Promotor rozprawy doktorskiej: prof. dr hab. inż. Andrzej Zieliński

Promotor pomocniczy rozprawy doktorskiej: dr inż. Beata Majkowska-Marzec

Data obrony: -

Słowa kluczowe rozprawy doktorskiej w języku polskim: wielościenne nanorurki węglowe, powłoka, nanosrebro, nanomiedź, tlenek tytanu, tytan II, Ti13Nb13Zr, osadzanie elektroforetyczne, właściwości mechaniczne, biomateriał

Słowa kluczowe rozprawy doktorskiej w języku angielskim: multi-wall carbon nanotubes, coating, nanosilver, nanocopper, titanium dioxide, titanium Grade II, Ti13Nb13Zr, electrophoretic deposition, mechanical properties, biomaterial

Streszczenie rozprawy w języku polskim: Głównymi problemami występującymi podczas zabiegu endoprotezoplastyki są infekcje bakteryjne, a w trakcie użytkowania endoprotezy, możliwość obluzowania implantu, wynikająca z przeciążenia lub niedociążenia materiału zastępującego ludzki staw biodrowy, co może prowadzić do konieczności przeprowadzenia ponownej alloplastyki. Bakteriami, które najczęściej kolonizują materiał, są *Staphylococcus aureus*, *Staphylococcus epidermidis*, *Pseudomonas aeruginosa* oraz *Escherichia coli*, stąd pożądanym byłoby stosowanie materiałów antybakteryjnych na pokrycia powierzchni endoprotez, co zminimalizowałoby prawdopodobieństwo powstania stanu zapalnego, będącego skutkiem zakażenia. Co więcej, materiał przeznaczony na endoprotezę powinien charakteryzować się właściwościami mechanicznymi oraz plastycznymi jak najbardziej zbliżonymi do właściwości naturalnej kości, dzięki czemu sztuczny staw dzieliłby przenoszone obciążenia razem z otaczającymi go żywymi tkankami, zapobiegając ich osteopenii. Materiały metaliczne, najbardziej trwałe, charakteryzują się jednak wyższymi właściwościami mechanicznymi, dlatego konieczne jest pokrycie podłoża powłoką, która spełniałaby powyższe wymagania, byłaby nietoksyczna w środowisku płynów ustrojowych, wspierała proliferację komórek osteoblastów, jak i charakteryzowała się wysoką adhezją do podłoża.

Niniejsza rozprawa miała na celu modyfikację podłoża z tytanu II oraz stopu Ti13Nb13Zr poprzez osadzenie elektroforetyczne (EPD) powłok na bazie wielościennych nanorurek węglowych (MWCNTs) z dodatkami wielkości nanometrycznej, przeznaczonych na pokrycia trzpieni endoprotez stawu biodrowego. Przygotowano trzy rodzaje powłok MWCNTs: z dodatkiem nanomiedzi (MWCNTs/Cu), nanosrebra (MWCNTs/Ag) oraz tlenku tytanu (MWCNTs/TiO_2), osadzone w procesie dwuetapowym, składającym się z I. EPD powłoki MWCNTs oraz II. EPD powłoki z dodatku. Zarówno MWCNTs, jak i zastosowane dodatki, charakteryzują się działaniem antybakteryjnym na bakterie najczęściej będące sprawcą zakażeń w obrębie endoprotez. Wytworzenie kompozytowej powłoki, składającej się z elastycznej matrycy w postaci nanorurek węglowych, o unikalnych właściwościach oraz wzmocnienia z twardych cząstek tlenku tytanu, miało nie tylko zapewniać właściwości antybakteryjne, ale również modyfikować właściwości podłoża, w kierunku zbliżenia do właściwości ludzkiej kości korowej.

Aby ocenić właściwości otrzymanych powłok na bazie MWCNTs dla każdej wykonano SEM, EDS, AFM, spektroskopię Raman'a (na podłożu Ti13Nb13Zr), badanie nanoindentacji, test nanozarysowania (z ang. *nano-scratch test*), badanie zwilżalności (na podłożu Ti13Nb13Zr) oraz przeprowadzono testy korozyjne (na podłożu Ti13Nb13Zr). W przypadku powłoki MWCNTs/TiO_2 osadzonej na podłożu ze stopu Ti13Nb13Zr dodatkowo dokonano oceny cytotoksyczności w teście MTT dla komórek ludzkich fibroblastów (HDF) oraz mysich prekursorów osteoblastów (MC3T3), które potwierdzono w teście dehydrogenazy mleczanowej (LDH).

Przeprowadzone badania wskazują na znaczący wpływ zastosowanych dodatków na morfologię, topografię, właściwości mechaniczne, plastyczne i sprężyste, odporność korozyjną oraz siłę adhezji powłok na bazie MWCNTs do podłoża tytanowego. Porównując właściwości mechaniczne oraz plastyczne powłok osadzonych na podłożu z tytanu II oraz stopu Ti13Nb13Zr, można zaobserwować znaczne różnice. Biorąc pod uwagę grubość powłok na bazie MWCNTs można wnioskować o nieznacznym wpływie podłoża, wynikającym ze stopnia utleniania podłoża oraz czasu osadzania EPD. Zarówno dodatki tlenkowe, jak i metaliczne zwiększały właściwości plastyczne oraz sprężyste powłoki MWCNTs, poprawiały jej odporność korozyjną (na podłożu Ti13Nb13Zr) oraz zwiększały adhezję do podłoża Ti13Nb13Zr. Ponadto, każda z powłok modyfikujących podłoże ze stopu Ti13Nb13Zr charakteryzowała się zwilżalnością pożądaną do zastosowania na biomateriały. Najbardziej obiecujące wyniki uzyskano dla powłoki MWCNTs z dodatkiem tlenku tytanu, dla której osiągnięto właściwości mechaniczne zbliżone do właściwości ludzkiej kości, właściwości plastyczne oraz sprężyste, interesujące do zastosowań na pokrycia trzpieni endoprotez oraz najwyższą ze wszystkich powłok adhezję do podłoża Ti13Nb13Zr. Co więcej, badania biologiczne wskazują na korzystne własności fizykochemiczne powłoki MWCNTs/TiO_2, które pozwalającą na adhezję komórek, jednak z powłoki mogą uwalniać się toksyczne substancje, hamujące ich proliferację. Zastosowanie tlenku tytanu w powłokach MWCNTs przeznaczonych do zastosowania na biomateriały wymaga więc dalszych badań.

Streszczenie rozprawy w języku angielskim: The main issues of the arthroplasty procedure are bacterial infections and loosening of the implant (inserted in the bone), which is a result of the over- or underloading of the hip endoprosthesis, which may require reimplantation. Bacteria colonizing the surrounding of the endoprosthesis material are *Staphylococcus aureus*, *Staphylococcus epidermidis*, *Pseudomonas aeruginosa*, and *Escherichia coli*, thus the use of antibacterial materials could minimize the inflammation caused by bacterial infection. Furthermore, the material intended for endoprosthesis should have mechanical and plastic properties the same or comparable to natural bone, leading to the shear of the applied load with surrounding tissues and preventing osteopenia. However, metallic materials are the most durable but are also characterized by higher mechanical properties than natural bone, therefore it is necessary to modify its surface, for instance by coating, which is required to be non-toxic in body fluids, promoting cell proliferation and well-adhered to the substrate material.

The study was aimed at modification of the titanium grade II and Ti13Nb13Zr alloy by electrophoretic deposition method (EPD) of multi-wall carbon nanotubes (MWCNTs) - based coatings with nanostructure additions, intended for hip endoprosthesis stem cover. Three types of MWCNTs coatings were prepared: with the addition of nanocopper (MWCNTs/Cu), nanosilver (MWCNTs/Ag), and titanium dioxide (MWCNTs/TiO_2), deposited in two-stage process I. EPD of MWCNTs coating and II. EPD of a coating composed of additions. Both, the MWCNTs and selected additions have antibacterial properties against bacteria responsible for infections within hip endoprosthesis. The synthesis of a composite coating, consisting of a carbon nanotube elastic matrix, with unique properties and reinforcement made of hard titanium dioxide, was aimed at providing antibacterial properties and substrate modification to achieve similar properties to natural human cortical bone.

To evaluate the properties of prepared MWCNTs- based coatings each of them was subjected to SEM, EDS, AFM, Raman spectroscopy (on Ti13Nb13Zr), nanoindentation, nano-scratch test, wettability studies (on Ti13Nb13Zr) and potentiodynamic corrosion tests (on Ti13Nb13Zr). Additionally, the cytotoxicity of the MWCNTs/TiO_2 coating, deposited on Ti13Nb13Zr alloy

substrate was determined using the MTT test on human dermal fibroblasts (HDF) and mouse osteoblast precursors (MC3T3), confirmed with lactate dehydrogenase (LDH) test.

The study revealed a significant impact of applied additions on the MWCNTs coatings morphology, topography, mechanical properties, plastic and elastic properties, corrosion resistance, and adhesion to a titanium substrate strength. Comparing mechanical and plastic properties of coatings deposited on titanium Grade II and Ti13Nb13Zr alloy, the differences might be observed; taking coatings thickness into account, the minimal substrate impact on coatings properties might be observed, resulting from the degree of oxidation and deposition time during EPD. Both metallic and oxide additions improve plastic and elastic properties, and corrosion resistance (on Ti13Nb13Zr) and increase the adhesion strength of the MWCNTs-based coatings to the Ti13Nb13Zr substrate. Furthermore, each coating modifying the Ti13Nb13Zr alloy substrate was characterized by wettability desired in biomedical applications. The most promising results were obtained for the MWCNTs coating with titanium dioxide addition, with mechanical properties near to those of natural bone, plastic, and elastic properties appropriate for application on hip endoprosthesis stem coating, and the highest adhesion strength to the Ti13Nb13Zr substrate among examined coatings. Nevertheless, the results of biological studies proved the physicochemical properties of the MWCNTs/TiO_2 coating improve cell adhesion, a coating might release toxic substances, thus inhibiting proliferation; MWCNTs coatings with the addition of titanium dioxide require further studies to apply in biomaterials.

ROZPRAWA DOKTORSKA

„Powłoki na osnowie pierwiastkowego węgla przeznaczone na implanty tytanowe”

mgr inż. Dorota Rogala-Wielgus

promotor: prof. dr hab. inż. Andrzej Zieliński

promotor pomocniczy: dr inż. Beata Majkowska-Marzec

Mam ogromne szczęście
mieć u swojego boku tak wspaniałych ludzi.

Bez nich nie byłoby tej pracy, dlatego
z całego serca dziękuję

mojemu Promotorowi
prof. dr hab. inż. Andrzejowi Zielińskiemu
za bycie moim mentorem, cierpliwym i zawsze otwartym na pomoc,

mojej Promotor Pomocniczej
dr inż. Beacie Majkowskiej-Marzec
za ogromne wsparcie i poświęcony czas

Dziękuję również

Mojej rodzinie, a w szczególności mamie i mężowi

oraz

moim kolegom i koleżankom

„Największy wysiłek rozumu to uznać,
że istnieje nieskończona mnogość rzeczy,
które go przerastają”

- Blaise Pascal

„Zawsze wydaje się, że coś jest niemożliwe,
dopóki nie zostanie to zrobione”

- Nelson Mandela.

Rozprawa doktorska została przygotowana w ramach jednotematycznego cyklu publikacji

SPIS TREŚCI

WYKAZ SKRÓTÓW I OZNACZEŃ

CNTs	- nanorurki węglowe
E	- moduł Young'a, moduł sprężystości wzdłużnej (GPa) (ang. *Young's modulus or elastic modulus*)
EPD	- metoda osadzania elektroforetycznego (ang. *electrophoretic deposition method*)
Er	- zredukowany moduł Young'a (GPa) (ang. *reduced Young's modulus*)
H	- nanotwardość (GPa) (ang. *nanohardness*)
HDF	- komórki fibroblastów ludzkich (ang. *human dermal cells*)
Lc	- krytyczna siła, po przekroczeniu której następuje delaminacja powłoki
LDH	- dehydrogenaza mleczanowa (ang. *lactate dehydrogenase*).
MC3T3	- mysie prekursory osteoblastów (ang. *mouse osteoblasts precursors*)
MWCNTs	- wielościenne nanorurki węglowe (ang. *multi-wall carbon nanotubes*)
MWCNTs/Ag	- powłoka z wielościennych nanorurek węglowych z dodatkiem nanosrebra
MWCNTs/Cu	- powłoka z wielościennych nanorurek węglowych z dodatkiem nanomiedzi
MWCNTs/TiO_2	- powłoka z wielościennych nanorurek węglowych z dodatkiem tlenku tytanu
test MTT	- test do analizy aktywności metabolicznej komórki (ang. *MTT assay*)

STRESZCZENIE I SŁOWA KLUCZOWE

Streszczenie

Głównymi problemami występującymi podczas zabiegu endoprotezoplastyki są infekcje bakteryjne, a w trakcie użytkowania endoprotezy, możliwość obluzowania implantu, wynikająca z przeciążenia lub niedociążenia materiału zastępującego ludzki staw biodrowy, co może prowadzić do konieczności przeprowadzenia ponownej alloplastyki. Bakteriami, które najczęściej kolonizują materiał, są *Staphylococcus aureus, Staphylococcus epidermidis, Pseudomonas aeruginosa* oraz *Escherichia coli,* stąd pożądanym byłoby stosowanie materiałów antybakteryjnych na pokrycia powierzchni endoprotez, co zminimalizowałoby prawdopodobieństwo powstania stanu zapalnego, będącego skutkiem zakażenia. Co więcej, materiał przeznaczony na endoprotezę powinien charakteryzować się właściwościami mechanicznymi oraz plastycznymi jak najbardziej zbliżonymi do właściwości naturalnej kości, dzięki czemu sztuczny staw dzieliłby przenoszone obciążenia razem z otaczającymi go żywymi tkankami, zapobiegając ich osteopenii. Materiały metaliczne, najbardziej trwałe, charakteryzują się jednak wyższymi właściwościami mechanicznymi, dlatego konieczne jest pokrycie podłoża powłoką, która spełniałaby powyższe wymagania, byłaby nietoksyczna w środowisku płynów ustrojowych, wspierała proliferację komórek osteoblastów, jak i charakteryzowała się wysoką adhezją do podłoża.

Niniejsza rozprawa miała na celu modyfikację podłoża z tytanu II oraz stopu Ti13Nb13Zr poprzez osadzenie elektroforetyczne (EPD) powłok na bazie wielościennych nanorurek węglowych (MWCNTs) z dodatkami wielkości nanometrycznej, przeznaczonych na pokrycia trzpieni endoprotez stawu biodrowego. Przygotowano trzy rodzaje powłok MWCNTs: z dodatkiem nanomiedzi (MWCNTs/Cu), nanosrebra (MWCNTs/Ag) oraz tlenku tytanu (MWCNTs/TiO_2), osadzone w procesie dwuetapowym, składającym się z I. EPD powłoki MWCNTs oraz II. EPD powłoki z dodatku. Zarówno MWCNTs, jak i zastosowane dodatki, charakteryzują się działaniem antybakteryjnym na bakterie najczęściej będące sprawcą zakażeń w obrębie endoprotez. Wytworzenie kompozytowej powłoki, składającej się z elastycznej matrycy w postaci nanorurek węglowych, o unikalnych właściwościach oraz wzmocnienia z twardych cząstek tlenku tytanu, miało nie tylko zapewniać właściwości antybakteryjne, ale również modyfikować właściwości podłoża, w kierunku zbliżenia do właściwości ludzkiej kości korowej.

Aby ocenić właściwości otrzymanych powłok na bazie MWCNTs dla każdej wykonano SEM, EDS, AFM, spektroskopię Raman'a (na podłożu Ti13Nb13Zr), badanie nanoindentacji, test nanozarysowania (z ang. *nano-scratch test*), badanie zwilżalności (na podłożu Ti13Nb13Zr) oraz przeprowadzono testy korozyjne (na podłożu Ti13Nb13Zr). W przypadku powłoki MWCNTs/TiO_2 osadzonej na podłożu ze stopu Ti13Nb13Zr dodatkowo dokonano oceny cytotoksyczności w teście MTT dla komórek ludzkich fibroblastów (HDF) oraz mysich prekursorów osteoblastów (MC3T3), które potwierdzono w teście dehydrogenazy mleczanowej (LDH).

Przeprowadzone badania wskazują na znaczący wpływ zastosowanych dodatków na morfologię, topografię, właściwości mechaniczne, plastyczne i sprężyste, odporność korozyjną oraz siłę adhezji powłok na bazie MWCNTs do podłoża tytanowego. Porównując właściwości mechaniczne oraz plastyczne powłok osadzonych na podłożu z tytanu II oraz stopu Ti13Nb13Zr, można zaobserwować znaczne różnice. Biorąc pod uwagę grubość powłok na bazie MWCNTs można wnioskować o nieznacznym wpływie podłoża, wynikającym ze stopnia utleniania podłoża oraz czasu osadzania EPD. Zarówno dodatki tlenkowe, jak i metaliczne zwiększały właściwości plastyczne oraz sprężyste powłoki MWCNTs, poprawiały jej odporność korozyjną (na podłożu Ti13Nb13Zr) oraz zwiększały adhezję do podłoża Ti13Nb13Zr. Ponadto, każda z powłok modyfikujących podłoże ze stopu Ti13Nb13Zr charakteryzowała się zwilżalnością pożądaną do zastosowania na biomateriały. Najbardziej obiecujące wyniki uzyskano dla powłoki MWCNTs z dodatkiem tlenku tytanu, dla której osiągnięto właściwości mechaniczne zbliżone do właściwości ludzkiej kości, właściwości plastyczne oraz sprężyste, interesujące do zastosowań na pokrycia trzpieni endoprotez oraz najwyższą ze wszystkich powłok adhezję do podłoża Ti13Nb13Zr. Co więcej, badania biologiczne wskazują na korzystne własności fizykochemiczne powłoki MWCNTs/TiO_2, które pozwalającą na adhezję komórek, jednak z powłoki mogą uwalniać się toksyczne substancje, hamujące ich proliferację. Zastosowanie tlenku tytanu w powłokach MWCNTs przeznaczonych do zastosowania na biomateriały wymaga więc dalszych badań.

Słowa kluczowe: wielościenne nanorurki węglowe, powłoka, nanosrebro, nanomiedź, tlenek tytanu, tytan II, Ti13Nb13Zr, osadzanie elektroforetyczne, właściwości mechaniczne, biomateriał

ABSTRACT AND KEYWORDS

Abstract

The main issues of the arthroplasty procedure are bacterial infections and loosening of the implant (inserted in the bone), which is a result of the over- or underloading of the hip endoprosthesis, which may require reimplantation. Bacteria colonizing the surrounding of the endoprosthesis material are *Staphylococcus aureus*, *Staphylococcus epidermidis*, *Pseudomonas aeruginosa*, and *Escherichia coli*, thus the use of antibacterial materials could minimize the inflammation caused by bacterial infection. Furthermore, the material intended for endoprosthesis should have mechanical and plastic properties the same or comparable to natural bone, leading to the shear of the applied load with surrounding tissues and preventing osteopenia. However, metallic materials are the most durable but are also characterized by higher mechanical properties than natural bone, therefore it is necessary to modify its surface, for instance by coating, which is required to be non-toxic in body fluids, promoting cell proliferation and well-adhered to the substrate material.

The study was aimed at modification of the titanium grade II and Ti13Nb13Zr alloy by electrophoretic deposition method (EPD) of multi-wall carbon nanotubes (MWCNTs) - based coatings with nanostructure additions, intended for hip endoprosthesis stem cover. Three types of MWCNTs coatings were prepared: with the addition of nanocopper (MWCNTs/Cu), nanosilver (MWCNTs/Ag), and titanium dioxide (MWCNTs/TiO_2), deposited in two-stage process I. EPD of MWCNTs coating and II. EPD of a coating composed of additions. Both, the MWCNTs and selected additions have antibacterial properties against bacteria responsible for infections within hip endoprosthesis. The synthesis of a composite coating, consisting of a carbon nanotube elastic matrix, with unique properties and reinforcement made of hard titanium dioxide, was aimed at providing antibacterial properties and substrate modification to achieve similar properties to natural human cortical bone.

To evaluate the properties of prepared MWCNTs- based coatings each of them was subjected to SEM, EDS, AFM, Raman spectroscopy (on Ti13Nb13Zr), nanoindentation, nano-scratch test, wettability studies (on Ti13Nb13Zr) and potentiodynamic corrosion tests (on Ti13Nb13Zr). Additionally, the cytotoxicity of the MWCNTs/TiO_2 coating, deposited on Ti13Nb13Zr alloy substrate was determined using the MTT test on human dermal fibroblasts (HDF) and mouse osteoblast precursors (MC3T3), confirmed with lactate dehydrogenase (LDH) test.

The study revealed a significant impact of applied additions on the MWCNTs coatings morphology, topography, mechanical properties, plastic and elastic properties, corrosion resistance, and adhesion to a titanium substrate strength. Comparing mechanical and plastic properties of coatings deposited on titanium Grade II and Ti13Nb13Zr alloy, the differences might be observed; taking coatings thickness into account, the minimal substrate impact on coatings properties might be observed,

resulting from the degree of oxidation and deposition time during EPD. Both metallic and oxide additions improve plastic and elastic properties, and corrosion resistance (on Ti13Nb13Zr) and increase the adhesion strength of the MWCNTs-based coatings to the Ti13Nb13Zr substrate. Furthermore, each coating modifying the Ti13Nb13Zr alloy substrate was characterized by wettability desired in biomedical applications. The most promising results were obtained for the MWCNTs coating with titanium dioxide addition, with mechanical properties near to those of natural bone, plastic, and elastic properties appropriate for application on hip endoprosthesis stem coating, and the highest adhesion strength to the Ti13Nb13Zr substrate among examined coatings. Nevertheless, the results of biological studies proved the physicochemical properties of the MWCNTs/TiO_2 coating improve cell adhesion, a coating might release toxic substances, thus inhibiting proliferation; MWCNTs coatings with the addition of titanium dioxide require further studies to apply in biomaterials.

Keywords: multi-wall carbon nanotubes, coating, nanosilver, nanocopper, titanium dioxide, titanium Grade II, Ti13Nb13Zr, electrophoretic deposition, mechanical properties, biomaterial

WYKAZ PUBLIKACJI BĘDĄCYCH PODSTAWĄ ROZPRAWY DOKTORSKIEJ

Publikacja przeglądowa:

[A1] **Rogala-Wielgus D.***, Zieliński A.: *Preparation and properties of composite coatings, based on carbon nanotubes, for medical applications*, Carbon Letters. (2023). https://doi.org/10.1007/s42823-023-00626-9
(IF: 4,5; MNiSW 40 pkt.)

Publikacje prac badawczych:

[A2] **Rogala-Wielgus D.*,** Majkowska-Marzec B., Zieliński A., Bartmański M., Bartosewicz B.: *Mechanical behavior of bi-layer and dispersion coatings composed of several nanostructures on Ti13Nb13Zr alloy*, Materials 14 (2021) 2905. https://doi.org/10.3390/ma14112905.
(IF=3,748, MNiSW 140 pkt.).

[A3] **Rogala-Wielgus D.***, Majkowska-Marzec B., Zieliński A., Jankiewicz B. J.: *Mechanical behavior of bi-layer and dispersion coatings composed of several nanostructures on Ti substrate*, Applied Sciences-Basel 11 (2021) 7862. https://doi.org/10.3390/app11177862.
(IF=2,838, MNiSW 100 pkt.).

[A4] **Rogala-Wielgus D.*,** Majkowska-Marzec B., Zieliński A.: *Characteristics of silver-dopped carbon nanotube coating destined for medical applications*, Materials Today Communications. 38 (2023) 107712.
https://doi.org/10.1016/j.mtcomm.2023.107712
(IF=3,8, MNiSW 70 pkt.)

[A5] **Rogala-Wielgus D.*,** Majkowska-Marzec B. Zieliński A., Roszek K., Liszewska M.: *Evaluation of adhesion strength, corrosion, and biological properties of the MWCNTs/TiO_2 coating intended for medical applications*, RSC Advances. 13 (2023) 30108-30117.
https://doi.org/10.1039/d3ra05331h
(IF=3,9, MNiSW 100 pkt.)

*autor korespondencyjny

Sumaryczny Impact Factor oraz punktacja wg MNiSW za powyższe publikacje wynosiły odpowiednio (#uwzględnienie procentowego udział doktoranta w przygotowaniu powyższych prac):

- Impact Factor: 18,786 (#13,59),
- punkty wg MNiSW: 450 pkt. (#316 pkt.)

TEZA PRACY NAUKOWEJ I PROBLEMY BADAWCZE

Projekt doktorski przygotowano na podstawie postawionej tezy, iż powłoki kompozytowe bazujące na wielościennych nanorurkach węglowych, modyfikowane dodatkami o wielkości nanometrycznej oraz kontrolowanej mikrostrukturze, wykazują:

I. właściwości mechaniczne, zbliżone do właściwości kości ludzkiej,
II. właściwości plastyczne i sprężyste, optymalne do zastosowań na pokrycia implantów;
III. właściwości biologiczne zadowalające w środowisku płynów ustrojowych.

Celem naukowym pracy było opracowanie parametrów wytwarzania bioaktywnych, bakteriostatycznych i bakteriobójczych powłok z wielościennych nanorurek węglowych z dodatkami o wielkości nanometrycznej przy użyciu metody osadzania elektroforetycznego oraz ocena ich właściwości mechanicznych, chemicznych oraz biologicznych.

Celem użytkowym przeprowadzonego projektu doktorskiego było wytworzenie powłok kompozytowych na bazie nanorurek węglowych z dodatkami o działaniu antybakteryjnym, mających na celu poprawę wytrzymałości powierzchni implantu w trakcie zabiegu endoprotezoplastyki oraz użytkowania endoprotezy.

Głównym problemem badawczym w projekcie doktorskim był wpływ dodatków o wielkości nanometrycznej na właściwości mechaniczne, odporność na prognozowane zużycie ścierne oraz właściwości biologiczne powłok na bazie MWCNTs. Natomiast, uszczegóławiając problematykę badawczą wyznaczono następujące problemy badawcze:

1. Jaki wpływ miały zmienne procesu wytwarzania powłok na bazie MWCNTs, takie, jak: napięcie EPD, czas EPD, odległość między elektrodami, skład zawiesiny w procesie EPD, na właściwości otrzymanych powłok?
2. Jakie dodatki do powłok MWCNTs o wielkości nanometrycznej będą charakteryzować się odpornością na bakterie *Staphylococcus aureus*, *Staphylococcus epidermidis, Pseudomonas aeruginosa* i *Escherichia coli*?
3. Czy dodatki do powłok MWCNTs, spełniające funkcję antybakteryjną, mogą też zoptymalizować właściwości mechaniczne powłok przeznaczonych na implanty?
4. Czy dodatki o wielkości nanometrycznej zmieniają topografię i morfologię powłok na bazie MWCNTs? I czy takie zjawisko wpłynie korzystnie na zwilżalność powłok?
5. Czy dodatki o wielkości nanometrycznej mają wpływ na właściwości mechaniczne, plastyczne oraz sprężyste, powłok na bazie MWCNTs?

6. Czy dodatki do powłok MWCNTs o wielkości nanometrycznej mogą zwiększyć adhezję powłok do podłoża tytanowego, a tym samym poprawić odporność na zużycie ścierne, czy kontaktowe?
7. Czy podłoże wpływa na właściwości mechaniczne otrzymanych powłok na bazie MWCNTs? I czy jest to zależne od grubości powłok?
8. Czy powłoka MWCNTs, bądź MWCNTs z dodatkami o wielkości nanometrycznej może być dobrze tolerowana przez organizm człowieka? Czy do takich powłok będą przylegać komórki osteoblastów i fibroblastów?

1. WPROWADZENIE

Rosnąca powszechność urazów w obrębie stawów biodrowych, powstałych w wyniku traumatycznych zdarzeń, bądź będących efektem wrodzonych wad anatomicznych lub spowodowanych wzrostem populacji osób starszych na świecie, doprowadziło do rozwoju w inżynierii biomateriałów elementów zastępujących naturalny staw biodrowy, zwanych endoprotezami. Około 60% pacjentów poddających się alloplastyce stawu biodrowego w ciągu 5 do 10 lat wymaga ponownej operacji ze względu na obluzowanie implantu, które może polegać na wysunięciu się głowy endoprotezy z panewki endoprotezy, bądź zmniejszeniu gęstości kości (resorpcja) w obrębie endoprotezy (wynikająca z prawa Wolff'a[2]), co prowadzi do przeciążenia albo niedociążenia implantu, a tym samym niezdolności do spełniania swojej funkcji [1,2].

Endoproteza stawu biodrowego, pokazana na *Rys. 1*, składa się z kilku części, jakimi są trzpień endoprotezy pełniący funkcję kości biodrowej, głowa endoprotezy, odwzorowująca głowę kości udowej, wkładka wraz z panewką endoprotezy, zapewniające ruchliwość w obrębie sztucznego stawu biodrowego. Na określone części endoprotezy działają naprężenia statyczne oraz dynamiczne, zależne od wielkości masy ciała, grawitacji, siły mięśni pracujących w obrębie stawu oraz przyjętej przez analizowaną jednostkę pozycji (siedząca, stojąca na dwóch nogach, stojąca na jednej nodze itp.) [3].

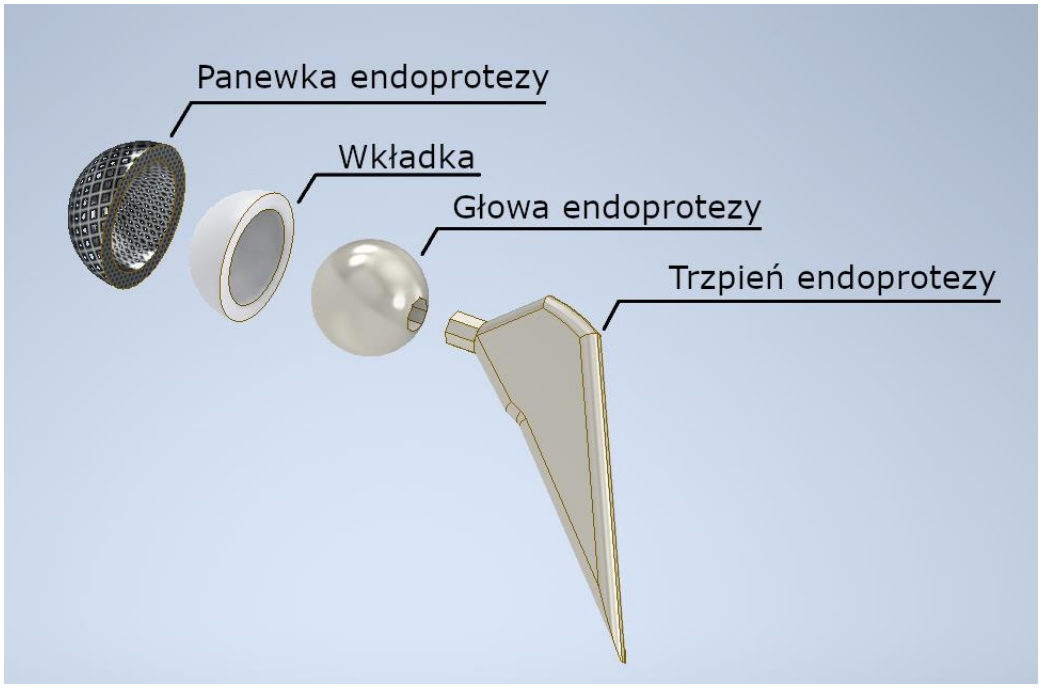

Rys. 1 Schematyczny model endoprotezy stawu biodrowego z wyszczególnionymi elementami (model zaprojektowany w programie Autodesk Inventor Professional)

[2] „*Every change in the function of bone or of their function alone is followed by certain definite changes in their internal architecture, and equally definite alteration in their external confirmation in accordance with mathematical laws*" *(Wolff, 1892).*

Dobór materiałów przeznaczonych na implanty oraz endoprotezy nie może być przypadkowy. Parametrami, które należy wziąć pod uwagę, są w szczególności moduł Young'a oraz wytrzymałość na rozciąganie [4], co jest podyktowane koniecznością przeciwstawienia się materiału naprężeniom występującym podczas procesu implantacji, jak i użytkowania. Większość materiałów bazujących na metalach, bądź ceramikach posiada wyższy moduł Young'a niż moduł kości korowej czy gąbczastej. W inżynierii biomateriałów dąży się do uzyskania modułu sprężystości materiału jak najbardziej zbliżonego do modułu naturalnej kości, bądź niższego. Zastosowanie na endoprotezę materiału o zbyt wysokim module Young'a (wiele wyższym niż moduł sprężystości kości) może być przyczyną miejscowego zmniejszenia gęstości kości (osteopenia) na skutek działających sił ścinających [5,6]. Według danych literaturowych moduł Young'a kości korowej wynosi średnio 18 GPa [7].

Jedne z najczęściej stosowanych materiałów przeznaczonych na endoprotezy to tytan i jego stopy. Są to materiały dobrze tolerowane przez organizm człowieka, biokompatybilne, a na ich powierzchni samorzutnie tworzy się warstwa pasywna, stanowiąca naturalną ochronę przed korozją [8]. Tytan II charakteryzuje się niską twardością (~ 6 GPa [9]) oraz niskim modułem Young'a (105 GPa [10]), jednak do zastosowań biomedycznych wymaga odpowiedniej modyfikacji, aby osiągnąć właściwości zbliżone do właściwości naturalnej kości, stąd przez wiele lat w medycynie na endoprotezy stosowano stop Ti-6Al-4V. Ze względu na obecność toksycznych pierwiastków (V, Al) oraz duże prawdopodobieństwo uwalniania się ich w organizmie pacjentów, zaczęto szukać nowych stopów. Badano m.in. Ti-6Al-7Nb, Ti–5Al–2.5Fe oraz TiNi, również nieodpowiednie pod kątem cytotoksyczności, aż zaczęto projektować materiały zawierające cyrkon oraz niob, które dodatkowo polepszają odporność korozyjną tytanu, jak np. Ti–13Nb–13Zr, którego moduł Young'a mieści się w granicach 79 ÷ 84 GPa [10] oraz charakteryzuje się twardością ~ 2,5 GPa (254 HV) [11]. Dodatek Nb poprawia właściwości mechaniczne materiału, co w połączeniu z Zr, zwiększającym wytrzymałość materiału, tworzy stop tytanu odpowiedni do zastosowań biomedycznych [12].

Oprócz modyfikacji właściwości tytanu poprzez zastosowanie dodatków stopowych [10] stosuje się powłoki wpływające na właściwości mechaniczne, odporność na zużycie ścierne oraz właściwości biologiczne materiału, m.in. polecane są powłoki na bazie węgla pierwiastkowego, jakimi mogą być powłoki z grafenu, diamentu, bądź z wielościennych nanorurek węglowych (MWCNTs). Materiały węglowe charakteryzują się chemiczną obojętnością, wysoką biokompatybilnością, są atrombogenne (nie powodują powstania skrzepów) oraz dobrze tolerowane przez ludzki organizm [13]. MWCNTs charakteryzują się unikalnymi właściwościami, jak wysoki współczynnik proporcjonalności (tzn. stosunek długości do średnicy nanorurki, z ang. *aspect ratio*), duża powierzchnia właściwa, wysoka wytrzymałość na rozciąganie (do 30 GPa), wysoki moduł Young'a (~ 1 TPa) oraz struktura stanowiąca doskonałe rusztowanie dla innych nanocząstek [14]. Stąd, dodatek MWCNTs do

powłok jest wykorzystywany jako wzmocnienie lub materiał zapobiegający powstaniu pęknięć. Co więcej, istnieją doniesienia o polepszeniu proliferacji komórek dla powłok z dodatkiem MWCNTs [15,16] oraz o ich działaniu antybakteryjnym [17]. Więcej szczegółowych informacji na temat właściwości powłok MWCNTs, metod ich wytwarzania oraz możliwe zastosowania zostały opisane w publikacji przeglądowej A1. Powłoki MWCNTs są stosowane z dodatkami w postaci ceramiki, metali, a także polimerów.

W niniejszym projekcie doktorskim podłoże do badań stanowił tytan II oraz stop Ti13Nb13Zr. Na pokrycia zastosowano powłoki na bazie MWCNTs oraz MWCNTs z dodatkami, takimi jak tlenek tytanu, nanomiedź oraz nanosrebro. Głównym zadaniem dodatków było wzmocnienie właściwości antybakteryjnych powłok MWCNTs, szczególnie przeciwko bakteriom, takim jak *Staphylococcus aureus*, *Staphylococcus epidermidis*, *Pseudomonas aeruginosa* i *Escherichia coli*, które są głównymi sprawcami infekcji w obrębie implantów i endoprotez [18].

Dodatkowo tlenek tytanu, którego najbardziej reaktywna forma, anataz, posiadająca najlepsze właściwości antybakteryjne [19], charakteryzuje się wysokim modułem Young'a [20] oraz niskim modułem ścinania [20], co korzystnie wpływa na właściwości mechaniczne powłok na bazie MWCNTs [20]. Co więcej, dodatek TiO_2 do powłok MWCNTs wytworzonych metodą EPD, powoduje zmniejszenie liczby i długości pęknięć powłoki, a tym samym poprawia adhezję do podłoża [21].

Powłoki na bazie nanorurek węglowych przygotowywano do zastosowania na pokrycia trzpieni endoprotezy stawu biodrowego, którego część została pokazana na *Rys. 2* (oznaczona ciemnym kolorem).

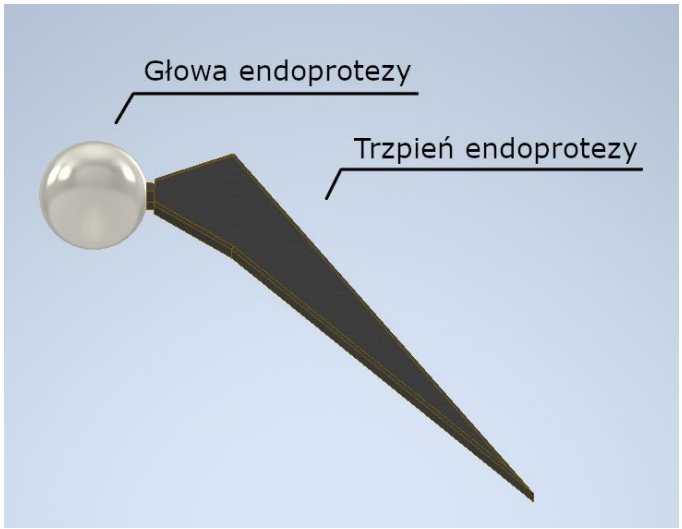

Rys. 2 Schemat części endoprotezy stawu biodrowego, przedstawiający potencjalne zastosowanie powłok MWCNTs na pokrycia trzpieni endoprotezy oznaczone kolorem ciemnym (rysunek został wykonany z użyciem programu Autodesk Inventor Professional)

W ramach projektu doktorskiego, czego efektem jest przygotowana rozprawa, wykonano:

1. Przegląd literatury odnośnie do powłok z nanorurek węglowych oraz ich właściwości (topografia, morfologia, adhezja do podłoża, właściwości mechaniczne, odporność korozyjna, zwilżalność, bioaktywność, cytotoksyczność i właściwości antybakteryjne) w zależności od zastosowanej metody wytwarzania oraz dodatków, czego efektem jest przygotowana publikacja przeglądowa A1.
2. Dobór odpowiednich parametrów osadzania elektroforetycznego (EPD) powłok z wielościennych nanorurek węglowych z dodatkami (napięcie EPD, czas EPD, stężenie dodatków - tlenek tytanu, nanomiedź, nanosrebro), czego efektem są przygotowane publikacje z prac badawczych A2, A3, A4.
3. Badania mechaniczne (ocena powierzchniowego modułu Young'a, nanotwardości, współczynników sprężystych oraz plastyczności), badania morfologii, ocena jakościowa składu chemicznego, topografii powierzchni oraz grubości otrzymanych powłok, których wyniki zostały opublikowane w pracach badawczych A2, A3, A4.
4. Badania kąta zwilżania, test nanozarysowania (z ang. *nanoscratch-test*; ocena adhezji powłoki do podłoża tytanowego), spektroskopia Raman'a oraz badania odporności korozyjnej, przedstawione w pracach badawczych A4 i A5.
5. Badania biologiczne na komórkach fibroblastów HDF (ang. *human dermal fibroblasts*) oraz mysich prekursorów osteoblastów MC3T3 (ang. *mouse osteoblasts precursors*) przeprowadzone dla powłoki z wielościennych nanorurek węglowych z dodatkiem tlenku tytanu, która osiągnęła najbardziej satysfakcjonujące wyniki w badaniach podstawowych, analizując zastosowanie powłoki w implantologii. Wyniki zostały opisane w publikacji A5.

2. METODYKA WYTWARZANIA POWŁOK MWCNTs

2.1 Przygotowanie podłoża

Odpowiednia modyfikacja podłoża ma kluczowe znaczenie m.in. wpływając na adhezję powłoki MWCNTs do podłoża tytanowego. Stosuje się wiele modyfikacji, w tym zastosowanie różnych metod trawienia podłoża: mechaniczne, chemiczne, elektrochemiczne oraz utlenianie mikro-łukowe (*micro-arc oxidation*, MAO) [22], modyfikacja wiązką lasera [22,23], poprzez zmianę kształtu podłoża, bądź parametrów chropowatości, a także naniesienie warstwy przejściowej [24]. Inne przykłady z literatury pokazujące wpływ przygotowania podłoża na adhezję powłok zostały pokazane w publikacji przeglądowej A1 w rozdziale 4.2 „Adhesion between CNTs and metallic substrate".

W niniejszym projekcie do przygotowania podłoża pod każdą z powłok zastosowano opisaną w [25,26] sekwencję, która miała na celu w pierwszej kolejności oczyścić powierzchnię z samorzutnie powstającej warstwy pasywnej na podłożu tytanowym oraz nadanie odpowiedniej chropowatości, poprzez zastosowanie szlifowania papierem ściernym do gradacji #800, a następnie płukanie w wodzie, aby usunąć resztki pozostałego, zeszlifowanego materiału.

W kolejnym etapie próbki były przetrzymywane w acetonie, aby odtłuścić podłoże oraz usunąć ewentualne zanieczyszczenia, a następnie moczone w wodzie i trawione chemicznie w 5% roztworze kwasu fluorowodorowego w celu usunięcia pozostałych zanieczyszczeń oraz zapewnienia optymalnej topografii podłoża pod powłokę z MWCNTs. Przed procesem osadzania elektroforetycznego próbki przetrzymywano w wodzie, aby ograniczyć powstawanie warstwy pasywnej na podłożu tytanowym. Tak przygotowane próbki, przytwierdzone do miedzianego drutu, mocowano w uchwycie, a następnie przystępowano do osadzania powłok.

2.2 Parametry osadzania elektroforetycznego powłok MWCNTs

Metoda osadzania elektroforetycznego (EPD) stanowi jedną z metod elektrochemicznych osadzania powłok MWCNTs z dodatkami, obok metod termicznych oraz wykorzystujących wiązkę lasera, które opisano w publikacji przeglądowej A1 w rozdziale 3 „CNTs- containing coating types and their deposition methods", gdzie pokazano wpływ metody wytwarzania na właściwości oraz strukturę otrzymanych powłok MWCNTs.

Ze względu na możliwość kontrolowania parametrów powłoki poprzez dostosowanie zmiennych procesu wytwarzania, takich jak napięcie, czas osadzania oraz skład zawiesiny, a także możliwość pokrywania powierzchni o różnych kształtach, do przygotowania powłok na bazie MWCNTs wykorzystano metodę EPD.

Parametry osadzania powłok z MWCNTs dobrano na podstawie analizy literatury oraz prób laboratoryjnych. Ustalenie odpowiedniego czasu osadzania miało wpływ przede wszystkim na grubość otrzymanych powłok z MWCNTs, ich jednorodność oraz przyczepność do podłoża tytanowego. Przeanalizowano dwa czasy osadzania 0,5 min oraz 1 min. Lepszą jakość powłok osadzonych na podłożu stopu Ti13Nb13Zr osiągano przy krótszym czasie EPD. Dłuższy czas osadzania powodował powstanie powłok o wyższej grubości, a tym samym gorszej przyczepności do podłoża. Odwrotnie -przy zastosowaniu podłoża z tytanu II. Czas osadzania powłok MWCNTs z dodatkami dobrano sugerując się parametrami zastosowanymi w publikacji [27], podobnie jak w przypadku napięcia EPD [21]. Zbyt niskie lub zbyt wysokie napięcie osadzania skutkowało brakiem powłoki na podłożu. Co więcej, odpowiednia odległość pomiędzy elektrodami, równoległe ustawienie elektrod do siebie oraz prawidłowe wyjęcie próbek z uchwytu również decydowały o jakości otrzymanych powłok.

Skład zawiesiny EPD dostosowano poprzez dobór odpowiedniego stężenia MWCNTs oraz dodatków. Wcześniejsze wyniki, przedstawione w publikacji [26], pokazały moduł Young'a zbliżony do modułu kości korowej dla powłoki MWCNTs o stężeniu 0,27% mas. w kąpieli EPD, stąd wytwarzając powłoki MWCNTs zastosowano podobne stężenie. Osadzanie MWCNTs metodą EPD było możliwe dzięki ich modyfikacji grupami –COOH.

Powłoki z dodatkami osadzano w dwóch etapach. W pierwszej kolejności na odpowiednio przygotowane podłoże nakładano powłokę MWCNTs, następnie osadzano powłokę z dodatkiem. Nie łączono składników powłoki w jednej zawiesinie ze względów technologicznych - powłoki z dodatkiem tlenku tytanu nie dało się w ten sposób osadzić. Zawartość procentową dodatków dobrano na podstawie przeglądu literaturowego, oceniając wpływ danego stężenia na właściwości antybakteryjne powłoki.

Stężenie tlenku tytanu wyznaczono na podstawie analizy literatury [28]. W celu uzyskania niskiej cytotoksyczności powłoki, przy zachowaniu optymalnych właściwości antybakteryjnych i właściwości mechanicznych, zawartość tlenku tytanu w zawiesinie została 3-krotnie obniżona. Wyniki badań nad powłokami MWCNTs/TiO_2 zostały opisane w publikacjach badawczych A2, A3 i A5 oraz są szerzej omówione w następnym rozdziale. Stężenie procentowe nanomiedzi w powłokach dobrano również na podstawie przeglądu literatury. Ze względu na potencjalną toksyczność miedzi [29,30] oraz możliwość porównania między sobą powłok na bazie MWCNTs, zastosowano stężenie wielokrotnie niższe niż podane w literaturze (1,5% [31], 1,92% [32] lub 2,5% [33]). Przegląd literatury dotyczący właściwości antybakteryjnych powłok z dodatkiem miedzi oraz wyniki badań dla powłoki MWCNTs/Cu osadzonej na podłożu Ti13Nb13Zr zostały przedstawione w publikacji A2. Podobnie, stężenie nanosrebra w powłokach ustalono na podstawie analizy danych literaturowych pod względem osiągnięcia optymalnych właściwości antybakteryjnych [34,35], a wyniki dla powłok MWCNTs/Ag opisano w publikacji A4.

Efektywność działania antybakteryjnego powłoki MWCNTs/Ag przeciwko bakteriom gram-ujemnym i gram-dodatnim, została omówiona w podrozdziale 4.7 „Antibacterial efficiency" publikacji przeglądowej A1.

3. ANALIZA WŁAŚCIWOŚCI OTRZYMANYCH POWŁOK

Poszczególne publikacje analizują określone właściwości powłok na bazie MWCNTs. Publikacja A2 i A3 stanowią porównanie właściwości mechanicznych, plastycznych oraz sprężystych, powłok z dodatkiem tlenku tytanu (MWCNTs/TiO_2) oraz nanomiedzi (MWCNTs/Cu) na podłożu stopu Ti13Nb13Zr (A2) oraz tytanu II (A3).

W publikacji A4 przedstawiono wyniki właściwości mechanicznych, korozyjnych oraz zwilżalności powłok MWCNTs z dodatkiem nanosrebra (MWCNTs/Ag) na podłożu Ti13Nb13Zr.

Natomiast publikacja A5 stanowi uzupełnienie badań pokazanych w publikacji A2 dla powłoki MWCNTs/TiO_2, która osiągnęła najlepsze wyniki w testach podstawowych. Artykuł A5 opisuje strukturę chemiczną, przedstawia wyniki pomiaru siły adhezji powłoki MWCNTs/TiO_2 do podłoża Ti13Nb13Zr, omawia odporność korozyjną, zwilżalność oraz cytotoksyczność dla komórek ludzkich fibroblastów oraz mysich prekursorów osteoblastów.

Poniżej przedstawiono podsumowanie wyników publikacji badawczych wchodzących w skład jednotematycznego cyklu publikacji.

3.1 Morfologia i topografia powierzchni

Parametry opisujące topografię powierzchni powłok z nanorurek węglowych oraz ich morfologię zostały opisane szerzej w publikacji przeglądowej A1. Omawiane właściwości są bardzo ważne w inżynierii materiałowej, gdyż wpływają nie tylko na właściwości biologiczne, takie jak odporność antybakteryjna, bioaktywność, cytotoksyczność, ale również na odporność korozyjną, a także adhezję powłoki do podłoża. Topografię powierzchni można modyfikować poprzez zastosowanie różnych materiałów powłokowych oraz rozmaitych technologii wytwarzania (przykłady wpływu metody wytwarzania na strukturę i właściwości powłok z MWCNTs zostały opisane w publikacji A1).

Wyniki przedstawione w publikacjach badawczych pokazują wysoką jednorodność osadzonych powłok MWCNTs. Nanorurki węglowe na podłożu tytanowym występowały w postaci nieuporządkowanej, zarówno na powierzchni tytanu II, jak i stopu Ti13Nb13Zr. Chropowatości powłoki MWCNTs osadzonej na podłożu z czystego tytanu oraz stopu Ti13Nb13Zr nie różniły się znacząco.

W przypadku powłok MWCNTs z dodatkami można było zaobserwować liczne aglomeraty. Tlenek tytanu w powłoce MWCNTs/TiO_2 przyjmował strukturę warstwową, wynikającą z zastosowanej metody osadzania. Natomiast w powłokach z

dodatkiem nanomiedzi, bądź nanosrebra, dodatki w postaci cząstek gromadziły się w miejscach, gdzie najprawdopodobniej występowały defekty strukturalne, tzn. na zgięciach nanorurek oraz na ich końcach. Co więcej, powłoka MWCNTs/Cu charakteryzowała się występowaniem pęknięć, zarówno na podłożu Ti13Nb13Zr, jak i z tytanu II. Badania chropowatości powłok pokazały, że powłoka MWCNTs/TiO_2 charakteryzowała się najwyższą wartością chropowatości, niezależnie od zastosowanego podłoża. Najniższy współczynnik chropowatości R_a wykazuje powłoka z samych MWCNTs. Natomiast powłoki z dodatkiem nanomiedzi i nanosrebra posiadają zbliżoną chropowatość, która wynika z podobnego lokalizowania się na powłoce MWCNTs obu dodatków.

Porównując grubości otrzymanych powłok, najwyższą charakteryzowała się powłoka MWCNTs/TiO_2, co wynikało z metody wytwarzania - najpierw osadzano powłokę MWCNTs, następnie TiO_2, a także - lokalizacji gromadzenia się aglomeratów oraz mikrometrycznego rozkładu ich wielkości.

3.2 Właściwości mechaniczne

Głównym celem projektu doktorskiego było przeprowadzenie podstawowych badań mechanicznych, aby ocenić przydatność otrzymanych powłok do zastosowań na pokrycia endoprotez i implantów stosowanych w biomedycynie. Publikacja przeglądowa A1 pokazuje przegląd literatury na temat właściwości mechanicznych powłok z MWCNTs z dodatkami. Publikacje badawcze A2, A3 oraz A4 omawiają wyniki badań powłok MWCNTs, MWCNTs/TiO_2, MWCNTs/Cu oraz MWCNTs/Ag. Co więcej, sprawdzono również, czy właściwości mechaniczne poszczególnych powłok będą się różniły w zależności od zastosowanego podłoża, dlatego publikacja A2 przedstawia powłoki na stopie Ti13Nb13Zr, a publikacja A3 - powłoki osadzone na tytanie II (z wyjątkiem powłoki MWCNTs/Ag).

Wyniki badań przedstawione w publikacji A2 oraz A4 pokazały, że najwyższym powierzchniowym modułem Young'a i jednocześnie najbardziej zbliżonym do modułu kości korowej charakteryzuje się powłoka z samych MWCNTs. Dodatki, takie jak nanomiedź, tlenek tytanu i nanosrebro obniżają powierzchniowy moduł Young'a powłoki. Powłoka MWCNTs/TiO_2, MWCNTs/Cu i MWCNTs/Ag charakteryzuję się odpowiednio niespełna 2-, 1,5- oraz ponad 3,5-razy niższym modułem Young'a w stosunku do powłoki MWCNTs. Natomiast w przypadku powłok osadzonych na podłożu z tytanu II (A3) moduł sprężystości w porównaniu do modułu kości korowej jest niższy odpowiednio prawie 4,5-krotnie dla powłok MWCNTs i MWCNTs/Cu oraz niespełna 2-krotnie dla powłoki MWCNTs/TiO_2.

Rodzaj zastosowanego podłoża dla powłok MWCNTs oraz MWCNTs z dodatkami generuje powstanie zależności między nanotwardością i powierzchniowym modułem Young'a. Dla powłok MWCNTs osadzonych na podłożu ze stopu Ti13Nb13Zr (A2) zastosowanie dodatków powodowało wzrost nanotwardości powłoki

i spadek powierzchniowego modułu Young'a. Natomiast na podłożu z tytanu II (A3), modyfikacja powłoki MWCNTs dodatkami powodowała zarówno wzrost nanotwardości, jak i powierzchniowego modułu Young'a. Powyższe zależności mogą wynikać z różnicy w strukturze materiałów podłoża, co jest przyczyną ich odmiennych właściwości. Stop Ti13Nb13Zr charakteryzuje się modułem Young'a oraz nanotwardością wynoszącymi odpowiednio 83.3 ± 11.6 GPa oraz 3,8 ± 1,05 GPa [26] (~300 HV [36]), natomiast tytan II odpowiednio 105 GPa oraz 350 HV [37]. Co więcej, wytwarzanie powłok na podłożu z tytanu II było trudniejsze technologicznie, ze względu na wyższy stopień utleniania podłoża podczas osadzania EPD w stosunku do stopu Ti13Nb13Zr, co mogło mieć wpływ na uzyskane wyniki. Wyższa nanotwardość powłoki MWCNTs/TiO_2 osadzonej na tytanie II w stosunku do powłoki osadzonej na stopie Ti13Nb13Zr może być skutkiem powstania międzywarstwy amorficznego tlenku tytanu.

Powłoka MWCNTs/Cu charakteryzuje się najwyższą nanotwardością na podłożu ze stopu Ti13Nb13Zr (A2). W porównaniu do powłoki MWCNTs, powłoki MWCNTs/Cu i MWCNTs/TiO_2 wykazały odpowiednio 2 i 1,5 razy wyższą nanotwardość, natomiast powłoka MWCNTs/Ag - 4 razy niższą. Wyniki pomiaru nanotwardości na podłożu z tytanu II (A3) ujawniają najwyższą nanotwardość dla powłoki MWCNTs/TiO_2. Porównując powłoki z dodatkami z powłoką MWCNTs, dodatek tlenku tytanu i nanomiedzi spowodował odpowiednio prawie 6- i 2,5-krotny wzrost nanotwardości. Powłoki MWCNTs/Ag nie badano na podłożu z tytanu II.

Badanie metodą nanoindentacji służyło również ocenie właściwości plastycznych oraz sprężystych powłok MWCNTs oraz ich odporności na zużycie ścierne (opisane w publikacjach badawczych A2 i A3). Parametrami opisującymi powyższe właściwości są praca plastyczna, praca sprężysta, współczynnik będący ilorazem nanotwardości (H) i zredukowanego modułu Young'a (Er) (nieuwzględniającego współczynnika Poisson'a materiałów: wgłębnika, materiału powłoki) oraz współczynnik H^2/Er^3, zwany *yield pressure*. Publikacja A2 szczegółowo omawia powyższe parametry, jednak dla lepszego zrozumienia tematu są one tu raz jeszcze wyjaśniane.

Praca plastyczna opisuje ilość energii magazynowanej w powłoce, która wynika z odkształcenia plastycznego powłoki; materiał pozostaje odkształcony po zniknięciu naprężenia zewnętrznego. Natomiast praca sprężysta reprezentuje energię uwolnioną z materiału pod wpływem działającego naprężenia; materiał powraca do swojego kształtu po ustąpieniu naprężenia zewnętrznego. Dodatek nanomiedzi oraz tlenku tytanu do powłok MWCNTs osadzonych na podłożu Ti13Nb13Zr (A2) spowodował polepszenie zarówno właściwości plastycznych, jak i sprężystych. Najwyższymi właściwościami plastycznymi charakteryzowała się powłoka MWCNTs/TiO_2, 1,5-razy wyższymi niż dla powłoki MWCNTs. Takie zjawisko wynika z zastosowania dodatku w postaci tlenku tytanu, który stanowi wzmocnienie w strukturze kompozytu. Natomiast właściwości sprężyste powłoki MWCNTs/TiO_2 były

zbliżone do właściwości powłoki MWCNTs/Cu i 2-krotnie wyższe w stosunku do powłoki MWCNTs, co wskazuje na zwiększenie właściwości sprężystych powłoki MWCNTs poprzez zastosowanie tlenkowych, jak i metalicznych dodatków. Zastosowanie dodatków metalicznych i tlenkowych do powłok MWCNTs na podłożu z tytanu II (A3) doprowadziło do odmiennych obserwacji; wyższa nanotwardość powłoki MWCNTs/TiO_2 oraz niższa dla MWCNTs/Cu spowodowała odwrotny efekt dla właściwości plastycznych i sprężystych omawianych powłok na podłożu z tytanu w stosunku do podłoża ze stopu Ti13Nb13Zr, co wynika z intensywnego utleniania podłoża z czystego tytanu podczas procesu osadzania powłok. Warto również podkreślić, że powłoka MWCNTs/Cu osiągnęła również najwyższe właściwości sprężyste spośród omawianych powłok, 20 razy wyższe niż powłoka MWCNTs.

Z wyników badań nanoindentacji wylicza się również współczynnik H/Er, bezpośrednio związany z adhezją powłoki do podłoża, dlatego wyniki dla poszczególnych powłok omówiono w kolejnym podrozdziale 3.3 „Adhezja powłoki MWCNTs do podłoża tytanowego".

Współczynnik H^3/Er^2 (omawiany w publikacjach A2 i A3) opisuje wytrzymałość powłok na odkształcenie plastyczne w wyniku przyłożonego nacisku. Powłoka MWCNTs/TiO_2 osadzona na podłożu Ti13Nb13Zr osiągnęła najwyższe właściwości plastyczne, co zostało też potwierdzone wyliczonym współczynnikiem H^3/Er^2. Najwyższy współczynnik *yield pressure* uzyskano dla powłoki MWCNTs/Cu, co wskazuje, że jest to materiał o niższych właściwościach plastycznych niż powłoka MWCNTs/TiO_2. Podobnie w przypadku powłok osadzonych na podłożu z tytanu II, wyliczone współczynniki H^3/Er^2 potwierdziły poprzednie wyniki opisujące właściwości plastyczne omawianych powłok.

3.3 Adhezja powłoki MWCNTs do podłoża tytanowego

Jednym z najważniejszych parametrów opisujących powłoki przeznaczone na pokrycia endoprotez i implantów jest ich siła przylegania do podłoża, a więc odporność powłoki na działanie naprężeń ścinających, która informuje, przy jakich siłach trących powłoka ulegnie delaminacji. Adhezja powłoki do podłoża jest zależna od wielu czynników, jakimi są grubość powłoki, struktura powłoki, zastosowana modyfikacja podłoża przed nałożeniem powłoki oraz zastosowana metoda osadzania powłoki [38].

Adhezję powłok MWCNTs, MWCNTs/Ag oraz MWCNTs/TiO_2 opisano w publikacjach badawczych A4 i A5. Najwyższą siłę krytyczną (Lc), dla której powłoka uległa zerwaniu zgodnie z analizą zdjęć uzyskanych podczas obserwacji na mikroskopie optycznym oraz testu nanozarysowania uzyskano dla powłoki MWCNTs/TiO_2. Jest to wartość prawie 3,5-krotnie wyższa niż dla powłoki MWCNTs oraz 1,5-krotnie wyższa niż dla powłoki MWCNTs/Ag.

Rys. 3 pokazuje nieopublikowane wyniki testu nanozarysowania dla powłoki MWCNTs/Cu, przeprowadzonego w takich samych warunkach, w jakich badano pozostałe powłoki (siła nacisku rosła od 0 do 200 mN z szybkością 1,3 $mN \cdot s^{-1}$, a długość zarysowania wynosiła 500 μm), który przedstawia wykres zależności krytycznej siły trącej (F_t) od krytycznej siły działającej prostopadle na próbkę (F_n).

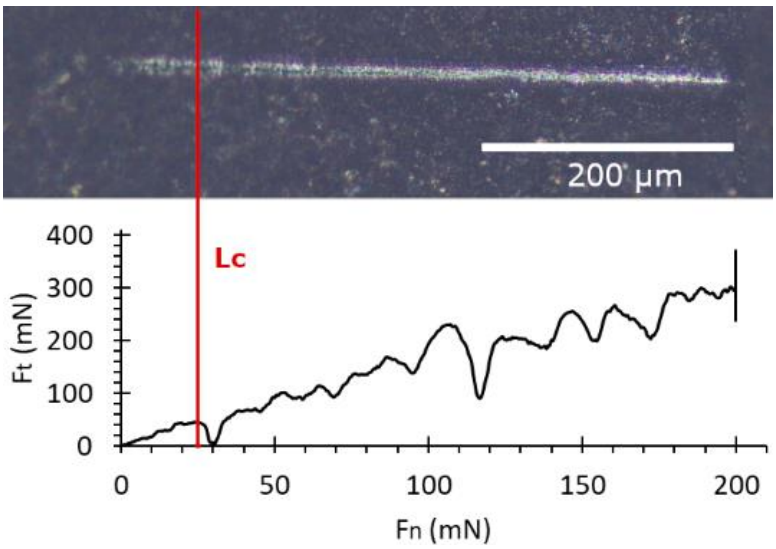

Rys. 3 Wykres zależności krytycznej siły trącej (F_t) oraz krytycznej siły normalnej (F_n) wraz ze zdjęciem zarysowania, uzyskanym podczas obserwacji na mikroskopie optycznym. Lc oznacza krytyczną siłę tarcia, w wyniku której następuje delaminacja powłoki

Na podstawie uzyskanych wyników wyznaczono średnią siłę krytyczną Lc, która wynosiła 23,9 ± 4,4 mN oraz krytyczną siłę tarcia 54,7 ± 9,02 mN, co pokazuje, że dodatek miedzi do powłoki MWCNTs nie wpływa na zmianę adhezji powłoki MWCNTs do podłoża ze stopu Ti13Nb13Zr.

Powłoka MWCNTs/TiO_2 wymagała użycia najwyższej siły, aby doszło do zerwania powłoki, co wynika z wysokiej twardości tlenku tytanu, która zgodnie z literaturą wynosi 1 GPa [39]. Co więcej, powłoka MWCNTs/TiO_2 charakteryzowała się najwyższą grubością spośród badanych powłok, a struktura zastosowanego tlenku tytanu, anatazu, jest bardziej reaktywna niż rutylu, co sprawia, że połączenie między nanorurkami węglowymi a tlenkiem tytanu mogło występować nie tylko fizycznie, ale również chemicznie (wiązania van der Waalsa). Dla lepszej oceny przyczyny uzyskanych wyników, w dalszych badaniach przydatna byłaby ocena występujących wiązań w powłoce poprzez zastosowanie spektroskopii Fouriera.

Oprócz testu nanozarysowania, na podstawie wyników badania nanoindentacji wyliczono współczynnik H/Er, który został omówiony w podrozdziale 3.2 „Właściwości mechaniczne”. Współczynnik H/Er opisuje zdolność powłoki do odkształcania się pod wpływem obciążenia, a więc odkształcania bez odpryskiwania, które mogłoby być związane z niedopasowaniem powłoki do podłoża. Analiza współczynników H/Er dla powłok MWCNTs została przeprowadzona w publikacjach

A2, A3 oraz A4. Najwyższy współczynnik H/Er na podłożu Ti13Nb13Zr, jak i z tytanu II uzyskano dla powłoki MWCNTs/Cu, co może wynikać z wysokiej plastyczności nanomiedzi i lokalizacji cząstek. Podobnych właściwości spodziewano się dla powłoki MWCNTs/Ag (na podłożu Ti13Nb13Zr), jednak powłoka ta uzyskała współczynnik H/Er zbliżony do powłoki MWCNTs, co wynikało z prawdopodobnego wpływu podłoża na wyniki dla powłoki MWCNTs/Cu, na której zaobserwowano pęknięcia. Powłoka MWCNTs/TiO_2 uzyskała najwyższy współczynnik H/Er po powłoce MWCNTs/Cu (niewielka różnica), co jest zgodne z wynikami testu nanozarysowania.

3.4 Odporność korozyjna powłok na bazie MWCNTs

Badanie odporności korozyjnej służy ocenie odporności danego materiału na działanie określonego czynnika elektrochemicznego. Dla powłok przeznaczonych do kontaktu z płynami ustrojowymi w ciele człowieka może być ono przeprowadzane m.in. w płynie Ringer'a. Omówienie odporności korozyjnej powłok MWCNTs zostało opisane w publikacji przeglądowej A1.

Zarówno powłoki MWCNTs, jak i MWCNTs z dodatkami wykazywały gorszą odporność korozyjną w stosunku do materiału podłoża. Niemniej jednak, zastosowane dodatki w postaci tlenku tytanu, nanosrebra czy nanomiedzi powodowały poprawę odporności korozyjnej samej powłoki MWCNTs.

Odporność korozyjną powłok MWCNTs, MWCNTs/Ag oraz MWCNTs/TiO_2 omówiono w publikacjach badawczych A4 oraz A5. Najwyższą odporność korozyjną w stosunku do MWCNTs uzyskano dla powłoki MWCNTs/TiO_2, czego przyczyną był nie tylko sam tlenek tytanu i jego zdolność do samopasywacji, ale również lokalizacja aglomeratów, izolujących nanorurki węglowe od środowiska zewnętrznego, a także zmniejszających porowatość powłoki. W przypadku powłoki MWCNTs/Cu wyniku nie opublikowano, jednak sprawdzono, że poszczególne parametry, takie jak prąd korozji j_{corr} oraz napięcie E_{corr} wynosiły odpowiednio, 155,4 ± 41,2 nA/cm^2 oraz -0,16 ± 0,003 V, blisko parametrów powłoki MWCNTs/Ag, w efekcie podobnej lokalizacji dodatków na podłożu nanorurkowym i zgodnie z oczekiwaniami.

3.5 Zwilżalność powłok na bazie MWCNTs

Pomiar kąta zwilżania, a więc ocena zwilżalności powłok, jest kluczowym parametrem charakteryzującym właściwości biologiczne (biokompatybilność) powłok, omówionym w publikacji przeglądowej A1.

Wyniki pomiaru kąta zwilżania dla powłoki MWCNTs, MWCNTs/Ag oraz MWCNTs/TiO_2 zostały opisane w publikacjach badawczych A4 oraz A5. Dokonano również pomiarów dla próbki z powłoką MWCNTs/Cu, których nie opublikowano, gdzie średni kąt zwilżania wynosił poniżej 20°.

Powłoki MWCNTs oraz MWCNTs z dodatkami charakteryzują się zwilżalnością odpowiednią do zastosowań medycznych, a więc występującą w granicach 40÷60°, gwarantującą odpowiednią adhezję komórek oraz bioaktywność powłoki (A1). Dodatek zarówno nanosrebra, jak i tlenku tytanu powoduje niewielki wzrost zwilżalności, wyższy dla powłoki MWCNTs/Ag, co może być wynikiem różnicy w porowatości powłoki, wynikającej ze sposobu osadzania się dodatku.

3.6 Właściwości biologiczne

Publikacja badawcza A5 przedstawia wyniki właściwości biologicznych powłoki MWCNTs/TiO_2, która wykazała najkorzystniejsze właściwości z punktu widzenia zastosowania na powłoki przeznaczone na endoprotezy i implanty tytanowe.

Badania biologiczne przeprowadzone na próbkach z powłoką MWCNTs oraz MWCNTs/TiO_2 obejmowały badanie *in vitro* cytotoksyczności dla komórek HDF (w teście bezpośrednim i pośrednim) oraz MC3T3 (w teście pośrednim). Żywotność komórek oceniono na podstawie testu MTT. Dla uzupełnienia wyników zbadano również poziom aktywności LDH (lactate dehydrogenase).

Wyniki testu bezpośredniego pokazują, że powłoka z samych MWCNTs, jak i MWCNTs/TiO_2 charakteryzuje się topografią korzystną do adhezji komórek HDF, co wynika z odpowiedniej porowatości powłoki. Dodatkowo, po 72 h inkubacji odnotowano wzrost proliferacji komórek HDF na powłoce MWCNTs, natomiast spadek na powłoce MWCNTs/TiO_2, gdzie dodatek tlenku tytanu zaczął toksycznie wpływać na komórki HDF.

Wyniki testu pośredniego wskazują na niekorzystny wpływ powłok MWCNTs oraz MWCNTs/TiO_2 na komórki HDF oraz MC3T3, spowodowany uwalnianiem toksycznych substancji z powłoki, bądź uniemożliwieniem przylegania składników odżywczych dla komórek, czy czynników ich wzrostu na powłoce.

Powyższe wyniki zostały potwierdzone w teście LDH. Po 24 h obie powłoki, MWCNTs, jak i MWCNTs/TiO_2, wykazały uszkodzenie komórek HDF na poziomie wyższym niż materiał rodzimy (podłoże Ti13Nb13Zr). Stopień ten jednak nie przekraczał 11% liczby komórek. Natomiast po 72 h poziom uszkodzenia komórek HDF na powłoce MWCNTs był zbliżony do materiału rodzimego, a dla MWCNTs/TiO_2 o 1,5% wyższy.

4. PODSUMOWANIE

W niniejszym projekcie doktorskim wytworzono powłoki na bazie MWCNTs z dodatkami, takimi jak nanomiedź, tlenek tytanu i nanosrebro na podłożu z tytanu II i stopu Ti13Nb13Zr, do zastosowań na pokrycia trzpieni endoprotez stawu biodrowego. Powłoki z dodatkami wytworzono metodą EPD w procesie składającym się z dwóch etapów: I. osadzenie powłoki MWCNTs na podłożu Ti13Nb13Zr (bądź tytan II), II. osadzenie powłoki z dodatkiem (nanosrebro lub nanomiedź, lub tlenek tytanu) na powłoce MWCNTs. Zastosowane dodatki miały za zadanie polepszać właściwości antybakteryjne oraz mechaniczne powłoki MWCNTs, a otrzymane powłoki modyfikować właściwości podłoża, tak aby były bardziej zbliżone do właściwości naturalnej kości.

Otrzymane powłoki MWCNTs charakteryzują się wysoką jednorodnością i porowatością, a zastosowane dodatki występują w postaci aglomeratów, zarówno na powierzchni powłoki, jak i w porach powłoki. Nanocząstki nanomiedzi oraz nanosrebra gromadzą się w miejscach zdefektowania nanorurek węglowych, natomiast tlenek tytanu tworzy aglomeraty o strukturze warstwowej, wynikającej z metody wytwarzania. Niezależnie od zastosowanego podłoża najwyższą chropowatością, wynikającą z mikrometrycznego rozkładu wielkości aglomeratów tlenku tytanu, charakteryzuje się powłoka MWCNTs/TiO_2, a najniższą powłoka z samych MWCNTs, co nieznacznie wpływa na zwilżalność powłok, która zarówno dla powłoki MWCNTs z dodatkami, jak i bez, mieściła się w granicach 40÷60°, zgodnie z literaturą gwarantując odpowiednią adhezję komórek oraz bioaktywność powłoki. Spośród badanych powłok MWCNTs z dodatkami, powłoka MWCNTs/TiO_2 charakteryzuje się modułem sprężystości najbardziej zbliżonym do modułu kości korowej, niezależnie od zastosowanego podłoża. Na podstawie otrzymanych różnic w wynikach badań mechanicznych powłok MWCNTs z dodatkami, uzyskanych na podłożu tytanu II oraz stopu Ti13Nb13Zr, a także analizując grubość powłok można podejrzewać wpływ podłoża na otrzymane właściwości. Różnice w nanotwardości powłok, a tym samym w ich właściwościach plastycznych oraz sprężystych, mogą w szczególności wynikać z szybszego utleniania podłoża z tytanu II (w stosunku do utleniania podłoża Ti13Nb13Zr) oraz zastosowania dłuższego czasu osadzania EPD. Niemniej jednak, właściwości mechaniczne podłoża, zarówno z tytanu, jak i jego stopu są wielokrotnie wyższe niż otrzymanych powłok MWCNTs, stąd można wnioskować o znikomym wpływie podłoża na właściwości analizowanych powłok MWCNTs oraz MWCNTs z dodatkami. Utworzenie struktury kompozytu z twardymi cząstkami w postaci dodatków tlenkowych, jak i metalicznych zawieszonych w sprężystej matrycy sprawia, że otrzymane powłoki na bazie MWCNTs charakteryzują się lepszymi właściwościami plastycznymi oraz sprężystymi w porównaniu z powłoką z samych MWCNTs, co w połączeniu z wysoką reaktywnością zastosowanego w powłokach tlenku tytanu powoduje, iż powłoka MWCNTs/TiO_2 osadzona na podłożu Ti13Nb13Zr osiąga najwyższą adhezję. Ponadto, powłoki MWCNTs są wysoce porowate, dlatego

charakteryzują się niższą odpornością korozyjną w stosunku do materiału podłoża (Ti13Nb13Zr). Zastosowanie dodatków o wielkości nanometrycznej do powłoki MWCNTs powoduje po pierwsze, zmniejszenie jej porowatości poprzez wnikanie dodatków w głąb struktury (MWCNTs/Ag, MWCNTs/Cu, MWCNTs/TiO_2), a po drugie izolację powłoki z nanorurek węglowych od środowiska zewnętrznego, tak jak ma to miejsce w przypadku powłoki MWCNTs/TiO_2, co znacząco poprawia odporność powłoki MWCNTs na działanie środowiska korozyjnego.

W związku z powyższym, dodatek tlenku tytanu spełnia wymagania, zarówno pod kątem właściwości antybakteryjnych, mechanicznych, w tym plastycznych do zastosowania na pokrycia trzpieni endoprotez wykonanych ze stopu Ti13Nb13Zr. Mimo iż powłoka MWCNTs/TiO_2 charakteryzuje się najwyższą siłą adhezji do podłoża Ti13Nb13Zr spośród badanych powłok, to jednak aby posiadać niezbędne cechy celowe jest zastosowanie innych rozwiązań, które miałyby na celu zwiększenie odporności powłoki na zużycie ścieranie, jak też wykonanie badań spektrometrycznych, aby sprawdzić, jakie są mechanizmy adhezji powłoki MWCNTs/TiO_2 do podłoża tytanowego. Cytotoksyczność powłoki MWCNTs z dodatkiem tlenku tytanu została wyznaczona na podstawie oceny żywotności komórek fibroblastów oraz mysich osteoblastów, a także testu LDH, które wskazują, iż powłoka MWCNTs/TiO_2 stanowi niekorzystne środowisko dla czynników wzrostu komórek, dostarczanych im substancji odżywczych, bądź z powłoki wydzielane są toksyczne substancje, co stanowi kolejny punkt, pozostający do dalszych rozważań w pracy badawczej.

Uzyskane wyniki jednoznacznie wskazują na znaczący wpływ dodatków na morfologię, topografię, właściwości mechaniczne, plastyczne i sprężyste, odporność korozyjną oraz siłę adhezji powłok MWCNTs do podłoża tytanowego. Co więcej, dodatek tlenku tytanu optymalizuje właściwości mechaniczne, plastyczne oraz sprężyste, powłok na bazie MWCNTs pod kątem ich zastosowania na biomateriały, jak też zwiększa ich adhezję do podłoża. W świetle powyższych wyników udowodniono punkt I i II tezy badawczej. Topografia powierzchni powłok MWCNTs oraz MWCNTs z dodatkiem tlenku tytanu promuje adhezję komórek fibroblastów, jak i osteoblastów mysich, niemniej jednak w przypadku powłoki MWCNTs/TiO_2 po 72 h inkubacji następuje obumieranie komórek potwierdzone testem LDH, co może być spowodowane zbyt wysoką zawartością tlenku tytanu w powłoce; w związku z tym udowodnienie III punktu tezy badawczej wymaga dalszych doświadczeń z zastosowaniem niższego stężenia tlenku tytanu w powłoce MWCNTs.

5. BIBIOGRAFIA

[1] V.P. Torchynskyi, T. V. Nizalov, L. V. Shmelyova, A.D. Suprun, Physical and mathematical modeling of the distribution of load forces on the feminal component of an endoprosthesis of the hip joint under real conditions, Reports of Morphology. 29 (2023) 52–57. https://doi.org/10.31393/morphology-journal-2023-29(3)-08.

[2] P. Pivatidevi, Y. Andy, S.B.K. Joyce, S.H. Tet, Z.A. Suraya, Endoprosthesis length affects stress shielding in proximal humeral replacement for tumour excision, Orthopaedic Proceedings. 103-B No.SUPP_13 (2021) 118.

[3] R. Karpiński, Ł. Jaworski, J. Szabelski, The design and structural analysis of the endoprosthesis of the hip joint, Applied Computer Science. 12 (2016) 87–95.

[4] L. Shanmuganantha, A. Baharudin, A.B. Sulong, R. Shamsudin, M.H. Ng, Prospect of Metal Ceramic (Titanium-Wollastonite) Composite as Permanent Bone Implants: A Narrative Review, Materials. 14 (2021) 277. https://doi.org/10.3390/ma14020277.

[5] M.L. Raffa, V.H. Nguyen, P. Hernigou, C.H. Flouzat-Lachaniette, G. Haiat, Stress shielding at the bone-implant interface: Influence of surface roughness and of the bone-implant contact ratio, Journal of Orthopaedic Research. 39 (2021) 1174–1183. https://doi.org/10.1002/jor.24840.

[6] M. Nakai, M. Niinomi, X. Zhao, X. Zhao, Self-adjustment of Young's modulus in biomedical titanium alloys during orthopaedic operation, Materials Letters. 65 (2011) 688–690. https://doi.org/10.1016/j.matlet.2010.11.006.

[7] A.G. Marty, Aging-related mechanical degradation of cortical bone is driven by microstrucural changes in addition to porosity, BioRxiv. (2023). https://doi.org/10.1101/2023.03.01.530672.

[8] B.D. Ratner, A Perspective on Titanium Biocompatibility, in: M. Rashabha, S. Sonali (Eds.), Titanium in Medicine. Engineering Materials., Springer, Berlin, 2001: pp. 1–12. https://doi.org/10.1007/978-3-642-56486-4_1.

[9] O. Unal, A. Cahit Karaoglanli, R. Varol, A. Kobayashi, Microstructure evolution and mechanical behavior of severe shot peened commercially pure titanium, Vacuum. 110 (2014) 202–206. https://doi.org/10.1016/j.vacuum.2014.08.004.

[10] L.-C. Zhang, L.-Y. Chen, L. Wang, Surface Modification of Titanium and Titanium Alloys: Technologies, Developments, and Future Interests, Advanced Engineering Materials. 22 (2020) 1901258. https://doi.org/10.1002/adem.201901258.

[11] M. Jażdżewska, B. Majkowska-Marzec, A. Zieliński, R. Ostrowski, A. Frączek, G. Karwowska, J.-M. Olive, Mechanical Properties and Wear Susceptibility Determined by Nanoindentation Technique of Ti13Nb13Zr Titanium Alloy after

"Direct Laser Writing," Materials. 16 (2023) 4834. https://doi.org/10.3390/ma16134834.

[12] I. Golvano, I. Garcia, A. Conde, W. Tato, A. Aginagalde, Influence of fluoride content and pH on corrosion and tribocorrosion behaviour of Ti13Nb13Zr alloy in oral environment, Journal of the Mechanical Behavior of Biomedical Materials. 49 (2015) 186–196. https://doi.org/10.1016/j.jmbbm.2015.05.008.

[13] J. Marciniak, Biomateriały, Wydawnictwo Politechniki Śląskiej, Gliwice, 2002.

[14] J.-E. Park, Y.-S. Jang, T.-S. Bae, M.-H. Lee, Biocompatibility Characteristics of Titanium Coated with Multi Walled Carbon Nanotubes—Hydroxyapatite Nanocomposites, Materials. 12 (2019) 224. https://doi.org/10.3390/ma12020224.

[15] H. Maleki-Ghaleh, J. Khalil-Allafi, Effect of hydroxyapatite-titanium-MWCNTs composite coating fabricated by electrophoretic deposition on corrosion and cellular behavior of NiTi alloy, Materials and Corrosion. 70 (2019) 2128–2138. https://doi.org/10.1002/maco.201910940.

[16] J.E. Park, I.-S. Park, M.P. Neupane, T.-S. Bae, M.-H. Lee, Effects of a carbon nanotube-collagen coating on a titanium surface on osteoblast growth, Applied Surface Science. 292 (2014) 828–836. https://doi.org/10.1016/j.apsusc.2013.12.058.

[17] Y. Zhu, X. Liu, K.W.K. Yeung, P.K. Chu, S. Wu, Biofunctionalization of carbon nanotubes/chitosan hybrids on Ti implants by atom layer deposited ZnO nanostructures, Applied Surface Science. 400 (2017) 14–23. https://doi.org/10.1016/j.apsusc.2016.12.158.

[18] B.M. Hidalgo-Robatto, M. López-Álvarez, A.S. Azevedo, J. Dorado, J. Serra, N.F. Azevedo, P. González, Pulsed laser deposition of copper and zinc doped hydroxyapatite coatings for biomedical applications, Surface Coating Technology. 333 (2018) 168–177. https://doi.org/10.1016/j.surfcoat.2017.11.006.

[19] S. Jafari, B. Mahyad, H. Hashemzadeh, S. Janfaza, T. Gholikhani, L. Tayebi, Biomedical Applications of TiO_2 Nanostructures: Recent Advances, International Journal of Nanomedicine. 15 (2020) 3447–3470. https://doi.org/10.2147/IJN.S249441.

[20] X. Liu, J. Fu, Electronic and elastic properties of the tetragonal anatase TiO_2 structure from first principle calculation, Optik (Stuttg). 206 (2020) 164342. https://doi.org/10.1016/j.ijleo.2020.164342.

[21] A.R. Boccaccini, J. Cho, J.A. Roether, B.J.C. Thomas, E. Jane Minay, M.S.P. Shaffer, Electrophoretic deposition of carbon nanotubes, Carbon N Y. 44 (2006) 3149–3160. https://doi.org/10.1016/j.carbon.2006.06.021.

[22] Ł. Pawłowski, M. Rościszewska, B. Majkowska-Marzec, M. Jażdżewska, M. Bartmański, A. Zieliński, N. Tybuszewska, P. Samsel, Influence of surface

modification of titanium and its alloys for medical implants on their corrosion behavior, Materials. 15 (2022) 7556. https://doi.org/10.3390/ma15217556.

[23] P. Tęczar, B. Majkowska-Marzec, M. Bartmański, The influence of laser alloying of Ti13Nb13Zr on surface topography and properties, Advances in Materials Science. 19 (2019) 44–56. https://doi.org/10.2478/adms-2019-0004.

[24] S. Hu, W. Huang, F. Meng, R.H.W. Lam, D. Lau, Adhesion strengthening mechanism of carbon nanotube-embedded epoxy composites: A fracture-based approach, ACS Applied Materials and Interfaces. 14 (2022) 7221–7229. https://doi.org/10.1021/acsami.1c20282.

[25] B. Majkowska-Marzec, P. Tęczar, M. Bartmański, B. Bartosewicz, B.J. Jankiewicz, Mechanical and corrosion properties of laser surface-treated Ti13Nb13Zr alloy with MWCNTs coatings, Materials. 13 (2020) 3991. https://doi.org/10.3390/ma13183991.

[26] B. Majkowska-Marzec, D. Rogala-Wielgus, M. Bartmański, B. Bartosewicz, A. Zieliński, Comparison of properties of the hybrid and bilayer MWCNTs—hydroxyapatite coatings on Ti alloy, Coatings. 9 (2019) 643. https://doi.org/10.3390/coatings9100643.

[27] J. Cho, S. Schaab, J.A. Roether, A.R. Boccaccini, Nanostructured carbon nanotube/TiO_2 composite coatings using electrophoretic deposition (EPD), Journal of Nanoparticle Research. 10 (2008) 99–105. https://doi.org/10.1007/s11051-007-9230-x.

[28] A.R. Boccaccini, P. Karapappas, J.M. Marijuan, C. Kaya, TiO_2 coatings on silicon carbide and carbon fibre substrates by electrophoretic deposition, Journal of Materials Science. 39 (2004) 851–859.

[29] P. Razmara, J.J. Imbery, E. Koide, C.C. Helbing, S.B. Wiseman, P.T. Gauthier, D.F. Bray, M. Needham, T. Haight, A. Zovoilis, G.G. Pyle, Mechanism of copper nanoparticle toxicity in rainbow trout olfactory mucosa, Environmental Pollution. 284 (2021) 117141. https://doi.org/10.1016/j.envpol.2021.117141.

[30] Z. Chen, H. Meng, G. Xing, C. Chen, Y. Zhao, G. Jia, T. Wang, H. Yuan, C. Ye, F. Zhao, Z. Chai, C. Zhu, X. Fang, B. Ma, L. Wan, Acute toxicological effects of copper nanoparticles in vivo, Toxicology Letters. 163 (2006) 109–120. https://doi.org/10.1016/j.toxlet.2005.10.003.

[31] J. Zhang, S. Zhu, K. Song, Z. Wang, Z. Han, K. Zhao, Z. Fan, X. Zhou, Q. Zhang, 3D reduced graphene oxide hybrid nano-copper scaffolds with a high antibacterial performance, Materials Letters. 267 (2020) 127527. https://doi.org/10.1016/j.matlet.2020.127527.

[32] T. Liang, Y. Wang, L. Zeng, Y. Liu, L. Qiao, S. Zhang, R. Zhao, G. Li, R. Zhang, J. Xiang, F. Xiong, A. Shanaghi, H. Pan, Y. Zhao, Copper-doped 3D porous coating developed on Ti-6Al-4V alloys and its in vitro long-term antibacterial ability, Applied Surface Science. 509 (2020) 144717. https://doi.org/10.1016/j.apsusc.2019.144717.

[33] B.M. Hidalgo-Robatto, M. López-Álvarez, A.S. Azevedo, J. Dorado, J. Serra, N.F. Azevedo, P. González, Pulsed laser deposition of copper and zinc doped hydroxyapatite coatings for biomedical applications, Surface Coating Technology. 333 (2018) 168–177. https://doi.org/10.1016/j.surfcoat.2017.11.006.

[34] Y. Seo, J. Hwang, J. Kim, Y. Jeong, M.P. Hwang, J. Choi, Antibacterial activity and cytotoxicity of multi-walled carbon nanotubes decorated with silver nanoparticles, International Journal of Nanomedicine. 9 (2014) 4621–4629. https://doi.org/10.2147/IJN.S69561.

[35] J.D. Kim, H. Yun, G.C. Kim, C.W. Lee, H.C. Choi, Antibacterial activity and reusability of CNT-Ag and GO-Ag nanocomposites, Applied Surface Science. 283 (2013) 227–233. https://doi.org/10.1016/j.apsusc.2013.06.086.

[36] T. Lee, Variation in Mechanical Properties of Ti-13Nb-13Zr Depending on Annealing Temperature, Applied Sciences. 10 (2020) 7896. https://doi.org/10.3390/app10217896.

[37] L. Klinge, C. Siemers, C. Jahnke, High-Strength, Low-Modulus Nanostructured: Ti13Nb13Zr Alloy, in: Proceedings of the 61st Conference of Metallurgists, COM 2022, Springer International Publishing, Cham, 2023: pp. 359–368. https://doi.org/10.1007/978-3-031-17425-4_48.

[38] J. Ramier, N. Da Costa, C.J.G. Plummer, Y. Leterrier, J.A.E. Månson, R. Eckert, R. Gaudiana, Cohesion and adhesion of nanoporous TiO_2 coatings on titanium wires for photovoltaic applications, Thin Solid Films. 516 (2008) 1913–1919. https://doi.org/10.1016/j.tsf.2007.08.057.

[39] Å.K. Jämting, J.M. Bell, M.V. Swain, L.S. Wielunski, R. Clissold, Measurement of the micro mechanical properties of sol-gel TiO_2 films, Thin Solid Films. 332 (1998) 189–194. https://doi.org/10.1016/S0040-6090(98)01102-X.

6. OŚWIADCZENIA WRAZ Z TREŚCIĄ PUBLIKACJI

6.1 [A1]

POLITECHNIKA GDAŃSKA | WYDZIAŁ INŻYNIERII MECHANICZNEJ I OKRĘTOWNICTWA

RESEARCH UNIVERSITY

OŚWIADCZENIE

Dotyczy publikacji w czasopiśmie naukowym:

Rogala-Wielgus D., Zieliński A.: *Preparation and properties of composite coatings, based on carbon nanotubes, for medical applications,* Carbon Letters. (2023). https://doi.org/10.1007/s42823-023-00626-9

Impact Factor: 4,5
Punkty wg MNiSW: 40 pkt

Oświadczamy, że wkład autorów w powstanie powyższej publikacji kształtuje się następująco:

L.p.	Współautor	Wkład, %	Wkład merytoryczny
1.	**Dorota Rogala-Wielgus**	**80**	**Realizacja przeglądu literaturowego z ostatnich 20 lat, korzystając z baz *Science Direct, Wiley, Springer, Google Schoolar*; przygotowanie manuskryptu; edycja manuskryptu; przygotowanie odpowiedzi na recenzje; rola autora korespondencyjnego**
2.	Andrzej Zieliński	20	nadzór merytoryczny; edycja manuskryptu; udział w przygotowaniu odpowiedzi na recenzje; korekta końcowa

Podpisy współautorów:

Dorota Rogala-Wielgus
mgr inż. Dorota Rogala-Wielgus

prof. dr hab. inż. Andrzej Zieliński

POLITECHNIKA GDAŃSKA pg.edu.pl
Ul. Gabriela Narutowicza 11/12
80-233 Gdańsk

Carbon Letters
https://doi.org/10.1007/s42823-023-00626-9

Online ISSN 2233-4998
Print ISSN 1976-4251

REVIEW

Preparation and properties of composite coatings, based on carbon nanotubes, for medical applications

Dorota Rogala-Wielgus[1] · Andrzej Zieliński[1]

Received: 9 January 2023 / Revised: 30 August 2023 / Accepted: 3 October 2023

Abstract

The coatings based on carbon nanotubes (CNTs) are increasingly developed for their applications, among others, in medicine, in particular for implants in implantology, cardiology, and neurology. The present review paper aims at a detailed demonstration of different preparation methods for such coatings, their performance, and relationships between deposition parameters and microstructure and material, mechanical, physical, chemical, and biological properties. The thermal and electrostatic spraying, electrophoretic and electrocathodic deposition, and laser methods are presented. Characterization of microstructure of coatings, topography, morphology, adhesion of CNTs to a substrate, mechanical behavior, corrosion resistance, wettability, cytotoxicity, bioactivity, and antibacterial protection are reviewed for different deposition methods and parameters. The state-of-the-art in the field of carbon nanotubes shows a considerable number of research performed on CNTs coatings. The different forms of CNTs, deposition methods, parameters, and substrates were applied as process variables. The microstructures and surface homogeneity, chemical and phase compositions, mechanical properties at the micro- and nanoscale such as coating Young`s modulus and hardness, interface adhesion strength and delaminating force, open corrosion potential and corrosion current density, contact angle in wettability assessment, and bioactivity, cytotoxicity, and antibacterial efficiency among biological properties were determined. The summary of so far achievements, strengths and weaknesses, and important future research necessary for clarification of some weak points, development of non-toxic, mechanically and chemically resistant, bioactive, and antibacterial multicomponent coatings based on functionalized CNTs are proposed.

Keywords Carbon nanotubes · Coatings · Composites · Hardness · Young's modulus · Biological properties

Abbreviations

ACCVD	Alcohol catalytic chemical vapor deposition
AFM	Atomic force microscopy
Ag NPs	Silver nanoparticles
CA	Cellulose acetate
CFs	Carbon fibers
CGDS	Cold gas dynamic spray
CNTs	Carbon nanotubes
CS	Cold spraying
CVD	Chemical vapor deposition
DWCNTs	Double-wall carbon nanotubes
ECD or ECAD	Electrocathodic deposition, electroplating, electro-co-deposition
EPD	Electrophoretic deposition
ER	Endoplasmic reticulum
ES	Electrostatic spraying
FM	Fully melted
f-MWCNTs	Functionalized multi-walled carbon nanotubes
GO	Graphene oxide
HAp	Hydroxyapatite
HPCS	High-pressure cold spraying
HSLC	High-speed laser cladding
HUVECs	Human umbilical vein endothelial cells
HVOF	High-velocity oxygen fuel or oxy-fuel
IBAD	Ion beam-assisted deposition
LC	Laser cladding
LPCS	Low-pressure cold spraying
LVOF	Low-velocity oxy-fuel
MTT	3-(4,5-Dimethylthiazol-2-yl)-2,5-diphenyltetrazolium bromide

✉ Dorota Rogala-Wielgus
dorota.wielgus@pg.edu.pl

[1] Division of Biomaterials Technology, Institute of Manufacturing and Materials Technology, Faculty of Mechanical Engineering and Ship Technology, Gdansk University of Technology, 11/12 Narutowicza Str., 80-233 Gdańsk, Poland

Published online: 16 November 2023

MWCNTs	Multi-wall carbon nanotubes
nanoAg	Nanosilver
nanoCu	Nanocopper
nanoHAp	Nanohydroxyapatite
NEMS	Nanoelectromechanical system
PBF	Powder bed fusion
PCL	Polycaprolactone
PECVD	Plasma enhanced chemical vapor deposition
PEG	Poly(ethylene glycol)
PEO	Plasma electrolytic oxidation
PLA	Poly(lactic acid)
PLGA	Poly(lactide-*co*-glycolide)
PLLA	Poly(L-lactide)
PM	Partially melted
PMMA	Poly(methyl methacrylate)
PS	Plasma spraying
PU	Polyurethane
PVA	Polyvinyl alcohol
rGO	Reduced graphene oxide
ROS	Reactive oxygen species
SBF	Simulated body fluid
SHVOF	Suspension high-velocity oxy-fuel
SWCNTs	Single-wall carbon nanotubes
YSZ	Yttria-stabilized zirconia

1 Introduction

Recent medical implantology has utilized or investigated a huge number of materials in the form of solid implants or scaffolds, and also meshes, sponges, hydrogels, and coatings to modify the surfaces of metallic implants. Among them, the most recently, have appeared different forms of elementary carbon, principally single-wall or multi-wall carbon nanotubes (SWCNTs or MWCNTs of different chirality) but also carbon fibers (CFs), graphene, mainly as graphene oxide (GO) or reduced graphene oxide (rGO), fullerenes (especially C60) [1, 2]. The carbon nanotubes were discovered by Iijima [3]. Various types of synthesis techniques for CNTs include the arc-discharge method, laser ablation method, chemical vapor deposition (CVD), vapor-phase growth, flame synthesis method, and plasma-assisted growth [2].

All nanocarbon forms, particularly carbon nanotubes (CNTs), demonstrate extraordinary mechanical, thermal, magnetic, optical, electrical, surface, and chemical properties. Their electronic properties, high electric and thermal conductivity, and stiffness and strength are over those shown by any other material [4]. Thanks to these features, the CNTs have been frequently applied or recommended for use in different fields of the economy: medicine, biomechanics, energy storage, molecular electronics, fabrics and fibers, air and water filtration, and others [5].

As an additive to construction materials, they are presumably mostly applied as a component of epoxy resins. They have been used to improve the electrical and mechanical construction of epoxy-based composites [6–8]. They were given as fillers to strengthen several construction polymers [2, 9, 10] and also as functionally graded CNTs reinforced composites [11]. They can be considered components of bifunctional electrocatalysts [12].

As a component of coatings, they have been proposed to enhance heat transfer of heat sinks [13], improve corrosion performance [14–17], reinforce the coatings [18], increase the friction behavior [19, 20], make coatings superhydrophobic and usable for different applications [15, 21–23], such as the abrasion-resistant, photothermal, and anti-icing [24], and self-adapting ultra-high-temperature ceramic coatings [25]. The CNTs were used in coatings for electromagnetic interference shielding [26] and as a flame-retardant coating or composite material [27–29]. They were applied against decontamination of organic chemical pollutants in water [30, 31] and also involved in building space stealth and cosmic radiation shielding [32].

They are widely used in electronics and energy systems. Their electrical and electronic properties are suitable for building artificial muscles, electrochemical, thermal actuators, solvent and vapor actuators, fiber-shaped batteries and supercapacitors, color-changed electroluminescent and electrochromic fibers, mechanical and electrochemical sensors [33], thermal management systems [33, 34], solar cells [35], high-performance metal-ion batteries [36–38], energy storage and conversion devices [39], nanogenerators for harvesting energy [40], NEMS and hydrogen storage modules [2].

They are also increasingly developed for medical applications. They can be applied in bone regeneration, artificial neural conduits, and in drug and gene delivery in cancer therapy, brain therapy [41, 42], vaccine delivery [42], tissue engineering, and regenerative medicine, in particular for bone and muscle, and nervous system regeneration by neuronal differentiation and neuronal stimulation [42–45], for culturing the human embryonic stem cells and preserving their viability [46], and dosage forms and biomedical substrates in the pharmaceutical industry [47], They can be utilized in diagnosis for biomedical imaging, biosensors, for biomolecular detection and nanotweezers [42, 48]. They are introduced as sensors, in drug targeting, cancer diagnosis, and treatment, as antibacterial and antifungal species [49]. The CNTs helped to create the coatings releasing the active ingredients [50] such as biphosphonates, nucleic acids,

proteins, and statins [51]. The integration of CNTs with polymeric scaffolds is promising for cardiac regeneration [52, 53]. The carbon nanotubes reinforced with chitosan, poly(lactic acid) (PLA), poly(lactide-*co*-glycolide) (PLGA), poly(ethylene glycol) (PEG), polyvinyl alcohol (PVA), and polycaprolactone (PCL) can mimic the extracellular matrices of bone [54]. These unique properties make CNTs promising candidates for cancer treatment and regenerative medicine, for bone, and nerve restoration [43, 55]. The incorporation of CNTs into polymer scaffolds results, among others, in increased scaffold strength and flexibility, improved biocompatibility, retardation of cancer cells` division, and enhancement of angiogenesis [1]. They are microbial and anti-adhesive [56–58]. They are used in various biosensors for biomolecular detection [59].

Besides the advantages, CNTs have two serious drawbacks. The first disadvantage important for medical applications is their anticipated toxicity which is a permanent feature of each nanoparticle; their small size and high surface area to volume ratio are associated with significant chemical reactivity, change in permeability and conductivity membranes of cells, lung penetration, and lung cancer risk [60]. The bioactivity and cytotoxicity of CNTs are affected by their diameter, length, and functionalization in vitro and in vivo, as well as by the fabrication method with nickel catalyst [61] and may make CNTs toxic for living organisms or the environment [60, 62]. The toxicity can manifest itself as membrane damage, DNA damage, an appearance of oxidative stress, and changes in mitochondrial activity and intracellular metabolic routes as a consequence of the highly hydrophobic surface and the non-biodegradable nature of the CNTs [1]. However, the CNTs are considered to have carcinogenicity mainly to enhance lung tumors, and the carcinogenicity may attenuate with decreasing tube length [63]. The MWCNTs are likely to be a more neural-friendly interface than SWCNTs since they allow for a wider external surface and effective functionalization [64].

The second disadvantage is the weak adhesion of CNTs (and all carbon nanoforms) to any material. It is critical to functionalize CNTs not only to make them more soluble, but also to allow their integration into many organic, inorganic, and biological systems and applications, and eliminate or at least minimize their toxicity. A proper functionalization of the CNTs is nowadays carried out by a variety of methods [65–68]. It may follow two strategies: (1) chemical reactions occurring at the sidewalls and tips of CNTs and (2) oxidation followed by an appearance of carboxyl-based bonding [41]. Functionalization of carbon nanofibers can be performed by CVD and plating of some compounds, and by chemical or biochemical reactions [69].

This review aims to show the newest data on carbon nanotubes creating coatings or being components of such, in particular (1) various synthesis methods, in particular the electrophoretic deposition (EPD) technique as the most preferred, (2) their properties, such as surface morphology and topography, mechanical, corrosion, and biological properties, and the relationships between output and input variables to optimize the deposition process.

2 Forms of carbon nanotubes

Carbon nanotubes are hollow structures created from rotating a graphene layer around one axis in a certain direction. It is an sp^2 form of hybridization of carbon derive, where carbon atoms are organized with strong covalent bonds in

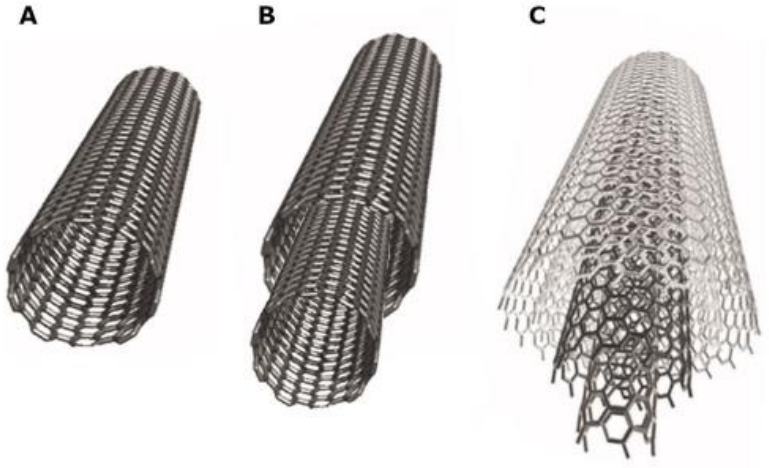

Fig. 1 CNTs types based on a number of walls, where **A** SWCNTs, **B** DWCNTs, and **C** MWCNTs. Figures **A** and **C** were reproduced with permission [74] Copyright 2011, InTech

a hexagonal lattice, very similar to graphene, graphite, and fullerenes. Carbon nanotubes can be divided into SWCNTs, double-wall carbon nanotubes (DWCNTs), and MWCNTs [70], which are demonstrated in Fig. 1. The first reported were MWCNTs by Iijima [3]. MWCNTs are composed of concentric cylinders with regular periodic interlayer spacing located around the ordinary central hollow. They form a layer construction with van der Waals bonding between cylinders [71–73].

Literature shows that the parameters of all types of carbon nanotubes are within certain limits as illustrated in Tables 1 and 2.

Besides the division grounding on the number of carbon nanotube walls, some SWCNTs forms differ in terms of wrapping to a cylinder structure, such as armchair (integers $n=m$), zigzag (integers $m=0$), and chiral (other integers) [72]. Figure 2 illustrates schematic types of wrapping graphite sheet to form different forms of SWCNTs.

There are several methods of synthesis of carbon nanotubes such as chemical vapor deposition, arc-discharge method, laser ablation method, spray pyrolysis, hydrothermal methods, and thermal plasma [48, 70, 85–87].

Table 1 The physical properties of three types of CNTs

Property	MWCNTs	DWCNTs	SWCNTs
Interlayer spacing	0.34÷0.39 nm [72]	0.33÷0.42 nm [75]	–
Inner diameter	4÷7 nm [76]	1÷3 nm [2]	–
Outer diameter	2÷30 nm [72]	2÷4 nm [2]	0.4÷3 nm [72, 77]
	15÷25 nm [76]		Made with CVD 1.3÷1.5 nm [78]
Length	Up to 50 μm [76]	100÷475 nm [79]	CVD 13 μm [78]
	100 nm÷1 cm [77]	100 nm÷1 cm [77]	CVD 140 nm÷3200 nm [80]
Ends	Closed and capped with half-fullerene molecules [72]	Capped and open-ended [81]	Can come together and form bundles [72]

Table 2 The mechanical properties of three types of CNTs

Property	MWCNTs	DWCNTs	SWCNTs
Young's modulus	1.7÷2.4 TPa [83]	0.33÷0.42 TPa [75]	2.8÷3.6 TPa [83]
Tensile strength	63 GPa [77]	77.51÷157.5 GPa[a] [84]	53 GPa [77]

[a]Predicted based on finite element method and chirality

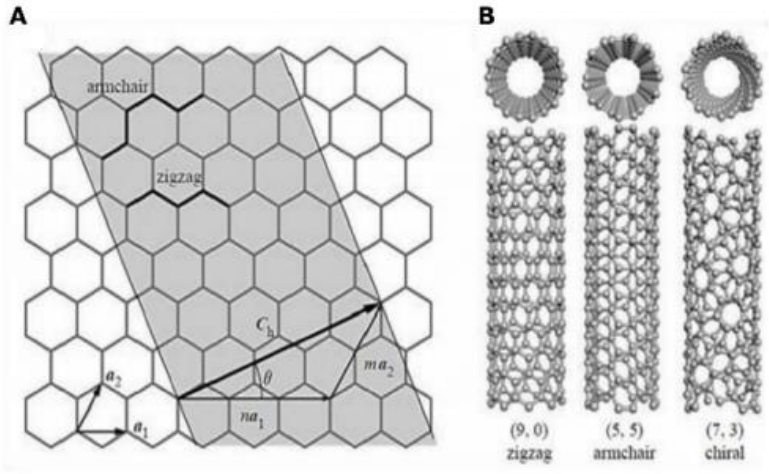

Fig. 2 A scheme illustrating **A** forms of wrapping graphite to achieve different structures of the SWCNTs and **B** different structures of SWCNTs based on the chiral angle. The figure is reproduced with permission [82] Copyright 2016, JACS Directory©2016

3 CNTs-containing coating types and their deposition methods

There are many types of CNT-included coatings, with ceramics, metals, polymers, or mixed. Examples of such coatings are shown in Fig. 3. Several deposition methods of CNTs-containing coatings, like the main groups: thermal spray, electrochemical deposition, and laser methods, are schematically shown in Fig. 7. The main advantages and disadvantages of the types of deposition methods are listed in Table 3. The examples of CNTs-containing coatings and their main parameters of synthesis with described impact on coatings properties are listed in Tables 4 and 5.

3.1 Thermal spraying

A thermal spray is a group of processes in which materials (metals, alloys, metal oxides, metal/ceramic blends, carbides, composite materials) are deposited using spraying. The processes differ from each other basically by the state of the material: molten, semi-molten, or solid state. The thermal spraying method is used in many fields in mechanical engineering, for corrosion protection, surface restoration, and repair, heat insulation or conduction; energy technology, and biomedical and industrial areas [88, 89]. Apart from many advantages, the technique has also some drawbacks. Covering parts with complex shapes, inner surfaces, and narrow parts is limited. Some advances in thermal spray technology enable covering a such surface, named the internal diameter thermal spray method [90, 91]. Figure 4 shows a schematic illustration of literature-based three most used methods of CNTs deposition techniques.

3.1.1 Plasma spraying

Plasma spraying (PS) is one of the thermal processes used to coat materials. This method uses a high-energy heat source, which melts (at a temperature of about 10,000 K) coating material inserted into a plasma jet and sprayed onto a prepared substrate [92–94]. The arc between two electrodes cathode (tungsten) and anode (copper) is initiated by high-frequency discharge in the presence of gases, such as Ar, He, H_2, and N_2 named plasma-forming gases [93, 94]. Figure 4 A shows a schematic illustration of the PS coating method.

3.1.2 Cold spraying

Cold spraying (CS) or cold gas dynamic spray (CGDS) is not only a thermal spraying process but also a solid-state spraying method. It differs from other thermal spraying methods by the state of powder feedstock, which is always unmelted. This method is used to produce metallic and metallic-ceramic coatings. Based on pressure level, the cold spraying process (Fig. 4C) can be divided into low-pressure cold spraying (LPCS) and high-pressure cold spraying (HPCS). This process is based on the acceleration of particles of the coating material by pressurized gas (air, N_2, He, or mixture) in a diverging-converging nozzle, leading to preparation layer-by-layer [89, 95] coating. The best adhesion of the cold-sprayed coatings is achieved only above a critical particle velocity [96].

3.1.3 High-velocity oxy-fuel thermal spraying

High-velocity oxygen fuel (HVOF) is a thermal spray technique that uses fuel, such as H_2, propylene, acetylene, or kerosene to achieve a high temperature that ranges from 2500 to 3000 °C and high pressure in the combustion chamber. Most commonly a powder, but also a suspension (another type of HVOF, named suspension high-velocity oxy-fuel SHVOF) is inserted in the nozzle and at the same time heated and accelerated (particle velocity of 550–1060 m/s) by a gas stream causing the formation of a relatively dense coating, with good adhesion properties. Coatings deposited by the HVOF method (Fig. 4 B) are widely used to enhance surface performance and protect against corrosion and wear, but it also is a convenient method to deposit nanomaterials [91, 97–100]

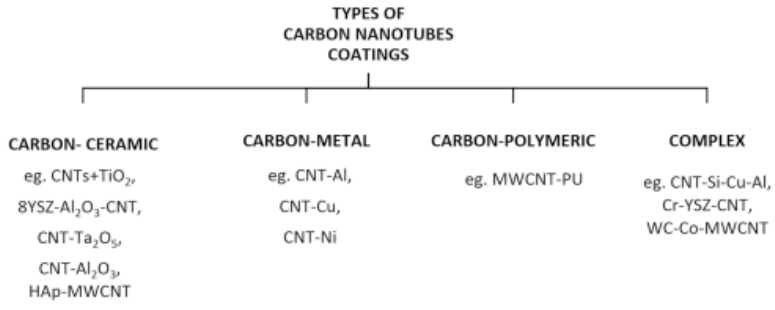

Fig. 3 Scheme of types of carbon nanotube coatings

Table 3 The main advantages and disadvantages of CNTs coating deposition techniques

The main group of a coating deposition method	Type of a coating deposition method	Advantages	Disadvantages	Reference
Thermal spraying	PS	Ability to coat a wide range of materials (a high-heat source, temperature ranging from 3000 to 25,000 °C), low thermal impact on working surfaces, high particle velocity in the range of 240–610 m/s, ability to change parameters according to the required effect (flame temperature, particle velocities, particle size distribution), comprehensive performance at a good level	Risk of CNTs structure deformation, due to high temperature in some cases was observed, regions with semi-molten material in the coating, generating defects, such as pores and cracks, the high temperature causes the substrate surface to (low level) melt during the PS process the coating material is molten during the PS process, the temperature and particle velocities in function with the distance between torch and substrate are crucial parameters to determine the appropriate coating microstructure, properties, and efficiency of the process, the deposition angle to the substrate has an impact on the microstructure and properties of the deposited coating, oxidation appears during the PS process, minimalized by using a vacuum chamber	[31, 88, 93, 94, 98]
	CS	High particle velocities in the range of 300–1200 m/s, sprayed material doesn't melt during the deposition process, the pureness of achieved coatings, the substrate maintains its properties due to low heat input, high-quality coatings, a wide range of coating materials, complex shape materials might be coated, minimal effects of oxidation, decomposition, grain growth, and phase change	High-pressure requirement, lower size distribution of the powders than in HVOF	[88, 107, 108]
	HVOF	The substrate maintains its properties due to low heat input (less than 150 °C), wide range of coating compositions, very high particle velocities of 550–1060 m/s (coatings with higher densities, smoother, lower oxide levels than in other thermal spraying methods with lower particle velocities), is used to prepare corrosion and wear-resistant coatings	The deposition angle to the substrate has an impact on the microstructure and properties of the deposited coating, less sensitive to the distance between the nozzle and substrate than the PS method, oxides with a higher melting point may be difficult to melt and thus to coat	[88, 98]
	LVOF	The substrate maintains its properties due to low heat input (lower than in HVOF), the particle velocities are higher than in the conventional PS method, improving coatings properties (level of oxides, density, surface topography), is used to prepare corrosion and wear-resistant coatings	Lower particle velocities than HVOF, give coatings with lower densities and higher oxide levels, the deposition angle to the substrate has an impact on the microstructure and properties of the deposited coating	[88, 98]

Table 3 (continued)

The main group of a coating deposition method	Type of a coating deposition method	Advantages	Disadvantages	Reference
Electrochemical methods	ES	Simplicity, low cost, time-saving, ability to achieve thin films, ability to deposit coatings with different morphologies, without vacuum requirement, sub-micrometer or nanoscale droplets of deposition material, self-dispersive and high-wettability droplets of deposition material, huge variety of compatible substrates, a large variety of coating materials, high deposition efficiencies due to charged droplets, and thus reduced material consumption, high coatings quality, low substrate temperatures, uniform distribution of CNTs in the polymer matrix (ex. PU)	The ES nozzle tip might be clogged when depositing graphene nanosheets, an additional annealing is required to obtain a particular crystalline phase	[103, 109, 110]
	EPD	A low-cost method, simplicity, ability to coat different shapes, a wide range of coating materials, low coating time and temperature, adjustable parameters of EPD, enabling control of deposit thickness and thus its parameters, uniformity of achieved coatings, a microstructural homogeneity of the coatings, a purity of deposited materials, the use of alternating current electric fields elongate nanoparticles, which align uniformly and orientate themselves along the electric field direction, thus enabling manipulation of the coating material deposition	The use of water as a solution to EPD bath may cause hydrolysis, thus bubble formation in the coating, the Joule heating appears when excessive voltage is applied, the use of lower voltages than the voltage of water electrolysis, causes deposited coatings to be of poor quality, an additional annealing might be required to obtain a particular crystalline phase or to improve coating quality	[111–117]
	ECD	Adjustable parameters of the ECD, thus control over deposit parameters, a low-cost method, simplicity, a wide range of coating materials, a purity of deposited materials, ability to coat different shapes	The method generates an excessive amount of sludge, to recover metals from suspension is problematic, the long-term impact of sludge disposal on the environment	[117, 118]
Laser methods	HSLC	The coating is uniform, higher melting speed than in the LC process, the coating might be thinner than in the LC process, ability to deposit smooth coatings, the cooling rate is higher than in the LC process, the deposited coatings are almost without defects, such as pores, or cracks, a wide range of coating materials, more limited heat-affect zone than in the LC, minimum dilution, small stress deformation, good metallurgical bonding	The substrate is melted during the HSLC process, the coating material is melted while deposited	[119–121]
	LC	High-flexibility deposition parameters, a rapid solidification of the deposit, wide range of coating materials, limited heat-affect zone, minimum dilution, small stress deformation, good metallurgical bonding	The substrate is melted during the LC process, the coating material is melted while deposited, lower melting speed than in HSLC, lower cooling rate than in HSLC	[121, 122]

Table 4 Examples of CNTs coating combinations and the parameters of synthesis

Coating	Substrate	Method	Main parameters	Coating specification	References
CNT–Al–Si	Mild steel	PS	A thoriated tungsten cathode; a concentric copper anode; the plasma power ~ 22 kW; the gun traverse velocity was 25 mm/s; a distance between a substrate and gun (standoff distance): 100 mm	Structure: two-phase microstructure composed of Al–Si matrix with uniformly distributed CNTs, and CNTs clusters, showing strengthening effect by fiber pull-out and crack bridging. The porosity of the coating is in the range of 10–12% Properties: the addition of CNTs in the concentration of 5 wt% and 10 wt% of CNTs to Al–Si coating improved the elastic modulus in the nanoindentation test of 19% and 39% respectively (with no difference in micro-scale compression test), the yield strength of 17.5% and 27%, respectively (in micro-scale compression test 27% and 77% respectively), and elastic recovery properties. Also, the wear volume in the nano-scratch test was decreased for the concentration of 5 wt% and 10 wt% of CNTs by 34% and 71% respectively, and in the macro-scale wear test was respectively decreased by 68% and increased by 15%. The nanoindentation elastic modulus for the 5 wt% and 10 wt% of CNTs in the coating was reported at 107 ± 6 GPa and 125 ± 7 GPa, respectively, and in the micro-scale of 4.95 ± 0.05 GPa and 5.65 ± 0.95 GPa, respectively	[123, 124]
TiO_2–CNTs	AISI 4140	PS	The working gas: a mixture of Ar (primary gas, 42 L/min) and H_2 (secondary gas, 10 L/min); the spraying voltage: 72 V; the spraying current: 550 A; the spraying distance: 80 mm	Structure: nanostructure coating, consisting of the following regions: fully melted (FM), and partially melted (PM) with solid elements and pores. The CNTs structure is destroyed due to the PS process. In some regions TiO_2 and C formed chemical bonding and in some physical Properties: the addition of CNTs to TiO_2 coating has a strengthening effect thus, the scratch resistance of the TiO_2–CNTs coating in comparison to TiO_2 coating was enhanced by around 38.6% and lubricating effect reduced the lateral friction force	[94]

Table 4 (continued)

Coating	Substrate	Method	Main parameters	Coating specification	References
MWCNTS–YSZ (yttria-stabilized zirconia)	INCONEL 738	Plasma thermal spray	Ionization of argon	Structure: a porosity and microcracks were distinguished Properties: the concentration of 8 wt% of CNTs improved the best hot corrosion resistance (at 950°C) of YSZ material (the weight change was of 0.0057 mg/cm^2), while the weight change for bare YSZ was 1.1 mg/cm^2, thus all coatings with the addition of CNTs exhibited improvement in hot corrosion resistance of the YSZ	[125]
CNTs	ADC12 Al alloy	Plasma electrolytic oxidation (PEO)	The voltage: 400 V; the pulse frequency: 400 Hz; the positive duty cycle: 35%; the negative duty cycle: 20%; the positive and negative pulse ratio: 1:1; the oxidation time was: 20 min, the anode: a substrate; the cathode: stainless steel; the temperature of the electrolyte: < 35 °C	Structure: the regulation of coating microstructure by the addition of CNTs. Porosity was observed Properties: the CNT-dopped PEO coatings improve the corrosion resistance of the ADC12 Al alloy (especially with a concentration of 1.5 g/L of the CNTs) by sealing pores. Also, the addition of CNTs improves thermal conductivity	[126]
Zirconia–alumina–CNT	P91 steel	PS	The gun: F-4 plasma gun; the plasma current: 500 A; the plasma voltage: 66 V; the primary gas argon flow: 38.5 nlpm[a]; the secondary gas hydrogen flow: 4 nlpm[a]; the carrier gas nitrogen flow: 3.30/4.25 L/min; the powder feed rate: 40 g/min; the spray distance: 120 mm The traverse speed: 0.0011 m/s	Structure: the CNTs are well dispersed in the zirconia-alumina matrix. The CNTs remained undamaged, despite high temperature during the PS process. Porosity was observed, while the CNTs addition reduced it (3 wt% of CNTs reduce coating porosity by 70%) Properties: the addition of CNTs increases thermal conductivity (from approximately 0.4 W/mK for base coating to 0.9 W/mK for coating with CNTs), microhardness, and corrosion resistance in contrary to the base alumina-reinforced coating	[127]
TiO_2/CNTs		PS	The argon flow rate: 80 L/min; the argon pressure: 0.69 MPa; the hydrogen flow rate: 15 L/min; the hydrogen pressure: 350 kPa; the arc current: 500 A; the arc voltage: 65/75 V; the powder feed rate: 40 g/min; the spray distance: 10 cm	Structure: the coating has low porosity and it doesn't change with the addition of CNTs Properties: the composite coating exhibited higher photocatalytic activities than the base TiO_2 coating, with the concentration of methylene blue solution decreased by approximately 35%	[128]

Table 4 (continued)

Coating	Substrate	Method	Main parameters	Coating specification	References
CNT-doped Ta_2O_5	Ti6Al4V alloy	Atmospheric-PS	The arc voltage: 70 V; the arc current: 500, 550, 600, 650 A; the primary plasma gas Ar: 50 L/min; the secondary plasma gas H_2: 12 L/min; the carrier gas Ar: 3 L/min; the powder feed rate: 40 g/min; the spray distance: 100 mm	Structure: the addition of CNTs increases the coating porosity Properties: the addition of CNTs doesn't impact coating roughness and reduces microhardness, while the increased concentration of CNTs increases elastic modulus and indentation fracture toughness. Also, the biological tests were conducted and showed excellent osteoblast-like osteosarcoma MG-63 cell adhesion and viability after 7 days of incubation	[31]
Al_2O_3–TiO_2–MWCNTs	Mild steel (C45 grade)	Air-PS	The plasma gun: 3 MB; the arc current: 490 A; the arc voltage: 70 V; the powder feed: 50 g/min; the argon flow rate: 33/38 L/min; the hydrogen flow rate: 7.1 L/min; the spray distance: 127 mm	Structure: the CNTs are well dispersed in the Al_2O_3–TiO_2 matrix, without damage that might appear due to high temperatures during the PS process. The addition of CNTs and their increased concentration decreases the porosity of the coating Properties: the addition of CNTs increases the adhesion strength and roughness of the coating and alumina alpha phase the resistance to high temperature	[129]
CNT–Al	AZ91 Mg alloy	CS + PEO	CS: the carrier gases: nitrogen; the gas pressure: 1.7 MPa; the gas temperature: 350 °C; the gun travel speed: 200 and 80 mm/s; the feeding rate: 2.7 g/mm; the standoff distance: 30 mm PEO: the pulsed power: 15 kW; the current combination of 0.3 and 0.6 A; the pulse frequency: 2000 Hz; the duty cycle: 20%; the oxidation time was: 10 min	Structure: good contact with base material without cracks but the roughness of PEO threated CNTs coating was higher Properties: the hardness and elastic modulus of the coating were 13.9 GPa and 185.4 GPa, respectively, and demonstrated almost the same corrosion resistance as the basic CS coating. The coating also showed a 59.8% lower wear rate and 15.6% lower friction coefficient than the CS coating	[107]
CNT–Al	AZ91 Mg alloy	CS	The carrier gases: nitrogen; the gas pressure: 1.7 MPa; the gas temperature: 350 °C; the gun travel speed: 200 and 80 mm/s; the feeding rate: 2.7 g/mm; the standoff distance: 30 mm	Structure: the coating has lower porosity than the Al coating Properties: the hardness and elastic modulus of the coating were 1.66 GPa and 77.6 GPa, respectively, and demonstrated higher corrosion and wear resistance than Al coating	[130]

Table 4 (continued)

Coating	Substrate	Method	Main parameters	Coating specification	References
CNT–Cu	Cu plate	CS	The carrier gases: nitrogen; the gas pressure: 3.2 and 2.8 MPa; the gas temperature: 200 and 500 °C; The gun travel speed: 10 mm/s; the feeding rate: 5.65 cm^3/min; the standoff distance: 35 mm	Structure: the 5 vol.% of CNTs coating demonstrated well-fused CNTs. Higher volume concentrations of CNTs showed noticeable particle interfaces Properties: the maximum heat transfer coefficient of the coatings was 1.21–1.74 times improved contrary to the plain Cu plate. The best-boiling heat transfer performance thus lowering the superheat and improving the heat transfer coefficient was achieved for the one-layer coating with 15 vol.% CNT	[131]
Cu–CNT–AlN Cu–CNT	Cu plate	CS	The carrier gases: nitrogen; the gas pressure: 3.2 and 2.8 MPa; the gas temperature: 200 and 500 °C; the gun travel speed: 25 mm/s; the feeding rate: 24.80 and 21.95 g/min; the standoff distance: 35 mm	Structure: the swerve particle deformation and lamellar structure, porous surface, and dense internal microstructure [132] Properties: the as-prepared coatings are more wettable in liquid R134a. The Cu–CNT coating exhibited a maximum boiling heat transfer enhancement ratio of 1.48. The heat transfer of the Cu–CNT decreased at high heat fluxes, where maximum improvement was observed at heat fluxes within 100–200 kW/m^2	[132, 133]
CNT–AlSi	Stainless steel	CS	The carrier gases: nitrogen; the gas pressure: 3.0 MPa; the gas temperature: 500 °C; the gun travel speed: 100 mm/s; the nozzle traverse speed: 500 mm/s; the standoff distance: 30 mm	Structure: microlaminated structure, containing fine grains, without damage to the CNTs structure and interfacial reaction between Al and CNTs	[108]
Nickel-plated CNTs/FeCoNbBSi	45-steel shaft	HSLC	The laser power: 2400 W The laser feed rate: 1 mm/s; the powder feed rate: 40 g/min; the gas flow: 10 m/min; the powder-defocusing amount: 13 mm; the laser defocusing amount: 9 mm	Structure: refined structure with an increase of Ni-plated CNTs Properties: with the increased concentration of Ni-plated CNTs the friction coefficient decreased and wear and corrosion resistance increased	[119]

Table 4 (continued)

Coating	Substrate	Method	Main parameters	Coating specification	References
Ti–MWCNT	Titanium	LC	The laser power: 700 W; the spot size: 2 mm; the scanning speed: 5 mm/s; the gas flow rate: 20 L/min	Structure: the increasing concentration of CNTs in the coatings caused TiC grain size enlargement Properties: the addition of the CNTs improved high-temperature corrosion resistance and lowered friction coefficient contrary to the Ti substrate	[120]
Al_3Ti–Cu–SiC–CNTs	TA2 titanium alloy	LC	The laser power: 800/1200 W, the laser beam diameter: 4 mm, the powder feeding rate: 20/30 g/min, the laser scanning speed: 2/8 mm/s, the gas flow rate: 30 L/min	Structure: the microstructure showed a large amount of point defects Properties: the addition of the CNTs decreased the friction coefficient	[134]
Ni–WC–CNT	Stainless steel	LC	The spot diameter: 4 mm; the laser power: 1000 W; the scanning velocity: 240 mm/min; the gas flow rate: 25 g/min	Structure: the addition of CNTs caused refined grains in the coating material Properties: the coatings with a concentration of 3 wt% of CNTs exhibit the highest microhardness and wear resistance	[122]
MWCNT/PU	Q235 steel	ES	The pressure of compressed air: 0.4÷0.7 MPa; the voltage: 50–60 kV; the distance between the spray gun and specimen: 100÷150 mm; the sintering temperature: 220 °C; the sintering time: 30 min	Structure: the MWCNTs were uniformly distributed in the PU matrix, forming a network structure Properties: the addition of MWCNTs to PU matrix enhanced the thermal conductivity of the coating and the corrosion resistance of the steel ground grid	[110]
Cu–CNT–TiO_2	Cooper tubes	ES	The electrostatic material: 2 wt% polyvinyl alcohol (PVA) solution; the sintering temperature: 350 °C; the sintering rate: 20 °C/min	Structure: porous structure Properties: the wettability of the coating (12.85°) is higher than the substrate material and also coating heat transfer is improved in comparison to the cooper tubes	[135]
CNT–CNP CNT–CNP–TiN	Al	High-voltage ES	The distance between the needle and substrate: 30 mm; the applied voltage: 9 kV; the spraying amount for each coating: 35 µL; the coatings drying temperature: 110 °C; the coatings drying time: 30 min	Structure: micron-sized porosity observed Properties: the addition of CNTs mesh into the structure improves light absorption properties	[103]

Table 4 (continued)

Coating	Substrate	Method	Main parameters	Coating specification	References
Cr–YSZ–CNT	Steel plate	ECD	The cathode: a substrate; the anode: graphite; the duration: 180 min; the current density: 400 mA/cm^2; the pH: 1.5; the temperature: 20 and 25 °C	Structure: well-dispersed CNTs in a matrix and cauliflower-like structure of the Cr–CNT coating. The coatings were almost free from microcracks and pores Properties: the addition of CNTs lowers friction coefficient and reduces wear rate in contrary to Cr and Cr–YSZ. The Cr–YSZ–CNT coating exhibited a hardness of 24 GPa and the lowest surface roughness of 0.22 µm according to Cr and Cr–YSZ coatings	[136]
Cr–YSZ–CNT	Steel plate	ECD	The cathode: a substrate; the anode: graphite; the duration: 120 min; the current density: 400 mA/cm^2; the pH: 1.5; the temperature: 20÷25 °C	Structure: dense and uniform coatings with reduced cracks appearance Properties: the coating exhibited a hardness of 25 GPa and elastic modulus of 206 GPa, and enhanced wear resistance in comparison to coatings without CNTs. The CNTs exhibited lubricating and bridging properties	[137]
Ni–CNT	Steel	ECD	The cathode: Ni plate; the anode: a substrate; the current density: 5 A/dm^2; the temperature: 50 °C; the ultrasonic agitation: 42 kHz, 30 W; the vibration frequency: 42 kHz; a bath consists of nickel sulphonate and CNTs	Structure: the CNTs were well dispersed and embedded in Ni-matrix Properties: the Vickers hardness of the Ni–CNTs coating exceeds 500 HV (for the concentration of CNTs of 1 g/L). The bonding strength of CNTs to Ni was 1.3 times improved by using the ECD technique, thus eightfold elongating tool life. The surface roughness of Ni–CNT coating was 0.28 µm	[138]
Fe–Cr–CNTs	Mild steel	LVOF	The C_2H_2 flow rate: 25.95 L/min; the C_2H_2 pressure: 0.1 MPa; the O_2 flow rate: 21.23 L/min; the O_2 pressure: 0.24 MPa; the N_2 flow rate: 33.03 L/min; the N_2 pressure: 0.72 MPa; the spray distance: 200 mm; The spray rate: 108 g/min	Structure: the homogenous and uniformly distributed CNTs in the coating Properties: the ID/IG ratio was less than 1, showing a low range of structural defects in CNTs coating, making the LVOF technique an excellent candidate for CNTs coatings deposition method	[102]

Table 4 (continued)

Coating	Substrate	Method	Main parameters	Coating specification	References
WC–Co–MWCNTs	AISI 416 stainless steel discs	HVOF	The combustion chamber pressure: 6–8 bar; a rotating substrate	Structure: the porosity was decreased in contrary to coating without MWCNTs Properties: the addition of CNTs caused the decreased microhardness and increased fracture toughness, and also the reduction of friction coefficient at high power conditions (improved wear performance). In medium and lower power the result was inverse	[90]
WC–Co–CNTs	Mild steel of AISI 1020	HVOF	The flow rate of O_2: 900÷950 L/min; the kerosene flow rate: 0.38 L/min; the gas (Ar) flow rate: 50÷60 L/min; the torch velocity: 700 mm/min; the powder feed rate: 70÷75 g/min; the spray distance: 200–250 mm	Structure: the porosity was reduced due to the addition of CNTs, which were well dispersed and adhered Properties: the addition of CNTs increased microhardness, reduced roughness, lower friction coefficient, and improved wear resistance	[97]
Ni–Cr/CNTs	Mild steel	HVOF	The C_3H_8 flow rate: 65.73 L/min; the C_3H_8 pressure: 0.97 MPa; the O_2 flow rate: 238.5 L/min; the O_2 pressure: 1.21 MPa; the air flow rate: 201.3 L/min; the air pressure: 0.9 MPa; the spray distance: 280 mm; the spray rate: 110 g/min	Structure: the porosity of the coating was in the range of 0.49–1.01 vol.%. The CNTs in the coating were well bonded Properties: the addition of CNTs 20% increased the Vickers hardness and improved wear and corrosion resistance	[139]

[a]Normal liter per minute; L/min, a unit of the volumetric flow rate of a gas at standard conditions for temperature and pressure

Table 5 Exemplary parameters of electrophoretically deposited CNTs coatings

Coating	Substrate	Main parameters	Coating specification	References
MWCNTs	Ti13Zr13Nb	The EPD voltage: 20 V; the EPD time: 0.5 min; the anode "+": substrate; the cathode "−": platinum; the content of MWCNTs: 0.19 wt%	Properties: The MWCNTs coatings were laser modified. It was reported the laser modification caused a lack of surface cracks. The contact angles of examined surfaces were in the range of 46°–82°, the hardness from 4.51 to 6. 36 GPa (higher for laser-melted layers than affected by the heat of the laser beam), and Young's modulus from 105.28 to 125.19 GPa (lower for laser-melted layers than affected by the heat of the laser beam)	[112]
CNTs	Ti pure	The EPD voltage: 28 V; the EPD time: 30 s; the EPD current range 6–13 mA; the anode "+": substrate; the cathode "−": no data; the content of CNTs: no data	Properties: The human osteoblasts NHOst cell viability was slightly increased after 7 days of incubation by the surface modification of Ti alloy with MWCNTs coating. The hardness of the coating was 1.664 ± 0.107 GPa (132 ± 37 HV), Young's modulus of 101 ± 15 GPa, and corrosion resistance was decreased in contrary to the substrate material	[140]
HAp/MWCNTs	Ti–6Al–4V	The EPD voltage: 5÷30 V; the EPD time: 2÷10 min; the anode "+": substrate; the cathode "−": stainless steel; the content of MWCNTs: 1÷5 wt%; sintered at 800 °C for 2h	Properties: The hardness of the MWCNTs coating containing 1 wt% and 5 wt% of MWCNTs was 6 GPa and 7.12 GPa, respectively, and the Young's modulus of 155 GPa and 160 GPa, respectively. The adhesion strength of the HAp/MWCNTs coating was higher than for the HAp coating	[141]
MWCNTs	Ti13Nb13Zr	The EPD voltage: 20 V; the EPD time: 0.5 min; the anode "+": substrate; the cathode "−": stainless steel; the content of MWCNTs: 0.25 wt%	Properties: The roughness of the coating was 0.34 µm, the hardness of 0.101 ± 0.049 GPa, and Young's modulus of 14.17 ± 4.32 GPa. The coating showed the worst resistance to plastic deformation and accommodation to substrate deflections in comparison with the MWCNTs/TiO_2 and MWCNTs_Cu coatings (described below)	[111]
MWCNTs	Ti13Nb13Zr	The EPD voltage: 11 V; the EPD time: 2 min; the anode "+": substrate; the cathode "−": stainless steel; the content of MWCNTs: 0.27 wt%	Properties: The roughness of the coating was 0.098 µm, the hardness of 0.101 ± 0.049 GPa, and Young's modulus of 14.17 ± 4.32 GPa. The adhesion strength of the coating was assessed using a nano-scratch test and the value of the critical load was 116.5 ± 32.07 mN. The coating was hydrophilic and in the final summary had the best properties in contrast with MWCNTs with additions (described below), when considering an application in endoprosthesis	[142]
MWCNTs	Ti Grade II	The EPD voltage: 20 V; the EPD time: 1 min; the anode "+": substrate; the cathode "−": stainless steel; the content of MWCNTs: 0.25 wt%	Properties: The roughness of the coating was 0.29 µm, the hardness of 0.032 ± 0.0003 GPa, and Young's modulus of 3.41 ± 0.03 GPa. The coating achieved the highest plastic properties in comparison with the base MWCNTs and MWCNTs_Cu coating (described below) and a high ability to accommodate substrate deflections	[143]

Table 5 (continued)

Coating	Substrate	Main parameters	Coating specification	References
MWCNTs–TiO_2	Ti13Nb13Zr	(1) EPD of MWCNTs: the EPD voltage: 20 V; the EPD time: 0.5 min; the anode "+": substrate; the cathode "−": stainless steel; the content of MWCNTs: 0.25 wt% (2) EPD of TiO_2: the EPD voltage: 50 V; the EPD time: 4 min; the anode "+": stainless steel; the cathode "−": a substrate	Properties: The roughness of the coating was 0.65 µm, the hardness of 0.137 ± 0.048 GPa, and Young's modulus of 7.69 ± 1.75 GPa. The coating achieved the lowest ability to accommodate substrate deflections and the lowest resistance to plastic deformation in comparison to the MWCNTs_Cu and MWCNTs/TiO_2 coatings	[111]
MWCNTs/Cu		The EPD voltage: 50 V; the EPD time: 4 min; the anode "+": stainless steel; the cathode "−": a substrate; the content of MWCNTs: 0.25 wt%	Properties: the roughness of the coating was 0.41 µm, the hardness of 0.213 ± 0.061 GPa, and Young's modulus of 10.83 ± 2.12 GPa. The coating achieved the best resistance to plastic deformation in comparison with the base MWCNTs and MWCNTs/TiO_2 coating	
MWCNTs–nanoHAp	Ti13Nb13Zr	(1) EPD of HAp: the EPD voltage: 30 V; the EPD time: 2 min; the anode "+": stainless steel; the cathode "−": a substrate (2) Sintering (3) EPD of MWCNTs: the EPD voltage: 30 V; the EPD time: 2 min; the anode "+": substrate; the cathode "−": stainless steel; the content of MWCNTs: 0.27 wt%	Properties: the roughness of the coating was 0.98 µm, the hardness of 0.022 ± 0.015 GPa, and Young's modulus of 5.63 ± 2.76 GPa. The adhesion strength of the coating was assessed using a nano-scratch test and the value of the critical load was 92.06 ± 34.3 mN. The coating was hydrophobic and in the final summary had worse properties than the base MWCNTs coating when considering an application in endoprosthesis	[142]
MWCNTs–nanoHAp–nanoAg–nanoCu		The EPD voltage: 30 V; the EPD time: 2 min; the anode "+": substrate; the cathode "−": stainless steel; the content of MWCNTs: 0.4 wt%	Properties: The roughness of the coating was 0.618 µm, the hardness of 0.035 ± 0.019 GPa, and Young's modulus of 8.88 ± 3.26 GPa. The adhesion strength of the coating was assessed using a nano-scratch test and the value of the critical load was 60.38 ± 10.21 mN. The coating was hydrophobic and in the final summary had worse properties than the base MWCNTs coating when considering an application in endoprosthesis	
MWCNTs–TiO_2	Ti Grade II	(1) EPD of MWCNTs: the EPD voltage: 20 V; the EPD time: 1 min; the anode "+": substrate; the cathode "−": stainless steel; the content of MWCNTs: 0.25 wt% (2) EPD of TiO_2: the EPD voltage: 50 V; the EPD time: 4 min; the anode "+": stainless steel; the cathode "−": a substrate	Properties: The roughness of the coating was 0.56 µm, the hardness of 0.183 ± 0.0572 GPa, and Young's modulus of 10.11 ± 2.42 GPa. The coating achieved the highest resistance to plastic deformation	[143]
MWCNTs/Cu		The EPD voltage: 50 V; the EPD time: 4 min; the anode "+": stainless steel; the cathode "−": a substrate; the content of MWCNTs: 0.25 wt%	Properties: The roughness of the coating was 0.36 µm, the hardness of 0.079 ± 0.0354 GPa, and Young's modulus of 3.51 ± 1.84 GPa. The coating achieved the highest plastic properties in comparison with the base MWCNTs and MWCNTs_TiO_2 coating and the highest ability to accommodate substrate deflections	
HAp–Si–MWCNTs	NiTi	The EPD voltage: 30 V; the EPD time: 1 min; the anode "+": platinum; the cathode "−": a substrate; the content of MWCNTs: 1 wt%	Properties: The coating showed a uniform and compact structure and the bonding strength was assessed at 27.47 ± 1 MPa	[113]
Mg–14Li–1Al/MWCNTs	Mg14Li1Al	The EPD voltage: 30 V; the EPD time: 5 min; the anode "+": stainless steel; the cathode "−": a substrate; the content of MWCNTs: 0.25 wt%	Properties: The coating properties, such as yield strength, ultimate tensile strength, and elongation were assessed respectively at 213 MPa, 266 MPa, and 21.6%, and were significantly increased in the contrary to the substrate material. The microhardness highest value for the Mg–14Li–1Al/MWCNTs material was 84.6 HV	[144]

Table 5 (continued)

Coating	Substrate	Main parameters	Coating specification	References
Hap–Ti–MWCNTs	NiTi	The EPD voltage: 60 V; the EPD time: 2 min; the electrodes: graphite and substrate; the content of MWCNTs: 1 wt%	Properties: The coating showed improved corrosion resistance and improved fibroblast cell (L929) proliferation in comparison to the NiTi substrate material. The coating demonstrated non-toxicity in the culture medium	[145]
MWCNT/TiO_2–Co	Cooper	The EPD voltage: 80 V; the EPD time: 5 min; the electrodes: platinum and substrate; the content of MWCNTs: 0.02 wt%	Properties: The MWCNT/TiO_2–Co showed a discharge capacity of 305 mAh/g, which is twofold higher than that of pure MWCNTs and 1.6-fold higher than CNT/TiO_2	[114]
MWCNT	Composite pencil graphite	The EPD voltage: 20–25 V; the EPD time: 1–3 min	Properties: The carboxylic MWCNTs has better current density, onset potentials, and charge transfer resistances in contrast to composite pencil graphite electrode and can be used as an electrochemical sensor in the analysis of hyperin	[146]

3.1.4 Low-velocity oxy-fuel thermal spraying

Low-velocity oxy-fuel (LVOF) thermal spraying is very similar to HVOF, except for particle velocities, which are here lower, with close (2300–2500 °C) or the same flame temperatures. At the same time, particle velocities in LVOF are higher than in plasma spraying [91, 101]. Coatings deposited by LVOF are corrosion- and wear-resistant [102].

3.2 Electrochemical methods

The electrochemical methods are among the most simple techniques. The deposition material is a suspension with charged micro- or nanoparticles, which are migrating to the substrate, mainly due to the applied electrical field. Figure 5 demonstrates electrochemical methods, which are mostly used to prepare CNTs coatings and CNTs coatings with additions.

3.2.1 Electrostatic spraying

The electrostatic spraying (electrospray method, ES, shown in Fig. 5C) is a simple technique used to deposit coatings by dispersing charged material under an applied electric field. The deposition system consists of a generator and micro-injector, where a charged coating suspension is placed. Coatings prepared using this method are characterized by good adhesion to the substrate [103].

3.2.2 Electrophoretic deposition

Electrophoretic deposition (EPD) is a simple method carried out in suspension, where two electrodes, an anode, and a cathode are placed parallel to each other and connected usually to a DC power supply (Fig. 5B). Due to the electric field, the particles suspended in the solution migrate to one of the electrodes (depending on particle charge) and coagulate, forming a coating [111, 112, 142, 143, 147].

3.2.3 Electrocathodic deposition

Electrocathodic deposition (ECD), which is also known as electrocathodically-assisted deposition (ECAD), electro-co-deposition, or electrolytic plating is a method used in water solutions of inorganic compounds appearing as cations and anions. Additionally, CNTs (or, e.g., their carboxylated complexes [148]) can be transported by large cationic particles with which they form hydrogen chemical bonds. Under an electric field, the cations or cation–CNTs complexes move toward the cathode being a covered

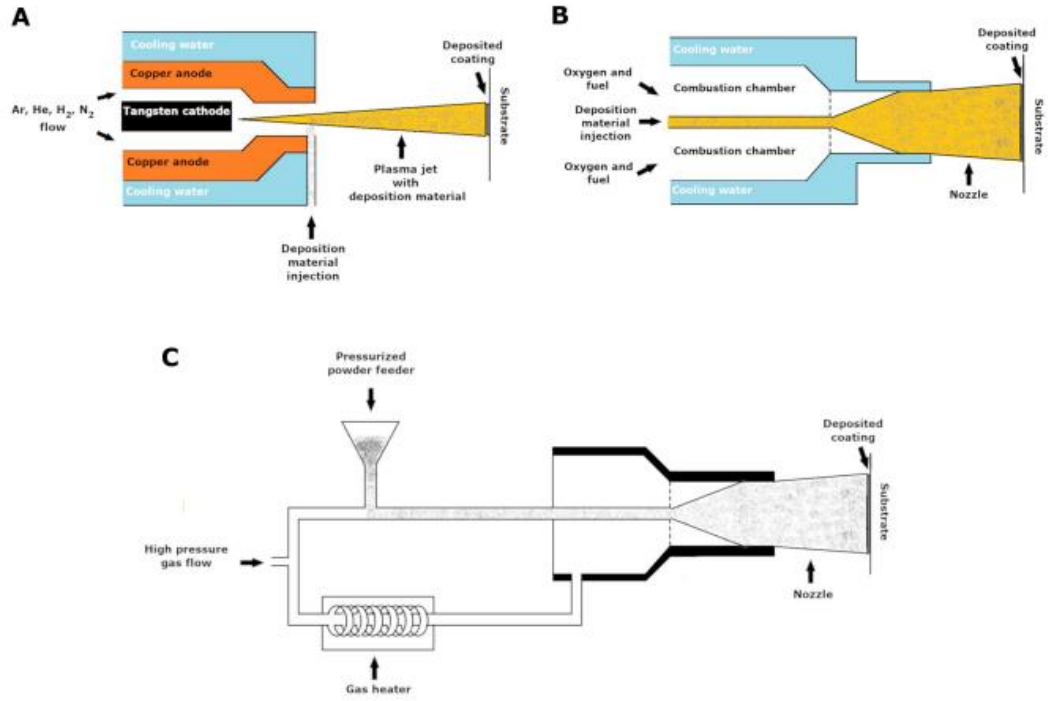

Fig. 4 Schematic illustration of thermal spraying methods: **A** plasma spraying, **B** high-velocity oxy-fuel thermal spraying, and **C** cold spraying

substrate, and form coatings [149, 150]. A schematic diagram of electrocathodic deposition is shown in Fig. 5A.

3.3 Laser methods

High-speed laser cladding (HSLC) is one of the methods applied to prepare CNT coatings, as shown in Fig. 7. Traditional laser cladding (LC) uses laser energy to melt additional material with the surface layer of the substrate. The additional material could be in the form of powder, wire, or strip [104]. LC method allows preparing surfaces free from porosity and cracks [105], but still too thick to produce wear and corrosion protective coatings because the surface preparation rate ranges from 10 to 50 cm^2/min. For ultra-high-speed laser cladding, the rate of cladding is approximately 500 cm^2/min, which is more efficient resulting in coatings of 10–250 μm thick [106]. For better understanding, Fig. 6 schematically demonstrates the idea of the HSLC technique (Fig. 7).

4 Properties of composite coatings

4.1 Topography and morphology

Surface topography is a qualitative feature of a surface shape, which is characterized by a quantitative feature, named surface roughness, expressed by the surface S_a parameter (multiple lines) or line R_a parameter. Table 6 shows a short review of the roughness of CNTs coatings. When discussing topography, it is also essential to point to surface morphology, which describes the coating chemical and phase composition, thus Table 4 also provides such information.

Table 6 shows that the roughness of electrochemically prepared CNTs-containing coatings is lower compared to other methods. Also, the plasma electrolytic oxidation has a lowering effect on the CNT–Al coating image. The microstructure of each coating depends on the method of synthesis. Plasma-sprayed coatings generally have

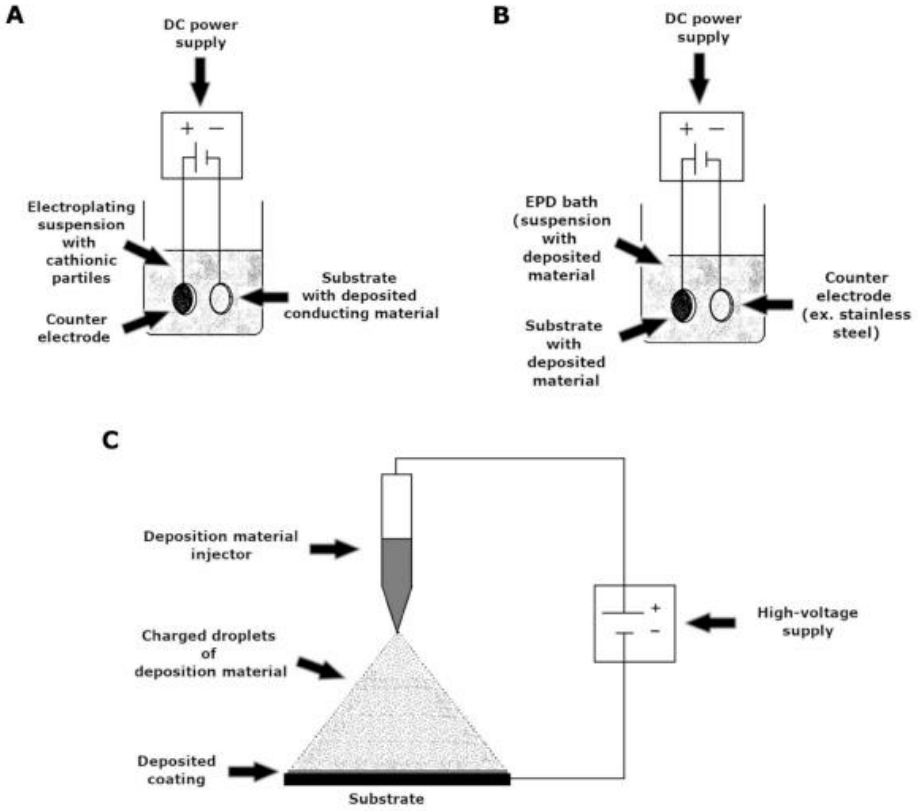

Fig. 5 Schematic illustration of electrochemical methods of CNTs coating deposition: **A** ECD, **B** EPD, and **C** ES

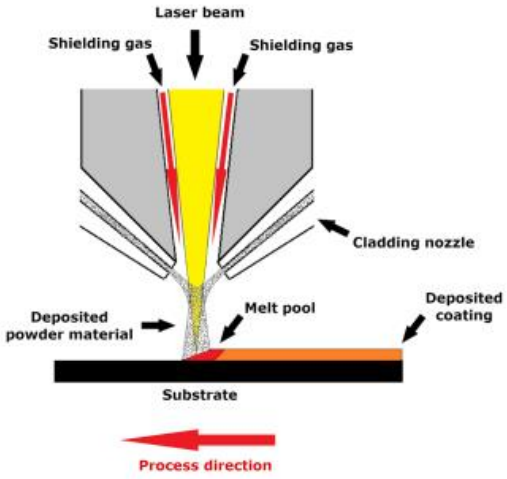

Fig. 6 Schematic illustration of HSLC method of coating synthesis

lamellar microstructure due to layer-by-layer deposition, where some microcracks, voids, and porosity can be distinguished [124, 125, 127, 136]. The porosity of Al–Si–CNTs coatings ranges from 10 to 12% and many agglomerates of size distribution 39÷57 μm could be observed [123]. For Ta_2O_5/CNT coatings the porosity ranges at 18÷26% and increases with the higher concentration of CNTs. Such coatings are intended for biomedical applications and reach a thickness of 540 ± 110 μm [31]. Generally, the coatings prepared using PS show regions, where the powder material is unmelted, partially melted or melted [94, 127]. Another method of CNTs coatings preparation is HSLC which gives coatings almost as flat as the substrate, without cracks in the micro-scale. For nickel-plated CNTs/Fe-based coatings, there could be seen phase transition from the columnar dendrite, through the crystal to amorphous resulting from a temperature gradient, and with the increase of CNTs content, all phases are refined [119]. CNTs coatings prepared with the CS method have

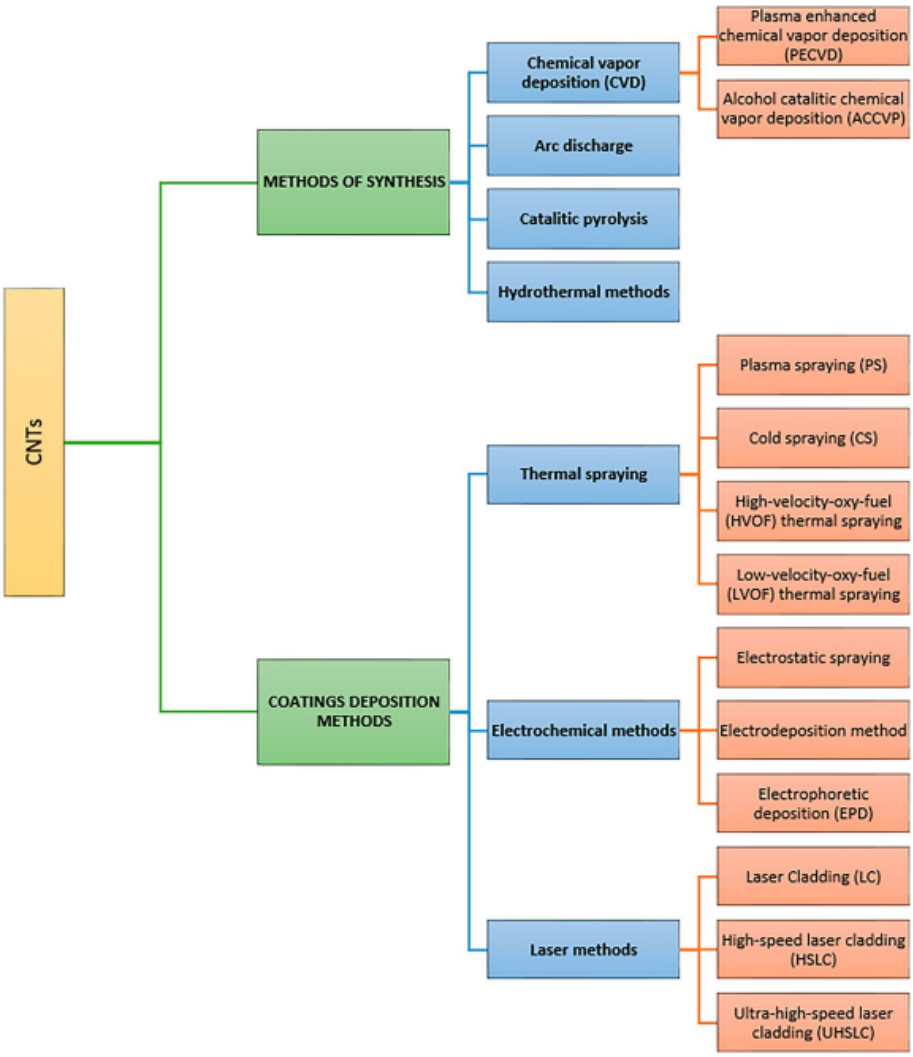

Fig. 7 A scheme of CNTs methods of synthesis and CNTs coatings deposition methods

flake-like morphology, whereas in cross-sectional images lamellar structure could be observed. Xie et al. reported CNT/AlSi coatings thickness to be several micrometers [108]. Moreover, 1wt%-CNT–Al coatings exhibit pores but their number and size are smaller than for the pure Al coating deposited on AZ91 Mg alloy [130]. EPD-prepared coatings have CNTs uniformly distributed. The other components such as nanometals and nanoceramics are mostly agglomerated [111, 142, 143] due to suspension instability and no possibility to stir during the process. Such coatings are also laser-modified, followed by scratches, folds, and bulges observed on their surface. The phases like TiC in the form of dendrites and spheres could be distinguished. The thickness of laser-modified MWCNTs coating was reported to be 7.88 ± 0.35 µm [112].

In materials science, morphology describes the shape, texture, and distribution of different elements and phases at a surface, whereas topography determines the quantitative 3D configuration of different geometrical features on a surface. The studies of both topography and morphology

Table 6 The roughness of coatings with CNTs

Coating	Substrate	Method of synthesis	Ra (μm)	Sa (μm)	Morphology description	References
Cr–CNT[a]	Steel	ECD	0.29	–	A cauliflower-like structure bulged deposit	[136]
Cr–YSZ–CNT[b]			0.22	–	A YSZ and CNTs are well dispersed in the Cr matrix, where a two-phase structure might be observed	
Ta_2O_5/CNT	Ti6Al4V	PS	9.6÷10.5	–	Characteristic to PS method coatings morphology, where layers of Ta_2O_5/CNT splats can be distinguished, homogenous CNTs coating, and uniformly distributed micropores of the distribution ranging from 1 to 5 μm	[31]
Cu–5CNT[c]	Cu	CS	20.69	–	The CNTs are not homogenously dispersed. No cracks observed	[132]
(Cu–5CNT)–10AlN[c]			14.37	–	Both, AlN particles and CNTs are not homogenously dispersed. No cracks observed	
(Cu–5CNT)–20AlN[c]			10.53	–		
CNT–Al	AZ91 Mg	CS + PEO	4.01	–	The structure of the CNT coating is lamellar, with microcracks, and Al_2O_3 volcanic-type pores. There could be distinguished α-Al_2O_3 and γ-Al_2O_3 forms of Al_2O_3 and graphitized carbon. The thickness of the coating is about 25 μm	[107]
MWCNT[d]	Ti13Nb13Zr	EPD	–	0.098	Uniform distribution of CNTs	[142]
MWCNT–HAp[d]			–	0.980	Many agglomerates of HAp observed, stuck to the CNTs	
MWCNT–Hap–nanoAg–nanoCu[d]			–	0.618	Many agglomerates of nanometals adsorbed to HAp particles	
MWCNTs[d]			–	0.34	Uniform distribution of CNTs. The thickness of the coating is about 0.5 μm	[111]
MWCNTs–TiO_2[d]			–	0.65	Uniform distribution of CNTs, many agglomerates of TiO_2 of micron size. The thickness of the coating is about 2 μm	
MWCNTs–Cu[d]			–	0.41	Uniform distribution of CNTs, the Cu nanoparticles located at the crossover of MWCNTs causing cracks. The thickness of the coating is not uniform; there are places of narrower and thicker coating	
MWCNTs[d]	Ti Grade II	EPD	–	0.353	Uniform distribution of CNTs	[143]
MWCNTs–TiO_2[d]			–	1.033	Uniform distribution of CNTs, many agglomerates of TiO_2 of micron size	
MWCNTs–Cu[d]			–	0.495	Uniform distribution of CNTs with Cu agglomerates built into	

[a]The roughness of the Cr surface is about 0.90 μm

[b]The roughness for Cr–YSZ is about 0.86 μm

[c]The roughness of the Cu surface is about 17.5 μm

[d]The roughness Sa parameter of Ti13Nb13Zr surface is about 0.203 μm

are always immanent parts of any materials investigations as their influence on bioactivity, i.e., bone growth rate, and also on corrosion behavior, is crucial. It might be assumed that in topography, the deciding is the proper development of the surface. For titanium, the geometry and dimensions of oxide nanotubes are important. In particular, the walls of rough and sharp nanotubes TiO_2 provide suitable places for the nucleation of biospecies [151]. The presence of titanium dioxide in the form of nanopatterns with heights of about 1.5 nm and nanotubes influenced protein adsorption kinetics and the thickness and morphology of the resulting protein layer which was attributed mainly to electrostatic interactions [152, 153]. The nanopatterned arrays developed by the chemical hydrothermal process at high temperatures mimic the dragonfly wing and are suggested as the origin of their activity against different bacteria [154]. The shot peening of titanium causes the substantial appearance of the micro- and nanoscale oxide layers which strongly affect adhesion, proliferation, and osteogenic differentiation of human cells, additionally enhancing wettability [154]. But not only the

presence of titanium oxide is a necessary condition for positive effects of topography. Osteoblasts showed a tendency to accelerate their proliferation on titanium spike structures [155]. The positive effects of the surface morphology, and micro and nano roughness, which improved osseointegration, were observed for hard titanium [155]. The additive designed manufacturing such as powder bed fusion (PBF) metal 3D printing makes porous structures of different local surface topography and pore shape that affects cell proliferation and differentiation. In particular, titanium with pores triangular and rectangular pores has higher roughness with a structure more concave (valley-like) than that with circular pores and effectively promotes the proliferation and differentiation of osteoblasts, thus improving osseointegration strength and implant fixation [156]. Similar phenomena were observed for porous topography for silicon [157, 158], hydroxyapatite [159, 160], poly(L-lactide) (PLLA) modified with femtosecond laser [161], poly(methyl methacrylate) (PMMA) [162]. For CNTs layers or composite coatings, there have been no important investigations, but it might be assumed that the presence of CNTs can enhance biological processes.

4.2 Adhesion between CNTs and metallic substrate

4.2.1 Adhesion mechanisms

The adhesion strength is mainly determined by mechanical and thermal interaction between particle and substrate depending on the method of coating synthesis. In the CS method deposition velocity and, thus, the degree of deformation plays an important role. At the critical velocity, the material is plastically deformed and a region (called adiabatic shear instability) where the temperature could reach the melting point of the material is formed, leading to viscoelastic material flow, formation of a conformal interface, and metallurgical bonding. Thus, the evaluation of adhesion strength is dependent on the particle velocity, particle or substrate temperature, substrate roughness, particle morphology, and mechanical properties of both the particle and the substrate [95, 163].

The CNTs formulate a mesh structure, with a large surface area, giving space for reaction. Direct reaction of CNTs with plasma plume in plasma spray method resulted in the generation of defects which leads to an increase in reaction sites [123]. In this method, there are seen three typical microstructures: fully melted region, partially melted region, and pores. In the fully melted region, some reduction processes may occur such as in the case of CNT–TiO_2 coating for which the carbothermal reduction appears followed by the formulation of some TiO_{2-x} species. In partially melted regions, CNTs and the other components stick to each other and bond with weak van der Waals forces [94].

Adhesion plays a very important role in implant coating. If the adhesion is poor, during implantation surgery the coating can be degraded or even totally removed. Therefore, even further properties are positive, the adhesion must be sufficient enough to counteract mechanical stresses during the insertion of whatever implant into the bone. Below different methods are described which are used to assess the anticipated integrity by measurements of the adhesion strength of the coating to the bone. Besides, as the coating is subject during surgery and after different loads, the coating must be also tough, but not brittle. Therefore, CNTs are added mainly to improve rigidity, hardness, and toughness.

Despite several described below tests to calculate adhesion strength, widely described in the literature, however, the best assessment of the coating behavior during implantation surgery is in vivo experiments on animals. The results of such successful studies are, however, not frequent. It is noted that to increase the clinical success rate of metal implants is to increase their bone-bonding properties, i.e., to develop a bone bioactive surface leading to reduced risks of interfacial problems. Much research has been devoted to modifying the surface of metals to make them bioactive. Many of the proposed methods include depositing a coating on the implant. However, there is a risk of coating failure due to low substrate adhesion. In [164], a method to obtain bioactivity combined with a high coating adhesion via a gradient structure of the coating [165]. The review of different techniques for HAp coatings on Ti6Al4V alloy, mostly still applied for hip joint implants, showed that three techniques, namely sputtering, IBAD (ion beam-assisted deposition) followed by heat treatment, and EPD give reasonably high adhesion values. To increase the adhesion, the substrate is usually properly prepared to develop its surface area and create micro and nanoforms such as grooves, pillars, columns, etc., by mechanical grinding, acidic and alkaline etching, chemical, electrochemical, and micro-arc oxidation, laser roughening, and patterning. In [166], such laser micromachining of titanium and its alloys created micro-grooves of diameter of about 10 μm, and then coating with arginine–glycine–aspartic acid to enhance cellular spreading and adhesion was deposited. The laser-grooved and coated rods had significantly higher pull-out strength than the only laser-grooved and control rods. This paper in an excellent way explains the core of this problem. To summarize, the coating for long-term implants must demonstrate several features, such as the bioactivity necessary to form quickly and strongly the bond between an implant and bone, mechanical behavior against anticipated stresses sufficient to avoid any serious damage or degradation, and high adhesion. Truly, we would like to achieve only bioactivity without cytotoxicity, but weak mechanical strength or weak coating adhesion might cause the coating to be destroyed and the main aim for its deposition will vanish.

4.2.2 Testing methods and adhesion strength of CNTs

Among different methods used to assess the adhesion of coatings, the standard ASTM F1044 based on shear testing of calcium phosphate and metallic coatings is the most often applied for CNTs composite coatings. It assesses the adhesion of coatings to substrates or the cohesion of a coating under shear stress to the interface. Commonly flat-coated specimens are glued to a proper counterpart and loaded up to the division of both parts. The more recent results of such investigations are shown in Table 7. The addition of the CNTs results in a significant increase in the adhesion strength, but as a rule at its higher contents or if a third component is present in a coating.

Exceptionally, the standard test method based on measuring adhesion force by tape test, ASTM D 3359-08, was applied for the chitosan–nanoHAp–CNTs on Ti substrate [171]. The tape tests displayed high adhesion strength (class 5B).

Nanoscratch testing is increasingly applied [141, 142] despite that mechanical force and not stress is measured which makes the results not comparable to those based on the shear technique. For the nanoHAp–CNTs coatings deposited on Ti and its alloys, [141], a critical load of 350 mN was noticed for the HAp–5% CNTs coating. In the other research [142] the values of critical force resulting in the delamination of coatings deposited on Ti13Nb13Zr alloy were 116.5 mN, 90.2 mN, and 60.4 mN under shear stress for CNTs, CNTs–HAp, and CNTs–nanometal coatings, respectively, at 0.27 wt% of CNTs only.

Finally, it is to emphasize a novel technique, called a nanomechanical pull-out method [172] that has used an atomic force microscopy cantilever acting as a force sensor and mounted vertically to a 3D piezo nanomanipulator. The interfacial shear strength and the maximum load-bearing capacity of the CNTs coatings on Al Ti and Zn substrates were 217 and 245 nN, and after quantitative analysis of the results, the shear stresses at the interfaces were calculated as 31÷40.01 MPa, depending on heat treatment, and 37.8 MPa, respectively [172, 173]. Based on the ASTM C-633 standard (European EN 582) and using the tensile tester for pull-out samples, the adhesion between cold-sprayed CNTs to Al matrix was assessed at 15–18 MPa [95].

Systematic research on the effects of some features and amounts of CNTs composites is rare. One of the reasons for increasing the adhesion strength with increasing the CNTs content in HAp coating is bridging formed by CNTs between coating and substrate [174, 175]. It is noted that an addition of CNTs has also been proposed for protective coatings based on epoxy resins [16].

Table 7 The shear strength of CNTs-containing coatings, determined by ASTM F1044 standard

Coating composition	Substrate	Shear strength (MPa)	References
HAp–20 wt% MWCNTs	Ti	34.94	[167]
HAp–30 wt% MWCNTs	Ti	35.44	[167]
HAp	Ti	20.62	[167]
HAp–0.1MWCNTs	Ti	19.0	[168]
HAp–1MWCNTs	Ti	24.2	[168]
HAp–2MWCNTs	Ti	22.4	[168]
HAp	Ti	18.1	[168]
HAp–0.1SWCNTs	Ti	17	[169]
HAp–0.3SWCNTs	Ti	~21	[169]
HAp–0.5SWCNTs	Ti	25.7	[169]
HAp-1.0SWCNTs	Ti	~25	[169]
HAp	Ti	15.3	[169]
HAp–20Si–1MWCNTs	NiTi	27.5	[113]
HAp–1MWCNTs	NiTi	19.3	[113]
HAp–20Si	NiTi	23.2	[113]
HAp	NiTi	18.0	[113]
HAp–20Ti–1MWCNTs	NiTi	32.1	[170]
HAp–20Ti	NiTi	~27	[170]
HAp	NiTi	17.2	[170]
HAp–Ta_2O_5–0.5MWCNTs	NiTi	30.2	[57]
HAp–Ta_2O_5–1MWCNTs	NiTi	32.4	[57]
HAp–2Ta_2O_5–1.5MWCNTs	NiTi	32.7	[57]
HAp–Ta_2O_5–2MWCNTs	NiTi	34.6	[57]
HAp–Ta_2O_5	NiTi	23.7	[57]
HAp	NiTi	18.9	[57]

4.3 Mechanical behavior

The mechanical behavior of a material is one of the most important features discussed when the material is considered for use in biomedical applications. Microhardness, nanohardness, elastic (Young`s) modulus, and yield strength less often, are the mechanical properties checked to describe the material and attribute it to an application. The difference between micro- and nanohardness is the area of the test. Microhardness gives information about the average hardness of a large area, while nanohardness is more specific and describes the little area using smaller loads. Young's modulus is used to assess material stiffness and is a very important factor in terms of biomedicine because the mismatch of implant and bone in Young's modulus could lead to complications for the patient and even the necessity to repeat the surgery. Usually, scientists are looking for materials, with lower values of elastic modulus than the natural bone elastic modulus, which is for cancellous bone about 3.78 GPa and cortical bone about 14.64 GPa [176]. Table 8 shows the mechanical properties of coatings composed of CNTs.

Table 8 Research of CNT-composite coatings deposited on a metallic substrate

Coating	CNTs wt%	Substrate	Microhardness (GPa)	Nanohardness (GPa)	Elastic modulus (GPa)	Yield strength (GPa)	References
Al–5CNT	6.2	Mild steel	1.350 ± 0.05	2.33 ± 0.27	107 ± 6	38.3 ± 1.9	[123]
Al–10CNT	12.4	Mild steel	2.100 ± 0.04	2.89 ± 0.27	125 ± 7	41.5 ± 1.8	
Al–Si–5CNT	5.0	Mild steel	–	–	107 ± 6	8.3 ± 1.9	[124]
Al–Si–10CNT	10.0	Mild steel	–	–	125 ± 7	41.5 ± 1.8	
CNT–Al	1.0	AZ91 Mg alloy	–	1.66 ± 0.2	77.6 ± 3.3	–	[130]
CNT–Al[a]	1.0	AZ91 Mg alloy	13.9	–	185.4	–	[107]
Cr–CNT	2	Steel[b]	15.0 ± 1.2	19.0÷3.0	196.0 ± 8.2	–	[137]
Cr–YSZ–CNT	2	Steel[b]	25.0 ± 0.28	32.0 ± 3.4	206 ± 11	–	
Cr–CNT	2	Steel[b]	14.0÷1.7	–	192÷22	–	[136]
Cr–YSZ–CNT	2	Steel[b]	24.0÷1.5	–	210÷20	–	
CNTs	0.5	Ti[c]	1.664 ± 0.107	–	101 ± 15	–	[140]
MWCNT	0.27	Ti13Nb13Zr[d]	–	0.101 ± 0.049	14.17 ± 4.32	–	[142]
MWCNT–HAp	0.27		–	0.022 ± 0.015	5.63 ± 2.76	–	
MWCNT–HAp–nanoAg–nanoCu	0.4		–	0.035 ± 0.019	8.88 ± 3.26	–	
MWCNT	0.25		–	0.101 ± 0.049	14.17 ± 4.32	–	[111]
MWCNT–TiO_2			–	0.137 ± 0.048	7.69 ± 1.75	–	
MWCNT–Cu			–	0.213 ± 0.061	10.83 ± 2.12	–	
MWCNT	0.25	Ti Grade II	–	0.032 ± 0.0003	3.14 ± 0.03	–	[143]
MWCNT–TiO_2			–	0.183 ± 0.0572	10.11 ± 2.42	–	
MWCNT–Cu			–	0.079 ± 0.0354	3.51 ± 1.84	–	

[a]The coating was first prepared by CS and second by PEO

[b]The elastic modulus for stainless steel is about 51.07 GPa [176]

[c]The elastic modulus for Ti is about 50.20 GPa [176]

[d]The elastic modulus for Ti13Nb13Zr is of 83.32 ± 11.63 GPa

CNT-based coatings are deposited on different substrates with variable CNTs and other additions` contents. Considering the value of Young's modulus of CNT-containing coatings for application in biomedicine we can observe that the coatings with 0.25 and 0.27 wt% addition of CNTs revealed elastic modulus values similar to cortical bone. The addition of nanometals and nanoceramics causes a decrease in Young's modulus. The CNTs applied in the YSZ and Al-based coatings improve mechanical properties [125, 130]. For Al-based coatings, the CNTs enhance coatings properties through thermal expansion mismatch, and Orowan looping as CNTs are generating high dislocation density and limit dislocation migration. Also, CNTs play a reinforcing role, dependent on content and distribution [130].

4.4 Corrosion resistance

The corrosion resistance testing focuses on the electrochemical behavior of the deposit by, almost exclusively, the electrochemical potentiodynamic polarization test. The increase in current density means the corrosion resistance decreases. The conditions of the test can be changed, such as temperature, electrolyte composition, scanning rate, and potential range. For biomedical applications mostly the temperature of the body is imitated and SBF solution is used as an electrolyte. Before the main test, the open circuit potential (OCP) value is checked, which is the potential at zero current value and gives information about the thermodynamic stability of the examined material. Mostly OCP value is negative, but sometimes it could be positive, which means a passivation phenomenon of the coating can occur [136]. The OCP value also gives a clue about the potential range that should be used during the electrochemical polarization test. Table 9 shows a brief conclusion about the corrosion behavior of CNTs-based coatings.

For the coatings with YSZ, Cr, and Al prepared using PS the addition of CNTs enhanced the corrosion resistance [125, 127, 130, 136]. Tripathi et al. [136] reported better corrosion resistance for the Cr–CNT and Cr–YSZ–CNT compared to the bare Cr material, with the highest potential achieved for the Cr–YSZ–CNT coating. For the Cr substrate the corrosion current density and corrosion potential

Table 9 A state-of-the-art corrosion behavior of CNT-containing coatings

Coating	Substrate	Crucial parameters of coating preparation	E_{corr} (V)	I_{corr} (nA/cm^2)	References
CNTs–TiO_2	Ti13Nb13Zr	EPD (0.25% CNTs, TiO_2 0.15 g, 50 V, 4 min)	−0.169	1.4	[177]
		EPD (0.25% CNTs, TiO_2 0.15 g, 60 V, 4 min)	−0.282	206.4	
		EPD (0.25% CNTs, TiO_2 0.30 g, 50 V, 4 min)	−0.217	17.5	
		EPD (0.25% CNTs, TiO_2 0.30 g, 60 V, 4 min)	−0.439	9.85	
CNTs		EPD (0.25% CNTs, 20V, 30 s)	−0.233	176.2	
NiTi + HAp–Ti–CNT	NiTi	EPD (1% CNTs, 60 V, 2 min)	−0.0391	0.91	[145]
Cr–CNT	Cr	ECD (20 g/L of CNTs)	−0.509	6900	[136]
Cr–YSZ–CNT	Cr	ECD (25 g/L of 3 mol% Y_2O_3, 20 g/L of CNTs)	−0.470	7200	
CNT–Al	AZ91 Mg alloy	CS (1 wt% CNTs)	−0.941	2030	[130]
CNT–Al	AZ91 Mg alloy	CS + PEO (1 wt% CNTs)	−1.126	3734	[107]
CNT	Ti	EPD (28V, 30 s)	0.270	112	[140]
Nickel-plated CNTs/FeCoNbBSi	45 steel	HSLC (0.25 wt% CNTs)	−0.592	547	[119]
Nickel-plated CNTs/FeCoNbBSi	45 steel	HSLC (0.5 wt% CNTs)	−0.502	454	
Nickel-plated CNTs/FeCoNbBSi	45 steel	HSLC (1 wt% CNTs)	−0.518	436	

were 15.9 ± 3.7 μA/cm^2 and − 534 ± 19 mV, respectively, and for Cr–CNT 6.9 ± 1.3 μA/cm^2 and − 509 ± 23 mV, and Cr–YSZ–CNT 7.2 ± 0.9 μA/cm^2 and − 470 ± 13 mV, what gives information that two-phase boundaries inhibit the cracks and limits corrosion [136]. On the other hand, the increase of MWCNTs content in MWCNTs/PU coatings increases the corrosion current density, thus weakening the corrosion resistance. This phenomenon could be explained by the formulation of micro-defects in the PU matrix, which facilitate the substrate metal corrosion. The maximum corrosion rate for MWCNTs/PU coating deposited on Q235 steel is at 8 wt% of MWNCTs and the maximum corrosion resistance appears for 2 wt% of MWCNTs [110]. The same effect was seen for 1 wt%-CNT–Al coating deposited on AZ91 Mg alloy, achieved using the CS method according to the substrate and pure Al coating. The phenomenon was explained by thermal mismatch between the Al matrix and CNTs, which can strengthen the matrix, limit dislocation looping, and suppress crack propagation [107, 130]. Maleki-Ghaleh et al. [145] prepared HAp–Ti–1wt%-MWCNTs coating using the EPD process on NiTi substrate, which possessed the best corrosion resistance in comparison to the substrate and coatings without MWCNTs addition. Nevertheless, there are the same reports about CNT coating EPD-deposited on Ti, which decreases corrosion resistance, due to the porous fibrous structure of the coating and the presence of TiO_2 [140]. Thus, the results are ambiguous indicating the complex roles of components and microstructure, roughness, and uniformity of the surface.

Another method to check corrosion resistance on a micro-scale is the scanning Kelvin probe. The test allows for achieving information about electron work. The higher the escape electron work is, the higher the corrosion resistance. The test indicated the best corrosion resistance for the CNTs/Fe-based coating with 1 wt% of CNTs prepared by HSLC, confirmed by the electrochemical corrosion test. The increase in CNT content caused the decrease in corrosion current density, and the CNTs presence allowed to join the cracks improving corrosion resistance [119].

4.5 Wettability

The contact angle is used to describe the wettability of CNTs coatings. The higher the contact angle is the higher the wettability of a surface, and thus such a surface is named hydrophilic. In the literature, the contact angle between 40 and 60° is the best in terms of promoting cells adhesion and improving the bioactivity of the coating [178]. Lin et al. reported on the decrease in contact angle of the Ta_2O_5/CNT coating deposited on Ti6Al4V to 1÷3° [31]. The wettability of Cu–CNT–TiO_2 coating is also hydrophilic (the contact angle value is 12.85°), due to the presence of TiO_2 particles [135]. The pure CNT coatings prepared using the EPD technique deposited on Ti13Nb13Zr are also hydrophilic and their contact angle is about 56°, while the contact angle of CNTs coatings with HAp and nanometal additions highly increases to hydrophobic values, which is unwelcome in biomedical applications [142]. The impact of laser modification on the wettability of CNTs coatings was also checked and revealed the increasing contact angle to the value of about 80° [112]. The wettability of CNTs coatings is then strongly dependent on the bonding effect and the method of synthesis. Most MWCNTs used to prepare coatings employing electrochemical methods are functionalized to give a negative charge and enable the deposition. Such a modification and changes in the pH of the solution during the process may impact the linking of CNTs to other components of the suspension, thus changing the contact angle of the coating

[142]. On the other hand, the wettability of CNTs coatings is dependent on the roughness.

4.6 Bioactivity and cytotoxicity

Most commonly the MWCNTs' bioactivity and cytotoxicity, namely positive and negative effects on adhesion, viability, proliferation, and mortality of cells were tested in human umbilical vein endothelial cells (HUVECs). Zhao et al. [52] examined three types of MWCNTs with different diameters, named XFM4 (diameter: 10–20 nm), XFM22 (length: 0.5–2 μm; diameter: 20–30 nm), and XFM34 (length: 0.5–2 μm; diameter: > 50 nm) and concluded that the smallest diameter, the higher level of cytotoxicity, the HUVECs are the most internalized, the level of cytokine released is the highest. They also observed the highest level of ER stress biomarkers, due to the highest specific surface area of the MWCNTs, causing autophagy of HUVECs, thus eliminating MWCNTs with such dimensions to be applied in biomedicine, especially in blood vessels. Also, the dose-dependence impact on cytotoxicity was seen. The MWCNTs with the smallest diameter exposed cytotoxicity at concentrations higher than 16 μg/mL. On the other hand, for higher MWCNTs diameters, a greater content of MWCNTs caused higher cytotoxicity to HUVECs, while its addition didn`t indicate obvious changes in the ultrastructure of HUVECs cells.

The MWCNTs diameter cytotoxicity impact on the other cells was also checked for NR8383 cells (normal rat alveolar macrophage cells) [179] and human mesothelial cell lines (MeT5A, E6/E7, and hTERT-immortalized human peritoneal mesothelial cells) [180] and the length impact of MWCNTs on cytotoxicity to HUVECs was investigated. Long et al. [181] examined two types of MWCNTs (XFM19 of length 10–30 μm and XFM22 of length 0.5–2 μm, both outer diameter of 20–30 nm and inner diameter of 5–10 nm) with different concentrations from 2 to 32 μg/mL. The longer the MWCNTs were, the higher level of cytotoxicity to HUVECs, the higher oxidative stress, the higher level of THP-1 monocyte adhesion to MWCNTs, the higher level of ER stress biomarkers were observed, which gives information about the inflammation-inducing effect of longer MWCNTs species. Another parameter discussed in the literature is a surface modification of MWCNTs, which could affect interaction with proteins and cells [182]. According to Sun et al. [183], pristine MWCNTs (XFM19, diameter: 28.97 nm, average length: 1181.14 nm), hydroxylated MWCNTs (XFM20, diameter: 30.46 nm, average length: 1323.94 nm), and carboxylated MWNCTs (XFM21, diameter: 31.03 nm, average length: 1256.59 nm) are cytotoxic to HUVECs and induce oxidative stress to a similar extent while used with MWCNTs concentration of 32 μg/mL or 64 μg/mL. Dinc et al. reported the functionalized (oxidized) MWCNTs were less toxic to HUVECs and MDA-MB-231 cells (breast cancer cells) than pristine MWCNTs [182]. Thus, MWCNTs with a longer length and smaller diameters could induce cytotoxicity to HUVECs, regardless of the type of used functionalization of MWCNTs. However, Dlugon et al. [140] checked the biological activity of CNTs coatings EPD deposited on Ti using the human osteoblast NHOst cell line and after 7 days observed higher cell viability for CNTs modified Ti than for pure substrate. Also, the SWCNTs were investigated in terms of cytotoxicity and showed that the oxidized SWCNTs caused malformed placentas in female mince already after administration of 100 ng/ml of oxidized SWCNTs [184, 185].

The toxicity of MWCNTs is then dependent on their dimensions, such as the diameter, length, and also physicochemical properties, like surface chemistry, and dose. So far studies show that the examined parameters in terms of cytotoxicity are: (1) the internalization of MWCNTs to human cells, (2) the release of inflammatory cytokines (THP-1 monocyte), (3) the mechanism of cytotoxicity activation-reactive oxygen species (ROS) or activation of endoplasmic reticulum (ER) stress biomarkers, such as *ddit3* (DNA damage-inducible transcript 3) or other named *chop* (C/EBP homologous protein); *xbp-1s* (spliced X-box binding protein 1), and the protein level of BiP (binding immunoglobulin protein; GRP78, 78 kDa glucose-regulated protein) [52, 181, 183].

The cytotoxicity is a serious problem that has been attempted to limit by several solutions. In [186] the toxicity of CNTs was shown to be mainly related to their dimensions: toxicity decreases with increasing length of the nanotubes. The toxicity was also reduced for CNTs of small diameter [187], thus the use of smooth CNTs is favorable. Besides this passive way, the functionalization of CNTs is likely the single approach to decrease cytotoxicity, with effectiveness dependent on chemical structure. The carboxylic SWCNTs and MWCNTs, with cytotoxicity investigated by adsorption of human serum albumin [188], of bovine serum albumin [189, 190], and by MTT assay [191] were the least toxic as compared to hydroxylated SWCNTs and amined SWCNTs. The natural bio-resin shellac applied for the functionalization of CNTs also reduces cytotoxicity [192].

The bioactivity of CNTs has been seldom investigated as elementary carbon is an inert body. The high surface properties, including the creation of chemical covalent or van der Waals bonds, are achieved due to nanosized tubes. However, it is now well known that to make CNTs bioactive, chemical functionalization is necessary. There are several indirect evidence for an enhancement or improvement of bioactivity by CNTs in multicomponent coatings. In [193] the multivalent polyanion-dispersed CNTs were used after their functionalization with polyglycerol sulfate and deposited on PCL. That results in higher neural differentiation efficiency creating then highly bioactive nanostructured

fibrous scaffolds. In [194] low-dimensional nanomaterials such as CNTs or graphene exhibited noticed in vitro bioactivity and osteoinductivity. In [195] polymer–bioglass–CNTs composite material was investigated. The results showed that the presence of MWCNTs in low quantities enhanced osteoblast-like cell attachment and proliferation compared to composites with high concentrations of MWCNTs, and the mechanism of CNTs-enhanced bioactivity is unclear. Considering the test results for [196] the coatings composed of functionalized multi-walled carbon nanotubes (f-MWCNTs) and hydroxyapatite on 316L steel, it was concluded that the addition of f-MWCNTs in the HAp increases the number of active sites responsible for the formation of carbonated apatite layer. In [197], the use of functionalized carbon nanotubes in the hybrid composition of chitosan/silica showed favorable tissue responses of the CNT-incorporated membrane.

The bioactivity is most often checked using in vitro tests, mostly in SBF solution. Lin et al. [31] reported a complete coverage by hemispherical-shaped particle samples of Ti6Al4V coated with Ta_2O_5 and Ta_2O_5/CNTs. Nevertheless, there could be an observed relationship between the increasing content of CNTs in the coating and with decreasing size of adhered apatite particles. The same team checked the adhesion of osteoblast-like cells, such as osteosarcoma MG-63 cells, which showed satisfactory adhesion and spreading behavior after 7 days of culture, but without an impact of CNTs presence. It means that CNT-decorated coatings could promote cell proliferation and differentiation, and thus they are candidates for use in biomaterials [183].

4.7 Antibacterial efficiency

CNTs have been reported to exhibit killing properties over a wide range of bacteria including human pathogens such as *Escherichia coli* (*E. coli*), *Salmonella typhimurium*, *Bacillus subtilis* (*B. subtilis*), *Staphylococcus aureus* (*S. aureus*), *Micrococcus lysodeikticus* and *Streptococcus mutans*. Several studies have disclosed that pristine CNTs exhibit antibacterial activity by physical contact and collisions leading to puncturing of the bacterial cell membrane and its damage [198, 199]. It was reported in [198] that the force of 100 nN is enough to make AFM-detectable holes in bacteria cells, even though the checked force is unrealistic to appear between bacteria and CNTs in normal conditions, thus this mechanism is unlike. The second mechanism assumed the CNTs are connecting to the bacteria cell membrane in the form of CNT dense network, thus changing cell membrane architecture, and its mechanical properties [198–200]. Liu et al. reported the SWCNTs after 10 min of exposure to *E.coli* and *B. subtilis* increasing cell wall roughness, causing increased cytoplasm leakage and bacteria cell death after 120 min [198], while Schifrano et al. reported a significant reduction of cell number after 24 h incubation in contact with CNTs [200]. Further investigation leads to the assertion that the antibacterial activity of CNTs is light-dependent [201, 202]. Rajavel et al. reported that the SWCNTs and MWCNTs are ROS generators (producing singlet oxygen $^1O_2$, superoxide anions $\dot{O}^{2-}$ and hydroxyl radicals ȮH) in sunlight with a light intensity of 903 lm/m^2 and ambient light of 180 lm/m^2 [201]. Such ROS production increases oxidative stress, makes bacteria cell membrane disruption (due to lipid peroxidation) and causes bacteria death [200–202]. Nevertheless, the antibacterial effectiveness of CNTs also depends on bacteria peptidoglycan cell wall thickness and strain resistance, showing the CNTs antibacterial properties are more significant for Gram-negative bacteria (e.g., *E.coli*, *P. aeruginosa*) than Gram-positive ones (e.g., *S. aureus, B. subtilis)* [198, 200]. The above mechanisms of antibacterial activity of CNTs are well established in [200], where both the mechanical injury and ROS production play important roles in the bactericidal effect of CNTs. Figure 8A shows a diagram, summarizing the antibacterial mechanisms of CNTs.

There are many reports about the antibacterial efficiency of CNTs with additions, where the main mechanism of antibacterial efficiency is again the generation of ROS. The cellulose acetate (CA)-CNT–Ag [203] was shown as effective against *E. coli* and *S. aureus*, with the CA matrix creating protection against the harmful effects of silver (i.e., argyria and argyrosis) [203]. Also, CNTs–Ag composites exhibit antibacterial properties against *E.coli* [204]. The addition of CNTs to Ag colloid lowers the minimal inhibitory concentration value of Ag particles in suspension, both against Gram-negative and Gram-positive bacteria. Here, a good dispersion of the Ag nanoparticles on the CNTs is the reason for the high antibacterial activity of CNT–Ag composites [204]. There is evidence about the antibacterial activity of MWCNTs–Ag composites against *E. coli* [205–207], *S. aureus* [203, 208–211], *Staphylococcus haemolyticus* [212], and also against *B. subtilis* and *Pseudomonas aeruginosa* [213]. The other CNTs-containing coating components were reported to have antibacterial properties [212], in particular for composite coatings such as the CNTs–ZnO [214, 215], hydroxyapatite/ZnO/CNT [216], Co doped-ZnO/MWCNTs [214] and MWCNTs–Ag/TiO_2 [217] against *E. coli* and *S. aureus*. Also, the MWCNTs–TiO_2 [218] and Ag–TiO_2–MWCNT [219] were lethal to *E. coli*, and CNTs/TiO_2/polyurethane films to *S. aureus* [220]. Also, SWCNTs composites with Ag nanoparticles inhibited the growth and multiplication of bacteria, such as *S. aureus*, *B. cereus*, *E. coli*, and *P. aeruginosa* [221]. Zhu et al. reported very strong antibacterial performance of SWCNTs in combination with silica and Ag against *E. coli* and *S. aureus* [222]. The same antibacterial activity showed SWCNTs–Ag/TiO_2 hybrids [217]. Although CNT

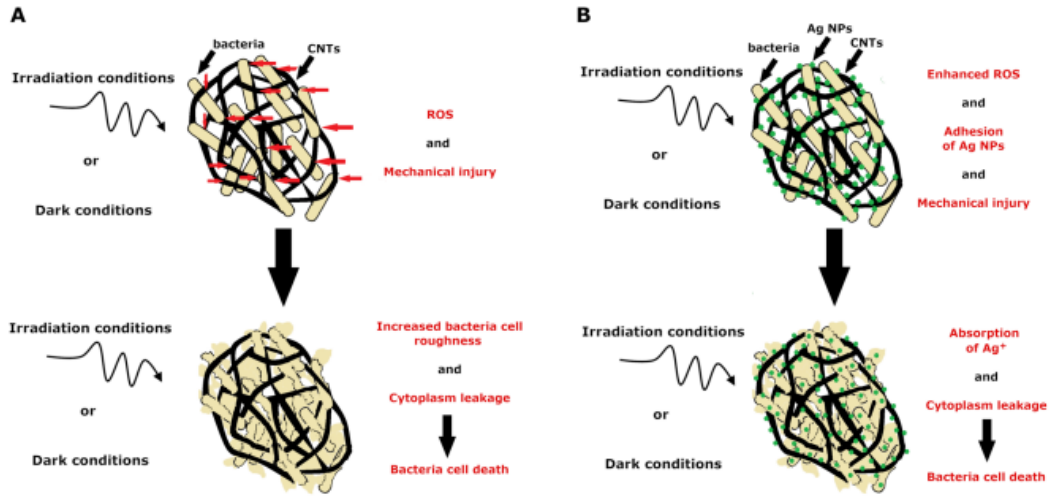

Fig. 8 A schematic illustration of antibacterial mechanisms for **A** CNTs and **B** CNTs with Ag NPs addition

coating improves cell adhesion, and antibacterial properties and promotes osteoblast differentiation of Ti species [202, 223], pristine CNTs are reported to increase oxidative stress and cause cell death [202].

In the example of Ag–MWCNTs coating, the mechanisms of antibacterial activity slightly differ depending on the form of silver, either ionic Ag^+ cations or NPs [153, 224, 225]. Both silver forms specifically interact with bacteria. For Ag NPs, the contact mechanism is typical which occurs through the touch of bacteria to silver particulates and ROS appearance, which leads to damage to the cell membrane and vacuolization of cytoplasm [226–230]. According to [231], all contacted Ag NPs influence the permeability and flow through the outer membrane, but only smaller Ag NPs can pass through the cell membrane, then interact with DNA, and affect the respiratory system. Whereas, the antibacterial mechanism for Ag^+ starts with their adhesion to the bacteria cell, its adsorption inside the bacteria cell, and the production of ROS [226, 228, 229, 232]. As Zhao et al. propose [230], the silver ions on the cell membrane inhibit the expression of outer membrane proteins, i.e., retard the reproduction of bacteria cells by inducing the release of nucleic acids, what is according to Du et al. [232] typical of large agglomerates of Ag NPs. The synergy of the combination of CNTs with Ag enhances the bactericidal efficiency of the CNTs, thus the Ag NPs are characterized by a high surface-to-volume ratio and MWCNTs high aspect ratio, this way produce a higher contact area [199]. Figure 8 schematically illustrates the differences in antibacterial mechanisms of CNTs and CNTs with Ag addition.

4.8 Perspectives and challanges

The CNTs gain more and more attention in biomedical, energy and thermal applications due to its excellent properties, such as crack bridging, increase in elastic modulus, improvement of thermal conductivity and heat transfer, and lubricating effect, which lowers the friction coefficient and improves wear resistance of coatings composed of CNTs. What is more, the CNTs addition generally improves the corrosion resistance of coatings by sealing pores, increases coating adhesion strength, due to the formation of a network in the coating and has antibacterial properties, especially against gram-negative bacteria. In endoprosthesis applications, Young's modulus near the cortical bone (of 15–30 GPa [233]), reported in [142] causes the MWCNTs coatings to be a suitable candidate for biomedical applications. Besides medical applications, the most promising perspectives for nanocarbon can be considered for the production of advanced, highly anticorrosive and self-repairing coatings [16], for green energy applications [234], for electronic and photonics [235].

Although there are many reports analyzing the properties of various CNTs coatings and composites, there are still several challenges and further questions to answer. The first one is the cytotoxicity issue of CNTs. Even if the studies demonstrate a general role of increasing the cytotoxicity of CNTs a high dose of CNTs in the coating, the smallest diameter, and the longer length of CNTs, the impact of functionalization on cytotoxic activity is still not enough known. The functionalization of CNTs enables its solubility, its deposition via electrochemical methods, thus the charged particles are

required in this group of methods to prepare the coating, but there are also reports about its impact on decreasing the CNTs cytotoxicity [188–192], which still should be an open question to scientists.

Also, the adhesion mechanism of the CNTs coatings is a challenge to discuss. Up to now the adhesion of CNTs to some substrate occurs probably due to physical contact or weak van der Waals interaction, when describing coatings deposited electrochemically or by thermal sprayed methods. Nevertheless, the knowledge of CNTs adhesion mechanisms might be valuable when creating the solution for the problem with improvement of the adhesion strength of CNTs, which is also still challenging.

The same question might be posed on the subject of the bioactivity mechanism of CNTs, which is connected with the functionalization and adhesion strength of the CNTs-containing coating. The CNTs functionalization has an impact on coating surface architecture and thus cell adhesion, while the poor adhesion strength might be the reason for the excessive release of toxic substances in the human body.

The least but not last challenge for CNTs coatings is an improvement of its antibacterial properties against gram-positive bacteria. The gram-negative bacteria are protected by a narrow membrane, thus it is easier to break it and cause bacteria cell leakage, while gram-positive bacteria have up to 10 times thicker peptidoglycan walls and for, e.g., *B. subtilis* has peritrichous flagella structures which have smooth structure, so are unfavorable substrate for CNTs adhesion [198].

This review is a summary of coating properties composed of CNTs and different metals, ceramics and polymers, deposited on different substrates. The development of CNTs coatings still needs more research.

5 Conclusions

The state-of-the-art in the carbon nanotubes field shows a huge amount of research performed on CNTs coatings. The different forms of CNTs, deposition methods, and parameters, and substrates were applied as process variables. The microstructures, chemical and phase compositions, mechanical properties at the micro and nanoscale such as coating Young`s modulus and hardness, interface adhesion strength and delaminating force, open corrosion potential and corrosion current density, contact angle in wettability assessment, and bioactivity, cytotoxicity, and antibacterial efficiency among biological properties were determined. The following conclusions demonstrating valuable results and their implications, and still observed inefficiencies, can be drawn:

1. The MWCNTs are the most frequently and promising carbon nanoforms presumably because of the highest strength and the lowest Young`s modulus which is important for the mechanical behavior of coatings on artificial implants.
2. There is a diversity of deposition techniques applied for CNTs-containing coatings, all relatively similarly used, a choice of which depends on the expected properties and destination of the coated substrate.
3. Electrophoretic deposition is widely used for titanium and its alloys at the most preferred voltage of 5–30 V, time 0.5–5 min.
4. The roughness is the most plausible for biological application by coatings obtained by EPD, 0.2–1.0 μm, and the roughness of coatings prepared by thermal spray and plasma electrochemical oxidation seems excessive, 4–20 μm.
5. The shear strength test seems the most used technique to assess the adhesion which ranges between 15 and 35 MPa. The nanoindentation scratch technique seems the most precise for a great number of softer coatings, but it urgently needs to be quantified and standardized.
6. Hardness and Young`s modulus are measured by microhardness and nanoindentation tests and their values vary in wide limits depending on the substrate and phase and microstructure of a coating. The best hardness values reach 19 and 32 MPa for pure CNTs and CNTs strengthened with YSZ on steel substrate, relatively, and the lowest Young`s modulus is observed for the softer coatings on titanium and its alloys, 3–15 GPa. The use of either micro or nanohardness testing depends on the presumed toughness of a coating, and in such coatings is not highly accurate as evidenced by high values of standard deviations as compared to means.
7. Corrosion current density is only determined by potentiodynamic technique, and the obtained values range between some or tens of $\mu A/cm^2$. The corrosion resistance can presumably increase with a fraction of CNTs due to increasing inhomogeneity of coatings, still, however, remaining in a low corrosion rate area. The highest corrosion resistivity was observed for coatings with 1 wt% of CNTs.
8. The coatings CNTs-containing are hydrophilic, but their increasing content seems to lead toward higher contact angles. Such an effect might be expected for carbon nanoforms and likely can disappear after proper CNTs` functionalization.
9. The CNTs promote bioactivity assessed by the deposition of bone-like phosphates. However, the cytotoxicity of coatings implemented with long and narrow carbon nanotubes can be toxic, and this problem needs further thorough studies.

10. The coatings based on the CNTs show significant killing properties against the number of various bacteria, including the most dangerous encountered in hospitals.
11. Further research on the design and deposition of CNTs-including coatings is desired, in particular, to improve the adhesion of CNTs and the other components or a substrate, optimization of hardness and elasticity of coatings, and an assessment of relationships between cytotoxicity, functionalization, and content of CNTs in the coating.

Declarations

Conflict of interest The authors declare that they have no conflicts of interest.

References

1. Hopley EL, Salmasi S, Kalaskar DM, Seifalian AM (2014) Carbon nanotubes leading the way forward in new generation 3D tissue engineering. Biotechnol Adv 32:1000–1014. https://doi.org/10.1016/j.biotechadv.2014.05.003
2. Rathinavel S, Priyadharshini K, Panda D (2021) A review on carbon nanotube: an overview of synthesis, properties, functionalization, characterization, and the application. Mater Sci Eng B 268:115095. https://doi.org/10.1016/j.mseb.2021.115095
3. Iijima S (1991) Helical microtubules of graphitic carbon. Nature 354:56–58. https://doi.org/10.1038/354056a0
4. Thostenson ET, Ren Z, Chou T-W (2001) Advances in the science and technology of carbon nanotubes and their composites: a review. Compos Sci Technol 61:1899–1912. https://doi.org/10.1016/S0266-3538(01)00094-X
5. Khaniki HB, Ghayesh MH (2020) A review on the mechanics of carbon nanotube strengthened deformable structures. Eng Struct 220:110711. https://doi.org/10.1016/j.engstruct.2020.110711
6. Mousavi SR, Estaji S, Kiaei H et al (2022) A review of electrical and thermal conductivities of epoxy resin systems reinforced with carbon nanotubes and graphene-based nanoparticles. Polym Test 112:107645. https://doi.org/10.1016/j.polymertesting.2022.107645
7. Souto LFC, Henriques RR, Soares BG (2022) Influence of acidic and alkaline environmental anticorrosive performance of epoxy coatings based on polyaniline/carbon nanotube hybrids modified with ionic liquid. Prog Org Coat 173:107206. https://doi.org/10.1016/j.porgcoat.2022.107206
8. Li X, Wang J, Tian Y et al (2022) Thermal enhancement by constructing ordered-orienting hybrid network with modified boron nitride, graphene and carbon nanotubes in epoxy composite coatings. Prog Org Coat. https://doi.org/10.1016/j.porgcoat.2022.107078
9. Han W, Zhou J, Shi Q (2023) Research progress on enhancement mechanism and mechanical properties of FRP composites reinforced with graphene and carbon nanotubes. Alex Eng J 64:541–579. https://doi.org/10.1016/j.aej.2022.09.019
10. Qi X, Yang J, Zhang N et al (2021) Selective localization of carbon nanotubes and its effect on the structure and properties of polymer blends. Prog Polym Sci 123:101471. https://doi.org/10.1016/j.progpolymsci.2021.101471
11. Soni SK, Thomas B, Swain A, Roy T (2022) Functionally graded carbon nanotubes reinforced composite structures: an extensive review. Compos Struct 299:116075. https://doi.org/10.1016/j.compstruct.2022.116075
12. Deng H, Sheng L, Zhao X et al (2022) Non-noble metal FeMn and single-walled carbon nanotubes nanocomposites as effective bifunctional electrocatalysts in alkaline media for oxygen/hydrogen revolution reactions. Chin J Anal Chem 50:100110. https://doi.org/10.1016/j.cjac.2022.100110
13. Lee J, Kyeong D, Kim J, Choi W (2022) Layer-by-layer self-assembled functional coatings of carbon nanotube-polyethylenimine for enhanced heat transfer of heat sinks. Int J Heat Mass Transf. https://doi.org/10.1016/j.ijheatmasstransfer.2021.122344
14. Xia Y, Zhang S, Tong L et al (2022) Introducing cyano-functionalized multiwalled carbon nanotubes to improve corrosion resistance and mechanical performance of poly(arylene ether nitrile) coating. Surf Coat Technol 432:128058. https://doi.org/10.1016/j.surfcoat.2021.128058
15. Mao T, Li C, Mao F et al (2022) A durable anti-corrosion superhydrophobic coating based on carbon nanotubes and SiO2 aerogel for superior protection for Q235 steel. Diam Relat Mater 129:109370. https://doi.org/10.1016/j.diamond.2022.109370
16. Hosseinpour A, Rezaei Abadchi M, Mirzaee M, Tabar FA, Ramezanzadeh B (2021) Recent advances and future perspectives for carbon nanostructures reinforced organic coating for anti-corrosion application. Surf Interfaces 23:100994. https://doi.org/10.1016/j.surfin.2021.100994
17. Yan D, Zhang Z, Zhang W et al (2022) Smart self-healing coating based on the highly dispersed silica/carbon nanotube nanomaterial for corrosion protection of steel. Prog Org Coat 164:106694. https://doi.org/10.1016/j.porgcoat.2021.106694
18. Islam A, Pandey KK, Singh P et al (2022) Microstructural, mechanical and tribological properties of carbon nanotubes reinforced plasma sprayed molybdenum disulphide composite coatings. Ceram Int 48:32757–32766. https://doi.org/10.1016/j.ceramint.2022.07.200
19. Han B, Chen Y, Tan C et al (2022) Microstructure and wear behavior of laser clad interstitial CoCrFeNi high entropy alloy coating reinforced by carbon nanotubes. Surf Coat Technol 434:128241. https://doi.org/10.1016/j.surfcoat.2022.128241
20. Gu Y, Ma L, Yan M et al (2022) Strategies for improving friction behavior based on carbon nanotube additive materials. Tribol Int 176:107875. https://doi.org/10.1016/j.triboint.2022.107875
21. Zhu Z, Kang S, Chen H et al (2022) Construction of superhydrophobic alkyl siloxane-modified carbon nanotubes/epoxy coating. Diam Relat Mater 129:109351. https://doi.org/10.1016/j.diamond.2022.109351
22. Ma Y, Zhang J, Zhu G et al (2022) Robust photothermal self-healing superhydrophobic coating based on carbon nanosphere/carbon nanotube composite. Mater Des 221:110897. https://doi.org/10.1016/j.matdes.2022.110897
23. Zhang X, Mo Z, Arenal R et al (2023) Efficient oil-water separation by a robust superhydrophobic coating prepared directly

from commercial lacquer using silanized multi-walled carbon nanotubes as filler. Appl Surf Sci 609:155208. https://doi.org/10.1016/j.apsusc.2022.155208
24. Liu Y, Shao Y, Wang Y, Wang J (2022) An abrasion-resistant, photothermal, superhydrophobic anti-icing coating prepared by polysiloxane-modified carbon nanotubes and fluorine-silicone resin. Colloids Surf A 648:129335. https://doi.org/10.1016/j.colsurfa.2022.129335
25. Liu N, Guo L, Kou G et al (2022) Carbon nanotube reinforced pyrocarbon matrix composites with high coefficient of thermal expansion for self-adapting ultra-high-temperature ceramic coatings. Ceram Int 48:15668–15676. https://doi.org/10.1016/j.ceramint.2022.02.101
26. Hu L, Kang Z (2021) Enhanced flexible polypropylene fabric with silver/magnetic carbon nanotubes coatings for electromagnetic interference shielding. Appl Surf Sci 568:150845. https://doi.org/10.1016/j.apsusc.2021.150845
27. Chen C, Xiao G, Zhong F et al (2022) Synergistic effect of carbon nanotubes bonded graphene oxide to enhance the flame retardant performance of waterborne intumescent epoxy coatings. Prog Org Coat 162:106598. https://doi.org/10.1016/j.porgcoat.2021.106598
28. Chen C, Xiao G, Zhong F et al (2022) Dendritic-hydroxyzinc stannate loaded carbon nanotubes for enhancing flame retardancy of composite coatings. Colloids Surf A Physicochem Eng Asp 648:129329. https://doi.org/10.1016/j.colsurfa.2022.129329
29. Zhan W, Ni L, Gu Z et al (2021) The influences of graphene and carbon nanotubes on properties of waterborne intumescent fire resistive coating. Powder Technol 385:572–579. https://doi.org/10.1016/j.powtec.2021.03.018
30. Agasti N, Gautam V, Priyanka N et al (2022) Carbon nanotube based magnetic composites for decontamination of organic chemical pollutants in water: a review. Appl Surf Sci Adv 10:100270. https://doi.org/10.1016/j.apsadv.2022.100270
31. Lin WT, Lin ZW, Kuo TY et al (2022) Mechanical and biological properties of atmospheric plasma-sprayed carbon nanotube-reinforced tantalum pentoxide composite coatings on Ti6Al4V alloy. Surf Coat Technol 437:128356. https://doi.org/10.1016/j.surfcoat.2022.128356
32. Cha JH, Jang WH, Noh JE et al (2022) A space stealth and cosmic radiation shielding composite: polydopamine-coating and multi-walled carbon nanotube grafting onto an ultra-high-molecular-weight polyethylene/hydrogen-rich benzoxazine composite. Compos Sci Technol 230:109711. https://doi.org/10.1016/j.compscitech.2022.109711
33. Wang F, Zhao S, Jiang Q et al (2022) Advanced functional carbon nanotube fibers from preparation to application. Cell Rep Phys Sci 3:100989. https://doi.org/10.1016/j.xcrp.2022.100989
34. Dong Z, Sun B, Zhu H et al (2021) A review of aligned carbon nanotube arrays and carbon/carbon composites: fabrication, thermal conduction properties and applications in thermal management. New Carbon Mater 36:873–892. https://doi.org/10.1016/S1872-5805(21)60090-2
35. Shahzad N, Lutfullah PT et al (2022) Counter electrode materials based on carbon nanotubes for dye-sensitized solar cells. Renew Sustain Energy Rev 159:112196. https://doi.org/10.1016/j.rser.2022.112196
36. Xia Y, Zhu X, Qiu P et al (2022) Nano-confinement coating strategy derived Matryoshka-like carbon nanotubes@anatase nanocrystalline@amorphous carbon nanofibers for ultrafast sodium ion storage. Electrochim Acta 428:140941. https://doi.org/10.1016/j.electacta.2022.140941
37. Zakaria MR, Omar MF, Zainol Abidin MS et al (2022) Recent progress in the three-dimensional structure of graphene-carbon nanotubes hybrid and their supercapacitor and high-performance battery applications. Compos Part 154:106756. https://doi.org/10.1016/j.compositesa.2021.106756
38. Khan N, Han G, Mazari SA (2022) Carbon nanotubes-based anode materials for potassium ion batteries: a review. J Electroanal Chem 907:116051. https://doi.org/10.1016/j.jelechem.2022.116051
39. Jyoti J, Gupta TK, Singh BP et al (2022) Recent advancement in three dimensional graphene-carbon nanotubes hybrid materials for energy storage and conversion applications. J Energy Storage 50:104235. https://doi.org/10.1016/j.est.2022.104235
40. Afsarimanesh N, Nag A, Eshrat e Alahi M et al (2022) A critical review of the recent progress on carbon nanotubes-based nanogenerators. Sens Actuators A 344:113743. https://doi.org/10.1016/j.sna.2022.113743
41. Tran PA, Zhang L, Webster TJ (2009) Carbon nanofibers and carbon nanotubes in regenerative medicine. Adv Drug Deliv Rev 61:1097–1114. https://doi.org/10.1016/j.addr.2009.07.010
42. Raphey VR, Henna TK, Nivitha KP et al (2019) Advanced biomedical applications of carbon nanotube. Mater Sci Eng C 100:616–630. https://doi.org/10.1016/j.msec.2019.03.043
43. Liu X, Miller AL, Park S et al (2017) Functionalized carbon nanotube and graphene oxide embedded electrically conductive hydrogel synergistically stimulates nerve cell differentiation. ACS Appl Mater Interfaces 9:14677–14690. https://doi.org/10.1021/acsami.7b02072
44. Xiang C, Zhang Y, Guo W, Liang X-J (2020) Biomimetic carbon nanotubes for neurological disease therapeutics as inherent medication. Acta Pharm Sin B 10:239–248. https://doi.org/10.1016/j.apsb.2019.11.003
45. Mezzasalma SA, Grassi L, Grassi M (2021) Physical and chemical properties of carbon nanotubes in view of mechanistic neuroscience investigations Some outlook from condensed matter, materials science and physical chemistry. Mater Sci Eng C 131:112480. https://doi.org/10.1016/j.msec.2021.112480
46. Sebaa M, Nguyen TY, Paul RK et al (2013) Graphene and carbon nanotube–graphene hybrid nanomaterials for human embryonic stem cell culture. Mater Lett 92:122–125. https://doi.org/10.1016/j.matlet.2012.10.035
47. Foldvari M, Bagonluri M (2008) Carbon nanotubes as functional excipients for nanomedicines: I. pharmaceutical properties. Nanomedicine 4:173–182. https://doi.org/10.1016/j.nano.2008.04.002
48. Murjani BO, Kadu PS, Bansod M et al (2022) Carbon nanotubes in biomedical applications: current status, promises, and challenges. Carbon Lett 32:1207–1226. https://doi.org/10.1007/s42823-022-00364-4
49. Anzar N, Hasan R, Tyagi M et al (2020) Carbon nanotube—a review on Synthesis, Properties and plethora of applications in the field of biomedical science. Sens Int 1:100003. https://doi.org/10.1016/j.sintl.2020.100003
50. Kravanja KA, Finšgar M (2022) A review of techniques for the application of bioactive coatings on metal-based implants to achieve controlled release of active ingredients. Mater Des 217:110653. https://doi.org/10.1016/j.matdes.2022.110653
51. Bjelić D, Finšgar M (2022) Bioactive coatings with anti-osteoclast therapeutic agents for bone implants: enhanced compliance and prolonged implant life. Pharmacol Res 176:106060. https://doi.org/10.1016/j.phrs.2022.106060
52. Zhao X, Chang S, Long J et al (2019) The toxicity of multi-walled carbon nanotubes (MWCNTs) to human endothelial cells: the influence of diameters of MWCNTs. Food Chem Toxicol 126:169–177. https://doi.org/10.1016/j.fct.2019.02.026
53. Barrejón M, Marchesan S, Alegret N, Prato M (2021) Carbon nanotubes for cardiac tissue regeneration: state of the art and

perspectives. Carbon 184:641–650. https://doi.org/10.1016/j.carbon.2021.08.059
54. Arumugam S, Ju Y (2021) Carbon nanotubes reinforced with natural/synthetic polymers to mimic the extracellular matrices of bone—a review. Mater Today Chem 20:100420. https://doi.org/10.1016/j.mtchem.2020.100420
55. Zieliński A, Majkowska-Marzec B (2022) Whether carbon nanotubes are capable, promising, and safe for their application in nervous system regeneration. Some critical remarks and research strategies. Coatings 12:1643. https://doi.org/10.3390/coatings12111643
56. Teixeira-Santos R, Gomes M, Gomes LC, Mergulhão FJ (2021) Antimicrobial and anti-adhesive properties of carbon nanotube-based surfaces for medical applications: a systematic review. iScience 24:102001. https://doi.org/10.1016/j.isci.2020.102001
57. Horandghadim N, Ghazanfar-Ahari Y, Khalil-Allafi J (2022) Multiwalled-carbon nanotubes reinforced hydroxyapatite-tantalum pentoxide nanocomposite coating on Nitinol alloy: antibacterial activity and Electrochemical properties. Surf Interfaces 29:101773. https://doi.org/10.1016/j.surfin.2022.101773
58. Hadzhieva Z, Boccaccini AR (2022) Recent developments in electrophoretic deposition (EPD) of antibacterial coatings for biomedical applications—a review. Curr Opin Biomed Eng 21:100367. https://doi.org/10.1016/j.cobme.2021.100367
59. Dai B, Zhou R, Ping J et al (2022) Recent advances in carbon nanotube-based biosensors for biomolecular detection. TrAC Trends Anal Chem 154:116658. https://doi.org/10.1016/j.trac.2022.116658
60. Hurt RH, Monthioux M, Kane A (2006) Toxicology of carbon nanomaterials: status, trends, and perspectives on the special issue. Carbon 44:1028–1033. https://doi.org/10.1016/j.carbon.2005.12.023
61. Alshehri R, Ilyas AM, Hasan A et al (2016) Carbon nanotubes in biomedical applications: factors, mechanisms, and remedies of toxicity. J Med Chem 59:8149–8167. https://doi.org/10.1021/acs.jmedchem.5b01770
62. Kong H, Wang L, Zhu Y et al (2015) Culture medium-associated physicochemical insights on the cytotoxicity of carbon nanomaterials. Chem Res Toxicol 28:290–295. https://doi.org/10.1021/tx500477y
63. Kobayashi N, Izumi H, Morimoto Y (2017) Review of toxicity studies of carbon nanotubes. J Occup Health 59:394–407. https://doi.org/10.1539/joh.17-0089-RA
64. Gaillard C, Cellot G, Li S et al (2009) Carbon nanotubes carrying cell-adhesion peptides do not interfere with neuronal functionality. Adv Mater 21:2903–2908. https://doi.org/10.1002/adma.200900050
65. Abousalman-Rezvani Z, Eskandari P, Roghani-Mamaqani H, Salami-Kalajahi M (2020) Functionalization of carbon nanotubes by combination of controlled radical polymerization and "grafting to" method. Adv Colloid Interface Sci 278:102126. https://doi.org/10.1016/j.cis.2020.102126
66. Eskandari P, Abousalman-Rezvani Z, Roghani-Mamaqani H, Salami-Kalajahi M (2021) Polymer-functionalization of carbon nanotube by in situ conventional and controlled radical polymerizations. Adv Colloid Interface Sci 294:102471. https://doi.org/10.1016/j.cis.2021.102471
67. Hosseini H, Ghaffarzadeh M (2022) Surface functionalization of carbon nanotubes via plasma discharge: a review. Inorg Chem Commun 138:109276. https://doi.org/10.1016/j.inoche.2022.109276
68. Lavagna L, Nisticò R, Musso S, Pavese M (2021) Functionalization as a way to enhance dispersion of carbon nanotubes in matrices: a review. Mater Today Chem 20:100477. https://doi.org/10.1016/j.mtchem.2021.100477
69. Klein KL, Melechko AV, McKnight TE et al (2008) Surface characterization and functionalization of carbon nanofibers. J Appl Phys 103:061301. https://doi.org/10.1063/1.2840049
70. Asghar F, Murtaza B, Shakoor B et al (2022) Properties, assembly and characterization of carbon nanotubes: their application in water purification, environmental pollution control and biomedicines—a comprehensive review. Carbon Lett 33:275–306. https://doi.org/10.1007/s42823-022-00432-9
71. Banhart F (2020) Elemental carbon in the sp1 hybridization. ChemTexts 6:3. https://doi.org/10.1007/s40828-019-0098-z
72. Eatemadi A, Daraee H, Karimkhanloo H et al (2014) Carbon nanotubes: properties, synthesis, purification, and medical applications. Nanoscale Res Lett 9:393. https://doi.org/10.1186/1556-276X-9-393
73. Guler O, Bagci N (2020) A short review on mechanical properties of graphene reinforced metal matrix composites. J Mater Res Technol 9:6808–6833. https://doi.org/10.1016/J.JMRT.2020.01.077
74. Choudhary V, Gupt A (2011) Polymer/carbon nanotube nanocomposites. In: Silva Y (ed) Carbon nanotubes—polymer nanocomposites. InTech, pp 65–90. ISBN: 978-953-307-498-6. http://www.intechopen.com/books/carbon-nanotubes-polymer-nanocomposites/polymer-carbon-nanotube-nanocomposites. Accessed Sept 2023
75. Cai Shen H, Brozena A, Wang YuHuang (2011) Double-walled carbon nanotubes: challenges and opportunities. Nanoscale 3:503–518. https://doi.org/10.1039/C0NR00620C
76. Fonseca A, Hernadi K, Piedigrosso P et al (1998) Synthesis of single- and multi-wall carbon nanotubes over supported catalysts. Appl Phys A 67:11–22. https://doi.org/10.1007/S003390050732
77. Kang J, Al-Sabah S, Théo R (2020) Effect of single-walled carbon nanotubes on strength properties of cement composites. Materials 13:1305. https://doi.org/10.3390/ma13061305
78. Hussain A, Liao Y, Zhang Q et al (2018) Floating catalyst CVD synthesis of single walled carbon nanotubes from ethylene for high performance transparent electrodes. Nanoscale 10:9752–9759. https://doi.org/10.1039/C8NR00716K
79. Liu Y, Qian W, Zhang Q et al (2008) The confined growth of double-walled carbon nanotubes in porous catalysts by chemical vapor deposition. Carbon 46:1860–1868. https://doi.org/10.1016/j.carbon.2008.07.040
80. He M, Magnin Y, Amara H et al (2017) Linking growth mode to lengths of single-walled carbon nanotubes. Carbon 113:231–236. https://doi.org/10.1016/j.carbon.2016.11.057
81. Saito Y, Nakahira T, Uemura S (2003) Growth conditions of double-walled carbon nanotubes in arc discharge. J Phys Chem B 107:931–934. https://doi.org/10.1021/jp021367o
82. Rashad AA, Abd S, Mohammed A et al (2016) Synthesis of carbon nanotube: a review. J Nanosci Technol 2:155–162
83. Choudhary V, Singh BP, Mathur RB (2013) Carbon nanotubes and their composites. In: Satoru S (ed) Syntheses and applications of carbon nanotubes and their composites. InTech, pp 193–222. https://doi.org/10.5772/52897 (**ISBN: 978-953-51-1125-2**)
84. Doh J, Lee J (2016) Prediction of the mechanical behavior of double walled-CNTs using a molecular mechanics-based finite element method: Effects of chirality. Comput Struct 169:91–100. https://doi.org/10.1016/j.compstruc.2016.03.006
85. Kumar R, Singh RK, Ghosh AK et al (2013) Synthesis of coal-derived single-walled carbon nanotube from coal by varying the ratio of Zr/Ni as bimetallic catalyst. J Nanopart Res 15:1406. https://doi.org/10.1007/s11051-012-1406-3
86. Tian Y, Zhang Y, Wang B et al (2004) Coal-derived carbon nanotubes by thermal plasma jet. Carbon 42:2597–2601. https://doi.org/10.1016/j.carbon.2004.05.042

87. Hoang VC, Hassan M, Gomes VG (2018) Coal derived carbon nanomaterials—recent advances in synthesis and applications. Appl Mater Today 12:342–358. https://doi.org/10.1016/j.apmt.2018.06.007
88. Dorfman MR (2018) Thermal spray coatings. In: Myer K (ed) Handbook of environmental degradation of materials, 3rd edn. Elsevier, New York, pp 469–488. https://doi.org/10.1016/B978-0-323-52472-8.00023-X
89. Vuoristo P (2014) Thermal spray coating processes. In: Saleem H, Gilmar FB, Chester JVT, Bekir Y (eds) Comprehensive materials processing. Elsevier, Woodhead Publishing, New York, pp 229–276. https://doi.org/10.1016/B978-0-08-096532-1.00407-6
90. Venturi F, Kamnis S, Hussain T (2021) Internal diameter HVOAF thermal spray of carbon nanotubes reinforced WC-Co composite coatings. Mater Des 202:109566. https://doi.org/10.1016/j.matdes.2021.109566
91. Lombardi AN, Casteletti LC, Totten GE (2013) Thermal spray technologies: an overview. In: Wang QJ, Chung YW (eds) Encyclopedia of tribology. Springer, US, Boston, pp 3607–3617. https://doi.org/10.1007/978-0-387-92897-5_684
92. Makhlouf ASH (2011) Current and advanced coating technologies for industrial applications. In: Abdel SHM, Ion T (eds) Nanocoatings and ultra-thin films. Elsevier, Woodhead Publishing, New York, pp 3–23. https://doi.org/10.1533/9780857094902.1.3
93. Wang M (2010) Composite coatings for implants and tissue engineering scaffolds. In: Luigi A (ed) Biomedical composites. Elsevier, Woodhead Publishing Series in Biomaterials, New York, pp 127–177. https://doi.org/10.1533/9781845697372.2.127
94. He P, Wang H, Chen S et al (2020) Interface characterization and scratch resistance of plasma sprayed TiO_2-CNTs nanocomposite coating. J Alloys Compd 819:153009. https://doi.org/10.1016/j.jallcom.2019.153009
95. Xie X, Tan Z, Chen C et al (2021) Synthesis of carbon nanotube reinforced Al matrix composite coatings via cold spray deposition. Surf Coat Technol 405:126676. https://doi.org/10.1016/j.surfcoat.2020.126676
96. Assadi H, Gärtner F, Stoltenhoff T, Kreye H (2003) Bonding mechanism in cold gas spraying. Acta Mater 51:4379–4394. https://doi.org/10.1016/S1359-6454(03)00274-X
97. Basha GMT, Bolleddu V (2021) Tribological behavior of carbon nanotubes reinforced high velocity oxy-fuel sprayed WC-20 wt% Co coatings. J Therm Spray Technol 30:1653–1665. https://doi.org/10.1007/s11666-021-01230-x
98. Li M, Christofides PD (2009) Modeling and control of high-velocity oxygen-fuel (HVOF) thermal spray: a tutorial review. J Therm Spray Technol 18:753–768. https://doi.org/10.1007/s11666-009-9309-2
99. Tucker RC (1995) Plasma spray, detonation gun, and HVOF deposition techniques. In: Yves P (ed) Materials and processes for surface and interface engineering, NATO ASI series, vol 290. Springer, Dordrecht, pp 245–284. https://doi.org/10.1007/978-94-011-0077-9_7
100. Murray JW, Rance GA, Xu F, Hussain T (2018) Alumina-graphene nanocomposite coatings fabricated by suspension high velocity oxy-fuel thermal spraying for ultra-low-wear. J Eur Ceram Soc 38:1819–1828. https://doi.org/10.1016/j.jeurceramsoc.2017.10.022
101. Mishra NK, Mishra SB (2015) Hot corrosion performance of LVOF sprayed Al_2O_3–40% TiO_2 coating on Superni 601 and Superco 605 superalloys at 800 and 900 °C. Bull Mater Sci 38:1679–1685. https://doi.org/10.1007/s12034-015-0986-9
102. Moonngam S, Tunjina P, Deesom D, Banjongprasert C (2016) Fe-Cr/CNTs nanocomposite feedstock powders produced by chemical vapor deposition for thermal spray coatings. Surf Coat Technol 306:323–327. https://doi.org/10.1016/j.surfcoat.2016.07.024
103. Huang Y, Zhu L, Huang Q, He Z (2022) The light absorption enhancement of nanostructured carbon-based coatings fabricated by high-voltage electrostatic spraying technique. Opt Mater (Amst) 133:112902. https://doi.org/10.1016/j.optmat.2022.112902
104. Quintino L (2014) Overview of coating technologies. In: Miranda R (ed) Surface modification by solid state processing. Elsevier, Woodhead Publishing, New York, pp 1–24. https://doi.org/10.1533/9780857094698.1
105. Shivamurthy RC, Kamaraj M, Nagarajan R, Shariff SM, Padmanabham G (2012) Laser surface modification of steel for slurry erosion resistance in power plants. In: Kwok CT (ed) Laser surface modification of alloys for corrosion and erosion resistance. In Woodhead Publishing series in metals and surface engineering. Elsevier, New York, pp 177–287. https://doi.org/10.1533/9780857095831.2.177
106. Yuan W, Li R, Chen Z et al (2021) A comparative study on microstructure and properties of traditional laser cladding and high-speed laser cladding of Ni45 alloy coatings. Surf Coat Technol 405:126582. https://doi.org/10.1016/j.surfcoat.2020.126582
107. Zhang Y, Wang Q, Ye R, Ramachandran CS (2022) Plasma electrolytic oxidation of cold spray kinetically metallized CNT-Al coating on AZ91-Mg alloy: evaluation of mechanical and surficial characteristics. J Alloys Compd 892:162094. https://doi.org/10.1016/j.jallcom.2021.162094
108. Xie X, Chen C, Ji G, Xu R, Tan Z, Xie Y, Li Z, Liao H (2019) A novel approach for fabricating a CNT/AlSi composite with the self-aligned nacre-like architecture by cold spraying. Nano Mater Sci 1:137–141. https://doi.org/10.1016/j.nanoms.2019.04.002
109. Joshi B, Samuel E, Kim Y, Yarin AL, Swihart MT, Yoon SS (2021) Electrostatically sprayed nanostructured electrodes for energy conversion and storage devices. Adv Funct Mater 31:2008181. https://doi.org/10.1002/adfm.202008181
110. Li G, Feng L, Tong P, Zhai Z (2016) The properties of MWCNT/polyurethane conductive composite coating prepared by electrostatic spraying. Prog Org Coat 90:284–290. https://doi.org/10.1016/j.porgcoat.2015.10.018
111. Rogala-Wielgus D, Majkowska-Marzec B, Zieliński A et al (2021) Mechanical behavior of bi-layer and dispersion coatings composed of several nanostructures on Ti13Nb13Zr alloy. Materials 14:2905. https://doi.org/10.3390/ma14112905
112. Majkowska-Marzec B, Tęczar P, Bartmański M et al (2020) Mechanical and corrosion properties of laser surface-treated Ti13Nb13Zr alloy with MWCNTs coatings. Materials 13:3991. https://doi.org/10.3390/ma13183991
113. Khalili V, Khalil-Allafi J, Maleki-Ghaleh H, Paulsen A, Frenzel J, Eggeler G (2016) The influence of Si as reactive bonding agent in the electrophoretic coatings of HA–Si–MWCNTs on NiTi alloys. J Mater Eng Perform 25:390–400. https://doi.org/10.1007/s11665-015-1824-3
114. Bordbar M, Alimohammadi T, Khoshnevisan B, Khodadadi B, Yeganeh-Faal A (2015) Preparation of MWCNT/TiO_2 –Co nanocomposite electrode by electrophoretic deposition and electrochemical study of hydrogen storage. Int J Hydrogen Energy 40:9613–9620. https://doi.org/10.1016/j.ijhydene.2015.05.138
115. Chávez-Valdez A, Boccaccini AR (2012) Innovations in electrophoretic deposition: alternating current and pulsed direct current methods. Electrochim Acta 65:70–89. https://doi.org/10.1016/j.electacta.2012.01.015
116. Dicu MM, Balteanu AM (2021) Coating techniques for materials medical: a mini-review. In: Proceedings of the 13th international conference on electronics, computers and artificial intelligence,

ECAI 2021. Institute of Electrical and Electronics Engineers Inc, pp: 1–5. https://doi.org/10.1109/ECAI52376.2021.9515152
117. Abdel-Karim R (2016) Electrochemical synthesis of nanocomposites. In: Mohamed AMA, Golden TD (eds) Electrodeposition of composite materials. InTech. https://doi.org/10.5772/62189 (**ISBN: 978-953-51-2270-8**)
118. Azmi AA, Jai J, Zamanhuri NA, Yahya A (2018) Precious metals recovery from electroplating wastewater: a review. IOP Conf Ser Mater Sci Eng 358:012024. https://doi.org/10.1088/1757-899X/358/1/012024
119. Yuan W, Li R, Zhu Y et al (2022) Structure and properties of nickel-plated CNTs/Fe-based amorphous composite coatings fabricated by high-speed laser cladding. Surf Coat Technol 438:128363. https://doi.org/10.1016/j.surfcoat.2022.128363
120. Li QH, Savalani MM, Zhang QM, Huo L (2014) High temperature wear characteristics of TiC composite coatings formed by laser cladding with CNT additives. Surf Coat Technol 239:206–211. https://doi.org/10.1016/j.surfcoat.2013.11.043
121. Zhai L, Ban C, Zhang J, Yao X (2019) Characteristics of dilution and microstructure in laser cladding Ni-Cr-B-Si coating assisted by electromagnetic compound field. Mater Lett 243:195–198. https://doi.org/10.1016/j.matlet.2019.01.133
122. Liu J, Sun W, Huang Y (2021) Effect of carbon nanotubes content on microstructure and properties of WC/Ni laser cladding coatings. Surf Eng 37:650–657. https://doi.org/10.1080/02670844.2020.1812481
123. Bakshi SR, Singh V, Seal S, Agarwal A (2009) Aluminum composite reinforced with multiwalled carbon nanotubes from plasma spraying of spray dried powders. Surf Coat Technol 203:1544–1554. https://doi.org/10.1016/j.surfcoat.2008.12.004
124. Bakshi SR, Keshri AK, Agarwal A (2011) A comparison of mechanical and wear properties of plasma sprayed carbon nanotube reinforced aluminum composites at nano and macro scale. Mater Sci Eng A 528:3375–3384. https://doi.org/10.1016/j.msea.2011.01.061
125. Abdulameer S, Al-Sultani KF, Majdi HS (2022) MWCNTS-YSZ coating deposited by plasma thermal spray on ICONEL 738 low carbon substrate. Mater Today Proc 60:1241–1247. https://doi.org/10.1016/j.matpr.2021.08.144
126. Yu L, Jia P, Song Y et al (2022) Effect of carbon nanotubes on the microstructure and properties of plasma electrolytic oxidized ceramic coatings on high silicon aluminum alloy. J Mater Res Technol 18:3541–3552. https://doi.org/10.1016/j.jmrt.2022.04.035
127. Thakare JG, Mulik RS, Mahapatra MM (2018) Effect of carbon nanotubes and aluminum oxide on the properties of a plasma sprayed thermal barrier coating. Ceram Int 44:438–451. https://doi.org/10.1016/j.ceramint.2017.09.196
128. Daram P, Banjongprasert C, Thongsuwan W, Jiansirisomboon S (2016) Microstructure and photocatalytic activities of thermal sprayed titanium dioxide/carbon nanotubes composite coatings. Surf Coat Technol 306:290–294. https://doi.org/10.1016/j.surfcoat.2016.06.068
129. Mohammed Thalib Basha G, Srikanth A, Venkateshwarlu B (2020) Effect of reinforcement of carbon nanotubes on air plasma sprayed conventional Al_2O_3–3%TiO_2 ceramic coatings. Mater Today Proc 20:191–194. https://doi.org/10.1016/J.MATPR.2019.11.025
130. Zhang Y, Wang Q, Chen G, Ramachandran CS (2020) Mechanical, tribological and corrosion physiognomies of CNT-Al metal matrix composite (MMC) coatings deposited by cold gas dynamic spray (CGDS) process. Surf Coat Technol 403:126380. https://doi.org/10.1016/j.surfcoat.2020.126380
131. Pialago EJT, Kwon OK, Park CW (2013) Nucleate boiling heat transfer of R134a on cold sprayed CNT–Cu composite coatings. Appl Therm Eng 56:112–119. https://doi.org/10.1016/j.applthermaleng.2013.03.046
132. Pialago EJT, Kwon OK, Kim M-S, Park CW (2015) Ternary Cu–CNT–AlN composite coatings consolidated by cold spray deposition of mechanically alloyed powders. J Alloys Compd 650:199–209. https://doi.org/10.1016/j.jallcom.2015.08.007
133. Pialago EJT, Kwon OK, Jin JS, Park CW (2016) Nucleate pool boiling of R134a on cold sprayed Cu–CNT–SiC and Cu–CNT–AlN composite coatings. Appl Therm Eng 103:684–694. https://doi.org/10.1016/j.applthermaleng.2016.04.022
134. Ye Z, Li J, Liu L et al (2021) Microstructure and wear performance enhancement of carbon nanotubes reinforced composite coatings fabricated by laser cladding on titanium alloy. Opt Laser Technol 139:106957. https://doi.org/10.1016/j.optlastec.2021.106957
135. Pialago EJT, Yoo J, Zheng X, Zhenga X, Kima BR, Honga SJ, Kwonb OK, Park CW (2020) Experimental investigation of the heat transfer performance of capillary-assisted horizontal evaporator tubes with sintered porous hydrophilic copper-carbon nanotube-titanium dioxide (Cu–CNT–TiO_2) composite coatings for adsorption chiller. Int J Heat Mass Transf 147:118958. https://doi.org/10.1016/j.ijheatmasstransfer.2019.118958
136. Tripathi P, Katiyar PK, Ramkumar J, Balani K (2020) Synergistic role of carbon nanotube and yttria stabilised zirconia reinforcement on wear and corrosion resistance of Cr-based nano-composite coatings. Surf Coat Technol 385:125381. https://doi.org/10.1016/j.surfcoat.2020.125381
137. Shukla P, Awasthi S, Ramkumar J, Balani K (2018) Protective trivalent Cr-based electrochemical coatings for gun barrels. J Alloys Compd 768:1039–1048. https://doi.org/10.1016/j.jallcom.2018.07.170
138. Suzuki T, Konno T (2014) Improvement in tool life of electroplated diamond tools by Ni-based carbon nanotube composite coatings. Precis Eng 38:659–665. https://doi.org/10.1016/j.precisioneng.2014.03.003
139. Deesom D, Charoenrut K, Moonngam S, Banjongprasert C (2016) Fabrication and properties of NiCr/CNTs nanocomposite coatings prepared by High Velocity Oxy-Fuel Spraying. Surf Coat Technol 306:240–244. https://doi.org/10.1016/j.surfcoat.2016.06.016
140. Dlugon E, Simka W, Fraczek-Szczypta A, Niemiec W, Markowski J, Szymanska M, Blazewicz M (2015) Carbon nanotube-based coatings on titanium. Bull Mater Sci 38:1339–1344. https://doi.org/10.1007/s12034-015-1019-4
141. Singh I, Allan P, London W (2007) Nano-mechanical testing of novel bioactive carbon nanotubes/HAP nano particles composite coating. NSTI Nanotech 4:145–148
142. Majkowska-Marzec B, Rogala-Wielgus D, Bartmański M et al (2019) Comparison of properties of the hybrid and bilayer MWCNTs—hydroxyapatite coatings on Ti Alloy. Coatings 9:643. https://doi.org/10.3390/coatings9100643
143. Rogala-Wielgus D, Majkowska-Marzec B, Zieliński A, Jankiewicz BJ (2021) Mechanical behavior of bi-layer and dispersion coatings composed of several nanostructures on Ti substrate. Appl Sci 11:7862. https://doi.org/10.3390/app11177862
144. Xu L, Wang J, Wu R, Wang J, Wu H, Li Y, Hou L, Zhang J (2021) Microstructure and mechanical properties of Mg-14Li-1Al/MWCNTs composites prepared by electrophoretic deposition and accumulative roll bonding. J Manuf Process 72:431–438. https://doi.org/10.1016/j.jmapro.2021.10.040
145. Maleki-Ghaleh H, Khalil-Allafi J (2019) Effect of hydroxyapatite-titanium-MWCNTs composite coating fabricated by electrophoretic deposition on corrosion and cellular behavior of NiTi alloy. Mater Corr 70:2128–2138. https://doi.org/10.1002/maco.201910940

146. Zhu QG, Sujari ANA, Ab Ghani S (2012) Electrophoretic deposited MWCNT composite graphite pencils and its uses to determine hyperin. J Solid State Electrochem 16:3179–3187. https://doi.org/10.1007/s10008-012-1749-9
147. Majkowska-Marzec B, Sypniewska J (2021) Microstructure and mechanical properties of laser surface-treated Ti13Nb13Zr alloy with MWCNTs coatings. Adv Mater Sci 21:5–18. https://doi.org/10.2478/adms-2021-0021
148. Nguyen TT, Pham NT, Dinh TTM, Vu TT, Nguyen HS, Tran LD (2020) Electrodeposition of hydroxyapatite-multiwalled carbon nanotube nanocomposite on Ti6Al4V. Adv Polym Technol 2020:1–10. https://doi.org/10.1155/2020/8639687
149. Sundaram RM, Sekiguchi A, Sekiya M et al (2018) Copper/carbon nanotube composites: research trends and outlook. R Soc Open Sci 5:180814. https://doi.org/10.1098/rsos.180814
150. Datta M (2009) Electrodeposition. In: Shacham-Diamand Y, Osaka T, Datta M, Ohba T (eds) Advanced nanoscale ULSI interconnects: fundamentals and applications. Springer, New York, pp 63–71. https://doi.org/10.1007/978-0-387-95868-2_4
151. Nasirpouri F, Yousefi I, Moslehifard E, Khalil-Allafi J (2017) Tuning surface morphology and crystallinity of anodic TiO_2 nanotubes and their response to biomimetic bone growth for implant applications. Surf Coat Technol 315:163–171. https://doi.org/10.1016/j.surfcoat.2017.02.006
152. Yang Y, Yu M, Böke F, Qina Q, Hübnerc R, Knusta S, Schwidereka S, Grundmeiera G, Fischerb H, Keller A (2021) Effect of nanoscale surface topography on the adsorption of globular proteins. Appl Surf Sci 535:147671. https://doi.org/10.1016/j.apsusc.2020.147671
153. Yang C, Jian R, Huang K, Wang Q, Feng B (2021) Antibacterial mechanism for inactivation of *E. coli* by AgNPs@polydoamine/titania nanotubes via speciation analysis of silver ions and silver nanoparticles by cation exchange reaction. Microchem J 160:105636. https://doi.org/10.1016/j.microc.2020.105636
154. Li N, Sun S, Bai H, Xu W, Xiao G, Zhang Y, Lu Y (2020) Evolution of nano/submicro-scale oxide structures on Ti6Al4V achieved by an ultrasonic shot peening-induction heating approach for high-performance surface design of bone implants. J Alloys Compd 831:154876. https://doi.org/10.1016/j.jallcom.2020.154876
155. Elias CN, Fernandes DJ, Resende CRS, Roestel J (2015) Mechanical properties, surface morphology and stability of a modified commercially pure high strength titanium alloy for dental implants. Dent Mater 31:e1–e13. https://doi.org/10.1016/j.dental.2014.10.002
156. Lee Y, Jung A, Heo S-J, Gweona B, Lim D (2023) Influences of surface topography of porous titanium scaffolds manufactured by powder bed fusion on osteogenesis. J Mater Res Technol 23:2784–2797. https://doi.org/10.1016/j.jmrt.2023.01.153
157. Alhmoud H, Brodoceanu D, Elnathan R, Kraus T, Voelcker NH (2021) A MACEing silicon: towards single-step etching of defined porous nanostructures for biomedicine. Prog Mater Sci 116:100636. https://doi.org/10.1016/j.pmatsci.2019.100636
158. Schlie S, Fadeeva E, Koroleva A, Ovsianikov A, Koch J, Ngezahayo A, Chichkov BN (2011) Laser-based nanoengineering of surface topographies for biomedical applications. Photonics Nanostruct 9:159–162. https://doi.org/10.1016/j.photonics.2010.09.006
159. Yazdani J, Ahmadian E, Sharifi S, Shahib S, Dizaj SM (2018) A short view on nanohydroxyapatite as coating of dental implants. Biomed Pharmacother 105:553–557. https://doi.org/10.1016/j.biopha.2018.06.013
160. Sonamuthu J, Samayanan S, Jeyaraman AR, Murugesana B, Krishnana B, Mahalingam S (2018) Influences of ionic liquid and temperature on the tailorable surface morphology of F-apatite nanocomposites for enhancing biological abilities for orthopedic implantation. Mater Sci Eng C 84:99–107. https://doi.org/10.1016/j.msec.2017.11.035
161. Kryszak B, Szustakiewicz K, Dzienny P, Junka K, Paleczny J, Szymczyk-Ziółkowska P, Hoppe V, Antończak A (2022) Functionalization of the PLLA surface with a femtosecond laser: tailored substrate properties for cellular response. Polym Test 116:107815. https://doi.org/10.1016/j.polymertesting.2022.107815
162. Hasturk O, Ermis M, Demirci U, Hasirci N, Hasirci V (2019) Square prism micropillars on poly(methyl methacrylate) surfaces modulate the morphology and differentiation of human dental pulp mesenchymal stem cells. Colloids Surf B Biointerfaces 178:44–55. https://doi.org/10.1016/j.colsurfb.2019.02.037
163. Goldbaum D, Shockley JM, Chromik RR, Rezaeian A, Yue S, Legoux JG, Irissou E (2012) The effect of deposition conditions on adhesion strength of Ti and Ti6Al4V cold spray splats. J Therm Spray Technol 21:288–303. https://doi.org/10.1007/s11666-011-9720-3
164. Brohede U, Zhao S, Lindberg F, Mihranyan A, Forsgren J, Strømme M, Engqvist H (2009) A novel graded bioactive high adhesion implant coating. Appl Surf Sci 255:7723–7728. https://doi.org/10.1016/j.apsusc.2009.04.149
165. Mohseni E, Zalnezhad E, Bushroa AR (2014) Comparative investigation on the adhesion of hydroxyapatite coating on Ti–6Al–4V implant: a review paper. Int J Adhes Adhes 48:238–257. https://doi.org/10.1016/j.ijadhadh.2013.09.030
166. Alkhodary MA (2023) Effect of controlled surface roughness and biomimetic coating on titanium implants adhesion to the bone: an experiment animal study. Saudi Dent J. https://doi.org/10.1016/j.sdentj.2023.07.010
167. Lin C, Han H, Zhang F, Li A (2008) Electrophoretic deposition of HA/MWNTs composite coating for biomaterial applications. J Mater Sci Mater Med 19:2569–2574. https://doi.org/10.1007/s10856-007-3196-1
168. Gopi D, Shinyjoy E, Sekar M, Surendiran M, Kavitha L, Kumar TSS (2013) Development of carbon nanotubes reinforced hydroxyapatite composite coatings on titanium by electrodeposition method. Corros Sci 73:321–330. https://doi.org/10.1016/j.corsci.2013.04.021
169. Pei X, Zeng Y, He R, Li Z, Tian L, Wang J, Wan Q, Li X, Bao H (2014) Single-walled carbon nanotubes/hydroxyapatite coatings on titanium obtained by electrochemical deposition. Appl Surf Sci 295:71–80. https://doi.org/10.1016/j.apsusc.2014.01.009
170. Maleki-Ghaleh H, Khalil-Allafi J (2019) Characterization, mechanical and in vitro biological behavior of hydroxyapatite-titanium-carbon nanotube composite coatings deposited on NiTi alloy by electrophoretic deposition. Surf Coat Technol 363:179–190. https://doi.org/10.1016/j.surfcoat.2019.02.029
171. Zhong Z, Qin J, Ma J (2015) Electrophoretic deposition of biomimetic zinc substituted hydroxyapatite coatings with chitosan and carbon nanotubes on titanium. Ceram Int 41:8878–8884. https://doi.org/10.1016/j.ceramint.2015.03.145
172. Yi C, Bagchi S, Dmuchowski CM, Gou F, Chen X, Park C, Chew HB, Ke C (2018) Direct nanomechanical characterization of carbon nanotubes—titanium interfaces. Carbon 132:548–555. https://doi.org/10.1016/j.carbon.2018.02.069
173. Yi C, Chen X, Gou F, Dmuchowski CM, Sharma A, Park C, Ke C (2017) Direct measurements of the mechanical strength of carbon nanotube—aluminum interfaces. Carbon 125:93–102. https://doi.org/10.1016/j.carbon.2017.09.020
174. Kaya C, Kaya F, Cho J, Roether JA, Boccaccini AR (2009) Carbon nanotube-reinforced hydroxyapatite coatings on metallic implants using electrophoretic deposition. Key Eng Mater 412:93–97. https://doi.org/10.4028/www.scientific.net/KEM.412.93

175. Lahiri D, Ghosh S, Agarwal A (2012) Carbon nanotube reinforced hydroxyapatite composite for orthopedic application: a review. Mater Sci Eng C 32:1727–1758. https://doi.org/10.1016/j.msec.2012.05.010
176. Heary RF, Parvathreddy N, Sampath S, Agarwal N (2017) Elastic modulus in the selection of interbody implants. J Spine Surg 3:163–167. https://doi.org/10.21037/jss.2017.05.01
177. Pawłowski Ł, Rościszewska M, Majkowska-Marzec B et al (2022) Influence of surface modification of titanium and its alloys for medical implants on their corrosion behavior. Materials 15:7556. https://doi.org/10.3390/ma15217556
178. Heise S, Forster C, Heer S, Qi H, Zhou J, Virtanen S, Lu T, Boccaccini AR (2019) Electrophoretic deposition of gelatine nanoparticle/chitosan coatings. Electrochim Acta 307:318–325. https://doi.org/10.1016/j.electacta.2019.03.145
179. Fujita K, Obara S, Maru J, Endoh S (2020) Cytotoxicity profiles of multi-walled carbon nanotubes with different physicochemical properties. Toxicol Mech Methods 30:477–489. https://doi.org/10.1080/15376516.2020.1761920
180. Nagai H, Okazaki Y, Chew SH et al (2011) Diameter and rigidity of multiwalled carbon nanotubes are critical factors in mesothelial injury and carcinogenesis. Proc Natl Acad Sci 108:E1330–E1338. https://doi.org/10.1073/pnas.1110013108
181. Long J, Xiao Y, Liu L, Cao Y (2017) The adverse vascular effects of multi-walled carbon nanotubes (MWCNTs) to human vein endothelial cells (HUVECs) in vitro: role of length of MWCNTs. J Nanobiotechnol 15:80. https://doi.org/10.1186/s12951-017-0318-x
182. Dinç B, Ünlü A, Bektaş M (2020) Characterization of short-length multi-walled carbon nanotubes and cytotoxicity on MDA-MB-231 and HUVEC cell lines. Carbon Lett 30:143–153. https://doi.org/10.1007/s42823-019-00081-5
183. Sun Y, Gong J, Cao Y (2019) Multi-walled carbon nanotubes (MWCNTs) activate apoptotic pathway through ER stress: does surface chemistry matter? Int J Nanomed 14:9285–9294. https://doi.org/10.2147/IJN.S217977
184. Shende P, Augustine S, Prabhakar B (2020) A review on graphene nanoribbons for advanced biomedical applications. Carbon Lett 30:465–475. https://doi.org/10.1007/s42823-020-00125-1
185. Pietroiusti A, Massimiani M, Fenoglio I et al (2011) Low doses of pristine and oxidized single-wall carbon nanotubes affect mammalian embryonic development. ACS Nano 5:4624–4633. https://doi.org/10.1021/nn200372g
186. Thakur A, Bharti R, Sharma R (2022) Carbon nanotubes: types, synthesis, cytotoxicity and applications in biomedical. Mater Today Proc 50:2256–2268. https://doi.org/10.1016/j.matpr.2021.10.002
187. Zhao X, Lu D, Hao F, Liu R (2015) Exploring the diameter and surface dependent conformational changes in carbon nanotube-protein corona and the related cytotoxicity. J Hazard Mater 292:98–107. https://doi.org/10.1016/j.jhazmat.2015.03.023
188. Lu N, Sui Y, Ding Y, Tian R, Li L, Liu F (2018) Adsorption of human serum albumin on functionalized single-walled carbon nanotubes reduced cytotoxicity. Chem Biol Interact 295:64–72. https://doi.org/10.1016/j.cbi.2018.03.015
189. Ding Y, Tian R, Yang Z, Chen J, Lu N (2017) Effects of serum albumin on the degradation and cytotoxicity of single-walled carbon nanotubes. Biophys Chem 222:1–6. https://doi.org/10.1016/j.bpc.2016.12.002
190. Tian R, Long X, Yang Z, Lu N, Peng YY (2020) Formation of a bovine serum albumin diligand complex with rutin and single-walled carbon nanotubes for the reduction of cytotoxicity. Biophys Chem 256:106268. https://doi.org/10.1016/j.bpc.2019.106268
191. Aghaleh M, Rafiee A, Morowvat MH, Ghasemi Y (2021) Evaluating the cytotoxicity of single-walled and multi-walled carbon nanotubes as a scaffold for human chondrocyte stem cell precursors and optimizing the operational conditions. Mater Today Commun 29:102979. https://doi.org/10.1016/j.mtcomm.2021.102979
192. Alam AKMM, Beg MDH, Yunus RM, Islam MR, Shubhra QTH (2021) Tailoring the dispersibility of non-covalent functionalized multi-walled carbon nanotube (MWCNT) nanosuspension using shellac (SL) bio-resin: structure-property relationship and cytotoxicity of shellac coated carbon nanotubes (SLCNTs). Colloid Interface Sci Commun 42:100395. https://doi.org/10.1016/j.colcom.2021.100395
193. Xia Y, Li S, Nie C et al (2019) A multivalent polyanion-dispersed carbon nanotube toward highly bioactive nanostructured fibrous stem cell scaffolds. Appl Mater Today 16:518–528. https://doi.org/10.1016/j.apmt.2019.07.006
194. Gao C, Feng P, Peng S, Shuai C (2017) Carbon nanotube, graphene and boron nitride nanotube reinforced bioactive ceramics for bone repair. Acta Biomater 61:1–20. https://doi.org/10.1016/j.actbio.2017.05.020
195. Misra SK, Ohashi F, Valappil SP et al (2010) Characterization of carbon nanotube (MWCNT) containing P(3HB)/bioactive glass composites for tissue engineering applications. Acta Biomater 6:735–742. https://doi.org/10.1016/j.actbio.2009.09.023
196. Stango AX, Vijayalakshmi U (2018) Electrochemically grown functionalized-multi-walled carbon nanotubes/hydroxyapatite hybrids on surgical grade 316L SS with enhanced corrosion resistance and bioactivity. Colloids Surf B Biointerfaces 171:186–196. https://doi.org/10.1016/j.colsurfb.2018.06.058
197. Seo S-J, Kim J-J, Kim J-H, Lee JY, Shin US, Li EJ, Kim HW (2014) Enhanced mechanical properties and bone bioactivity of chitosan/silica membrane by functionalized-carbon nanotube incorporation. Compos Sci Technol 96:31–37. https://doi.org/10.1016/j.compscitech.2014.03.004
198. Liu S, Ng AK, Xu R, Wei J, Tan CM, Yang Y, Chen Y (2010) Antibacterial action of dispersed single-walled carbon nanotubes on *Escherichia coli* and *Bacillus subtilis* investigated by atomic force microscopy. Nanoscale 2:2744–2750. https://doi.org/10.1039/c0nr00441c
199. Dinh NX, Van QN, Huy TQ, Le AT (2015) Decoration of silver nanoparticles on multiwalled carbon nanotubes: antibacterial mechanism and ultrastructural analysis. J Nanomater 2015:1–11. https://doi.org/10.1155/2015/814379
200. Schifano E, Cavoto G, Pandolfi F et al (2023) Plasma-etched vertically aligned CNTs with enhanced antibacterial power. Nanomaterials 13:1081. https://doi.org/10.3390/nano13061081
201. Rajavel K, Gomathi R, Manian S, Rajendra Kumar RT (2014) In vitro bacterial cytotoxicity of CNTS: reactive oxygen species mediate cell damage edges over direct physical puncturing. Langmuir 30:592–601. https://doi.org/10.1021/la403332b
202. Zhu Y, Liu X, Yeung KWK, Yeung KWK, Chu PK, Wu S (2017) Biofunctionalization of carbon nanotubes/chitosan hybrids on Ti implants by atom layer deposited ZnO nanostructures. Appl Surf Sci 400:14–23. https://doi.org/10.1016/j.apsusc.2016.12.158
203. Jatoi AW, Ogasawara H, Kim IS, Ni Q-Q (2020) Cellulose acetate/multi-wall carbon nanotube/Ag nanofiber composite for antibacterial applications. Mater Sci Eng C 110:110679. https://doi.org/10.1016/j.msec.2020.110679
204. Yun H, Kim JD, Choi HC, Lee CW (2013) Antibacterial activity of CNT-Ag and GO-Ag nanocomposites against gram-negative and gram-positive bacteria. Bull Korean Chem Soc 34:3261–3264. https://doi.org/10.5012/bkcs.2013.34.11.3261
205. Baek S, Joo SH, Su C, Toborek M (2019) Antibacterial effects of graphene- and carbon-nanotube-based nanohybrids on *Escherichia coli*: implications for treating multidrug-resistant bacteria. J Environ Manag 247:214–223. https://doi.org/10.1016/j.jenvman.2019.06.077
206. Ma Y, Liu J, Yin H et al (2018) Remarkably improvement in antibacterial activity of carbon nanotubes by hybridizing with

silver nanodots. J Nanosci Nanotechnol 18:5704–5710. https://doi.org/10.1166/jnn.2018.15383
207. Zhao A, Zhang N, Li Q et al (2021) Incorporation of silver-embedded carbon nanotubes coated with tannic acid into polyamide reverse osmosis membranes toward high permeability, antifouling, and antibacterial properties. ACS Sustain Chem Eng 9:11388–11402. https://doi.org/10.1021/acssuschemeng.1c03313
208. Hamouda HI, Abdel-Ghafar HM, Mahmoud MHH (2021) Multi-walled carbon nanotubes decorated with silver nanoparticles for antimicrobial applications. J Environ Chem Eng 9:105034. https://doi.org/10.1016/j.jece.2021.105034
209. Kim JD, Yun H, Kim GC, Lee CW, Choi HC (2013) Antibacterial activity and reusability of CNT-Ag and GO-Ag nanocomposites. Appl Surf Sci 283:227–233. https://doi.org/10.1016/j.apsusc.2013.06.086
210. Xia L, Xu M, Cheng G et al (2018) Facile construction of Ag nanoparticles encapsulated into carbon nanotubes with robust antibacterial activity. Carbon 130:775–781. https://doi.org/10.1016/j.carbon.2018.01.073
211. Yin M, Huang D, Zhang X et al (2018) Preparation of Ag@CNT nanohybrids and investigations on their antibacterial and cytotoxicological effects. Nanosci Nanotechnol Lett 10:1671–1676. https://doi.org/10.1166/nnl.2018.2844
212. Gan L, Geng A, Jin L, Zhong Q, Wang L, Xu L, Mei C (2019) Antibacterial nanocomposite based on carbon nanotubes–silver nanoparticles-co-doped polylactic acid. Polymer Bull 77:793–804. https://doi.org/10.1007/S00289-019-02776-1
213. Joghataeian M, Bahari A, Qavami A, Raeisi MJ (2020) An antibacterial study of a new magnetic carbon nanotube/core-shell nanohybrids. J Environ Chem Eng 8:104150. https://doi.org/10.1016/j.jece.2020.104150
214. Khedaer Z, Ahmed D, Al-Jawad S (2021) Investigation of morphological, optical, and antibacterial properties of hybrid ZnO-MWCNT prepared by sol-gel. J Appl Sci Nanotechnol 1:66–77. https://doi.org/10.53293/jasn.2021.11634
215. Yazhini KB, Prabu HG (2014) Antibacterial activity of cotton coated with ZnO and ZnO-CNT composites. Appl Biochem Biotechnol 175:85–92. https://doi.org/10.1007/S12010-014-1257-8
216. Ding M, Sahebgharani N, Musharavati F, Jaber F, Zalnezhad E, Yoon GH (2018) Synthesis and properties of HA/ZnO/CNT nanocomposite. Ceram Int 44:7746–7753. https://doi.org/10.1016/j.ceramint.2018.01.203
217. Mohammad MR, Ahmed DS, Mohammed MKA (2019) Synthesis of Ag-doped TiO_2 nanoparticles coated with carbon nanotubes by the sol–gel method and their antibacterial activities. J Solgel Sci Technol 90:498–509. https://doi.org/10.1007/s10971-019-04973-w
218. Sukkar K, Duha SA, Hussein A, Mohammad RM (2019) Synthesis and characterization hybrid materials (TiO_2/MWCNTs) by chemical method and evaluating antibacterial activity against common microbial pathogens. Acta Phys Pol A 135:588–592. https://doi.org/10.12693/APhysPolA.135.588
219. Hossain MdA, Elias Md, Sarker DR et al (2018) Synthesis of Fe- or Ag-doped TiO_2–MWCNT nanocomposite thin films and their visible-light-induced catalysis of dye degradation and antibacterial activity. Res Chem Intermed 44:2667–2683. https://doi.org/10.1007/s11164-018-3253-z
220. Nguyen QX, Nguyen TT, Pham NM, Khong TT, Cao TM, Pham VV (2022) A fabrication of CNTs/TiO_2/polyurethane films toward antibacterial and protective coatings. Prog Org Coat 167:106838. https://doi.org/10.1016/j.porgcoat.2022.106838
221. Singh A, Goswami A, Nain S (2020) Enhanced antibacterial activity and photo-remediation of toxic dyes using Ag/SWCNT/PPy based nanocomposite with core–shell structure. Appl Nanosci 10:2255–2268. https://doi.org/10.1007/s13204-020-01394-y
222. Zhu Y, Xu J, Wang Y, Chen C, Gu H, Chai Y, Wang Y (2020) Silver nanoparticles-decorated and mesoporous silica coated single-walled carbon nanotubes with an enhanced antibacterial activity for killing drug-resistant bacteria. Nano Res 13:389–400. https://doi.org/10.1007/s12274-020-2621-3
223. Park JE, Park I-S, Neupane MP, Bae TS, Lee MH (2014) Effects of a carbon nanotube-collagen coating on a titanium surface on osteoblast growth. Appl Surf Sci 292:828–836. https://doi.org/10.1016/j.apsusc.2013.12.058
224. Li H, Gao Y, Li C, Ma G, Shang Y, Sun Y (2016) A comparative study of the antibacterial mechanisms of silver ion and silver nanoparticles by Fourier transform infrared spectroscopy. Vib Spectrosc 85:112–121. https://doi.org/10.1016/j.vibspec.2016.04.007
225. Wu Y, Yang Y, Zhang Z, Wang Z, Zhao Y, Sun L (2018) A facile method to prepare size-tunable silver nanoparticles and its antibacterial mechanism. Adv Powder Technol 29:407–415. https://doi.org/10.1016/j.apt.2017.11.028
226. Liu S, Zhang D, Chen W, Wang X, Ji H, Fu Y, Lü C (2023) Synthesis, antibacterial activity and action mechanism of silver-based nanomaterials with thermosensitive polymer-decorated graphene oxide as a stable support. Mater Today Commun 36:106598. https://doi.org/10.1016/j.mtcomm.2023.106598
227. Zhao Z, Li P, Xie R, Cao X, Su D, Shan Y (2022) Biosynthesis of silver nanoparticle composites based on hesperidin and pectin and their synergistic antibacterial mechanism. Int J Biol Macromol 214:220–229. https://doi.org/10.1016/j.ijbiomac.2022.06.048
228. Ji H, Zhou S, Fu Y, Wang Y, Mi J, Lu T, Wang X, Lü C (2020) Size-controllable preparation and antibacterial mechanism of thermo-responsive copolymer-stabilized silver nanoparticles with high antimicrobial activity. Mater Sci Eng C 110:110735. https://doi.org/10.1016/j.msec.2020.110735
229. Gallón SMN, Alpaslan E, Wang M et al (2019) Characterization and study of the antibacterial mechanisms of silver nanoparticles prepared with microalgal exopolysaccharides. Mater Sci Eng C 99:685–695. https://doi.org/10.1016/j.msec.2019.01.134
230. Zhao Y, Wee CY, Zhang H, Yang Z, Wang WEJ, Thian ES (2022) Silver-substituted hydroxyapatite inhibits *Pseudomonas aeruginosa* outer membrane protein F: a potential antibacterial mechanism. Biomater Adv 134:112713. https://doi.org/10.1016/j.msec.2022.112713
231. Jin Y, Zhu L, Xue W, Li W (2015) Fabrication of superaligned carbon nanotubes reinforced copper matrix laminar composite by electrodeposition. Trans Nonferrous Met Soc China 25:2994–3001. https://doi.org/10.1016/S1003-6326(15)63926-7
232. Du J, Hu Z, Dong W, Wang Y, Wu S, Bai Y (2019) Biosynthesis of large-sized silver nanoparticles using Angelica keiskei extract and its antibacterial activity and mechanisms investigation. Microchem J 147:333–338. https://doi.org/10.1016/j.microc.2019.03.046
233. Moghadasi K, Isa MSM, Ariffin MA et al (2022) A review on biomedical implant materials and the effect of friction stir based techniques on their mechanical and tribological properties. J Mater Res Technol 17:1054–1121
234. Ong YT, Ahmad AL, Zein SHS, Tan SH (2010) A review on carbon nanotubes in an environmental protection and green engineering perspective. Braz J Chem Eng 27:227–242
235. Kamanina N, Kuzhakov P, Kvashnin D (2020) Novel perspective coatings for the optoelectronic elements: features of the carbon nanotubes to modify the surface relief of BaF2 materials. Coatings 10:661. https://doi.org/10.3390/coatings10070661

6.2 [A2]

POLITECHNIKA GDAŃSKA | WYDZIAŁ INŻYNIERII MECHANICZNEJ I OKRĘTOWNICTWA | RESEARCH UNIVERSITY

OŚWIADCZENIE

Dotyczy publikacji w czasopiśmie naukowym:

Rogala-Wielgus D., Majkowska-Marzec B., Zieliński A., Bartmański M., Bartosewicz B.: *Mechanical behavior of bi-layer and dispersion coatings composed of several nanostructures on Ti13Nb13Zr alloy,* Materials. 14 (2021) 2905. https://doi.org/10.3390/ma14112905.

Impact Factor: 3,748
Punkty wg MNiSW: 140 pkt.

Oświadczamy, że wkład autorów w powstanie powyższej publikacji kształtuje się następująco:

L.p.	Współautor	Wkład, %	Wkład merytoryczny
1.	**Dorota Rogala-Wielgus**	**70**	**realizacja przeglądu literaturowego; opracowanie koncepcji badań; przygotowanie powłok; przeprowadzenie badań; analiza wyników; przygotowanie manuskryptu; edycja manuskryptu; przygotowanie odpowiedzi na recenzje; rola autora korespondencyjnego**
2.	Beata Majkowska-Marzec	15	udział w opracowaniu koncepcji badań; udział w realizacji badań; udział w analizie wyników; udział w przygotowaniu odpowiedzi na recenzje
3.	Andrzej Zieliński	5	nadzór merytoryczny; korekta końcowa; edycja manuskryptu; udział w przygotowaniu odpowiedzi na recenzje
4.	Michał Bartmański	5	przeprowadzenie badań nanoindentacji; korekta końcowa
5,	Bartosz Bartosewicz	5	funkcjonalizacja nanorurek węglowych; korekta końcowa

Podpisy współautorów:

Dorota Rogala-Wielgus
mgr inż. Dorota Rogala-Wielgus

Majkowska-Marzec Beata
dr inż. Beata Majkowska-Marzec

prof. dr hab. inż. Andrzej Zieliński

Michał Bartmański
dr inż. Michał Bartmański

Bartosz Bartosewicz
mgr inż. Bartosz Bartosewicz

POLITECHNIKA GDAŃSKA
Ul. Gabriela Narutowicza 11/12
80-233 Gdańsk
pg.edu.pl

materials

MDPI

Article

Mechanical Behavior of Bi-Layer and Dispersion Coatings Composed of Several Nanostructures on Ti13Nb13Zr Alloy

Dorota Rogala-Wielgus [1,*], Beata Majkowska-Marzec [1], Andrzej Zieliński [1], Michał Bartmański [1] and Bartosz Bartosewicz [2]

[1] Division of Biomaterials Technology, Faculty of Mechanical Engineering and Shipbuilding, Gdansk University of Technology, 11 Narutowicza str., 80-233 Gdańsk, Poland; beata.majkowska@pg.edu.pl (B.M.-M.); andrzej.zielinski@pg.edu.pl (A.Z.); michal.bartmanski@pg.edu.pl (M.B.)

[2] Institute of Optoelectronics, Military University of Technology, gen. S. Kaliskiego 2, 00-908 Warsaw, Poland; bartosz.bartosewicz@wat.edu.pl

* Correspondence: dorota.wielgus@pg.edu.pl; Tel.: +48-534-897-893

Abstract: Titanium implants are commonly used because of several advantages, but their surface modification is necessary to enhance bioactivity. Recently, their surface coatings were developed to induce local antibacterial properties. The aim of this research was to investigate and compare mechanical properties of three coatings: multi-wall carbon nanotubes (MWCNTs), bi-layer composed of an inner MWCNTs layer and an outer TiO_2 layer, and dispersion coatings comprised of simultaneously deposited MWCNTs and nanoCu, each electrophoretically deposited on the Ti13Nb13Zr alloy. Optical microscopy, scanning electron microscopy, X-ray electron diffraction spectroscopy, and nanoindentation technique were applied to study topography, chemical composition, hardness, plastic and elastic properties. The results demonstrate that the addition of nanocopper or titanium dioxide to MWCNTs coating increases hardness, lowers Young's modulus, improves plastic and elastic properties, wear resistance under deflection, and plastic deformation resistance. The results can be attributed to different properties, structure and geometry of applied particles, various deposition techniques, and the possible appearance of porous structures. These innovative coatings of simultaneously high strength and elasticity are promising to apply for deposition on long-term titanium implants.

Keywords: coatings; composites; electrophoretic deposition; carbon nanotubes; nanocopper; titanium oxide; nanoindentation; hardness; Young's modulus; titanium alloy

Citation: Rogala-Wielgus, D.; Majkowska-Marzec, B.; Zieliński, A.; Bartmański, M.; Bartosewicz, B. Mechanical Behavior of Bi-Layer and Dispersion Coatings Composed of Several Nanostructures on Ti13Nb13Zr Alloy. *Materials* **2021**, *14*, 2905. https://doi.org/10.3390/ma14112905

Academic Editor: Christopher C. Berndt

Received: 22 April 2021
Accepted: 24 May 2021
Published: 28 May 2021

1. Introduction

Carbon thin coatings continue to attract attention, fueled by their potential for industrial and commercial applications. Carbon nanotubes (CNTs) demonstrate unique properties, such as high aspect ratio, enhanced tensile (tensile strength up to 30 GPa [1]) and elastic properties (elastic modulus of 1 TPa or more [1]), and excellent electrical and thermal conductivity, resulting from their unique molecular structure and dependent on the synthesis method [2]. Extraordinary high mechanical properties led to extensive research on the use of CNTs as a reinforcing agent to produce composites [3–5] and laminar coatings [5] with various materials, such as Al_2O_3 [6–8], hydroxyapatite (HAp) [4,9–13], titanium [4], titanium dioxide (TiO_2) [5,8,14–16], ultra-high molecular weight polyethylene (UHMWPE) [17,18], nickel [19–22], aluminum [23–25], chromium [26], and copper [22].

After the reports on CNTs bioactive properties, their application in the biomedical field increased [1,27]. Sasani et al. [28] used copper decorated multi-wall carbon nanotubes (MWCNTs) to incorporate fluorapatite-titania coating onto a Ti-based implant, which improved composite coating in terms of nanomechanical properties. The toxicity profile and biocompatibility of CNTs were the main concerns as confirmed by numerous reports available on this issue [2,29–37]. The size (diameter and length [30,31]) and surface area

of the CNTs play an important role in toxicology—the smaller the size structure and increased surface area, the larger probability of the interactions with living cells and translocation into the cells, thus adverse biological effects. Kumar et al. [34]. reported on many other important factors determining the cytotoxicity of CNTs, such as the type of CNTs, the type of functionalization, the purification of the product, and dispersion. These parameters should be controlled to reduce the adverse effects of MWCNTs [31,32]. Benko et al. [29] conducted biocompatibility tests on titanium modified with CNTs using the human osteoblast-like cell line MG63. The result confirmed the non-toxic character of the tested materials and showed improvement in the biocompatibility of the modified titanium substrate. What is more, structural disorder and the presence of functional groups, together with an increased surface area of the material, caused better cell adhesion and growth, than for pure titanium [29]. Portan et al. [33] investigated the human bone cells (osteoblasts) behavior when cultured on biomaterials like polymer, titanium, titania nanotubes (TNTs), and CNTs. In this case, osteoblasts cultured on nanostructured topographies, like TNTs and CNTs, improved the proliferation. However, Li et al. [31] reported on MWCNTs harmful activity in the human immune system as impairment of the phagocytic ability, which finally led to cell apoptosis or necrosis. General assumption is that MWCNTs with larger dimensions (long, rigid, a needle-like shape) show higher bioactivity and the shorter the MWCNTs are, the lower the inflammatory response. Literature shows that MWCNTs with a smaller dimension and smaller agglomerate size or with less metal impurities demonstrate lower cytotoxicity [30]. Another study of Zhao et al. [30] revealed that, at the same mass concentration, the cytotoxicity decreased with an increase in the diameter of MWCNTs. Whereas, smaller diameters of MWCNTs generally displayed stronger toxicity towards bacteria [30]. Thus, as so far reports on suspected toxicity are inconsistent and the use of CNTs against bacteria as promising and easy, to achieve titanium surface modification cannot be excluded.

Titanium dioxide (TiO_2) appears in four natural polymorphs-TiO_2(B), brookite, anatase, and rutile. Most widely studied are the anatase and rutile crystalline polymorphs, but there is also an amorphous form of TiO_2 [38]. TiO_2 is a biocompatible ceramic, which can be used to achieve the antibacterial effect, corrosion resistance, and high biocompatibility in biomedical appliances [5]. For this reason, titanium dioxide is a candidate material for developing protective coatings on metallic substrates [39]. What is more, TiO_2 is widely used in many different areas, such as gas sensors, and for air purification or dye-sensitized solar cell applications [15]. TiO_2 has some prominent properties, it is photocatalytically active, has a self-cleaning ability on surfaces, is low-toxic [40]. Ikono et al. [40] carried out cytotoxicity analysis for chitosan-50% TiO_2 nanoparticles sponges which proved the material to be biocompatible; the cells could proliferate well with a trend of increasing cell number with TiO_2 concentration. This suggests that such a huge percentage of TiO_2 nanoparticles in the material could be used for bone tissue engineering. Hsiao et al. [41] also checked TiO_2 nanoparticles in terms of cytotoxicity which showed that not only the size, surface area, and shape, but also the phase of the nanoparticles played an important role. The cytotoxicity of the TiO_2 nanoparticles increased in the following order: amorphous > anatase > anatase/rutile. Uboldi et al. [42] showed that rutile induced toxic effects in Balb/3T3 mouse fibroblasts, whereas it was dependent on the particle size. Additionally, Louro [32] claimed that widely used TiO_2 (as a pigment in paints, varnishes, and plastics, as an additive to food—E171, as UV-filter in cosmetic products), especially the rutile, presented the most genotoxic effects. The literature showed also the induction of micronuclei by anatase TiO_2 and negative results for rutile when testing genotoxicity using human cell lines [42].

CNTs have a high surface area, which gives them the possibility to build a mesoporous structure, thus they are excellent carrier substrates for TiO_2 nanoparticles. The combination of CNTs and TiO_2 nanoparticles can lead to achieving relevant properties for a variety of functional applications. There are some reports on preparing CNTs/TiO_2 nanoparticle coatings. Boccaccini et al. [43] discussed the mechanism of electrophoretic deposition (EPD)

of CNT/TiO_2 nanoparticle composites and laminates. The subject of the investigation was a four-layer laminate coating of CNTs and TiO_2, which showed that non-sintered ceramic coating could be reinforced by the addition of CNTs, which provided a crack deflection and delamination path. Jarernboon et al. [15] used CNTs to protect TiO_2 coating against microcracks. The TiO_2 coatings deposited using the EPD process showed that the number and length of the microcracks increased with the TiO_2 layer thickness. The addition of multiwalled carbon nanotubes (MWCNTs) minimized the crack problem because hydroxyl groups and carboxylic groups from CNTs bind to TiO_2 particles. As a result, microcrack formation was diminished. The reinforcement effect of CNTs was also seen when the CNTs coating was synthesized by air plasma spraying [43]. The CNTs were resistant to damage at increasing temperatures during the spraying process, and the pores of such coatings and their roughness demonstrated to decrease with an increasing percentage of CNTs in the coating microstructure [44]. Jambagi et al. [8] tested plasma-sprayed CNTs/TiO_2 and CNTs/alumina (Al_2O_3) coatings, noticing an improvement of scratch resistance of the listed ceramic coatings. Wang et al. [14] verified the CNTs influence on the friction coefficient of the CNTs/TiO_2 nanocomposite coating using a ball-on-disk tribometer under dry-sliding conditions. The comparison between nanocomposite and TiO_2 showed a moderate decrease in friction coefficient and a significant reduction (~93.6%) in wear volume. There were also reports about hydroxyapatite (HAp) coating with titanium and MWCNTs addition (HAp-Ti(20 wt.%)-MWCNTs (1 wt.%) [4] deposited using the EPD method, which showed relevant improvement in hardness and adhesion strength. Moreover, the biological tests revealed an incredible improvement in the apatite and bone cell growth on the nanocomposite coating compared to pure HAp coating.

Copper is an element with proved antibacterial efficiency attributed to its influence on cellular permeability, resulting in malfunction and death of bacteria [45]. Such effects against *S. aureus* and *E. coli* were shown by Hidalgo-Robatto et al. [46] for the nanocopper—HAp coating. The antibacterial activity was observed against *E. coli*, *S. aureus*, and *C. albicans* by Shanmugam and Gopal [47] for Cu substituted HAp coating. For bone phosphate an addition of copper ions eliminated *E. coli*, *P. aeruginosa*, and *S. enteritidis* bacteria [48]. Copper is tolerated by human body, but nanocopper is suspected to destroy the liver and kidneys [49]. The safe content of copper in coatings can be estimated as 2 wt.% as concerns the compatibility [46]. However, as demonstrated by Radovanovic et al. [50] high antibacterial functions can be obtained at low cytotoxicity of coatings. As such, no harmful content of Cu was assessed as of 2 wt.pct in a coating [46]. Moreover, there are several reports of introducing antibacterial properties together with increasing bioactivity and biocompatibility for Cu-incorporated HAp [51], Cu-doped polymer–ceramic coating [52], and Cu-implemented anodic coatings [53].

The most commonly used processing method for the production of ceramic and ceramic-based composite coatings is EPD, which is characterized by many advantages including, low cost, simplicity, low coating time and temperature, control of deposit thickness, uniformity of deposits, the ability to coat the complicated shapes, and microstructural homogeneity [15,54–56]. The EPD method has proved to be effective in a relatively simple way to obtain layers from nanometric particles, whose adhesiveness to the substrate may be higher than those containing micrometric size particles [57]. In order to obtain a homogenous deposition, the suspension used in the process has to be well-dispersed and stable [5]. EPD is fundamentally combined with two processes, electrophoresis and deposition. In the first step, material (charged particles) suspended in a liquid is forced to migrate towards an electrode under an applied electric field. In the second step, the particles coagulate at the electrode and form a coherent deposit [4,5,55]. There are numerous publications of CNTs coatings and their hybrids obtained using the EPD process, like [4,5,15,22,54–56,58–63].

Due to excellent physical (low density, the strength of ~500 MPa and relatively low Young's modulus close to the value of cortical bone [64]) and chemical properties, titanium and its alloys are applied in medicine, especially in the field of tissue engineering [65]. For long-term bearing implants, mostly Ti6Al4V or Ti6Al7Nb alloys are used. There are also

studies about the Ti13Nb13Zr alloy, which show the relatively low Young modulus and its non-toxic potential on the human body (the elements Ti, Nb, Zr are non-toxic) [64,66].

So far, research has shown that surface coatings are numerous as well as their properties, and different determinants for optimization of surface treatment can be chosen. In this research, we have focused only on the creation of two composite coatings which would possess greater hardness at simultaneously high elasticity than the present coatings to prevent possible damage by stresses imposed during surgery and use of an implant. To achieve this objective, we have decided to apply nanoparticles of carbon (carbon nanotubes with high surface/volume ratio), ceramic nanooxides (nanotitania) and nanocopper, in different combinations. The nanoparticles are well-known to have high mechanical properties. We have also assumed that electrophoretically deposited coatings would possess a certain porosity, resulting in lowering Young's modulus and enlarging the elastic region. Therefore, we have prepared composite coatings as bi-layer (sandwich) deposits obtained by two consecutive processes, and the dispersion coating, formed in a one-stage process.

2. Materials and Methods

2.1. Surface Preparation

The Ti13Nb13Zr alloy (Xi'an SATE Metal Materials Development Co., Ltd., Xi'an, China) of the composition shown in Table 1 was used as substrate. Specimens of 40 mm in diameter and 4 mm thick slices were cut from the rod and divided into quarters using a precision cutter (Brillant 220, ATM GmbH, Mammelzen, Germany). The surface was ground using abrasive paper SiC up to grit # 800 on a metallographic grinding machine (Saphir 330, ATM GmbH, Mammelzen, Germany). Then, specimens were rinsed with acetone for analysis (Chempur, Piekary Śląskie, Poland), distilled water, dried in the air, picked in 5% hydrofluoric acid (Chempur, Piekary Śląskie, Poland) for 30 s to remove oxide layers from the surface and finally rinsed with distilled water.

Table 1. Chemical composition of the Ti13Nb13Zr alloy.

Element	Nb	Zr	Fe	C	H	O	S	Hf	Ti
wt. pct.	13.18	13.49	0.085	0.035	0.004	0.078	<0.001	0.055	rem.

The multi-wall carbon nanotubes (MWCNTs) had an outer diameter 10–15 nm, inner diameter 2–6 nm, length 1–10 μm, number of walls 3–15 (3D-Nano, Krakow, Poland). Nanocopper (nanoCu) had a mean grain size distribution of 80 nm (Hongwu International Group Ltd., Guangzhou, Guangdong, China). Titanium dioxide (TiO_2), rutile structure, (3D-Nano, Krakow, Poland) possessed an extremely small grain size in the range of 1 to 2 nm.

2.2. Preparation of MWCNTs/TiO_2 Bi-Layer and MWCNTs_Cu Dispersion Coatings

The electrophoretic deposition (EPD) method was used to prepare coatings, of which parameters of synthesis are shown in Table 2. The Ti13Nb13Zr substrate was used as an anode and stainless steel as a counter electrode. The electrodes were placed parallel to each other within a distance of 5 mm and connected to the DC power source (MCP/SPN110-01C, Shanghai MCP Corp., Shanghai, China).

The EPD process was conducted at parameters selected from preliminary studies and based on the Cho et al. report [5]. The MWCNTs/TiO_2 bi-layer coating was prepared in two steps. First, the electrophoretic suspension comprised of 0.1 g MWCNTs suspended in 40 mL of distilled water was prepared and the EPD process on the Ti13Nb13Zr substrate was proceeded. At this stage, preparation of the MWCNTs coating was finished. The MWCNTs coated samples were then subjected to EPD in suspension consisting of 0.15 g TiO_2 dispersed in 50 mL of isopropanol and 0.5 mL of surfactant Polysorbate 20 (Tween 20, Sigma-Aldrich Sp. z.o.o, Poznan, Poland).

Table 2. Parameters of synthesis of coatings.

Coating	Substrate	Deposited Materials	Content of Component in a Bath (wt. pct.)	EPD Time (min)	EPD Voltage (V)
MWCNTs	Ti13Nb13Zr	MWCNTs	0.25	0.5	20
$MWCNTs/TiO_2$	Ti13Nb13Zr	(I) MWCNTs (II) TiO_2	0.25 0.30	0.5 4	20 50
MWCNTs_Cu	Ti13Zr13Nb	MWCNTs + nanoCu	0.25 0.0125	4	50

To prepare the MWCNTs_Cu dispersion coating, 0.1 g of MWCNTs, 0.005 g of nanoCu, and 0.5 mL of Polysorbate 20 were dispersed in 40 mL of distilled water and deposited using the EPD method on the Ti13Nb13Zr substrate.

2.3. Structure and Morphology

To study the surface topography, the optical microscope (VHX Keyence, Keyence International (Belgium) NV/SA, Mechelen, Belgium) was used. The average roughness index Sa values were estimated based on 512 lines made in the area of approximately 150 μm × 140 μm.

The specimens' surfaces and cross-sections were observed using a high-resolution scanning electron microscope (SEM) (JSM-7800F, JOEL, Tokyo, Japan) with a LED detector, at 5 kV acceleration voltage.

The chemical composition of the coatings was investigated by the X-ray energy dispersive spectrometer (EDS) (Octane Elite 25, EDAX Ametek, Berwyn, PA, USA).

2.4. Nanoindentation Studies

Nanoindentation tests were performed with the NanoTest™ Vantage (NanoTest™ Vantage, Micro Materials, Wrexham, Great Britain) using a Berkovich three-sided pyramidal diamond. The twenty-five measurements were carried out on each sample. The maximum applied force was 10 mN, the loading and unloading rate were set up at 20 s, and the dwell period at maximum load was 10 s. The distances between the subsequent indents were 20 μm. During the indent, the load–displacement curves were determined by the Oliver and Pharr method. Based on the load–penetration curves, surface hardness (H), reduced Young's modulus (E_r), plasticity index (PI), and elastic recovery index (EI) were calculated using the integrated software. Young's modulus (E) parameter was calculated based on E_r value and the Poisson's ratio (ν). The ν of 0.25 [67] was preconceived for the MWCNTs coating, 0.26 for TiO_2 [68], and 0.352 for Cu [69]. Assuming the $MWCNTs/TiO_2$ and MWCNTs_Cu coatings as unidirectional composite materials, the Halpin–Tsai (H-P) model was used to evaluate their ν, E [70], and H [71] values using the following relations:

$$\nu = \nu_m V_m + \nu_r V_r \quad (1)$$

$$E = E_m V_m + E_r V_r \quad (2)$$

$$H = H_m V_m + H_r V_r \quad (3)$$

where V_r, ν_r, E_r, H_r and V_m, ν_m, E_m, H_m are volume fraction, Poisson's ratio, Young's modulus, and hardness of the reinforcement and matrix, respectively. The volume fraction was calculated according to [71] and assuming densities of 2.10 g/cm^3 [72], 4.23 g/cm^3 [73], and 8.94 g/cm^3 [74] for MWCNTs, TiO_2, and nanoCu, respectively.

According to Equation (1), the ν values of 0.254 and 0.251 were assessed for the $MWCNTs/TiO_2$ and MWCNTs_Cu coating, respectively.

3. Results and Discussion

3.1. Structure and Morphology

Figure 1 shows the topography of the MWCNTs coating, MWCNTs/TiO_2 bi-layer coating, and MWCNTs_Cu dispersion coating. The coating surface roughness increased after composition modification with both metal and oxide particles, as proven by the results presented in Table 3 (the experimental error has been estimated as of <0.05 µm). A similar effect was shown previously in our earlier work [57] for MWCNTs coating with the addition of nanoCu particles. The observed effects are easy to explain. For bi-layer coating, small titania particles located on the surface form a rough surface. For dispersion coating, the geometries of MWCNTs and nanocopper particles are different, i.e., misfit occurs. The increase in hardness is not large and can be positive for biological applications as such roughness enhances the adhesion of cells.

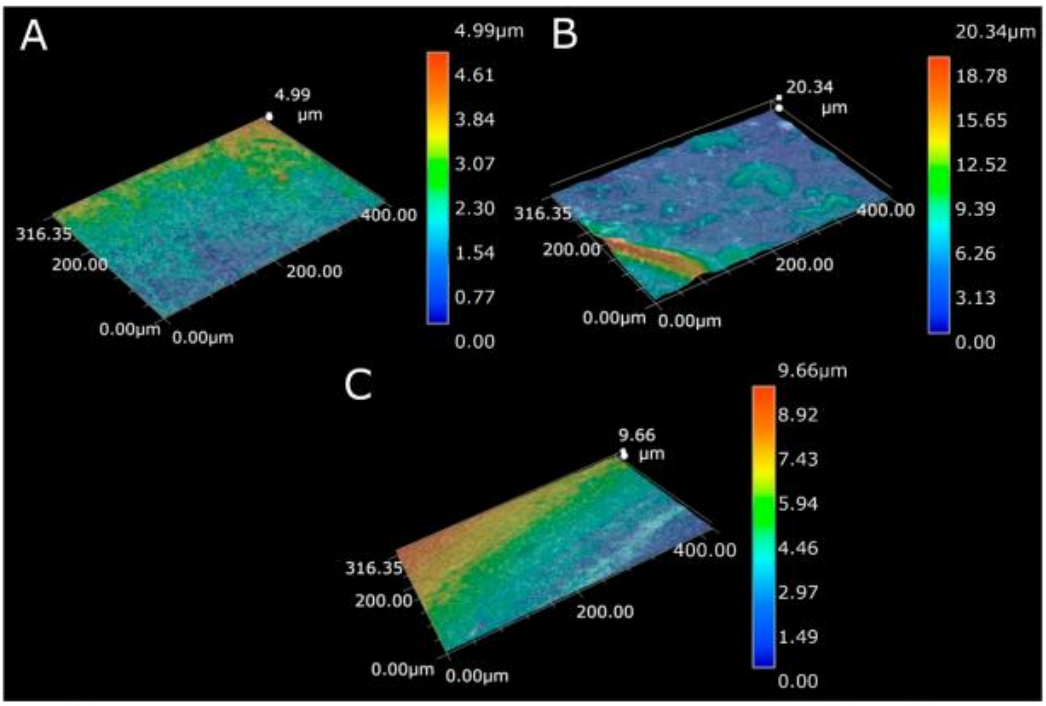

Figure 1. Surface topography for (**A**) the MWCNTs coating, (**B**) the MWCNTs/TiO_2 coating, (**C**) the MWCNTs_Cu coating.

Table 3. The surface roughness of the deposited coatings.

Sample	Roughness Sa (µm)
MWCNTs	0.34
MWCNTs/TiO_2	0.65
MWCNTs_Cu	0.41

Figure 2 present SEM images of the MWCNTs sample, the MWCNTs/TiO_2 bi-layer coating, and the MWCNTs_Cu dispersion coating deposited on the Ti13Nb13Zr alloy. Figure 2 demonstrates the uniform distribution of MWCNTs. Figure 2C,D illustrates a more diverse surface with visible agglomerates of many TiO_2 particles with an average aggregates surface area of about 1.5 μm^2. The surface topography of the MWCNTs_Cu

coating (Figure 3E,F) is different: The MWCNTs coating is significantly cracked due to deposition of nanoCu particles, especially at the crossover and edge-contact locations of MWCNTs as previously observed [28,75,76]. Such a phenomenon can be attributed again to a significant difference in geometry (misfit) in both nanoforms.

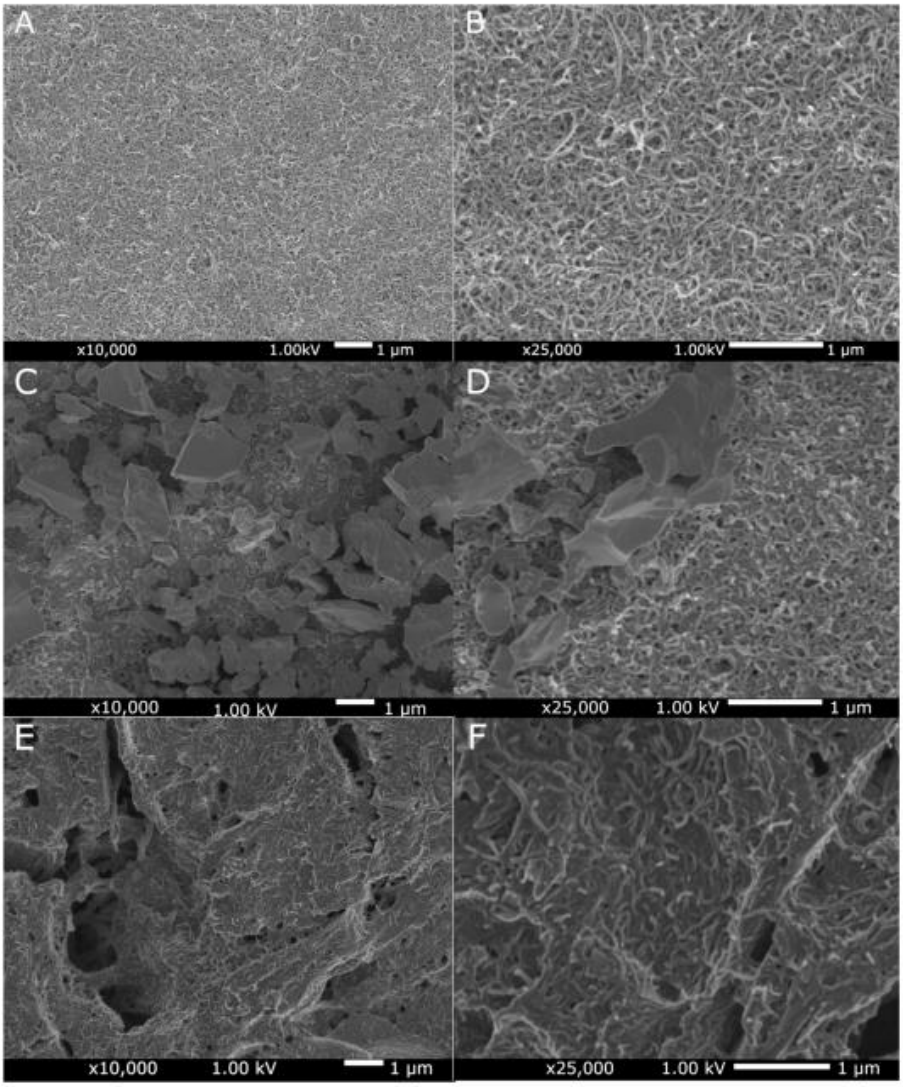

Figure 2. SEM surface topography of the MWCNTs coating (**A**,**B**), the MWCNTs/TiO2 bi-layer coating (**C**,**D**) and the MWCNTs_Cu dispersion coating (**E**,**F**) in different resolutions.

Figure 3 illustrates the EDS spectrum of the MWCNTs, the MWCNTs_Cu dispersion coating, and the MWCNTs/TiO_2 bi-layer coating, confirming its formation by the presence of carbon, copper, titanium, and oxide peaks together with those from alloying elements (except the MWCNTs/TiO_2 coating as a result of the largest thickness of examined coatings, which is shown in Figure 4), and iron, sodium, chlorine, and copper in MWCNTs/TiO_2, likely as possible contaminants.

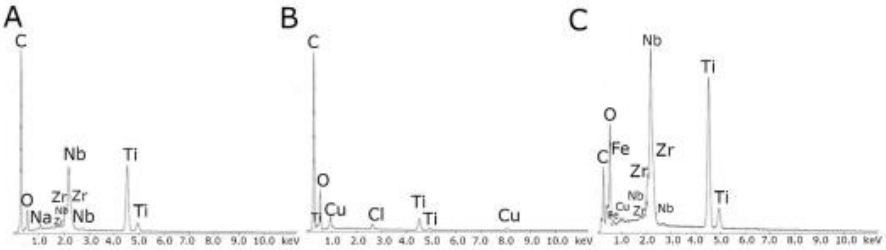

Figure 3. EDS spectra of the (**A**) MWCNTs reference coating, (**B**) MWCNTs/TiO_2 bi-layer coating, (**C**) MWCNTs_Cu dispersion coating.

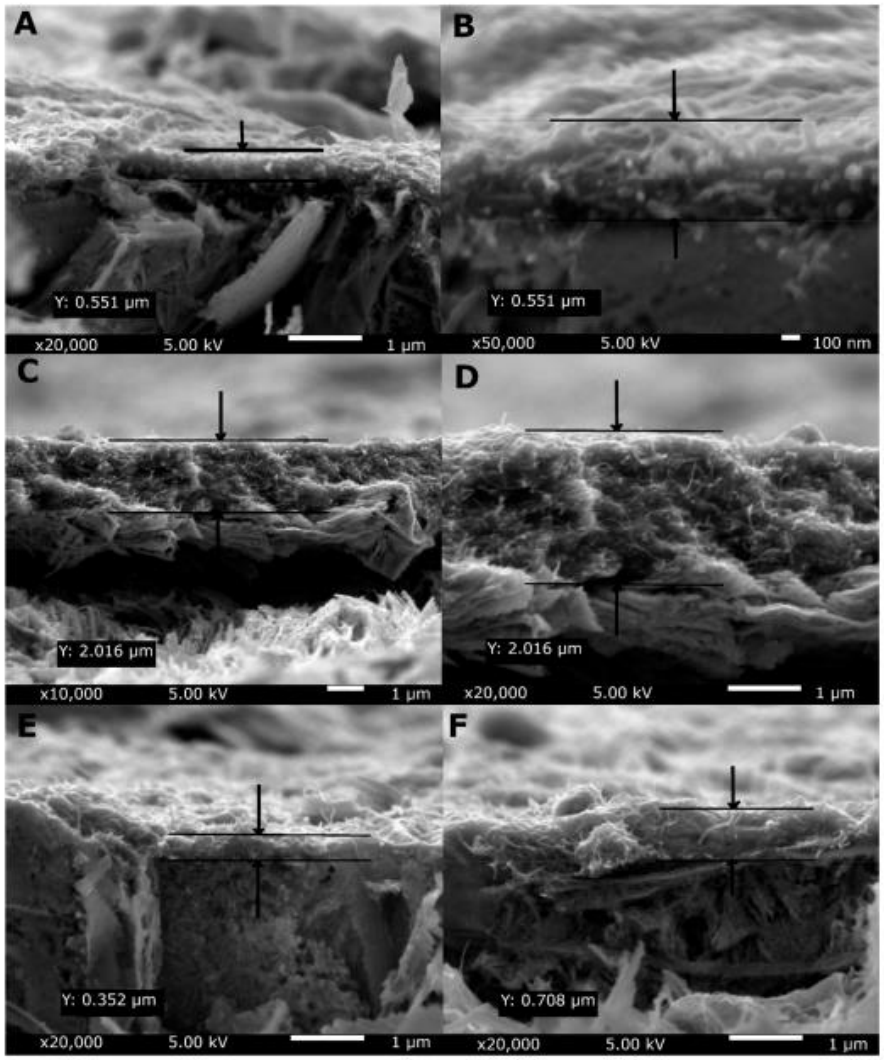

Figure 4. Cross-sectional SEM images of the MWCNTs reference coating (**A**,**B**), MWCNTs/TiO_2 bi-layer coating (**C**,**D**) in different resolutions and MWCNTs_Cu dispersion coating (**E**,**F**) in different places, with an indicated coating thickness.

Figure 4 shows the cross-sectional SEM images of the MWCNTs reference coating, the MWCNTs/TiO_2 bi-layer coating, and the MWCNTs_Cu dispersion coating with an indicated coatings thickness (Y). As seen, the thickness of the coatings, shown in both images, extended roughly between 0.5 and 2 µm. The greatest values are observed for the MWCNTs/TiO_2 coating which could be explained by the deposition method resulting in the bi-layer coating. What is important, all coatings possess the thickness sufficient to separate the substrate surface, with the greatest thickness of the MWCNTs/TiO_2 coating being the most appropriate for application as sufficiently thick for retardation of possible penetration of liquids.

3.2. Nanoindentation Studies

The load–displacement hysteresis curve, as an example of the results of nanoindentation tests, is shown in Figure 5. Three stages of the nanoindentation test can be distinguished in the graph: raising the load until maximum value, a pause (to stabilize the probe at maximum depth), and offloading. Due to temperature drift, an irregularity in the form of the stage can be observed. The drift is adjusted at the end of nanoindentation.

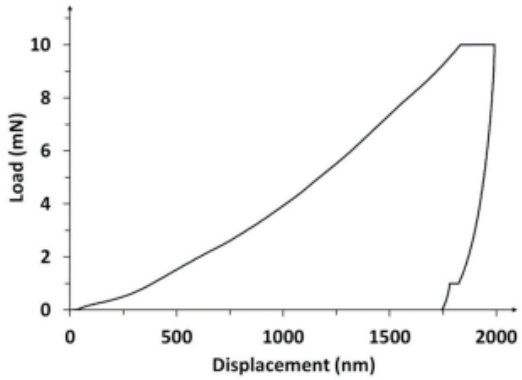

Figure 5. Nanoindentation load–displacement curve obtained for the MWCNTs/TiO_2 coating.

The exact values of measured mechanical properties are listed in Table 4. The addition of both metal and oxide particles resulted in an increase in nanohardness over 100% and over 36%, respectively, with regard to the reference. The composite coatings demonstrate Young's modulus lower than that of the reference coating and measured values are approximately close to that of bone, reported as of 18.6 GPa for cortical bone [63], but only 1 GPa for immature and 6 GPa for mature bone [77].

Such behavior, an inverse relationship between hardness and Young's modulus, already anticipated by us [67], has been achieved. The decreasing Young's modulus may be explained by several reasons as the most obvious strengthening of material under nanoindenter load by freshly created dislocations [78]. However, we believe that the main mechanism is related to the presence of local pores/voids in the microstructure of investigated composite coatings. As well-known, for homogenous composites, both hardness (strictly: strength) and Young's modulus are additive values calculated based on values of mechanical properties and relative fractions of components. Table 4 shows the values of hardness and Young's modulus for pure components (for MWCNTs twice, as isolated nanofilm and as a coating on Ti alloy). Taking into account the weight fractions in composite coatings, theoretical hardness, and Young's modulus values were calculated (using Equations (2) and (3)).

Table 4. A statement of weight fraction, real H, and real E parameters for pure components and MWCNTs composite coatings, compared with H and E parameters calculated based on H-P model for MWCNTs composite coatings.

Material	Weight Fraction of MWCNTs	Weight Fraction of TiO_2	Weight Fraction of nanoCu	Calculated H (GPa)	Calculated E (GPa)	Real H (GPa)	Real E (GPa)
Ti13Zr13Nb alloy	0	0	0	-	-	3.760 [67]	83.32 [67]
MWCNTs	1	0	0	-	-	0.204 [79]	2.659 [79]
TiO_2	0	1	0	-	-	1.000 [80]	68.00 [80]
nanoCu	0	0	1	-	-	1.200 [81]	104.20 [69]
MWCNTs coating	1	0	0	-	-	0.101	14.17
MWCNTs/TiO_2 coating	0.4	0.6	0	0.485	37.15	0.137	7.69
MWCNTs_Cu coating	0.952	0	0.048	0.114	15.22	0.213	10.83

Assuming that Young's modulus values are also additive, porosity might be expressed as a ratio of real Young's modulus to the calculated above value. However, such an approach is unjustified as it is no perfect composite. Zhang et al. tried to find a relation between porosity and mechanical properties (such as microhardness and Young's modulus) and reported that, from the statistical trend, the coating porosity increases when microhardness decreases, the same as Young's modulus decreases [82]. In literature, porosity phenomenon is related to a presence of empty spaces, named pores, and manifests itself as lower density and compactness of porous material than those of the same bulk material. Most methods evaluating the porosity of the coatings are based on image analysis, which is subjective [82,83]. On the other hand, coating porosity affects also the corrosion resistance of the coating's substrate, as revealed in [83,84]. Besides, as Praveen et al. reported [85], the CNTs addition to zinc deposit reduces pore volume, and thus improves the corrosion resistance of CNT-Zn coatings. The decrease in Young's modulus can be caused by pores which do not oppose the nanoindenter, but also by weak adhesion between MWCNTs and other nanoparticles. The physical image of occurring processes is different in solid materials and composites. Moreover, this composite coating has a specific structure: the main component, always placed on a metallic base, is a film composed of carbon nanotubes. If the ceramic layer is deposited on the previous MWCNTs layer, the randomly positioned nanotubes relatively easily bend off under a load of the penetrating nanoindenter and allow the layer comprised of titanium oxide nanoparticles also to deflect. Thus, the elastic elongation is easy and Young's modulus is low. For the dispersion composite coating with nanocopper particles, the course of the process is similar even if, in this case, the nanocopper particles directly penetrate the "forest" of nanotubes not encountering any serious opposition, to some extent.

The hardness, on the other side, has an understandable relation with the strengths of the components. The higher hardness values of layers comprising of titania or nanocopper can be explained by a specific nanohardness measurement which starts at the surface provided then that the minimal hardness is required to begin measurement (no test in the air might start). In such a case, in composite coatings, the hardness values which are means of several measurements may fulfill the relation between properties of composites, properties of each component, and fractions of individual components (Table 4). Differences between hardness values here measured and those assessed by the Halpin–Tsai model are simple to understand as the considered model has been prepared for composite materials in which there have been no empty spaces (pores, voids, cracks) and, on the other hand, a specific nature of isolated various nanoforms, bonded by presumably weak chemical and physical bonds. Despite that, these differences in hardness are not very high and, therefore, the obtained coatings may be assumed as of composite type, roughly approaching the properties of ideal composite solid. The applicable models for such composites which would take into account the inhomogeneous structure of a solid and adhesion forces between nanoparticles are, unfortunately, unknown at the moment.

Even more exciting is a comparison of real and theoretical values for Young's modulus. For both coatings, these values are lower than those predicted by the model, and again the 3D structure is useful to understand such behavior. For the bi-layer, the nanoindenter tip likely bends the titania layer and this motion is not substantially impeded by the MWCNTs inner layer with its long tubes, random positioning and significant free space between nanotubes. For MWCNTs_Cu, the mechanism of deformation is different and related likely more to the misfit between MWCNTs and nanocopper particles creating additional free spaces. Therefore, the difference between real and anticipated values is, in the last case, distinctly lower than for the bi-layer coating.

Figure 6 shows the 3D Young's modulus and nanohardness distribution for the MWCNTs sample, the MWCNTs/TiO_2 bi-layer coating, and the MWCNTs_Cu dispersion coating. As high fluctuations of both values can be observed depending on the specific measured area, these results are evidence that the coatings possess a highly non-uniform rough surface as already shown in topography tests and by great standard deviations in Table 5. The 3D-mechanical properties' distributions demonstrate "elevations", which result from the probe's contact with the surface of the native material for the MWCNTs reference coating, the presence of TiO_2 agglomerates for the MWCNTs/TiO_2 bi-layer coating and the presence of nanoCu aggregates, or in the aftermath of the microcracks, the probe's contact with the substrate of the MWCNTs_Cu dispersion coating.

Table 5. Mechanical properties and maximum indent depth for the substrate and achieved coatings.

Sample	Nanohardness H (GPa)	Reduced Young's Modulus Er (GPa)	Young's Modulus E (GPa)	Maximum Indent Depth (μm)	Plasticity Index PI (nJ)	Elastic Recovery Index EI (nJ)
MWCNTs	0.101 ± 0.049	18.59 ± 5.66	14.17 ± 4.32	2.07 ± 0.35	3.88 ± 0.85	0.378 ± 0.056
MWCNTs/TiO_2	0.137 ± 0.048	10.22 ± 2.33	7.69 ± 1.75	1.81 ± 0.33	5.87 ± 1.08	0.722 ± 0.084
MWCNTs_Cu	0.213 ± 0.061	14.28 ± 2.80	10.83 ± 2.12	1.43 ± 0.23	3.53 ± 0.53	0.688 ± 0.065

Generally, when hardness decreases, Young's modulus decreases as well, and vice versa, as shown by several examples such as for Ti-based alloys with Ta and Fe additions [86], MWCNTs [87], La_2O_3-modified HfC-SiC coating for SiC-coated C/C composites [88], HAp-Ti-CNTs [4], YSZ-C-alumina [89], Ti-C-TiN coatings [90], MWCNTs/graphene Al nanocomposite [91], YSZ/Al_2O_3 coatings [92], MWCNTs/HAp [4,9,93], and our previous results [67], but also such simple relationships have not been observed in presence of TiO_2 in BN sheets [94] and for Cu-Si composites [95]. Moreover, as perfectly shown in the review [96], nanoindentation measurements in multiphase solids are very complicated. For coatings, also the ratio of indenter displacement to coating thickness as it is important to know whether coating or substrate determines the indentation response.

Among the problems that contribute to the difficulty in the application of indentation techniques to natural inhomogeneous materials is the presence of pores, microcracks, and voids [97]. In porous materials, mechanical properties usually decrease with increasing porosity as flexural strength and hardness in ZrB_2-based composites [98], hardness in porous chromium carbide [99], Young's modulus for plasma-sprayed YSZ coatings [100]. In [101], Young's modulus and strength of single-phase TCP distinctly decrease with increasing porosity, for the first property over 50% at 20% porosity, but toughness was independent on porosity. On the other hand, for Cr_3C_2 ceramics, hardness increased at increasing pore size in the range 0.8 to 3.5 μm [99], but no explanation of this observation was proposed. Even for ZrO_2-Y_2O_3 coatings, again the same relationship between Young's modulus and hardness on porosity was observed, but only in some side regions so that this relation was sensitive to the morphology of the coating [102]. It is also to underline that hardness is related not only to elastic modulus but also to flexural strength, toughness, compression, and wear resistance in a complex way.

Two factors in multicomponent components determine mechanical properties. The first is the presence of tough particles, such as here, rutile nanograins and nanocopper

particles (tough species in nanoform). The hard particles counteract the indenter penetration through the matrix due to the accumulation of dislocations in the deformed area. Another determinant is adhesion and bond strength between components [95]. We think that in tested composite coatings, the dislocation effect is negligible, hardness is determined by tough particles, but weak adhesion of components results in easy separation of nanoparticles and movement of the nanoindenter tip between them, utilizing the free spaces (intrinsic pores).

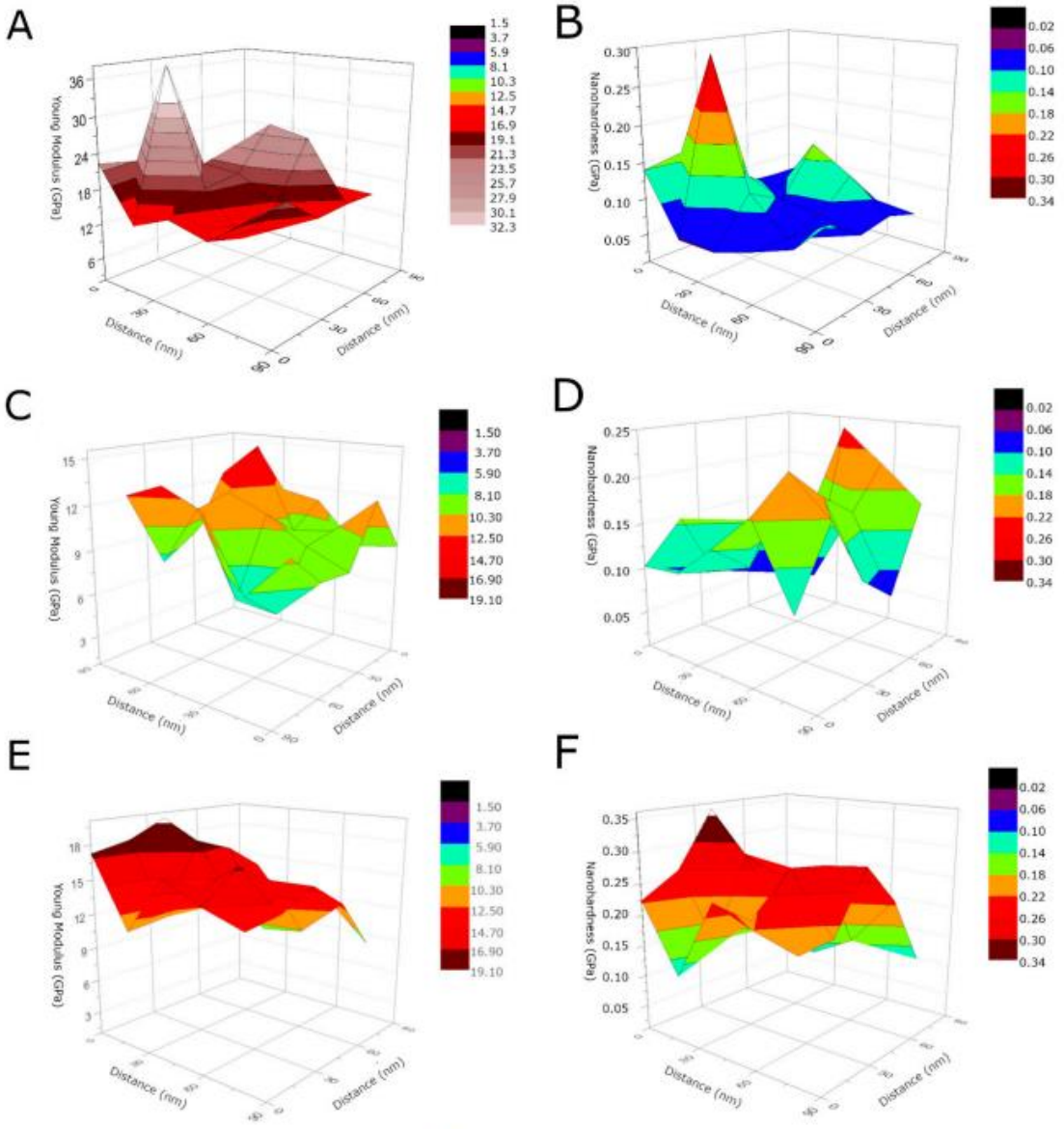

Figure 6. 3D Young's modulus and nanohardness distribution for the MWCNTs sample (**A**,**B**), the MWCNTs/TiO_2 coating (**C**,**D**), the MWCNTs_Cu coating (**E**,**F**), respectively.

The mechanical behavior and the wear resistance of the examined coatings were further assessed from the nanoindentation results by evaluating elastic recovery index (EI), plasticity index (PI), ratio of the nanohardness to the reduced elastic modulus (H/Er) and yield pressure (H^2/Er^3). The EI represents the amount of energy released by the material under the influence of load. Whereas, the PI demonstrates the energy dissipated in the coating due to plastic deformation [86,87,103]. Figure 7 shows the EI and PI of the MWCNTs sample, the MWCNTs/TiO_2 bi-layer and the MWCNTs_Cu dispersion coating deposited on the Ti13Nb13Zr alloy. The highest PI is observed for the MWCNTs/TiO_2 coating, indicating its highest plastic deformation during the nanoindentation test, while the PI for MWCNTs_Cu is the lowest. Nevertheless, the EI of the nanoCu and TiO_2-modified coatings were 2-fold improved in the contrary to the MWCNTs sample, which demonstrates the stiffening effect of the additives.

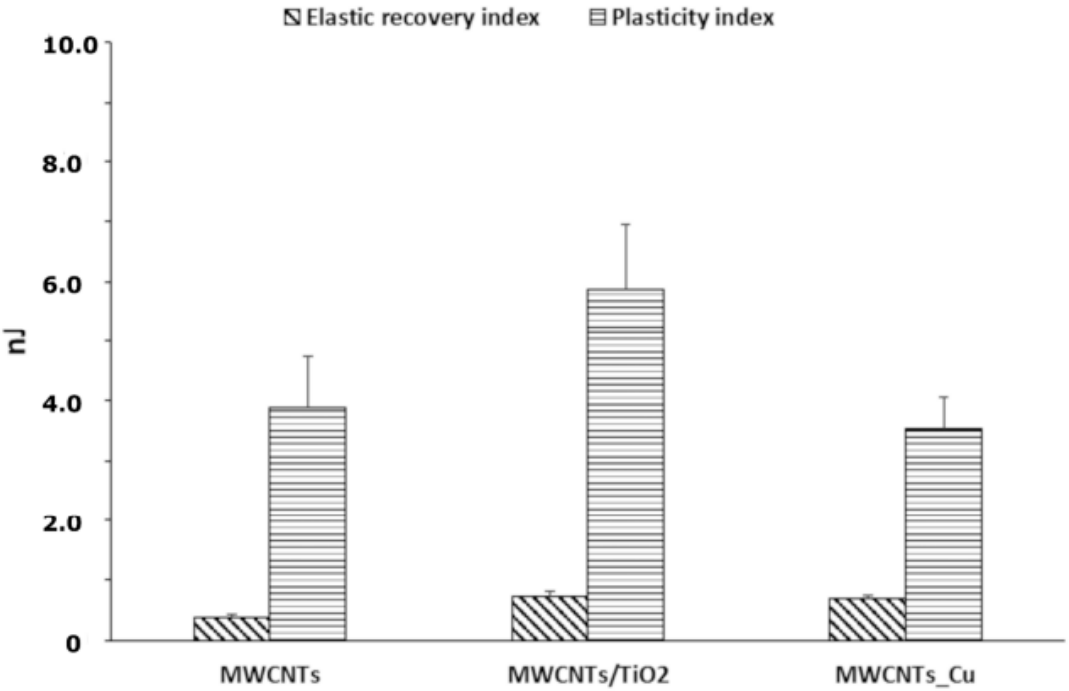

Figure 7. The diagram of EI and PI calculated for the MWCNTs coating, MWCNTs/TiO_2 bi-layer, and MWCNTs_Cu deposition coating, examined under indentation load of 10 mN.

Further crucial parameters are the ratio of the nanohardness to elastic modulus (H/Er), which shows the endurance capability of a surface coating, especially its ability to accommodate substrate deflections under load [103], and the yield pressure (H^3/Er^2), used to evaluate the resistance to plastic deformation of materials under nanoindenter tip load [56]. The H/Er and H^3/Er^2 parameters for the MWCNTs sample, the MWCNTs/TiO_2 bi-layer, and the MWCNTs_Cu dispersion coating, examined under indentation load of 10 mN are shown in Figure 8. The addition to the MWCNTs coating-based Ti13Nb13Zr substrate, several nanoCu or TiO_2 particles improves the wear resistance under surface deflections and the resistance to plastic deformation under applied load [86]. This means that the higher the H^3/Er^2 parameter is, the higher the fraction of plastic work during stress applying on coating surface should be. Conversely, the diagram showed in Figure 8 demonstrates the lowest PI for the MWCNTs_Cu dispersion coating, what indicates the release of energy

dissipated in the coating under nanoindenter tip load and explains the appearance of the cracks shown in Figure 2.

These results are favorable for both composite coatings. These coatings are innovative and, being able to oppose some stresses during and after implantation surgery, are plausible for clinical practice. Moreover, they potentially may express some antibacterial efficiency, all of the tested components. However, the coating composed of two layers, inner MWCNTs and rutile outer layer, is sufficiently thick and does not contain Cu, that above certain limits of content might be toxic for a biological organism. Therefore, in the next step, we are going to verify, for both coatings, their biological properties, including their wettability, bioactivity of live cells, cytotoxicity, and antibacterial efficiency.

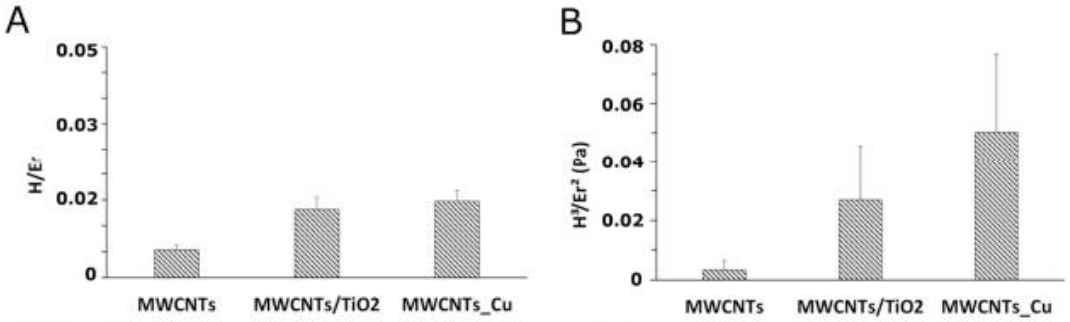

Figure 8. The diagrams for the H/Er (**A**) and the H^3/Er^2 parameter (**B**) calculated for the MWCNTs bi-layer and the MWCNTs_Cu dispersion coating, examined under indentation load of 10 mN.

4. Conclusions

In this study, the influence of titanium dioxide and nanocopper additions on the mechanical properties of the Ti13Nb13Zr substrate covered with the multi-wall carbon nanotube-based nanocomposites was investigated. The mechanical properties of the coatings were evaluated using the nanoindentation technique and the following conclusions were drawn from the investigations:

(1) The results show Young's modulus value tends to decrease with rising nanohardness, which is a positive effect resulting from the structure of composite coatings, i.e., a simultaneous presence of elastic carbon nanotubes and tough nanoparticles of copper or rutile.

(2) Both composite coatings demonstrate the mechanical properties better than the MWCNTs coating on Ti alloy. The additions of nanocopper or titanium dioxide to the MWCNTs coating-based Ti13Nb13Zr alloy substrate improve plastic and elastic recovery index, wear resistance to surface deflection, and to plastic deformation under applied load.

(3) Comparing composite coatings to each other, the dispersion coating with nanocopper has distinctly higher hardness, slightly higher yield pressure and Young's modulus, comparable endurance capability and elasticity recovery index, and substantially lower plasticity index. On the other side, the bi-layer coating has the greatest thickness combined with a satisfactory ability to accommodate the substrate under applied load, and the highest plasticity index, which indicates its best resistance to plastic deformation.

(4) The yield pressure parameter is strictly related to the plasticity index, which shows the endurance of material to plastic deformation.

(5) The observed stiffening effect can be attributed to dislocation strengthening under a load of the nanoindenter tip in presence of tough and hard nanoparticles.

(6) The noticed decreasing Young's modulus in both composite coatings compared to the MWCNTs coating may be explained by an appearance of porosity of coatings.

Author Contributions: Conceptualization, D.R.-W. and B.M.-M.; methodology, D.R.-W., B.M.-M., M.B. and B.B.; software, D.R.-W., M.B.; validation, D.R.-W., B.M.-M., and A.Z.; formal analysis, A.Z, D.R.-W.; investigation, D.R.-W., B.M.-M., M.B.; resources, D.R.-W., B.M.-M.; writing—original draft, D.R.-W.; writing—review and editing, A.Z.; visualization, D.R.-W.; supervision, A.Z.; project administration, B.M.-M. All authors have read and agreed to the published version of the manuscript.

Funding: This research received no external funding.

Institutional Review Board Statement: Not applicable.

Informed Consent Statement: Not applicable.

Data Availability Statement: Not applicable.

Acknowledgments: We would like to express our sincere gratitude to Grzegorz Gajowiec for their support in carrying out nanoindentation experiment and SEM analysis, Dawid Chojnowski—Team Leader Microscopes from Keyence International (Belgium) NV/SA for sharing microscope VHX Keyence equipment and support in preparing data to the above publication, Aleksandra Kowalska and Justyna Kiljan for their immense support in preparing coatings.

Conflicts of Interest: The authors declare no conflict of interest.

References

1. Park, J.E.; Jang, Y.S.; Bae, T.S.; Lee, M.H. Biocompatibility characteristics of titanium coated with multiwalled carbon nanotubes-hydroxyapatite nanocomposites. *Materials* **2019**, *12*, 224. [CrossRef]
2. Ji, X.; Li, X.; Yu, H.; Zhang, W.; Dong, H. Study on the carbon nanotubes reinforced nanocomposite coatings. *Diam. Relat. Mater.* **2019**, *91*, 247–254. [CrossRef]
3. Curtin, W.A.; Sheldon, B.W. CNT-reinforced ceramics and metals. *Mater. Today* **2004**, *7*, 44–49. [CrossRef]
4. Maleki-Ghaleh, H.; Khalil-Alla, J. Characterization, mechanical and in vitro biological behavior of hydroxyapatite-titanium-carbon nanotube composite coatings deposited on NiTi alloy by electrophoretic deposition. *Surf. Coat. Technol.* **2019**, *363*, 179–190. [CrossRef]
5. Cho, J.; Schaab, S.; Roether, J.A.; Boccaccini, A.R. Nanostructured carbon nanotube/TiO_2 composite coatings using electrophoretic deposition (EPD). *J. Nanopart. Res.* **2008**, *10*, 99–105. [CrossRef]
6. Priyadershini, S.; Rahman, O.S.A.; Pandey, K.K.; Keshri, A.K. Remarkable improvement in tribological behavior of plasma sprayed carbon nanotube and graphene nanoplatelates hybrid reinforced alumina nanocomposite coating. *Ceram. Int.* **2019**, *45*, 5768–5778. [CrossRef]
7. Ahmad, I.; Kennedy, A.; Zhu, Y.Q. Wear resistant properties of multi-walled carbon nanotubes reinforced Al_2O_3 nanocomposites. *Wear* **2010**, *269*, 71–78. [CrossRef]
8. Jambagi, S.C. Scratch adhesion strength of plasma sprayed carbon nanotube reinforced ceramic coatings. *J. Alloys Compd.* **2017**, *728*, 126–137. [CrossRef]
9. Lahiri, D.; Singh, V.; Keshri, A.K.; Seal, S.; Agarwal, A. Carbon nanotube toughened hydroxyapatite by spark plasma sintering: Microstructural evolution and multiscale tribological properties. *Carbon* **2010**, *48*, 3103–3120. [CrossRef]
10. Rajesh, R.; Senthilkumar, N.; Hariharasubramanian, A.; Ravichandran, Y.D. Review on hydroxyapatite-carbon nanotube composites and some of their applications. *Int. J. Pharm. Pharm. Sci.* **2012**, *4*, 2–6.
11. Singh, I.; Allan, P.; London, W. Nano-mechanical testing of novel bioactive carbon nanotubes/HAP nano particles composite coating. *NSTI Nanotechol.* **2007**, *4*, 145–148.
12. Farrokhi-rad, M.; Shahrabi, T.; Mahmoodi, S.; Khanmohammadi, S. Electrophoretic deposition of hydroxyapatite-chitosan-CNTs nanocomposite coatings. *Ceram. Int.* **2017**, *43*, 4663–4669. [CrossRef]
13. Kaya, C.; Singh, I.; Boccaccini, A.R. Multi-walled carbon nanotube-reinforced hydroxyapatite layers on Ti6Al4V medical implants by electrophoretic deposition (EPD). *Adv. Eng. Mater.* **2008**, *10*, 131–138. [CrossRef]
14. Wang, H.; He, P.; Ma, G.; Xu, B.; Xing, Z.; Chen, S.; Liu, Z.; Wang, Y. Tribological behavior of plasma sprayed carbon nanotubes reinforced TiO_2 coatings. *J. Eur. Ceram. Soc.* **2018**, *38*, 3660–3672. [CrossRef]
15. Jarernboon, W.; Pimanpang, S.; Maensiri, S.; Swatsitang, E.; Amornkitbamrung, V. Effects of multiwall carbon nanotubes in reducing microcrack formation on electrophoretically deposited TiO_2 film. *J. Alloys Compd.* **2009**, *476*, 840–846. [CrossRef]

Jażdżewska, M.; Bartmański, M. Nanotubular Oxide Layer Formed on Helix Surfaces of Dental Screw Implants. *Coatings* **2021**, *11*, 115. [CrossRef]

Golchin, A.; Wikner, A.; Emami, N. An investigation into tribological behaviour of multi-walled carbon nanotube/graphene oxide reinforced UHMWPE in water lubricated contacts. *Tribiol. Int.* **2016**, *95*, 156–161. [CrossRef]

18. Samad, M.A.; Sinha, S.K. Mechanical, thermal and tribological characterization of a UHMWPE film reinforced with carbon nanotubes coated on steel. *Tribiol. Int.* **2011**, *44*, 1932–1941. [CrossRef]
19. Lee, C.K. Wear and corrosion behavior of electrodeposited nickel–carbon nanotube composite coatings on Ti–6Al–4V alloy in Hanks' solution. *Tribiol. Int.* **2012**, *55*, 7–14. [CrossRef]
20. Chen, X.H.; Chen, C.S.; Xiao, H.N.; Liu, H.B.; Zhou, L.P.; Li, S.L.; Zhang, G. Dry friction and wear characteristics of nickel/carbon nanotube electroless composite deposits. *Tribiol. Int.* **2006**, *39*, 22–28. [CrossRef]
21. Zhen-Qiang, M.; Xi-Bin, L.I.; Yong-Jun, X.; Jing, Z. Preparation and tribological performances of Ni − P − multi-walled carbon nanotubes composite coatings. *Trans. Nonferrous Met. Soc. China* **2012**, *22*, 2719–2725. [CrossRef]
22. Ammara, S.; Shamaila, S.; Bokhari, A.; Sabah, A. Nonenzymatic glucose sensor with high performance electrodeposited nickel/copper/carbon nanotubes nanocomposite electrode. *J. Phys. Chem. Solids* **2018**, *120*, 12–19. [CrossRef]
23. Bakshi, S.R.; Lahiri, D.; Patel, R.R.; Agarwal, A. Nanoscratch behavior of carbon nanotube reinforced aluminum coatings. *Thin Solid Films* **2010**, *518*, 1703–1711. [CrossRef]
24. Bakshi, S.R.; Keshri, A.K.; Agarwal, A. A comparison of mechanical and wear properties of plasma sprayed carbon nanotube reinforced aluminum composites at nano and macro scale. *Mater. Sci. Eng. A* **2011**, *528*, 3375–3384. [CrossRef]
25. Maiti, A.; Laha, T. Study of distribution of Carbon nanotube in Al-CNT nanocomposite synthesized via Spark-Plasma sintering. *IOP Conf. Ser. Mater. Sci. Eng.* **2018**, *338*, 012014. [CrossRef]
26. Zeng, Z.; Lin, Y. Mechanical properties of hard Cr—MWNT composite coatings. *Surf. Coat. Technol.* **2009**, *203*, 3610–3613. [CrossRef]
27. Zanello, L.P.; Zhao, B.; Hu, H.; Haddon, R.C. Bone Cell Proliferation on Carbon Nanotubes. *Nano Lett.* **2006**, *6*, 562–567. [CrossRef]
28. Sasani, N.; Vahdati Khaki, J.; Mojtaba Zebarjad, S. Characterization and nanomechanical properties of novel dental implant coatings containing copper decorated-carbon nanotubes. *J. Mech. Behav. Biomed. Mater.* **2014**, *37*, 125–132. [CrossRef] [PubMed]
29. Benko, A.; Wiecheć, A.; Rajchel, B.; Długoń, E.; Błażewicz, M. Titanium surface modification with carbon nanotubes. Towards improved biocompatibility. *Acta Phys. Pol. A* **2016**, *129*, 176–178. [CrossRef]
30. Zhao, X.; Chang, S.; Long, J.; Li, J.; Li, X.; Cao, Y. The toxicity of multi-walled carbon nanotubes (MWCNTs) to human endothelial cells: The influence of diameters of MWCNTs. *Food Chem. Toxicol.* **2019**, *126*, 169–177. [CrossRef]
31. Li, Y.; Cao, J. The impact of multi-walled carbon nanotubes (MWCNTs) on macrophages: Contribution of MWCNT characteristics. *Sci. China Life Sci.* **2018**, *61*, 1333–1351. [CrossRef] [PubMed]
32. Louro, H. Relevance of physicochemical characterization of nanomaterials for understanding nano-cellular interactions. *Adv. Exp. Med. Biol.* **2018**, *1048*, 123–142. [CrossRef] [PubMed]
33. Portan, D.V.; Deligianni, D.D.; Deligianni, K.; Kroustalli, A.A.; Tyllianakis, M.; Papanicolaou, G.C. Modeling of the interaction between osteoblasts and biocompatible substrates as a function of adhesion strength. *J. Biomed. Mater. Res. Part A* **2018**, *106*, 621–628. [CrossRef] [PubMed]
34. Kumar, P. Nano-TiO_2 doped chitosan scaffold for the bone tissue engineering applications. *Int. J. Biomater.* **2018**, *2018*, 1–7. [CrossRef]
35. Fathi-Achachelouei, M.; Knopf-Marques, H.; Ribeiro da Silva, C.E.; Barthès, J.; Bat, E.; Tezcaner, A.; Vrana, N.E. Use of nanoparticles in tissue engineering and regenerative medicine. *Front. Bioeng. Biotechnol.* **2019**, *7*, 1–22. [CrossRef] [PubMed]
36. Park, H.; Yeo, M. Effects of TiO_2 nanoparticles and nanotubes on zebrafish caudal fin regeneration. *Mol. Cell. Toxicol.* **2013**, *9*, 375–383. [CrossRef]
37. Kumar, S.; Rani, R.; Dilbaghi, N.; Tankeshwar, K.; Kim, K.-H. Carbon nanotubes: A novel material for multifaceted applications in human healthcare. *Chem. Soc. Rev.* **2017**, *46*, 158–196. [CrossRef]
38. Vargas, M.A.; Rodríguez-Páez, J.E. Amorphous TiO_2 nanoparticles: Synthesis and antibacterial capacity. *J. Non. Cryst. Solids* **2017**, *459*, 192–205. [CrossRef]
39. Raddaha, N.; Cordero-Arias, L.; Cabanas-Polo, S.; Virtanen, S.; Roether, J.; Boccaccini, A. Electrophoretic deposition of chitosan/h-BN and chitosan/h-BN/TiO_2 composite coatings on stainless steel (316L) substrates. *Materials* **2014**, *7*, 1814–1829. [CrossRef] [PubMed]
40. Ikono, R.; Li, N.; Pratama, N.H.; Vibriani, A.; Yuniarni, D.R.; Luthfansyah, M.; Bachtiar, B.M.; Bachtiar, E.W.; Mulia, K.; Nasikin, M.; et al. Enhanced bone regeneration capability of chitosan sponge coated with TiO_2 nanoparticles. *Biotechnol. Rep.* **2019**, *24*, e00350. [CrossRef]
41. Hsiao, I.-L.; Huang, Y.-J. Effects of various physicochemical characteristics on the toxicities of ZnO and TiO_2 nanoparticles toward human lung epithelial cells. *Sci. Total Environ.* **2011**, *409*, 1219–1228. [CrossRef] [PubMed]
42. Uboldi, C.; Urbán, P.; Gilliland, D.; Bajak, E.; Valsami-Jones, E.; Ponti, J.; Rossi, F. Role of the crystalline form of titanium dioxide nanoparticles: Rutile, and not anatase, induces toxic effects in Balb/3T3 mouse fibroblasts. *Toxicol. Vitr.* **2016**, *31*, 137–145. [CrossRef]
43. Boccaccini, A.R.; Cho, J.; Roether, J.A.; Thomas, B.J.C.; Minay, E.J.; Shaffer, M.S.P. Electrophoretic deposition of carbon nanotubes. *Carbon* **2006**, *44*, 3149–3160. [CrossRef]
44. Mohammed Thalib Basha, G.; Srikanth, A.; Venkateshwarlu, B. Effect of reinforcement of carbon nanotubes on air plasma sprayed conventional Al_2O_3-3%TiO_2 ceramic coatings. *Mater. Today Proc.* **2020**, *20*, 191–194. [CrossRef]
45. Kolmas, J.; Groszyk, E.; Kwiatkowska-Różycka, D. Substituted hydroxyapatites with antibacterial properties. *Biomed. Res. Int.* **2014**, *2014*, 1–15. [CrossRef] [PubMed]

46. Hidalgo-Robatto, B.M.; López-Álvarez, M.; Azevedo, A.S.; Dorado, J.; Serra, J.; Azevedo, N.F.; González, P. Pulsed laser deposition of copper and zinc doped hydroxyapatite coatings for biomedical applications. *Surf. Coat. Technol.* **2018**, *333*, 168–177. [CrossRef]
47. Shanmugam, S.; Gopal, B. Copper substituted hydroxyapatite and fluorapatite: Synthesis, characterization and antimicrobial properties. *Ceram. Int.* **2014**, *40*, 15655–15662. [CrossRef]
48. Rau, J.V.; Wu, V.M.; Graziani, V.; Fadeeva, I.V.; Fomin, A.S.; Fosca, M.; Uskoković, V. The bone building blues: Self-hardening copper-doped calcium phosphate cement and its in vitro assessment against mammalian cells and bacteria. *Mater. Sci. Eng. C* **2017**, *79*, 270–279. [CrossRef]
49. Chen, Z.; Meng, H.; Xing, G.; Chen, C.; Zhao, Y.; Jia, G.; Wang, T.; Yuan, H.; Ye, C.; Zhao, F.; et al. Acute toxicological effects of copper nanoparticles in vivo. *Toxicol. Lett.* **2006**, *163*, 109–120. [CrossRef]
50. Radovanović, Ž.; Jokić, B.; Veljović, D.; Dimitrijević, S.; Kojić, V.; Petrović, R.; Janaćković, D. Antimicrobial activity and biocompatibility of Ag+- and Cu^{2+}-doped biphasic hydroxyapatite/α-tricalcium phosphate obtained from hydrothermally synthesized Ag+- and Cu^{2+}-doped hydroxyapatite. *Appl. Surf. Sci.* **2014**, *307*, 513–519. [CrossRef]
51. Karthika, A. Biocompatible iron and copper incorporated nanohydroxyapatite coating for biomedical implant applications. *Mater. Today Proc.* **2021**, in press. [CrossRef]
52. Rivera, L.R.; Cochis, A.; Biser, S.; Canciani, E.; Ferraris, S.; Rimondini, L.; Boccaccini, A.R. Antibacterial, pro-angiogenic and pro-osteointegrative zein-bioactive glass/copper based coatings for implantable stainless steel aimed at bone healing. *Bioact. Mater.* **2021**, *6*, 1479–1490. [CrossRef]
53. Liang, T.; Wang, Y.; Zeng, L.; Liu, Y.; Qiao, L.; Zhang, S.; Zhao, R.; Li, G.; Zhang, R.; Xiang, J.; et al. Copper-doped 3D porous coating developed on Ti-6Al-4V alloys and its in vitro long-term antibacterial ability. *Appl. Surf. Sci.* **2020**, *509*, 144717. [CrossRef]
54. Fraczek-Szczypta, A.; Wedel-Grzenda, A.; Benko, A.; Grzonka, J.; Mizera, J. Interaction of carbon nanotubes coatings with titanium substrate. *Appl. Phys. A* **2017**, *123*, 120. [CrossRef]
55. Cho, J.; Konopka, K.; Rożniatowski, K.; García-Lecina, E.; Shaffer, M.S.P.; Boccaccini, A.R. Characterisation of carbon nanotube films deposited by electrophoretic deposition. *Carbon* **2009**, *47*, 58–67. [CrossRef]
56. Zhong, Z.; Qian, L.; Tan, Y.; Wang, G.; Yang, L.; Hou, C.; Liu, A. A high-performance glucose/oxygen biofuel cell based on multi-walled carbon nanotube films with electrophoretic deposition. *J. Electroanal. Chem.* **2018**, *823*, 723–729. [CrossRef]
57. Fraczek-Szczypta, A.; Dlugon, E.; Weselucha-Birczynska, A.; Nocun, M.; Blazewicz, M. Multi walled carbon nanotubes deposited on metal substrate using EPD technique. A spectroscopic study. *J. Mol. Struct.* **2013**, *1040*, 238–245. [CrossRef]
58. Benko, A.; Przekora, A.; Wesełucha-Birczyńska, A.; Nocuń, M.; Ginalska, G.; Błażewicz, M. Fabrication of multi-walled carbon nanotube layers with selected properties via electrophoretic deposition: Physicochemical and biological characterization. *Appl. Phys. A* **2016**, *122*, 447. [CrossRef]
59. Zhong, Z.; Qin, J.; Ma, J. Electrophoretic deposition of biomimetic zinc substituted hydroxyapatite coatings with chitosan and carbon nanotubes on titanium. *Ceram. Int.* **2015**, *41*, 8878–8884. [CrossRef]
60. Wedel-Grzenda, K.; Tran, A.F.-S. The influence different types of carbon nanomaterial on the properties of coatings obtained by EPD process. *Eng. Biomater.* **2016**, *135*, 13–20.
61. Dlugon, E.; Simka, W.; Fraczek-Szczypta, A.; Niemiec, W.; Markowski, J.; Szymanska, M.; Blazewicz, M. Carbon nanotube-based coatings on titanium. *Bull. Mater. Sci.* **2015**, *38*, 1339–1344. [CrossRef]
62. Singh, I.; Kaya, C.; Shaffer, M.S.P.; Thomas, B.C.; Boccaccini, A.R. Bioactive ceramic coatings containing carbon nanotubes on metallic substrates by electrophoretic deposition. *J. Mater. Sci.* **2006**, *41*, 8144–8151. [CrossRef]
63. Fraczek-Szczypta, A.; Jantas, D.; Ciepiela, F.; Grzonka, J.; Bernasik, A.; Marzec, M. Carbon nanomaterials coatings–Properties and influence on nerve cells response. *Diam. Relat. Mater.* **2018**, *84*, 127–140. [CrossRef]
64. Ibrahim, M.Z.; Sarhan, A.A.D.; Yusuf, F.; Hamdi, M. Biomedical materials and techniques to improve the tribological, mechanical and biomedical properties of orthopedic implants—A review article. *J. Alloys Compd.* **2017**, *714*, 636–667. [CrossRef]
65. Feizi Mohazzab, B.; Jaleh, B.; Kakuee, O.; Fattah-alhosseini, A. Formation of titanium carbide on the titanium surface using laser ablation in n-heptane and investigating its corrosion resistance. *Appl. Surf. Sci.* **2019**, *478*, 623–635. [CrossRef]
66. Bartmanski, M.; Cieslik, B.; Glodowska, J.; Kalka, P.; Pawlowski, L.; Pieper, M.; Zielinski, A. Electrophoretic deposition (EPD) of nanohydroxyapatite—nanosilver coatings on Ti13Zr13Nb alloy. *Ceram. Int.* **2017**, *43*, 11820–11829. [CrossRef]
67. Majkowska-Marzec, B.; Rogala-Wielgus, D.; Bartmański, M.; Bartosewicz, B.; Zieliński, A. Comparison of properties of the hybrid and bilayer MWCNTs—hydroxyapatite coatings on Ti alloy. *Coatings* **2019**, *9*, 643. [CrossRef]
68. Borgese, L.; Gelfi, M.; Bontempi, E.; Goudeau, P.; Geandier, G.; Thiaudière, D.; Depero, L.E. Young modulus and Poisson ratio measurements of TiO_2 thin films deposited with Atomic Layer Deposition. *Surf. Coat. Technol.* **2012**, *206*, 2459–2463. [CrossRef]
69. Zhao, J.-H.; Du, Y.; Morgen, M.; Ho, P.S. Simultaneous measurement of Young's modulus, Poisson ratio, and coefficient of thermal expansion of thin films on substrates. *J. Appl. Phys.* **2000**, *87*, 1575–1577. [CrossRef]
70. Mahmun, A.; Kirtania, S. Evaluation of elastic properties of graphene nanoplatelet/epoxy nanocomposites. *Mater. Today Proc.* **2021**, *44*, 1531–1535. [CrossRef]
71. Goyal, R.K.; Tiwari, A.N.; Negi, Y.S. Microhardness of PEEK/ceramic micro- and nanocomposites: Correlation with Halpin–Tsai model. *Mater. Sci. Eng. A* **2008**, *491*, 230–236. [CrossRef]

Adegbenjo, A.O.; Obadele, B.A.; Olubambi, P.A. Densification, hardness and tribological characteristics of MWCNTs reinforced Ti6Al4V compacts consolidated by spark plasma sintering. *J. Alloys Compd.* **2018**, *749*, 818–833. [CrossRef]

73. Ramganesh, V.; Ananth Kumar, M.; Mini, K.; Vignesh, V.; Karthikeyan, R. Effect of nano TiO_2-epoxy composite in bond strength and corrosion resistance of rebar embedded in micro-silica modified concrete. *J. Phys. Conf. Ser.* **2020**, *1706*, 012122. [CrossRef]
74. Kaczmar, J.W.; Granat, K.; Kurzawa, A.; Grodzka, E. Physical Properties of Copper Based MMC Strengthened with Alumina. *Arch. Foundry Eng.* **2014**, *14*, 85–90. [CrossRef]
75. Lee, W.; Lee, S.-B.; Choi, O.; Yi, J.-W.; Um, M.-K.; Byun, J.-H.; Thostenson, E.T.; Chou, T.-W. Formicary-like carbon nanotube/copper hybrid nanostructures for carbon fiber-reinforced composites by electrophoretic deposition. *J. Mater. Sci.* **2011**, *46*, 2359–2364. [CrossRef]
76. Chen, Y.; Jiang, H.; Li, D.; Song, H.; Li, Z.; Sun, X.; Miao, G.; Zhao, H. Improved field emission performance of carbon nanotube by introducing copper metallic particles. *Nanoscale Res. Lett.* **2011**, *6*, 537. [CrossRef]
77. Byrne, D.P.; Lacroix, D.; Planell, J.A.; Kelly, D.J.; Prendergast, P.J. Simulation of tissue differentiation in a scaffold as a function of porosity, Young's modulus and dissolution rate: Application of mechanobiological models in tissue engineering. *Biomaterials* **2007**, *28*, 5544–5554. [CrossRef]
78. Javaid, F.; Pouriayevali, H.; Durst, K. Dislocation–grain boundary interactions: Recent advances on the underlying mechanisms studied via nanoindentation testing. *J. Mater. Res.* **2021**. [CrossRef]
79. Zheng, C.; Chen, W.; Ye, X. Study on Au nanoparticles, TiO_2 nanoclusters, and SiO_2 nanoshells coated multi-wall carbon nanotubes/silica gel-glass. *Opt. Mater.* **2012**, *34*, 1042–1047. [CrossRef]
80. Jämting, Å.K.; Bell, J.M.; Swain, M.V.; Wielunski, L.S.; Clissold, R. Measurement of the micro mechanical properties of sol-gel TiO_2 films. *Thin Solid Films* **1998**, *332*, 189–194. [CrossRef]
81. Pavithra, C.L.P.; Sarada, B.V.; Rajulapati, K.V.; Rao, T.N.; Sundararajan, G. A new electrochemical approach for the synthesis of copper-graphene nanocomposite foils with high hardness. *Sci. Rep.* **2015**, *4*, 4049. [CrossRef]
82. Zhang, X.C.; Xu, B.S.; Xuan, F.Z.; Tu, S.T.; Wang, H.D.; Wu, Y.X. Porosity and effective mechanical properties of plasma-sprayed Ni-based alloy coatings. *Appl. Surf. Sci.* **2009**, *255*, 4362–4371. [CrossRef]
83. Ahn, S.; Lee, J.; Kim, H.; Kim, J. A study on the quantitative determination of through-coating porosity in PVD-grown coatings. *Appl. Surf. Sci.* **2004**, *233*, 105–114. [CrossRef]
84. Zhang, S.D.; Zhang, W.L.; Wang, S.G.; Gu, X.J.; Wang, J.Q. Characterisation of three-dimensional porosity in an Fe-based amorphous coating and its correlation with corrosion behaviour. *Corros. Sci.* **2015**, *93*, 211–221. [CrossRef]
85. Praveen, B.M.; Venkatesha, T.V.; Arthoba Naik, Y.; Prashantha, K. Corrosion studies of carbon nanotubes–Zn composite coating. *Surf. Coat. Technol.* **2007**, *201*, 5836–5842. [CrossRef]
86. Ehtemam-Haghighi, S.; Cao, G.; Zhang, L. Nanoindentation study of mechanical properties of Ti based alloys with Fe and Ta additions. *J. Alloys Compd.* **2017**, *692*, 892–897. [CrossRef]
87. Okoro, A.M.; Machaka, R.; Lephuthing, S.S.; Oke, S.R.; Awotunde, M.A.; Olubambi, P.A. Nanoindentation studies of the mechanical behaviours of spark plasma sintered multiwall carbon nanotubes reinforced Ti6Al4V nanocomposites. *Mater. Sci. Eng. A* **2019**, *765*, 138320. [CrossRef]
88. Feng, G.; Li, H.; Yao, X.; Liu, T.; Jia, Y.; Yang, L.; Li, B. Mechanical properties and ablation resistance of La_2O_3-modified HfC-SiC coating for SiC-coated C/C composites. *Corros. Sci.* **2021**, *182*, 109259. [CrossRef]
89. Thakare, J.G.; Pandey, C.; Mulik, R.S.; Mahapatra, M.M. Mechanical property evaluation of carbon nanotubes reinforced plasma sprayed YSZ-alumina composite coating. *Ceram. Int.* **2018**, *44*, 6980–6989. [CrossRef]
90. Zhao, Y.; Zhang, T.; Chen, L.; Yu, T.; Sun, J.; Guan, C. Microstructure and mechanical properties of Ti–C–TiN-reinforced Ni204-based laser-cladding composite coating. *Ceram. Int.* **2021**, *47*, 5918–5928. [CrossRef]
91. Kumar, V.; Kempaiah, U.N.; Shivasharanayyaswamy; Bopanna, S.B. Nanoindentation studies on multiwalled carbon nanotubes/graphene reinforced aluminium alloy 6061 nanocomposites. *Mater. Today Proc.* **2020**, *45*, 202–206. [CrossRef]
92. Lu, X.-J.; Wang, X.; Xiao, P. Nanoindentation and residual stress measurements of yttria-stablized zirconia composite coatings produced by electrophoretic deposition. *Thin Solid Films* **2006**, *494*, 223–227. [CrossRef]
93. Hahn, B.; Lee, J.-M.; Park, D.; Choi, J.; Ryu, J.; Yoon, W.; Lee, B.; Shin, D.; Kim, H. Mechanical and in vitro biological performances of hydroxyapatite–carbon nanotube composite coatings deposited on Ti by aerosol deposition. *Acta Biomater.* **2009**, *5*, 3205–3214. [CrossRef]
94. Huang, Z.; Zhao, W. Coupling hybrid of HBN nanosheets and TiO_2 to enhance the mechanical and tribological properties of composite coatings. *Prog. Org. Coat.* **2020**, *148*, 105881. [CrossRef]
95. Chmielewski, M.; Nosewicz, S.; Wyszkowska, E.; Kurpaska, Ł.; Strojny-Nedza, A.; Pi, A.; Bazarnik, P.; Pietrzak, K. Analysis of the micromechanical properties of copper-silicon carbide composites using nanoindentation measurements. *Ceram. Int.* **2019**, *45*, 9164–9173. [CrossRef]
96. Bull, S.J. Nanoindentation of coatings. *J. Phys. D Appl. Phys.* **2005**, *38*, R393–R413. [CrossRef]
97. Epshtein, S.A.; Borodich, F.M.; Bull, S.J. Evaluation of elastic modulus and hardness of highly inhomogeneous materials by nanoindentation. *Appl. Phys. A* **2015**, *119*, 325–335. [CrossRef]
98. Balak, Z.; Zakeri, M.; Rahimipur, M.R.; Salahi, E.; Nasiri, H. Effect of open porosity on flexural strength and hardness of ZrB2-based composites. *Ceram. Int.* **2015**, *41*, 8312–8319. [CrossRef]
99. Zhang, L.; Gao, K.; Elias, A.; Dong, Z.; Chen, W. Porosity dependence of elastic modulus of porous Cr_3C_2 ceramics. *Ceram. Int.* **2014**, *40*, 191–198. [CrossRef]

100. Karthikeyan, S.; Balasubramanian, V.; Rajendran, R. Developing empirical relationships to estimate porosity and Young's modulus of plasma sprayed YSZ coatings. *Appl. Surf. Sci.* **2014**, *296*, 31–46. [CrossRef]
101. Garcia-Prieto, A.; Hornez, J.C.; Leriche, A.; Pena, P.; Baudín, C. Influence of porosity on the mechanical behaviour of single phase β-TCP ceramics. *Ceram. Int.* **2017**, *43*, 6048–6053. [CrossRef]
102. Jang, B.; Matsubara, H. Influence of porosity on hardness and Young's modulus of nanoporous EB-PVD TBCs by nanoindentation. *Mater. Lett.* **2005**, *59*, 3462–3466. [CrossRef]
103. Musil, J.; Kunc, F.; Zeman, H.; Poláková, H. Relationships between hardness, Young's modulus and elastic recovery in hard nanocomposite coatings. *Surf. Coat. Technol.* **2002**, *154*, 304–313. [CrossRef]

6.3 [A3]

POLITECHNIKA GDAŃSKA | WYDZIAŁ INŻYNIERII MECHANICZNEJ I OKRĘTOWNICTWA

RESEARCH UNIVERSITY

OŚWIADCZENIE

Dotyczy publikacji w czasopiśmie naukowym:

Rogala-Wielgus D., Majkowska-Marzec B., Zieliński A., Jankiewicz B. J.: *Mechanical behavior of bi-layer and dispersion coatings composed of several nanostructures on Ti substrate*, Applied Sciences-Basel. 11 (2021) 7862.
https://doi.org/10.3390/app11177862

Impact Factor: 2,838
Punkty wg MNiSW: 100 pkt.

Oświadczamy, że wkład autorów w powstanie powyższej publikacji kształtuje się następująco:

L.p.	Współautor	Wkład, %	Wkład merytoryczny
1.	**Dorota Rogala-Wielgus**	**70**	**realizacja przeglądu literaturowego; opracowanie koncepcji badań; przygotowanie powłok; przeprowadzenie badań; analiza wyników; przygotowanie manuskryptu; edycja manuskryptu; przygotowanie odpowiedzi na recenzje; rola autora korespondencyjnego**
2.	Beata Majkowska-Marzec	15	udział w opracowaniu koncepcji badań; udział w realizacji badań; udział w analizie wyników
3.	Andrzej Zieliński	10	nadzór merytoryczny; korekta końcowa; edycja manuskryptu; udział w przygotowaniu odpowiedzi na recenzje
4.	Bartłomiej Jankiewicz	5	udział w analizie wyników; korekta końcowa

Podpisy współautorów:

Dorota Rogala-Wielgus
mgr inż. Dorota Rogala-Wielgus

Majkowska-Marzec Beata
dr inż. Beata Majkowska-Marzec

prof. dr hab. inż. Andrzej Zieliński

Bartłomiej Jankiewicz
dr inż. Bartłomiej Jankiewicz

POLITECHNIKA GDAŃSKA pg.edu.pl
Ul. Gabriela Narutowicza 11/12
80-233 Gdańsk

applied sciences

MDPI

Article

Mechanical Behavior of Bi-Layer and Dispersion Coatings Composed of Several Nanostructures on Ti Substrate

Dorota Rogala-Wielgus [1,*], Beata Majkowska-Marzec [1], Andrzej Zieliński [1] and Bartłomiej J. Jankiewicz [2]

[1] Division of Biomaterials Technology, Faculty of Mechanical Engineering and Shipbuilding, Gdansk University of Technology, 11 Narutowicza Street, 80-233 Gdańsk, Poland; beata.majkowska@pg.edu.pl (B.M.-M.); andrzej.zielinski@pg.edu.pl (A.Z.)
[2] Institute of Optoelectronics, Military University of Technology, Gen. S. Kaliskiego 2, 00-908 Warszawa, Poland; bartlomiej.jankiewicz@wat.edu.pl
* Correspondence: dorota.wielgus@pg.edu.pl; Tel.: +48-534-897-893

Abstract: Three coatings suitable for biomedical applications, including the dispersion coating composed of multi-wall carbon nanotubes (MWCNTs), MWCNTs/TiO_2 bi-layer coating, and MWCNTs-Cu dispersion coating, were fabricated by electrophoretic deposition (EPD) on Ti Grade II substrate. Optical microscopy, scanning electron microscopy, energy-dispersive X-ray spectroscopy, and nanoindentation were applied to study topography, chemical, and phase composition, roughness, hardness, Young's modulus, plastic, and elastic behavior. The results showed that the best mechanical properties in terms of biomedical application were achieved for the MWCNTs coating with titania outer layer. Nevertheless, both the addition of nanocopper and titania improved the mechanical resistance of the base MWCNTs coating. Compared to our previous experiments on Ti13Nb13Zr alloy, a general tendency is observed to form more homogenous coatings on pure metal than on the alloy, in which chemical and phase compositions are more complex.

Keywords: carbon nanotubes; coatings; nanohardness; Young's modulus

Citation: Rogala-Wielgus, D.; Majkowska-Marzec, B.; Zieliński, A.; Jankiewicz, B.J. Mechanical Behavior of Bi-Layer and Dispersion Coatings Composed of Several Nanostructures on Ti Substrate. *Appl. Sci.* **2021**, *11*, 7862. https://doi.org/10.3390/app11177862

Academic Editor: Elzbieta Pach

Received: 30 July 2021
Accepted: 24 August 2021
Published: 26 August 2021

1. Introduction

The carbon nanotubes (CNTs) belong to highly promising functional materials due to their extraordinary properties as electrical semiconductivity, high mechanical stiffness, tensile strength, high elasticity, significant thermal conductivity, and, in certain conditions, superconductivity [1,2]. The CNTs may appear in different forms as single-, double-, and multi-wall carbon nanotubes (MWCNTs) [3], nanohorns, and nanobuds [1]. They find applications in different fields as many branches of nanotechnology, nanomedicine, membranes and biosensors, electrochemical, piezoelectric and gas sensors, capacitors, and transistors in electronics [3], and high-performance batteries [4,5]. In particular, in medicine, they are proposed for drug targeting, cancer diagnosis, and treatment, as antibacterial and antifungal structures [2], and as gene carriers [6].

The most popular development direction of CNTs is their application in multi-component materials. The typical recent examples include cellulose—CNTs for methylene adsorption [7], nitrogen-doped graphene—CNTs for microwave absorption [8], polypyrrole—CNTs for storage devices [9], ZnO—CNTs dispersed in PU for better anti-corrosion resistance [10], cement [11,12], and Al alloy reinforced with CNTs [13]. The specific optical and electrical properties, high specific surface area, high chemical activity, and significant mechanical behavior are the reasons for the development of a great number of such composite materials [14,15].

CNTs can also form coatings, layers, or films. They have been, rather seldomly, proposed as single coating, e.g., to enhance the adsorption of albumins on Ti [16], in condensation heat transfer systems [17], to enhance biotribological resistance of Ti alloy [18], to mitigate biofouling [19], and in environmental protection [20]. However, they

are more often used as one of the layers in sandwich (hybrid) coatings, or as one of the components of the coating. The most frequently studied composite coatings are those based on CNTs and CNTs reinforced hydroxyapatite (HAp) [21–23], and HAp substituted by (Sr + Mg + Zn) [24], Hap-collagen-MWCNTs [25], and Hap-titanium-CNTs [26]. Other research focused on composite coatings such as tantalum oxide-CNTs [27], collagen-CNTs [28], collagen-CNTs-acrylic acid [29], CNTs-polysiloxane [30], and Al_3Ti-Cu-SiC-CNTs [31]. As concerns the noble metals, it is important to note the electrodes obtained by atomic layer deposition and composed of MWCNTs, TiO_2, and Pt [32]. The possibility of interaction of Ni, Ti, Pd, and Au with CNTs was shown for different forms of carbon nanotubes [33]. Nanochitosan capped gold nanoparticles were also obtained [34]. The important role of nanogold in the immobilization of proteins associated with SARS-CoV-2 was shown by Yokohama et al. [35,36].

The use of noble or semi-noble metals is justified by their antibacterial properties. However, if silver is assumed to be a safe element to human cells [37], the higher potential risk comes from the use of nanocopper than two-valent copper ions, related to different mechanisms of their toxic effects [38]. On the other hand, rGO (reduced graphene oxide)—nanoCu scaffolds demonstrated high antibacterial efficiency [39]. The nanogold was shown to eliminate pathogenic bacteria and even cancer cells [40], but no data about the side effects of this element are known.

The research studies described in this article are aimed at determining several properties of some new promising multi-component systems for medicine, which are based on MWCNTs. The titanium dioxide is added to the MWCNTs-based coating to enhance its mechanical behavior, while nanocopper is implemented to create the antibacterial activity of titanium implants. The MWCNTs-titanium oxide systems were developed for different purposes as nanocomposites obtained by sol-gel technique [41], by high energy ball milling [42], and by atomic layer deposition of titania on MWCNTs [43]. Nanocopper was a component of several coatings: HAp-nanoCu [44,45] and polyelectrolyte-nanoCu [46]. However, there is no sufficient research or knowledge on such material systems, which are potentially promising in the development of antibacterial, bioactive, and mechanically strong coatings for titanium implants.

2. Materials and Methods

2.1. Materials

The Ti Grade II (EkspresStal, Luboń, Poland) was used as a substrate. Specimens in form of 40 mm in diameter and 4 mm thick slices were cut from the rod and divided into quarters using a precision cutter (Brillant 220, ATM GmbH, Mammelzen, Germany). The surface was ground using abrasive paper SiC up to grit # 800 on a metallographic grinding machine (Saphir 330, ATM GmbH, Mammelzen, Germany). Then, specimens were rinsed with acetone (Chempur, Piekary Śląskie, Poland), distilled water, dried in the air, and pickled in 5% HF (Chempur, Piekary Śląskie, Poland) for 30 s to remove oxide layers from the surface, and finally rinsed with distilled water.

The multi-wall carbon nanotubes (MWCNTs) had an outer diameter of 10–15 nm, an inner diameter of 2–6 nm, a length of 1–10 µm, and the number of walls 3–15 (3D-Nano, Krakow, Poland). Nanocopper (nanoCu) had a mean grain size of 80 nm (Hongwu International Group Ltd., Guangzhou, Guangdong, China). Titanium dioxide (TiO_2) of rutile structure (3D-Nano, Krakow, Poland), possessed a grain size in the range of 1 to 2 nm.

2.2. Fabrication of the Bi-Layer MWCNTs/TiO_2 Coating and MWCNTs_Cu Dispersion Coating

The electrophoretic deposition (EPD) method was used to prepare coatings, for which synthesis parameters are shown in Table 1. The Ti Grade II substrate was used as an anode and stainless steel as a counter-electrode for the MWCNTs coating, and inversely for both other coatings. The electrodes were placed parallel to each other within a distance of 5 mm and connected to the DC power source (MCP/SPN110-01C, Shanghai MCP Corp., Shanghai, China).

Table 1. Parameters of synthesis of coatings.

Coating	Substrate	Deposited Materials	Content of Component in a Bath (wt. pct.)	EPD Time (min)	EPD Voltage (V)
MWCNTs	Ti Grade II	MWCNTs	0.25	1	20
MWCNTs_TiO_2	Ti Grade II	(I) MWCNTs (II) TiO_2	0.25 0.30	1 4	20 50
MWCNTs/Cu	Ti Grade II	MWCNTs + nanoCu	0.25 0.0125	4	50

The EPD process was conducted at parameters selected based on the preliminary studies. The bi-layer coating MWNCTs_TiO_2 was prepared in two steps. First, the electrophoretic suspension of 0.1 g MWCNTs in 40 mL of distilled water was prepared and the EPD process on Ti Grade II substrate proceeded (designation: MWCNTs). Second, the same samples were deposited in suspension consisted of 0.15 g TiO_2 dispersed in 50 mL of isopropanol together with 0.5 mL of surfactant -Polysorbate 20 (Tween 20, Sigma-Aldrich, Poznan, Poland).

To prepare the dispersion coating MWCNTs_Cu, 0.1 g of MWCNTs, 0.005 g of nanoCu, and 0.5 mL of Polysorbate 20 were dispersed in 40 mL of distilled water and deposited using the EPD method on Ti Grade II substrate.

2.3. Structure and Morphology

To study the surface topography, the optical microscope (VHX Keyence, Keyence International (Belgium) NV/SA, Mechelen, Belgium) was used. The average roughness index S_a values were estimated based on 512 lines made in the area of approximately 150 μm × 140 μm. Additionally, the atomic force microscopy (NaniteAFM, Nanosurf AG, Liestal, Switzerland) at a non-contact mode of testing with a 20 nN force was applied for the same purpose. Tests were made on the surface of dimensions 50 μm × 50 μm and the S_a parameter was estimated based on 256 lines (time for a single line of 2 s).

The specimens' surfaces and cross-sections were observed using a high-resolution scanning electron microscope (SEM) (JSM-7800F, JOEL, Tokyo, Japan) with a LED detector, at 5 kV acceleration voltage.

The chemical composition of the coatings was investigated by the X-ray energy dispersive spectrometer (EDS) (Octane Elite 25, EDAX Ametek, Berwyn, PA, USA).

2.4. Nanoindentation Studies

Nanoindentation tests were performed with the NanoTest™ Vantage (Micro Materials, Wrexham, Great Britain) equipment, except for the MWCNTs reference coating which was measured with the nanoindentation tester NHT^3 (Anton Paar, Buchs, Switzerland), equipped with an optical microscope. All samples were tested using a Berkovich three-sided pyramidal diamond probe. The combined samples: the MWCNTs/TiO_2 and the MWCNTs_Cu coatings were measured in twenty-five (5 × 5) points, while the MWCNTs reference coating was tested in the best place, based on optical microscopy observation. The measurements were carried out according to a test method following the ISO 14577 standard (the maximum applied force: 10 mN, the loading and unloading rate: 20 s, the dwell period at maximum load: 10 s). The distances between the subsequent indents were 20 μm. The load-displacement curve was determined by the Oliver and Pharr method, and surface hardness (H), reduced Young's modulus (Er), elastic and plastic deformation energies were calculated using the integrated software. Young's modulus (E) parameter was estimated based on the reduced Young's modulus (Er) parameter and the Poisson's ratio (v). Assuming the MWCNTs/TiO_2 and MWCNTs_Cu coatings as unidirectional composite materials, the values of v, E, and H parameters were calculated from the Halpin-Tsai (H-P) model, explained in our previous publication [47]. The volume fraction was calculated according to [48] and assuming densities of 2.10 g/cm^3 [49], 4.23 g/cm^3 [50], and 8.94 g/cm^3 [51] for MWCNTs, TiO_2, and nanoCu, respectively.

The v values of 0.254 and 0.251 were assessed for the MWCNTs/TiO_2 and MWCNTs_Cu coating, respectively.

3. Results

3.1. Structure and Morphology

The surface topographies of the MWCNTs, MWCNTs/TiO_2, and MWCNTs_Cu coatings are shown in Figure 1. The reference MWCNTs coating is characterized with high ups and downs, while for the MWCNTs/TiO_2 and the MWCNTs_Cu coatings, the roughness is higher, but the distance between ups and downs is lower. The surface of the MWCNTs_Cu coating is significantly leaned—the left side of the sample is higher than the other, which could be the reason for an unevenly put force during the grinding process or the difference in the MWCNTs_Cu coating thickness on both sides of the sample. The values of the roughness parameter (S_a) calculated both with the optical microscope and the atomic force microscope are demonstrated in Table 2. It could be observed that the S_a parameter is higher for all surfaces when using the atomic force microscopy, which could be attributed to the use of the non-contact mode AFM and thus lower accuracy.

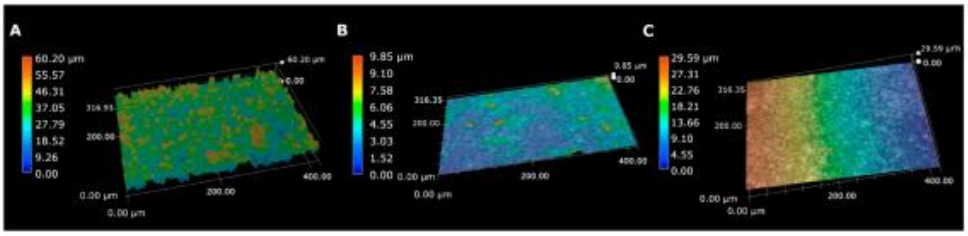

Figure 1. Surface topography based on optical microscopy tests for (**A**) the MWCNTs coating, (**B**) the MWCNTs/TiO_2 coating, and (**C**) the MWCNTs_Cu coating.

Table 2. Surface roughness of the deposited coatings.

Sample	Roughness S_a Based on Optical Microscopy Tests (µm)	Roughness S_a Based on Atomic Force Microscopy Tests (µm)
MWCNTs	0.29 *	0.353 ± 0.107
MWCNTs/TiO_2	0.56 *	1.033 ± 0.107
MWCNTs_Cu	0.36 *	0.495 ± 0.034

* the experimental error has been estimated as less than 0.05 µm.

Figure 2 shows the AFM images for tested surfaces, confirming the roughness Sa parameter values shown in Table 2. The surface of the MWCNTs/TiO_2 demonstrates the highest ups and downs, which is caused by the TiO_2 agglomerates deposited on the MWCNTs surface, while the MWCNTs surface is the smoothest, as assumed.

Figure 3 demonstrates the SEM images of the surface topography of the MWCNTs, MWCNTs/TiO_2, and MWCNTs_Cu coatings at different resolutions. The surface of the MWCNTs coating shows uniformly distributed carbon nanotubes. There are light points/areas for high ups, as demonstrated in Figure 1A, supposedly places where the coating is thicker. There are many agglomerates on the combined MWCNTs/TiO_2 and MWCNTs_Cu coatings, however the structure of agglomerates is different. The MWCNTs/TiO_2 contains uniformly positioned angular particles of TiO_2, which adhere to the surface of the MWCNTs coating, while the Cu agglomerates in the MWCNTs_Cu coating are built into the MWCNTs structure. Therefore, they are almost invisible, but nevertheless influence mechanical properties of the coating, as previously observed in [47]. The areas, where the SEM image of the MWCNTs_Cu coating is blurred, are probably spaces in which the cracks of the MWCNTs coating occur.

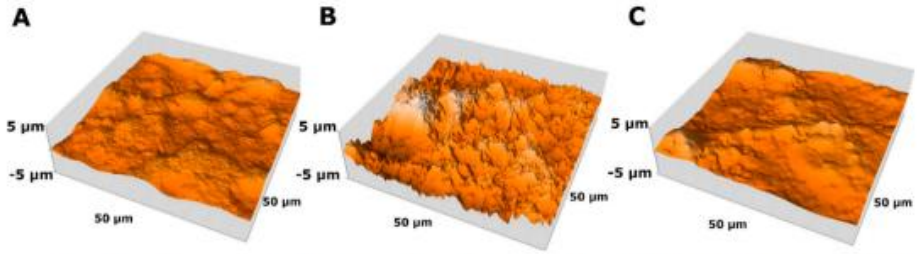

Figure 2. Surface topography based on atomic force microscopy tests for (**A**) the MWCNTs coating, (**B**) the MWCNTs/TiO_2 coating, (**C**) the MWCNTs_Cu coating.

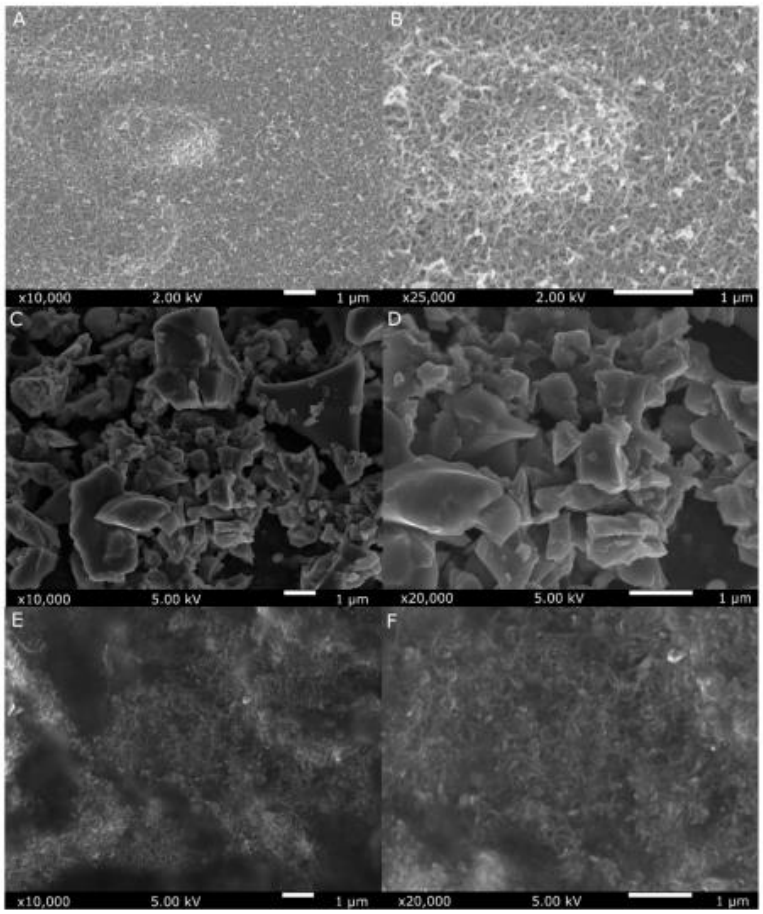

Figure 3. SEM surface topography of the MWCNTs coating (**A**,**B**), the MWCNTs/TiO_2 bi-layer coating (**C**,**D**), and the MWCNTs_Cu dispersion coating (**E**,**F**) at different resolutions.

The EDS spectra of the examined coatings are shown in Figure 4, confirming the appearance of the MWCNTs, MWCNTs/TiO_2, and MWCNTs_Cu coatings. There are also present some impurities (silicon, chlorine, sodium, and fluorine) that result from the samples preparation.

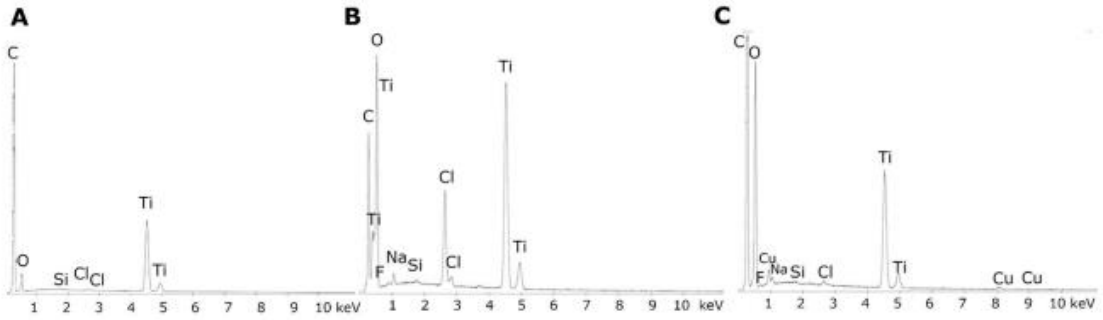

Figure 4. EDS spectra of the (**A**) MWCNTs reference, (**B**) MWCNTs/TiO_2 bi-layer coating, and (**C**) MWCNTs_Cu dispersion coating.

Moreover, the ASTM D3359-97 pressure-sensitive tape test was carried out on every single coating to check the thickness and the adhesion to the substrate. None of the examined coatings was removed during the test, which gives us valuable information of significantly strong coatings' adhesion to the Ti grade II substrate.

3.2. Nanoindentation Studies

The results of the nanoindentation test are illustrated as the load-displacement hysteresis curves in Figure 5. There are three stages distinguished in the nanoindentation test, which are pointed in the graph. Firstly, the increasing curve shows the force raising during the test until the maximum load is achieved. Secondly, the horizontal line demonstrates the pause, where the probe is stabilized at maximum depth. The third stage is the result of temperature drift, adjusted at the end of the nanoindentation measurement. The displacement, and thus maximum indent depth, was observed for the MWCNTs coating. Both the metal and metallic oxide additions to the MWCNTs based coating made it harder, as confirmed by mechanical properties (Table 3).

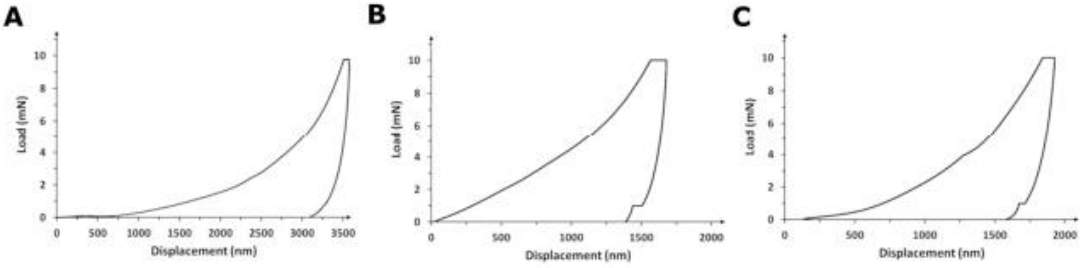

Figure 5. Nanoindentation load–displacement curves obtained for (**A**) the MWCNTs coating, (**B**) the MWCNTs/TiO_2 coating, and (**C**) the MWCNTs_Cu coating.

Table 3. Mechanical properties and maximum indent depth for the substrate and tested coatings.

Sample	Nanohardness H (GPa)	Reduced Young's Modulus E_r (GPa)	Young's Modulus E (GPa)	Maximum Indent Depth h_{max} (µm)	Plastic Deformation Energy (nJ)	Elastic Recovery Energy (nJ)
MWCNTs[1]	0.032 ± 0.0003	4.5 ± 0.05	3.41 ± 0.03	3.58 ± 0.04	7.06 ± 0.07	0.958 ± 0.0096
MWCNTs/TiO_2	0.183 ± 0.0572	13.4 ± 3.20	10.11 ± 2.42	1.55 ± 0.28	5.01 ± 0.87	0.644 ± 0.0664
MWCNTs_Cu	0.079 ± 0.0354	4.7 ± 2.40	3.51 ± 1.84	2.55 ± 0.69	19.23 ± 6.83	6.821 ± 2.0237

Table 3 demonstrates the mean values and standard deviations of several mechanical properties of the MWCNTs, MWCNTs/TiO_2, and MWCNTs_Cu coatings. The hybrid and composite coatings have higher hardness and Young's modulus, and lower maximum indent depth compared to the reference MWCNTs coating, as the addition of nanoceramics and nanometals, in general, improves mechanical properties. However, we can observe the nanohardness increase when Young's modulus decreases (regarding the reference MWCNTs coating), differently than in our previous research [47], in which the same coatings have been deposited on Ti alloy substrate. The mechanical properties of the MWCNTs_Cu coating are pretty close to the reference sample, except plastic and elastic properties, while different for the MWCNTs/TiO_2 coating.

The elastic recovery and plastic deformation energies are also shown by an area under load-displacement curves during the nanoindentation test.

Figure 6 shows the comparison of elastic recovery and plastic deformation energy of the examined coatings. The MWCNTs_Cu coating was the most both plastically and elastically deformed, comparing to the others. It can be attributed to the nanoCu presence in the crossover sections of carbon nanotubes, which influences the coating's properties, whereas the MWCNTs/TiO_2 coating achieved better properties. After the nanoindentation test, the material was the least deformed both plastically and elastically, even less than the reference sample, which was certainly caused by hard TiO_2 particles strengthening the MWCNTs coating.

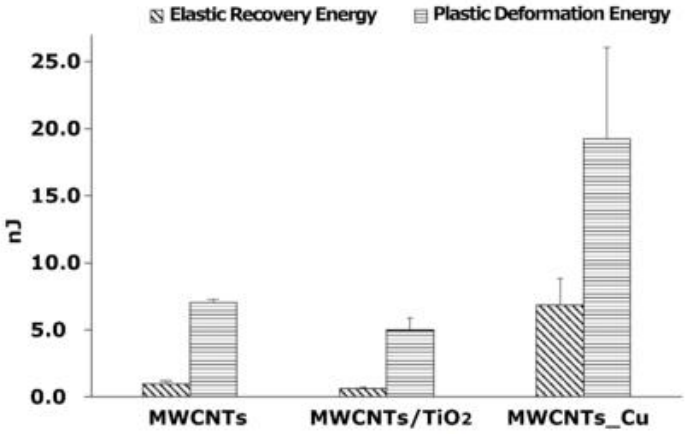

Figure 6. The comparison of plastic deformation and elastic energy for the tested coatings.

Other crucial parameters, further explaining mechanical properties of the MWCNTs, MWCNTs/TiO_2, and MWCNTs_Cu, are the ratio of the nanohardness to reduced elastic modulus (H/E_r), which shows the coating ability to accommodate substrate deflections under load (the coating endurance for chipping off under substrate bending), and the yield pressure (H^3/E_r^2), determining the resistance to plastic deformation under the nanoindenter probe load (the distortion of the coating material during nanoindentation test), as previously discussed in [47] for the Ti alloy. The addition of nanoceramics and nanometals to the MWCNTs coating improves its ability to accommodate the substrate deformation under applied load as the H/E_r parameter for both composite coatings is higher than that of the MWCNTs as illustrated in Figure 7A. In particular, the resistance to plastic deformation was significantly increased for coating implemented with hard ceramic nanotitania particles.

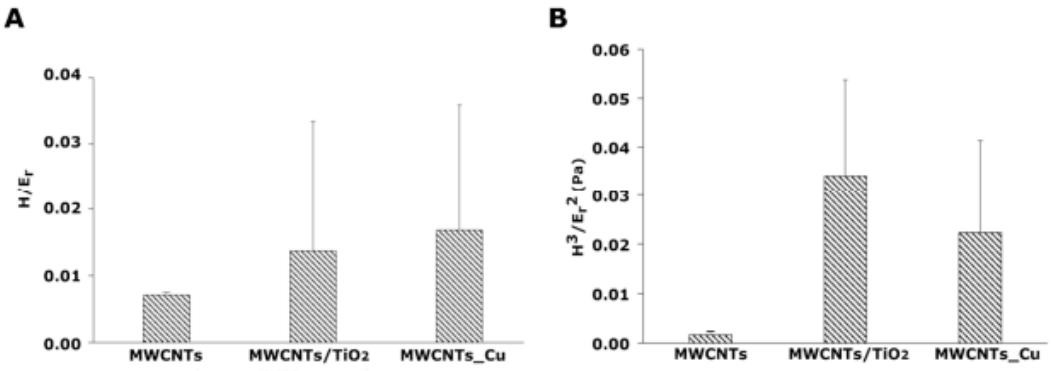

Figure 7. The diagrams for the H/E_r (**A**) and the H^3/E_r^2 parameter (**B**), calculated for the MWCNTs, MWCNTs/TiO_2 bi-layer, and the MWCNTs_Cu dispersion coating, examined under indentation load of 10 mN.

Figure 7B shows the best ability to resist plastic deformation under nanoindenter tip load for the MWCNTs/TiO_2 coating, as also demonstrated in Figure 6, where the same coating was the least plastically deformed. The MWCNTs_Cu coating was significantly less susceptible to plastic deformation under nanoindenter tip action (Figure 7B) than the MWCNTs coating with the TiO_2 addition. Figure 6 shows the MWCNTs_Cu coating as the most elastically deformed during the nanoindentation test (the coating partially returned to its shape).

4. Discussion

The results can be discussed in two aspects. At first, the change in surface properties due to surface modification by either of the two tested coatings can be attributed to different phenomena and determinants. Secondly, the influence of substrate surface on observed topography and mechanical appearance can be considered. To summarize, two variables, the coating microstructure and composition, and substrate composition are two variables to discuss.

The ceramic-carbon coating has roughness greater than the MWCNTs layer (Figures 1 and 2, and Table 2). It is a hybrid coating with inner CNTs and an outer titania layer. Highly rough topography is observed (Figure 3) with many separated nanoparticles of titanium dioxide or their aggregates. Figure 4 justifies the real presence of titanium in the layer. Unfortunately, the authors have failed to obtain a homogenous coating by simultaneous deposition of MWCNTs and TiO_2. On the other hand, the design and preparation of such bi-layer coatings on the titanium alloys appears a highly fruitful strategy if the inner layer is elastic (soft) and allows cracks to bridge, deviate or passivate, or absorb energy [52]. In other words, the layered structure (hybrid or sandwich structure) of a coating permits the simultaneous creation of the hard outer layer and the elastic, impact and high stress absorbent, resistant-to-damage inner layer. The last phenomenon results from preventing the occurrence of cracks and, in particular, their movement across the whole coating. There are opinions [53] that such a two-stage deposition process offers more flexibility in the composition of the coatings, but as it has been shown here, the EPD mechanisms are in such a case becoming complex, and to develop the coatings with optimal characteristics is difficult and needs several attempts, which will be made in the future for the most promising MWCNTs/TiO_2. In particular, an aggregation of nanoparticles is an unnecessary phenomenon that should be avoided or eliminated by chemical functionalization, solvent exchange, ultrasonication, or in another way [54,55].

The composite carbon-metal coating also has roughness greater than the MWCNTs coating (Table 2), but lower than that of the hybrid coating, and a more homogenous surface (Figure 3). The Cu nanoparticles are well dispersed in the matrix, and in such a manner

they do not seriously contribute to the roughness. Figure 4 proves the real presence of copper in the layer.

When comparing the mechanical values for both tested coatings, the difference between hybrid MWCNTs-titania and composite MWCNTs_Cu coatings is apparent. The MWCNTs-oxide coating has greater hardness and Young's modulus than the carbon nanotube-metal coating. The first coating may be then considered in such applications in which the coating opposes high stresses and must be resistant to wear or cracking. The second coating, which includes antibacterial metal, can be recommended for particular coatings that should actively kill bacteria in their neighborhood [56], but with no excessive loads during surgery and further use of the implant.

The obtained results are similar to those previously obtained for Ti alloy [47], but to some extent only. For hybrid coating, the network of carbon nanotubes forms an elastic sub-layer that immobilizes the titania nanoparticles; in such a way, the hardness is similar to that of titanium dioxide. Such a formula gives hard coating, but presumably, due to nanoform and the existence of inner layer, it is also not prone to brittle cracking which appears often in the case of ceramic coatings. For composite coating, low hardness can be attributed to small, relatively soft metallic nanoparticles, well-positioned in the CNTs network. Therefore, in this case, they do not play an important role in creating hardness and strength.

As concerns Young's modulus value, it is close to the values observed for human bones: about 19 GPa for cortical bone [57] and 6 GPa for mature bone [58]. It may be expected that the hardness and Young's modulus either both increase or decrease as observed for CNTs-Ti6Al4V nanocomposite [59], MWCNTs-graphene-Al alloy [60], and HAp-CNTs on Ti [61].

The mechanical behavior can also be characterized by the elastic recovery energy, plastic deformation energy, a ratio of the nanohardness to the reduced elastic modulus (H/E_r), and the yield pressure (H^3/E_r^2). The deep plastic deformation during the nanoindentation test is, based on these results, observed for composite coating MWCNT_Cu.

The thickness of obtained coatings has not been here determined, but comparing to previous reports and applied voltage and time of deposition it is likely to be in the range of 50–80 μm [53]. Therefore, the nanoindentation results have not been influenced by the substrate.

Finally, it is interesting to assess whether the chemical and phase composition of a substrate may affect the mechanical appearance after deposition of coatings at the same conditions. The appropriate values are listed in Table 4. Considering the above results, almost all of them can be satisfactorily explained. In particular, the higher hardness, the greater Young's modulus. However, it is true only for the same substrate, either titanium or its alloy, and with the exception of MWCNTs-titania coating, likely due to the highly nonhomogeneous surface. More importantly, the chemical and phase composition for substrate seems to play a significant role. For titanium substrate, the MWCNTs-oxide coating has a greater hardness, Young's modulus, and lower indent depth than the MWCNTs-nanocopper coating. For Ti alloy, the opposite relation was observed. These results might be considered as not fully reliable as the standard deviations approach even 30–50%. Therefore, this issue needs further experiments. On the other side, observed phenomena can be explained by: (i) deposition of coating dependent on surface characteristics, and (ii) interaction between nanoindenter tip and substrate (size effect) [62].

The mechanical properties of hybrid carbon-ceramic coatings on both substrates are, within the limits of an experimental error, close to one another. It is acceptable, as the MWCNTs are deposited in both cases as inner layers, and become adherent to the surface by chemical bonding and physical adsorption. They both depend on surface chemical composition [18]. The weaker coating observed on the Ti alloy as a substrate may be attributed to a general tendency to form more homogenous coatings on pure metals than on alloys with their chemical segregation and two or more phase constituents. The elastic and plastic resistances indicate that the outer titania layer is strong and brittle, which may

be expected for the ceramic layer. The opposite effect is observed for composite coatings. It is postulated that, in this case, the much harder surface for coating deposited on the alloy, as compared to the pure titanium, may contribute to the hardness value at relatively deep indents.

Table 4. Comparison of mechanical properties of two coatings deposited on different substrates: Ti (present work) and Ti13Nb13Zr (previous research [47]).

Coating	Substrate	S_a (µm)	H (GPa)	E (GPa)	h_{max} (µm)	PDE (nJ)	ERE (nJ)	H/E_r 10(6)
MWCNTs	Ti	0.29	0.032	3.41	3.58	7.06	0.958	7.1
MWCNTs	Ti13Nb13Zr	0.34	0.101	14.17	2.07	3.88	0.378	5.3
MWCNTs_TiO_2	Ti	0.56	0.183	10.11	1.55	5.01	0.644	13.7
MWCNTs_TiO_2	Ti13Zr13Nb	0.65	0.137	7.69	1.81	5.87	0.722	13.1
MWCNTs/Cu	Ti	0.36	0.079	3.51	2.55	19.23	6.821	16.8
MWCNTs/Cu	Ti13Zr13Nb	0.41	0.213	10.83	1.43	3.53	0.688	14.7

Table 4 shows the mechanical parameters of coatings obtained on two different substrates. The values to compare the previous results to those obtained in the present work have not been found in the literature, except the MWCNTs coating. The elastic modulus of MWCNTs ranged between 270 and 2400 GPa [55], while in other work it was 467–507 GPa [63]. For TiO_2 reinforced with CNTs composites [64], hardness was about 250 GPa and elastic modulus about 190 GPa, and for fluorapatite-TiO_2 and fluorapatite-TiO_2-CNT(Cu) coatings hardness was only 0.72 and 0.58 GPa, and Young's modulus 14.5 and 19.3 GPa, respectively [65]. As regards composites with carbon nanotubes and copper, hardness was determined as above 600 GPa for CNTs-1Cu composites in [66], hardness was of 1.1–1.4 GPa and Young's modulus 96–108 GPa in CNTs-Cu nanocomposites [67], and H of 85–96 MPa and E of 9–10 GPa in other work of the same team was reported [68], copper-based hybrid nanocomposites with 4 wt. pct. of SiC and MWCNTs showed hardness increased from 0.96 to 1.61 GPa, and Young's modulus from 98 to 120 GPa for pure copper and nanocomposite, respectively [69], for Cu-10MWCNTs the hardness was about 1 GPa and Young's modulus about 100 GPa in [70] and for HAp-CNTs (20 wt. pct.) the hardness and Young's modulus were 13.3 GPa and 189.5 GPa, respectively [71]. Here, determined values of hardness and Young's modulus are lower than the above-reported values which may be attributed to the specific microstructure of tested coatings, relatively thick and containing not closely packed carbon nanotubes.

Figure 8 shows the comparison between the yield pressure parameter for each coating deposited, both on Ti and Ti alloy substrate. It could be observed that also, in this case, different relationships for coatings deposited either on Ti or Ti alloy appear. For Ti alloy, the nanocopper addition improved the resistance to plastic deformation under indenter tip load, but it also caused cracking in the MWCNTs coating. For Ti substrate, the cracks were invisible, but the MWCNTs-nanocopper coating achieved a lower yield pressure parameter than for the MWCNTs-titania coating. This shows that the substrate affects the properties of deposited coatings.

Both coatings have been developed for the medical implantology field, for long-term titanium implants. It is well-known that high mechanical stresses may appear during implantation surgery. Therefore, the coatings need to be both elastic and resistant to plastic deformation, well adjacent to the titanium surface, and possess Young's modulus close to that of a bone. The present results show that the MWCNTs-titania coating, never before investigated at the present setting, is especially plausible for such application.

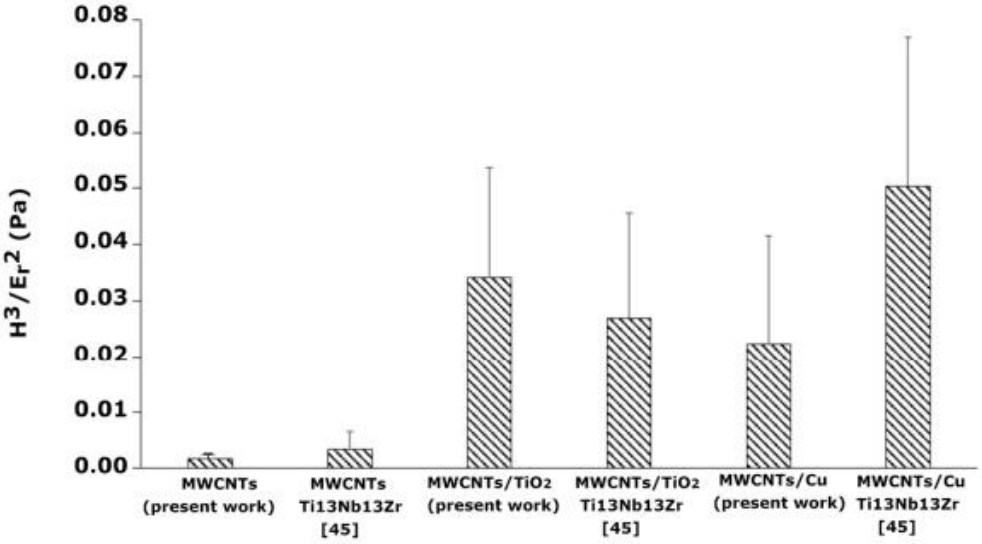

Figure 8. The diagram comparing the H^3/Er^2 parameter for the MWCNTs, MWCNTs/TiO_2 bi-layer, and the MWCNTs_Cu dispersion coating deposited on Ti (present work) and Ti13Nb13Zr [47], examined under indentation load of 10 mN.

5. Conclusions

The best mechanical, plastic, and elastic properties were achieved for the multi-wall carbon nanotubes coating combined with titania particles. This coating possesses the highest Young's modulus, close to that of natural human bone, and the best resistance to plastic deformation so that it substantially improved the capability of the MWCNTs coating to accommodate stresses appearing under applied load during surgery or further use of an implant. The addition of nanocopper to the MWCNTs coating made the material more susceptible to plastic deformation; nevertheless, it also improved the MWCNTs coating resistance to chipping off under deflection loading.

There is a general rule that more homogenous coatings form on pure metals than on their alloys. The latter materials are more complex in terms of chemical and phase composition, but also demonstrate a much harder surface compared to the pure titanium. Therefore, the observed different mechanical behavior of coatings on the different substrates is related to the difference in surface composition of the substrate and its influence on the EDP process, mainly on the adhesion of the coating.

The applications of obtained coatings may be different, but they can be considered plausible as coatings for implants for orthopedic applications. Such coatings need to be both elastic and resistant to relatively high stresses during implantation surgery and possess Young's modulus close to that of a bone. From a mechanical point of view, the tested coatings, in particular MWCNTs–titania nanocomposite structure, can be particularly considered useful for medical implantology if biological properties become appropriate.

Author Contributions: Conceptualization, D.R.-W. and B.M.-M.; methodology, D.R.-W. and B.M.-M.; software, D.R.-W.; validation, D.R.-W., B.M.-M., A.Z., and B.J.J.; formal analysis, D.R.-W.; investigation, D.R.-W. and B.M.-M.; resources, D.R.-W.; writing—original draft preparation, D.R.-W. and A.Z.; writing—review and editing, A.Z. and B.J.J.; visualization, D.R.-W.; supervision, A.Z.; and project administration, B.M.-M. All authors have read and agreed to the published version of the manuscript.

Funding: This research received no external funding.

Institutional Review Board Statement: Not applicable.

Informed Consent Statement: Not applicable.

Data Availability Statement: Not applicable.

Acknowledgments: We would like to express our sincere gratitude to Michał Bartmański for his support in carrying out the nanoindentation experiment and Grzegorz Gajowiec for SEM analysis, Dawid Chojnowski—Team Leader Microscopes from Keyence International (Belgium) NV/SA for sharing microscope VHX Keyence equipment, and support in preparing data to the above publication, Aleksandra Kowalska and Justyna Kiljan for their immense support in preparing coatings, and Patrycja Kowalik—Product Manager from Technolutions for sharing nanoindentation tester NHT^3.

Conflicts of Interest: The authors declare no conflict of interest.

References

1. Manikandan, N.; Suresh Kumar, V.P.; Siva Murugan, S.; Rathis, G.; Vishnu Saran, K.; Shabariganesh, T.K. Carbon nanotubes and their properties-The review. *Mater. Today Proc.* **2021**, 2–5, in press. [CrossRef]
2. Anzar, N.; Hasan, R.; Tyagi, M.; Yadav, N.; Narang, J. Carbon nanotube—A review on synthesis, properties and plethora of applications in the field of biomedical science. *Sens. Int.* **2020**, *1*, 100003. [CrossRef]
3. Rathinavel, S.; Priyadharshini, K.; Panda, D. A review on carbon nanotube: An overview of synthesis, properties, functionalization, characterization, and the application. *Mater. Sci. Eng. B* **2021**, *268*, 115095. [CrossRef]
4. Tao, F.; Liu, Y.; Ren, X.; Jiang, A.; Wei, H.; Zhai, X.; Wang, F.; Stock, H.-R.; Wen, S.; Ren, F. Carbon nanotube-based nanomaterials for high-performance sodium-ion batteries: Recent advances and perspectives. *J. Alloys Compd.* **2021**, *873*, 159742. [CrossRef]
5. Gao, X.; Yin, W.; Liu, X. Carbon nanotubes-based electrode for Zn ion batteries. *Mater. Res. Bull.* **2021**, *138*, 111246. [CrossRef]
6. Caoduro, C.; Hervouet, E.; Girard-Thernier, C.; Gharbi, T.; Boulahdour, H.; Delage-Mourroux, R.; Pudlo, M. Carbon nanotubes as gene carriers: Focus on internalization pathways related to functionalization and properties. *Acta Biomater.* **2017**, *49*, 36–44. [CrossRef]
7. Ding, F.; Ren, P.; Wang, G.; Wu, S.; Du, Y.; Zou, X. Hollow cellulose-carbon nanotubes composite beads with aligned porous structure for fast methylene blue adsorption. *Int. J. Biol. Macromol.* **2021**, *182*, 750–759. [CrossRef] [PubMed]
8. Gao, X.; Xue, W.; Ye, W.; Zhao, R.; Ma, X.; He, D. Large-scale synthesis of nitrogen doped graphene/carbon nanotube composites by solid-state pyrolysis of nickel phthalocyanine and its synergistic effect for microwave absorption properties. *Mater. Lett.* **2021**, *294*, 129767. [CrossRef]
9. Grądzka, E.; Dłużewski, P.; Wigda, I.; Wysocka-Żołopa, M.; Winkler, K. Formation and electrochemical properties of multiwalled carbon nanotubes and polypyrrole composite with (n-Oc4N)Br binder. *Synth. Met.* **2021**, *272*, 116661. [CrossRef]
10. Rajitha, K.; Mohana, K.N.S.; Hegde, M.B.; Nayak, S.R.; Swamy, N.K. Fabrication of ZnO/rGO and ZnO/MWCNT nanohybrids to reinforce the anticorrosion performance of polyurethane coating. *FlatChem* **2020**, *24*, 100208. [CrossRef]
11. Yakovlev, G.; Pervushin, G.; Maeva, I.; Keriene, J.; Pudov, I.; Shaybadullina, A.; Buryanov, A.; Korzhenko, A.; Senkov, S. Modification of Construction Materials with Multi-Walled Carbon Nanotubes. *Procedia Eng.* **2013**, *57*, 407–413. [CrossRef]
12. Kim, G.M.; Nam, I.W.; Yang, B.; Yoon, H.N.; Lee, H.K.; Park, S. Carbon nanotube (CNT) incorporated cementitious composites for functional construction materials: The state of the art. *Compos. Struct.* **2019**, *227*, 111244. [CrossRef]
13. Preethi, K.; Raju, T.N.; Shivappa, H.A.; Shashidhar, S.; Nagral, M. Processing, microstructure, hardness and wear behavior of carbon nanotube particulates reinforced Al6061 alloy composites. *Mater. Today Proc.* **2021**, in press. [CrossRef]
14. Chen, X.; Liu, H.; Hu, D.; Liu, H.; Ma, W. Recent advances in carbon nanotubes-based microwave absorbing composites. *Ceram. Int.* **2021**, in press. [CrossRef]
15. Garg, A.; Chalak, H.D.; Belarbi, M.-O.; Zenkour, A.M.; Sahoo, R. Estimation of carbon nanotubes and their applications as reinforcing composite materials–an engineering review. *Compos. Struct.* **2021**, *272*, 114234. [CrossRef]
16. Wesełucha-Birczyńska, A.; Stodolak-Zych, E.; Piś, W.; Długoń, E.; Benko, A.; Błażewicz, M. A model of adsorption of albumin on the implant surface titanium and titanium modified carbon coatings (MWCNT-EPD). 2D correlation analysis. *J. Mol. Struct.* **2016**, *1124*, 61–70. [CrossRef]
17. Kim, T.; Shin, D.; Lee, J.; Kim, S.J. Effect of layer-by-layer assembled carbon nanotube coatings on dropwise condensation heat transfer associated with non-condensable gas effect. *Int. J. Heat Mass Transf.* **2021**, *175*, 121345. [CrossRef]
18. Deng, J.; Pang, S.; Wang, C.; Ren, T. Biotribological properties of Ti-6Al-4V alloy treated with self-assembly multi-walled carbon nanotube coating. *Surf. Coat. Technol.* **2020**, *382*, 125169. [CrossRef]
19. Rice, D.; Rajwade, K.; Zuo, K.; Bansal, R.; Li, Q.; Garcia-Segura, S.; Perreault, F. Electrochemically-active carbon nanotube coatings for biofouling mitigation: Cleaning kinetics and energy consumption for cathodic and anodic regimes. *J. Colloid Interface Sci.* **2021**, *603*, 391–397. [CrossRef]
20. Szabó, A.; Nánai, L.; Tóth, Z.R.; Hernadi, K. Simplification of the CCVD method used in the growth of carbon nanotube forests on titanium substrate. *Solid State Sci.* **2021**, *117*, 106648. [CrossRef]

21. Gopi, D.; Shinyjoy, E.; Sekar, M.; Surendiran, M.; Kavitha, L.; Sampath Kumar, T.S. Development of carbon nanotubes reinforced hydroxyapatite composite coatings on titanium by electrodeposition method. *Corros. Sci.* **2013**, *73*, 321–330. [CrossRef]
22. Pei, X.; Zeng, Y.; He, R.; Li, Z.; Tian, L.; Wang, J.; Wan, Q.; Li, X.; Bao, H. Single-walled carbon nanotubes/hydroxyapatite coatings on titanium obtained by electrochemical deposition. *Appl. Surf. Sci.* **2014**, *295*, 71–80. [CrossRef]
23. Devgan, S.; Sidhu, S.S. Surface modification of β-type titanium with multi-walled CNTs/ μ-HAp powder mixed Electro Discharge Treatment process. *Mater. Chem. Phys.* **2020**, *239*, 122005. [CrossRef]
24. Gopi, D.; Shinyjoy, E.; Kavitha, L. Influence of ionic substitution in improving the biological property of carbon nanotubes reinforced hydroxyapatite composite coating on titanium for orthopedic applications. *Ceram. Int.* **2015**, *41*, 5454–5463. [CrossRef]
25. Chen, B.; Li, X.; Jia, Y.; Xu, L.; Liang, H.; Li, X.; Yang, J.; Li, C.; Yan, F. Fabrication of ternary hybrid of carbon nanotubes/graphene oxide/MoS2 and its enhancement on the tribological properties of epoxy composite coatings. *Compos. Part A Appl. Sci. Manuf.* **2018**, *115*, 157–165. [CrossRef]
26. Maleki-Ghaleh, H.; Khalil-Allafi, J. Characterization, mechanical and in vitro biological behavior of hydroxyapatite-titanium-carbon nanotube composite coatings deposited on NiTi alloy by electrophoretic deposition. *Surf. Coatings Technol.* **2019**, *363*, 179–190. [CrossRef]
27. Maho, A.; Detriche, S.; Delhalle, J.; Mekhalif, Z. Sol-gel synthesis of tantalum oxide and phosphonic acid-modified carbon nanotubes composite coatings on titanium surfaces. *Mater. Sci. Eng. C* **2013**, *33*, 2686–2697. [CrossRef] [PubMed]
28. Park, J.E.; Park, I.-S.; Neupane, M.P.; Bae, T.-S.; Lee, M.-H. Effects of a carbon nanotube-collagen coating on a titanium surface on osteoblast growth. *Appl. Surf. Sci.* **2014**, *292*, 828–836. [CrossRef]
29. Gizawy, M.A.; Shamsel-Din, H.A.; Abdelmonem, I.M.; Ibrahim, M.I.A.; Mohamed, L.A.; Metwally, E. Synthesis of chitosan-acrylic acid/multiwalled carbon nanotubes composite for theranostic 47Sc separation from neutron irradiated titanium target. *Int. J. Biol. Macromol.* **2020**, *163*, 79–86. [CrossRef]
30. Marchewka, J.; Jeleń, P.; Długoń, E.; Sitarz, M.; Błażewicz, M. Spectroscopic investigation of the carbon nanotubes and polysiloxane coatings on titanium surface. *J. Mol. Struct.* **2020**, *1212*, 128176. [CrossRef]
31. Ye, Z.; Li, J.; Liu, L.; Ma, F.; Zhao, B.; Wang, X. Microstructure and wear performance enhancement of carbon nanotubes reinforced composite coatings fabricated by laser cladding on titanium alloy. *Opt. Laser Technol.* **2021**, *139*, 106957. [CrossRef]
32. Hussain, S.; Erikson, H.; Kongi, N.; Tarre, A.; Ritslaid, P.; Rähn, M.; Matisen, L.; Merisalu, M.; Sammelselg, V.; Tammeveski, K. Pt nanoparticles sputter-deposited on TiO_2/MWCNT composites prepared by atomic layer deposition: Improved electrocatalytic activity towards the oxygen reduction reaction and durability in acid media. *Int. J. Hydrogen Energy* **2018**, *43*, 4967–4977. [CrossRef]
33. Kayang, K.W.; Nyankson, E.; Efavi, J.K.; Apalangya, V.A.; Adetunji, B.I.; Gebreyesus, G.; Tia, R.; Abavare, E.K.K.; Onwona-Agyeman, B.; Yaya, A. A comparative study of the interaction of nickel, titanium, palladium, and gold metals with single-walled carbon nanotubes: A DFT approach. *Results Phys.* **2019**, *12*, 2100–2106. [CrossRef]
34. Saravanakumar, K.; Mariadoss, A.V.A.; Sathiyaseelan, A.; Wang, M.-H. Synthesis and characterization of nano-chitosan capped gold nanoparticles with multifunctional bioactive properties. *Int. J. Biol. Macromol.* **2020**, *165*, 747–757. [CrossRef]
35. Yokoyama, K.; Ichiki, A. Nano-size dependence in the adsorption by the SARS-CoV-2 spike protein over gold colloid. *Colloids Surfaces A Physicochem. Eng. Asp.* **2021**, *615*, 126275. [CrossRef]
36. Yokoyama, K.; Ichiki, A. Spectroscopic investigation on the affinity of SARS-CoV-2 spike protein to gold nano-particles. *Colloid Interface Sci. Commun.* **2021**, *40*, 100356. [CrossRef] [PubMed]
37. Dziaduszewska, M.; Wekwejt, M.; Bartmański, M.; Pałubicka, A.; Gajowiec, G.; Seramak, T.; Osyczka, A.M.; Zieliński, A. The Effect of Surface Modification of Ti13Zr13Nb Alloy on Adhesion of Antibiotic and Nanosilver-Loaded Bone Cement Coatings Dedicated for Application as Spacers. *Materials* **2019**, *12*, 2964. [CrossRef] [PubMed]
38. Razmara, P.; Imbery, J.J.; Koide, E.; Helbing, C.C.; Wiseman, S.B.; Gauthier, P.T.; Bray, D.F.; Needham, M.; Haight, T.; Zovoilis, A.; et al. Mechanism of copper nanoparticle toxicity in rainbow trout olfactory mucosa. *Environ. Pollut.* **2021**, *284*, 117141. [CrossRef]
39. Zhang, J.; Zhu, S.; Song, K.; Wang, Z.; Han, Z.; Zhao, K.; Fan, Z.; Zhou, X.; Zhang, Q. 3D reduced graphene oxide hybrid nano-copper scaffolds with a high antibacterial performance. *Mater. Lett.* **2020**, *267*, 127527. [CrossRef]
40. Ahmed, F.; Faisal, S.M.; Ahmed, A.; Husain, Q. Beta galactosidase mediated bio-enzymatically synthesized nano-gold with aggrandized cytotoxic potential against pathogenic bacteria and cancer cells. *J. Photochem. Photobiol. B Biol.* **2020**, *209*, 111923. [CrossRef] [PubMed]
41. Kumar, P. Nano-TiO_2 Doped Chitosan Scaffold for the Bone Tissue Engineering Applications. *Int. J. Biomater.* **2018**, *2018*, 6576157. [CrossRef] [PubMed]
42. Lephuthing, S.S.; Okoro, A.M.; Ige, O.O.; Olubambi, P.A. Comparison of dispersion methods of multi-walled carbon nanotubes in titanium oxide. *Mater. Today Proc.* **2020**, *28*, 704–709. [CrossRef]
43. Kaushik, P.; Eliáš, M.; Michalička, J.; Hegemann, D.; Pytlíček, Z.; Nečas, D.; Zajíčková, L. Atomic layer deposition of titanium dioxide on multi-walled carbon nanotubes for ammonia gas sensing. *Surf. Coatings Technol.* **2019**, *370*, 235–243. [CrossRef]
44. Bartmanski, M.; Zielinski, A.; Jazdzewska, M.; Głodowska, J.; Kalka, P. Effects of electrophoretic deposition times and nanotubular oxide surfaces on properties of the nanohydroxyapatite/nanocopper coating on the Ti13Zr13Nb alloy. *Ceram. Int.* **2019**, *45*, 20002–20010. [CrossRef]

45. Bartmański, M.; Pawłowski, Ł.; Strugała, G.; Mielewczyk-Gryń, A.; Zieliński, A. Properties of Nanohydroxyapatite Coatings Doped with Nanocopper, Obtained by Electrophoretic Deposition on Ti13Zr13Nb Alloy. *Materials* **2019**, *12*, 3741. [CrossRef] [PubMed]
46. Kruk, T.; Gołda-Cępa, M.; Szczepanowicz, K.; Szyk-Warszyńska, L.; Brzychczy-Włoch, M.; Kotarba, A.; Warszyński, P. Nanocomposite multifunctional polyelectrolyte thin films with copper nanoparticles as the antimicrobial coatings. *Colloids Surfaces B Biointerfaces* **2019**, *181*, 112–118. [CrossRef]
47. Rogala-Wielgus, D.; Majkowska-Marzec, B.; Zieliński, A.; Bartmański, M.; Bartosewicz, B. Mechanical Behavior of Bi-Layer and Dispersion Coatings Composed of Several Nanostructures on Ti13Nb13Zr Alloy. *Materials* **2021**, *14*, 2905. [CrossRef]
48. Goyal, R.K.; Tiwari, A.N.; Negi, Y.S. Microhardness of PEEK/ceramic micro- and nanocomposites: Correlation with Halpin–Tsai model. *Mater. Sci. Eng. A* **2008**, *491*, 230–236. [CrossRef]
49. Adegbenjo, A.O.; Obadele, B.A.; Olubambi, P.A. Densification, hardness and tribological characteristics of MWCNTs reinforced Ti6Al4V compacts consolidated by spark plasma sintering. *J. Alloys Compd.* **2018**, *749*, 818–833. [CrossRef]
50. Ramganesh, V.; Ananth Kumar, M.; Mini, K.; Vignesh, V.; Karthikeyan, R. Effect of nano TiO2-epoxy composite in bond strength and corrosion resistance of rebar embedded in micro-silica modified concrete. *J. Phys. Conf. Ser.* **2020**, *1706*, 012122. [CrossRef]
51. Kaczmar, J.W.; Granat, K.; Kurzawa, A.; Grodzka, E. Physical Properties of Copper Based MMC Strengthened with Alumina. *Arch. Foundry Eng.* **2014**, *14*, 85–90. [CrossRef]
52. Bai, H.; Zhong, L.; Kang, L.; Liu, J.; Zhuang, W.; Lv, Z.; Xu, Y. A review on wear-resistant coating with high hardness and high toughness on the surface of titanium alloy. *J. Alloys Compd.* **2021**, *882*, 160645. [CrossRef]
53. Atiq Ur Rehman, M.; Chen, Q.; Braem, A.; Shaffer, M.S.P.; Boccaccini, A.R. Electrophoretic deposition of carbon nanotubes: Recent progress and remaining challenges. *Int. Mater. Rev.* **2020**, 1–30. [CrossRef]
54. Castro-Muñoz, R.; Ahmad, M.Z.; Fíla, V. Tuning of Nano-Based Materials for Embedding Into Low-Permeability Polyimides for a Featured Gas Separation. *Front. Chem.* **2020**, *7*, 897. [CrossRef] [PubMed]
55. Soni, S.K.; Thomas, B.; Kar, V.R. A comprehensive review on CNTs and CNT-reinforced composites: Syntheses, characteristics and applications. *Mater. Today Commun.* **2020**, *25*, 101546. [CrossRef]
56. Dziaduszewska, M.; Zieliński, A. Structural and Material Determinants Influencing the Behavior of Porous Ti and Its Alloys Made by Additive Manufacturing Techniques for Biomedical Applications. *Materials* **2021**, *14*, 712. [CrossRef]
57. Fraczek-Szczypta, A.; Jantas, D.; Ciepiela, F.; Grzonka, J.; Bernasik, A.; Marzec, M. Carbon nanomaterials coatings—Properties and influence on nerve cells response. *Diam. Relat. Mater.* **2018**, *84*, 127–140. [CrossRef]
58. Byrne, D.P.; Lacroix, D.; Planell, J.A.; Kelly, D.J.; Prendergast, P.J. Simulation of tissue differentiation in a scaffold as a function of porosity, Young's modulus and dissolution rate: Application of mechanobiological models in tissue engineering. *Biomaterials* **2007**, *28*, 5544–5554. [CrossRef]
59. Okoro, A.M.; Machaka, R.; Lephuthing, S.S.; Oke, S.R.; Awotunde, M.A.; Olubambi, P.A. Nanoindentation studies of the mechanical behaviours of spark plasma sintered multiwall carbon nanotubes reinforced Ti6Al4V nanocomposites. *Mater. Sci. Eng. A* **2019**, *765*, 138320. [CrossRef]
60. Kumar, V.; Kempaiah, U.N.; Shivasharanayyaswamy; Bopanna, S.B. Nanoindentation studies on multiwalled carbon nanotubes/graphene reinforced aluminium alloy 6061 nanocomposites. *Mater. Today Proc.* **2020**, *45*, 202–206. [CrossRef]
61. Hahn, B.; Lee, J.-M.; Park, D.; Choi, J.; Ryu, J.; Yoon, W.; Lee, B.; Shin, D.; Kim, H. Mechanical and in vitro biological performances of hydroxyapatite–carbon nanotube composite coatings deposited on Ti by aerosol deposition. *Acta Biomater.* **2009**, *5*, 3205–3214. [CrossRef]
62. Le Bourhis, E. Appendix 8: Instrumented Nanoindentation Applied to Thin Films. In *Glass*; Wiley-VCH Verlag GmbH & Co. KGaA: Weinheim, Germany, 2007; pp. 291–309. [CrossRef]
63. Belhenini, S.; Labbaye, T.; Boulmer-Leborgne, C.; Kovacevic, E.; Tougui, A.; Dosseul, F. Elastic modulus measurements of vertically aligned multi walled carbon nanotubes carpets by using the nanoindentation technique. *Mech. Res. Commun.* **2017**, *85*, 16–20. [CrossRef]
64. Debalina, B.; Vaishakh, N.; Jagannatham, M.; Vasanthakumar, K.; Karthiselva, N.S.; Vinu, R.; Haridoss, P.; Bakshi, S.R. Effect of different nano-carbon reinforcements on microstructure and properties of TiO_2 composites prepared by spark plasma sintering. *Ceram. Int.* **2016**, *42*, 14266–14277. [CrossRef]
65. Sasani, N.; Vahdati Khaki, J.; Mojtaba Zebarjad, S. Characterization and nanomechanical properties of novel dental implant coatings containing copper decorated-carbon nanotubes. *J. Mech. Behav. Biomed. Mater.* **2014**, *37*, 125–132. [CrossRef]
66. Tsai, P.-C.; Jeng, Y.-R.; Lee, J.-T.; Stachiv, I.; Sittner, P. Effects of carbon nanotube reinforcement and grain size refinement mechanical properties and wear behaviors of carbon nanotube/copper composites. *Diam. Relat. Mater.* **2017**, *74*, 197–204. [CrossRef]
67. Tsai, P.-C.; Jeng, Y.-R. Enhanced mechanical properties and viscoelastic characterizations of nanonecklace-reinforced carbon nanotube/copper composite films. *Appl. Surf. Sci.* **2015**, *326*, 131–138. [CrossRef]
68. Tsai, P.-C.; Jeng, Y.-R. Experimental and numerical investigation into the effect of carbon nanotube buckling on the reinforcement of CNT/Cu composites. *Compos. Sci. Technol.* **2013**, *79*, 28–34. [CrossRef]
69. Mallikarjuna, H.M.; Ramesh, C.S.; Koppad, P.G.; Keshavamurthy, R.; Sethuram, D. Nanoindentation and wear behaviour of copper based hybrid composites reinforced with SiC and MWCNTs synthesized by spark plasma sintering. *Vacuum* **2017**, *145*, 320–333. [CrossRef]

70. Nayan, N.; Shukla, A.K.; Chandran, P.; Bakshi, S.R.; Murty, S.V.S.N.; Pant, B.; Venkitakrishnan, P.V. Processing and characterization of spark plasma sintered copper/carbon nanotube composites. *Mater. Sci. Eng. A* **2017**, *682*, 229–237. [CrossRef]
71. Chen, Y.; Zhang, Y.Q.; Zhang, T.H.; Gan, C.H.; Zheng, C.Y.; Yu, G. Carbon nanotube reinforced hydroxyapatite composite coatings produced through laser surface alloying. *Carbon N. Y.* **2006**, *44*, 37–45. [CrossRef]

6.4 [A4]

POLITECHNIKA GDAŃSKA | WYDZIAŁ INŻYNIERII MECHANICZNEJ I OKRĘTOWNICTWA

RESEARCH UNIVERSITY

OŚWIADCZENIE

Dotyczy publikacji w czasopiśmie naukowym:

Rogala-Wielgus D., Majkowska-Marzec B., Zieliński A.: *Characteristics of silver-dopped carbon nanotube coating destined for medical applications,* Materials Today Communications. 38 (2023) 107712. https://doi.org/10.1016/j.mtcomm.2023.107712

Impact Factor: 3,8
Punkty wg MNiSW: 70 pkt.

Oświadczamy, że wkład autorów w powstanie powyższej publikacji kształtuje się następująco:

L.p.	Współautor	Wkład, %	Wkład merytoryczny
1.	**Dorota Rogala-Wielgus**	**80**	**realizacja przeglądu literaturowego; opracowanie koncepcji badań; samodzielne przeprowadzenie badań zwilżalności powłok i testów korozyjnych; analiza wyników; przygotowanie manuskryptu; edycja manuskryptu; przygotowanie odpowiedzi na recenzje; rola autora korespondencyjnego**
2.	Beata Majkowska-Marzec	**10**	udział w opracowaniu koncepcji badań; korekta końcowa
3.	Andrzej Zieliński	10	nadzór merytoryczny; korekta końcowa; edycja manuskryptu; udział w przygotowaniu odpowiedzi na recenzje

Podpisy współautorów:

Dorota Rogala-Wielgus
mgr inż. Dorota Rogala-Wielgus

Majkowska-Marzec Beata
dr inż. Beata Majkowska-Marzec

prof. dr hab. inż. Andrzej Zieliński

POLITECHNIKA GDAŃSKA
Ul. Gabriela Narutowicza 11/12
80-233 Gdańsk
pg.edu.pl

Materials Today Communications 38 (2024) 107712

Contents lists available at ScienceDirect

Materials Today Communications

journal homepage: www.elsevier.com/locate/mtcomm

Characteristics of silver-dopped carbon nanotube coating destined for medical applications

Dorota Rogala-Wielgus *, Beata Majkowska-Marzec, Andrzej Zieliński

Division of Biomaterials Technology, Institute of Manufacturing and Materials Technology, Faculty of Mechanical Engineering and Ship Technology, Gdańsk University of Technology, 11 Narutowicza str., 80-233 Gdańsk, Poland

ARTICLE INFO

Keywords:
Carbon nanotubes
Silver
Composite coatings
Young's modulus
Adhesion
Corrosion resistance

ABSTRACT

Carbon nanotubes are materials demonstrating outstanding mechanical, chemical, and physical properties and are considered coatings of titanium implants. The present research is aimed to characterize the microstructure and properties of the multi-wall carbon nanotubes (MWCNTs) layer decorated with silver nanoparticles (Ag NPs) on the Ti13Nb13Zr alloy destined for long-term implants. The electrophoretic deposition of coatings was performed in a two-stage process, at first at 0.25 wt. pct. of MWCNTs, and next at 0.30 wt. pct. of Ag NPs content in the bath. The SEM, EDS, AFM, Raman spectroscopy, nanoindentation tests, nano-scratch test, wettability assessments, and corrosion tests were carried out. The effects of the presence of Ag NPs onto the MWCNTs coating were observed as the roughness increased to 0.380 μm and thickness to 5.26 μm, the improved adhesion and corrosion resistance, the water contact angle of 62.94°, the decreased nanohardness, Young's modulus and resistance to plastic deformation under load, and slightly improved adhesion. The obtained results can be explained by a specific two-layer structure of the coating, in which the Ag NPs agglomerates create the coating less porous and permeable, but softer structure. Future research will focus on the improvement of the adhesion of the component coatings in different ways.

1. Introduction

Titanium and its alloys have excellent biocompatibility, the appropriate mechanical properties except for hardness, and are highly resistant to corrosion, while demonstrating low bioactivity and no bactericidal protection. Therefore, they are usually surface-modified by several well-known techniques [1–4], mainly to attain antibacterial properties [5–8] and bioactivity [9–11].

Nanotechnologies play an important role in civilization's progress. The different nanoforms, especially nanoparticles, nanofilms, and surface nanostructuring are increasingly applied in the economy. The nanoparticles and nanofilms are nowadays proposed for different medical and pharmaceutical applications [12–15], in electronics and energy storage [16–18], environment protection [19,20], agriculture and food packaging [21,22], for inkjets [23], and in other applications. Among them, appear such nanoforms as carbon nanotubes (CNTs) and silver nanoparticles (Ag NPs), the components of coatings developed in the present research.

Carbon nanotubes and related structures include single-walled carbon nanotubes (SWCNTs), multi-wall carbon nanotubes (MWCNTs), nanohorns, nanobus, and nanotorus known for their outstanding mechanical, electronic, thermal, optical, and chemical properties [24,25]. Specifically, they approach 30 GPa in tensile strength, can have an elastic modulus of about 1 GPa [26,27], and demonstrate high mechanical stiffness, remarkable thermal conductivity, and electrical semiconductivity or superconductivity [25,28]. The CNTs were considered, among others, for use in diagnostic and therapy [28–30], specifically in drug transport [28], as gene carriers [31], in bone tissue regeneration [32], neuroscience [29,33], and to improve the wear resistance of Ti implants [34].

The coatings based on CNTs are less popular than composite materials because of their specific loose microstructure. They were developed to enhance the adsorption of proteins on titanium [35], improving the resistance to tribocorrosion in biological conditions [36], strengthening hydroxyapatite (HAp) deposits [37–40], as HAp-collagen [41], HAp-Ti [42], and CNTs with Cu NPs or titania [43,44], with collagen-acrylic acid [45], polysiloxane [46], or Al_3Ti-Cu-SiC [47], and also as electrospun chitosan/CNT coatings on Mg alloy [48].

The silver nanoparticles Ag NPs are well-known for their strong antibacterial properties [49]. In medicine, the chitosan – Ag NPs [50],

* Corresponding author.
E-mail address: dorota.wielgus@pg.edu.pl (D. Rogala-Wielgus).

https://doi.org/10.1016/j.mtcomm.2023.107712
Received 21 August 2023; Received in revised form 5 November 2023; Accepted 27 November 2023
Available online 29 November 2023

silk fibroin/Ag co-functionalized strontium titanate nanotubes [51], Ag NPs – polyaniline [52], Ag NPs – hydroxychloroquine [53], hyaluronic acid – Ag NPs [54], PEG – Ag NPs [55], nanosilver - chitosan/Eudragit polymers [56–58]. In particular, they were proposed for the improvement of behavior of orthodontic brackets [59], for drug delivery [60] and bone engineering [61,62], as plant-based Ag NPs for cardioprotective treatment [63], in cancer therapy [64–66], anti-diabetic treatment [67], wound healing [68], and for kidney injuries [69]. The other popular technical applications include anti-corrosion protection [70–74], environment protection [75,76], conductive inks [77], covering the touch screen panels [78], in antibacterial protection of cultural monuments [79], to improve thermal properties [80] and reduce the wear of silicon-based components [81], and in photocatalysis [82]. The antibacterial barrier on titanium can also be achieved by other approaches, as recently proposed strontium titanate nanotubes functionalized with peptides [83,84], and Mg-Cu/doped titanium oxide layer [85].

Carbon nanotubes together with Ag nanoparticles are also frequent. Silver nanoparticles are often used as antibacterial compounds in bulk composites or coatings. They are considered for catalysis in enhancing oxygen reduction [86], and in electrochemistry as the CNTs-silver borate for ion-selective electrodes [87]. They can be used in construction materials such as a reinforcement of the copper matrix composites [88], CNTs, Ag NPs, and PVA for electrospun nanofiber mate [89], as titanium dioxide functionalized MWCNTs with Ag NPS to reinforce PU nanofibers [90], and PTFE, Ag NPs, CNTs, and graphene oxide (GO) for cement pastes [91]. Similar solutions are considered in electronics and energy storage as the combination of PP, CNTs, and Ag for electromagnetic interference shielding [92], for hydrogen storage [93], as film composed of Ag selenide and MWCNTs to improve surface thermoelectric properties [94], to increase durability of silicon solar cells [95], as Ag-decorated MnO2/CNTs electrodes for supercapacitors [96], together with GO for doping of amorphous selenium for optoelectronic devices [97,98].

Our previous research was focused on checking the mechanical properties of the coating composed of MWCNTs, hydroxyapatite, Ag NPs, and Cu NPs [18] demonstrating satisfactory values for Young's modulus of 8.88 GPa, but improper hardness, wettability, and adhesion. The present research aims to verify whether the MWCNTs layer decorated with Ag nanoparticles at a three-fold higher amount of silver, desired for antibacterial prevention, has all necessary mechanical, corrosion, and wettability properties, and how microstructural features can explain them.

2. Materials and methods

2.1. Materials

The 20 mm in diameter and 4 mm thick samples of Ti13Nb13Zr alloy (MR) (Xi'an SATE Metal Materials Development Co., China), composed of 13.18 wt. pct. Nb, 13.49 wt. pct. Zr, 0.085 wt. pct. Fe, 0.035 wt. pct. C, 0.004 wt. pct. H, 0.078 wt. pct. O, < 0.001 wt. pct. S, 0.055 wt. pct. Hf and remaining Ti were cut from the rod and grounded with abrasive paper ended at # 800 grit (Saphir 330, ATM GmbH, Germany). The surfaces were subsequently rinsed with acetone (Chempur, Poland) for 2 min and distilled water, air-dried, pickled in 5% HF (Chempur, Poland) for 30 s, and again water-rinsed.

2.2. Electrophoretic deposition

The MWCNTs modified with –COOH (3D-Nano, Poland), of outer diameter 10–15 nm, inner diameter 2–6 nm, length 1–10 μm, number of walls 3–15, were deposited on Ti13Nb13Zr substrate using EPD method at the parameters shown in Table 1 and based on previous research [43]. The MWCNTs were ultrasonically dispersed in distilled water by stirring for 1 h. The DC power source (MCP/SPN110–01 C, Shanghai MCP Corp., China), and two electrodes, an anode of the Ti13Zr13Nb alloy and a counter electrode of the stainless steel 316 L were placed parallel to each other at a distance of 5 mm.

Table 1
The parameters of the EPD synthesis of MWCNTs coatings.

Coating assignment	Deposited material	Component content (wt. pct.)	Deposition time (min)	Deposition voltage (V)
MWCNTs	MWCNTs	0.25	1	20
MWCNTs/Ag	MWCNTs	0.25	1	20
	Ag NPs	0.30	4	50

The Ag layer was prepared by EPD on the previous MWCNTs layer in the bath containing 0.30 wt. pct. of Ag NPs (Hongwu International Group Ltd., China) of 30 nm size as an average, and 1 wt. pct. of Polysorbate 20 (Tween 20, Sigma-Aldrich, Poland) in isopropanol, ultrasonically dispersed for 2 h.

2.3. Investigations of the microstructural features

A high-resolution scanning electron microscope (SEM JEOL JSM-7800 F, Japan) with a LED detector, was applied at a 5 kV to examine the morphology of surfaces and cross-sections of coatings. The surface topography was evaluated using an atomic force microscope (AFM NaniteAFM, Nanosurf, Great Britain) in the non-contact mode at 20 mN force. The average roughness index S_a was estimated based on 512 lines made in the area of 80.4 × 80.4 μm^2. The cross-sections were prepared using a pressure-sensitive tape test according to the ASTM D3359–97 to assess the thickness of the coatings. The chemical composition of the coatings was investigated by the X-ray energy dispersive spectrometer (EDS) (Octane Elite 25, EDAX Ametek, USA).

2.4. Wettability assessment

The wettability was examined at room temperature by the water contact angle (CA) measurements (Contact Angle Goniometer, Zeiss, Germany). The falling drop method was applied at 5 s time for a dropout. Each specimen was tested three times in different areas, and the means and standard deviations (SD) were calculated.

2.5. Raman spectroscopy

The Raman microscope (Renishaw InVia plc., UK) with an EMCCD detector (Andor Technology Ltd, Oxford Instruments, Belfast, UK) and the objective lens set at 20x was used. The results were the graphs of the means and SDs based on 100 points. The wavelength of the laser during tests was 532 nm, the single measurement time 1 s or 0.5 s, the measurement counts 5 or 10, and the laser power 0.2 or 1 mW, for the coatings without or with Ag NPs, respectively.

2.6. Nanoindentation testing

The NanoTest™ Vantage (Micro Materials, Great Britain) with a Berkovich indenter was used. The 25 measurements were carried out on each sample, at the maximum applied force of 10 mN, loading and unloading times set up at 20 s, the dwell period at a maximum load of 10 s, and the distance between the subsequent indents of 20 μm. The Oliver and Pharr method was used to determine the load–displacement (L-D) curve, and then the surface nanohardness (H), reduced Young's modulus (E_r), maximum indent depth (h_{max}), plasticity energy (PE), and elastic recovery energy (ERE) with an integrated software. To assess the surface Young's modulus (E), the Poisson's ratio (ν) values of 0.25, 0.37, and 0.36, for the MWCNTs coating, Ag NPs, and Ti13Nb13Zr alloy [40,99]. Then the Halpin-Tsai (H-P) model was used to evaluate the ν, E, and H values for unidirectional composite MWCNTs/Ag coating, as described in [44]. The volume fraction [100] was calculated assuming the density of 4.0 g cm^{-3} [99] and 2.1 g cm^{-3} [101] for the MWCNTs and Ag NPs

[99,101], respectively. Therefore, the assessed ν value for the MWCNTs/Ag coating was set at 0.213.

Nanoscratch tests were performed also with NanoTest™ Vantage. During the scratch tests, the load increased from 0 to 200 mN, and the loading rate and distance were 1.3 mN s^{-1}, and 500 µm, respectively. The assessment of coating adhesion was based on an abrupt change in frictional force (F_t) and indicated as critical load (L_c). In the end, the scratches were observed under an optical microscope (BX51, OLYMPUS, Japan).

2.7. Corrosion tests

The potentiodynamic polarization tests were carried out with a potentiostat (Atlas 0531, Atlas Sollich, Poland), with software calculating the corrosion potential (E_{corr}), and corrosion current density (j_{corr}) based on Tafel extrapolation. The sample was the working electrode,

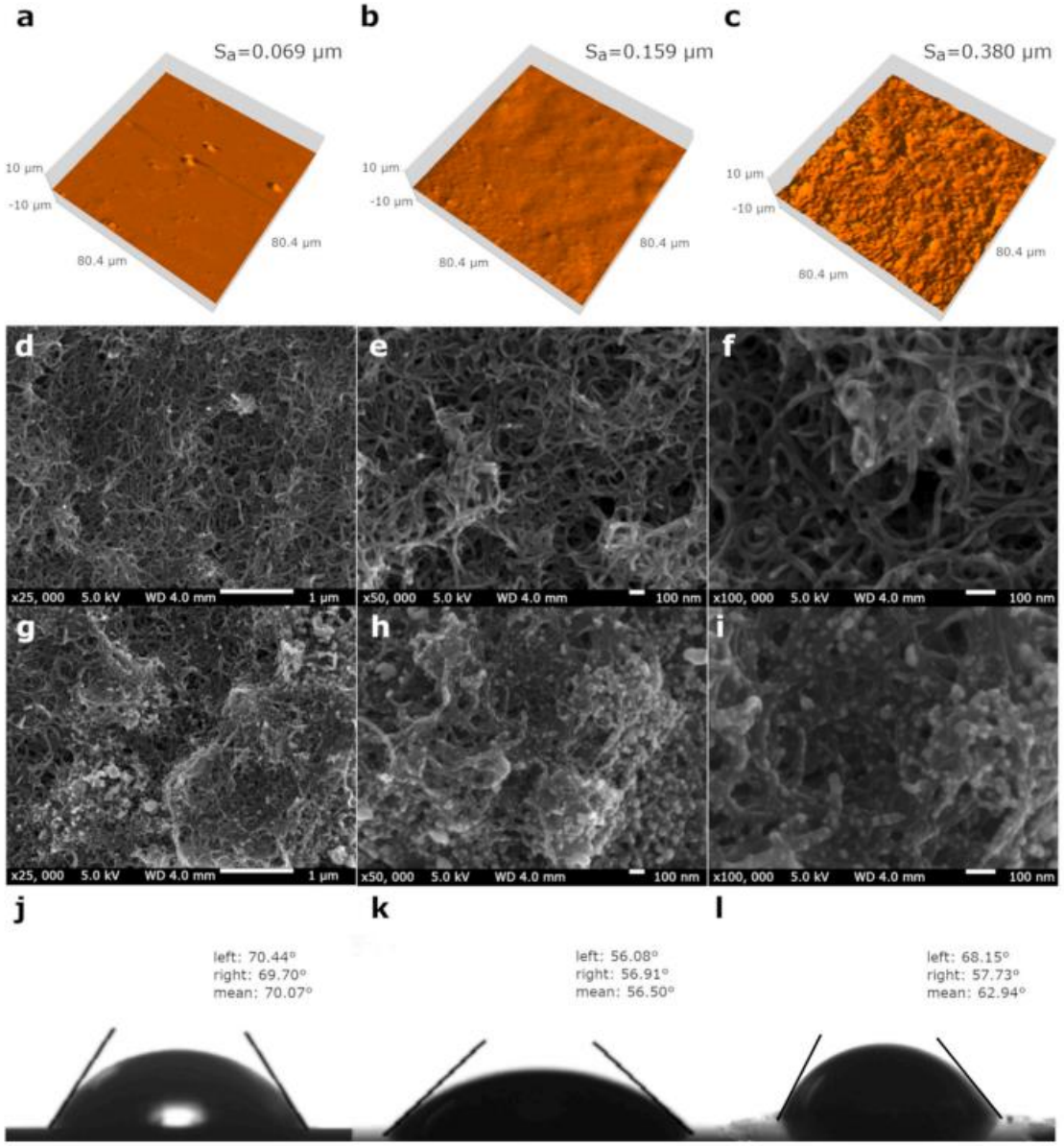

Fig. 1. The AFM-estimated S_a roughness for the MR (a), the MWCNTs coating (b), and the MWCNTs/Ag coating (c); the SEM surface topography for the MWCNTs coating (d, e, f) and the MWCNTs/Ag coating (g, h, i), and the CA results for the MR (j), the MWCNTs coating (k) and the MWCNTs/Ag coating (l).

platinum the counter-electrode, and a saturated calomel electrode (SCE) the reference electrode. The tests were performed in the Ringer's solution (in g L^{-1}: NaCl, 8.6; $CaCl_2$, 0.33; KCl, 0.30) at a temperature of 37 °C. The open circuit potential (OCP) was measured after 1 h and then the measurements were performed from − 1.0–1.0 V at a scan rate of 1 mV s^{-1}.

3. Results

The surface roughness of MWCNTs coating increased after the deposition of the Ag NPs layer (Fig. 1a-c). The Ag-formed agglomerates sized at 35 ± 5.7 nm were located on the edges and surface of the coatings. Each coating covered the substrate surface uniformly (Fig. 1d-i).

In the wettability assessment, all surfaces were hydrophilic (Fig. 1j-l). The Ag layer slightly increased the CA.

The EDS results for the MWCNTs/Ag coating (Fig. 2a) indicate the alloy elements, carbon from the MWCNTs, and silver. Some impurities, such as Cl and Si also appear. The Raman spectra of the MWCNTs/Ag coating (Fig. 2b) indicate the characteristic bands for the MWCNTs, such as the D band at 1375.5 cm^{-1} and G band at 1584.5 cm^{-1} [102], and less intense G′ band at 2937 cm^{-1} also attributed to the [103]. The intensity ratio I_D/I_G, which informs about the degree of structural defecting, reached 0.48 for the MWCNTs/Ag coating.

The addition of Ag NPs brings out hardness H of 0.024 ± 0.009 MPa, E of 3.06 ± 0.74 GPa, and h_{max} of 4.29 ± 0.80 μm. Fig. 3a shows the comparison between PE and ERE characterizing the elastic and plastic properties. Young`s modulus of the MWCNTs/Ag coating is 7-fold lower than for the MWCNTs layer (Fig. 3b). The MWCNTs/Ag coating demonstrates energy dissipated in the material higher than that released under the influence of tip load, thus it is almost 5-fold more plastic than the MWCNTs reference coating. The parameters such as the ratio of nanohardness to reduced Young's modulus (E/H_r) and the yield pressure (H^3/E_r^2) were also compared for the MWCNTs and MWCNTs/Ag coating (Fig. 3c-d) showing the MWCNTs/Ag coating is slightly more resistant to substrate deflections and thus coating chipping (Fig. 3c), and is 3-fold less resistant to plastic deformation under tip load (Fig. 3d). The observed L-D curves are shown in Fig. 4a-b.

Fig. 4c-d illustrates the relation of critical force (F_n) to critical friction (F_t) for each coating subjected to a nano-scratch test together with images of each scratch. The addition of Ag NPs to MWCNTs coating increased the L_c value to 57.74 ± 3.03 mN, thus improving its adhesion strength.

Fig. 5 shows the cross-section images of the MWCNTs and MWCNTs/Ag coating in two places with indicated coating thickness d. The MWCNTs and MWCNTs/Ag average coating thicknesses were, respectively, 3.58 ± 0.84 μm and 5.26 ± 0.31 μm.

The results of corrosion tests are shown in Fig. 6. The MWCNTs coatings exhibit higher j_{corr} and E_{corr} values than the MR reference sample (Table 2), whereas the addition of the Ag NPs improved more than twice the corrosion resistance of the coating. It is to note a high OCP shift to anodic potentials for the MWNCTs coating.

4. Discussion

The EDS elementary analysis of the MWCNTs/Ag coating shows the presence of all anticipated elements, where picks attributed to silver clearly confirm the presence of this element in the coating. The Raman spectra show all characteristics of MWCNTs. The low I_D/I_G ratio in contrary to another report [104] can be attributed to the high degree of structural defects in the coating, decreased size and the number of sp^2 clusters, or the degree of functionalization [105]. In this case, FTIR spectroscopy is a better tool to show the presence of specific chemical bonds, such as Ag-O, which was reported in literature between 613 and 481 cm^{-1} [104].

The silver addition certainly increases the surface roughness of coatings. The silver agglomerates are sized at 35 ± 5.7 nm and located on the edges and surface of the carbon nanotubes as already observed [106]. Each MWCNTs coating covered evenly the substrate surface (Fig. 1d-i). The previous results suggested the best osteoblast adhesion at a roughness R_a of 3–5 μm [107,108], but nanoroughness is also important [109]. In our previous publication for the coating composed of MWCNTs, Cu NPs, Ag NPs, and HAp, the achieved roughness was almost twice higher as here [40]. This difference can be attributed to the presence of HAp presumably increasing roughness as expected from ceramic coatings, but in each case, the roughness is acceptable for titanium implants.

The addition of Ag nanoparticles on the coating of MWCNTs resulted in a significant decrease in H and E values, and an increasing h_{max} (Table 3), calculated based on the L-D curves, revealing three stages of nanoindentation, observed previously [18]. Some earlier nanoindentation results [40,44] were added to the table to have a full spectrum of the results to discuss the effects.

The investigated coatings are softer than the four-component

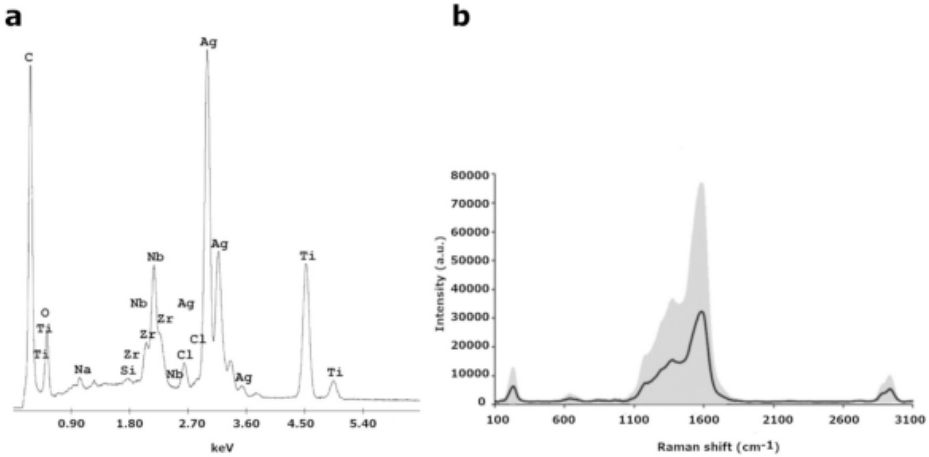

Fig. 2. The EDS (a) and Raman (b) spectra achieved for the MWCNTs/Ag coating.

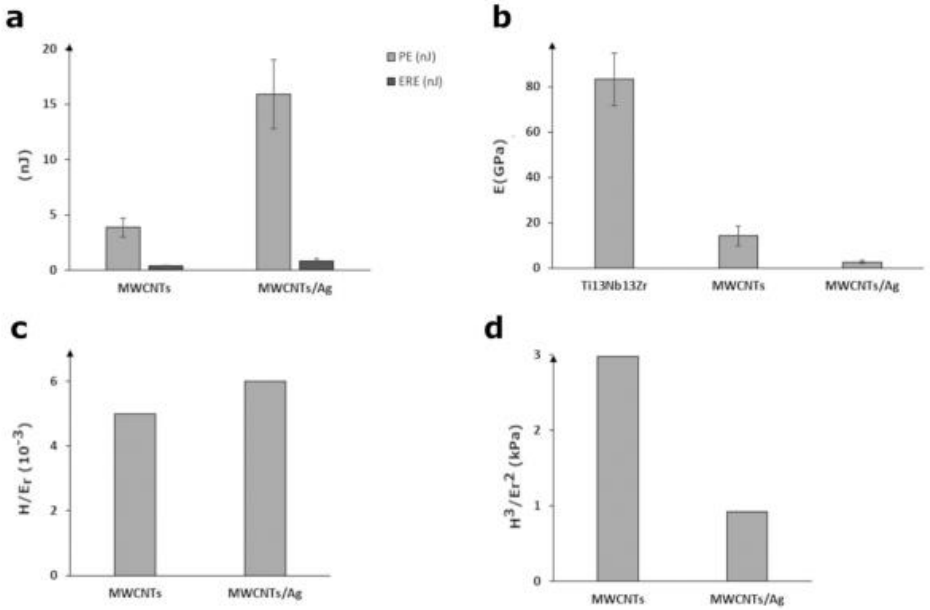

Fig. 3. The graphical comparison of nanoindentation test results between the tested materials: (a) PE and ERE, (b) E, (c), H/E_r, and (d) H^3/E_r^2.

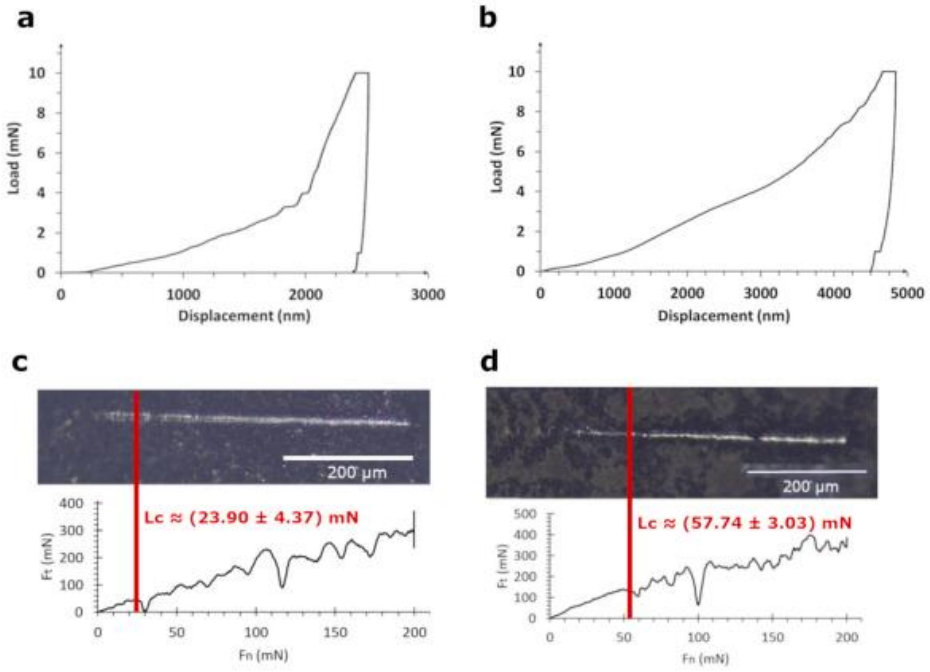

Fig. 4. The L-D curves and the nano-scratch test results with optical microscopy images of a specific scratch and indicated L_c for the MWCNTs coating (a, c) and the MWCNTs/Ag coating (b, d).

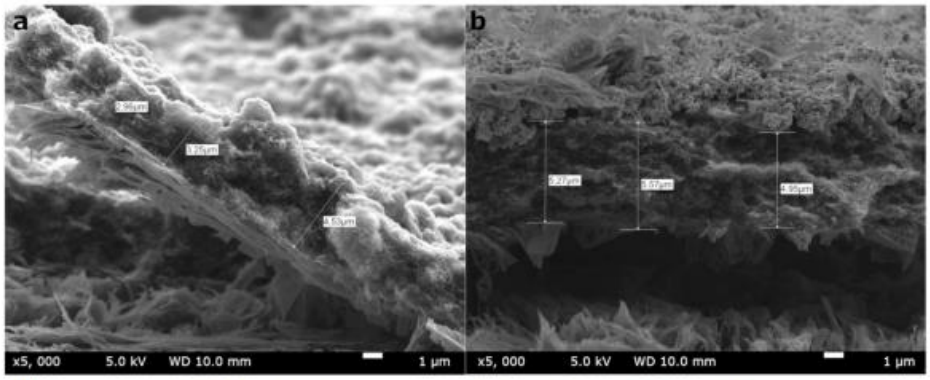

Fig. 5. Cross-sectional SEM images of the MWCNTs coating (a) and MWCNTs/Ag coating (b) with an indicated coating thickness.

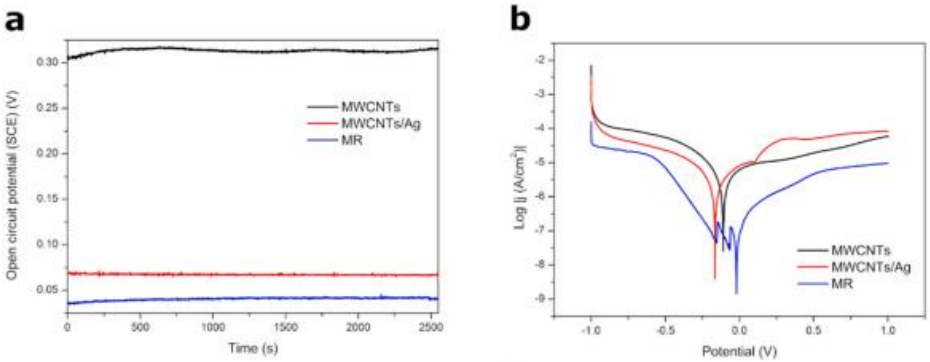

Fig. 6. The OCP vs. time (a) and potentiodynamic polarization curves for all tested samples (b).

Table 2
Corrosion test results for examined coatings.

Sample	E_{corr} (V (SCE))	j_{corr} (nA cm^{-2})
Ti13Nb13Zr	-0.019 ± 0.007	38.66 ± 5.92
MWCNTs	-0.109 ± 0.002	325.61 ± 33.61
MWCNTs/Ag	-0.165 ± 0.001	147.38 ± 13.73

MWCNTs-based tested previously, for them the H and E reached, respectively, 0.035 ± 0.019 GPa and 8.88 ± 3.26 GPa [40]. Moreover, the deposition of Ag NPs additionally decreases both parameters, presumably because silver aggregates are only physically adsorbed by MWCNTs and cannot resist indenter load.

The H/E and H^3/E^2 indexes can characterize elastic strain to failure, and resistance to plastic deformation. Comparing the other mechanical indexes here calculated with the previous ones [40], in which the H/E_r and H^3/E_r^2 values were, respectively, 0.003 and 0.31 kPa, the present coatings demonstrate improved behavior, likely because of a specific build-up of the coating. The slight increase of H/E_r and decrease of H^3/E_r^2 nanoindentation parameters may be the reason for the addition of the aggregated Ag NPs which are located on the MWCNTs walls, making it more plastic. Such a conclusion is by PE and ERE results: the first values, for the MWCNTs and MWCNTs/Ag, respectively, are 3.88 ± 0.85 nJ and 15.91 ± 3.12 nJ, and the second values, 0.38 ± 0.056 nJ and 0.85 ± 0.18 nJ (Fig. 3a), making the MWCNTs/Ag coating more plastic than the MWCNTs coating. However, the model describing the mechanical behavior of a complex composite structure of MWCNs/Ag NPs coating cannot be proposed yet.

The coating adhesion was improved by the addition of Ag NPs achieving the highest L_c value. The adhesion determination by nanoscratch tests is infrequent, but here obtained values, 23.90 and 57.74 mN, are comparable to 12–45 mN observed for PEO-made ceramic

Table 3
The nanoindentation results of the examined materials.

Sample	Nanohardness H (GPa)	Reduced Young's modulus E_r (GPa)	Surface Young's modulus E (GPa)	H/E_r (-)	H^3/E_r^2 (kPa)	Maximum indent depth (µm)
Ti13Nb13Zr	3.758 ± 1.045 *	116.91 ± 16.32 *	83.32 ± 11.63 *	0.032	3880	0.34 ± 0.037 *
MWCNTs	0.101 ± 0.049 *	18.59 ± 5.66 *	14.17 ± 4.32 *	0.005	2.98	2.07 ± 0.35 *
MWCNTs/Ag	0.024 ± 0.009	3.87 ± 0.94	3.06 ± 0.74	0.006	0.92	4.29 ± 0.80

* earlier results [40,44]

coatings on Mg-MWCNTs composite [110]. Whereas, the MWCNTs coatings in our previous research achieved different values for the MWCNTs and MWCNTs-based multicomponent coatings, respectively 89.42 ± 36.19 mN and 29.56 ± 6.92 mN [40]. The higher adhesion of previously developed bi-layer coating can be attributed, however, to higher h_{max} and the more remarkable substrate influence.

In the wettability assessment, all surfaces were hydrophilic. The Ag layer slightly increased the CA, resulting in the values already observed for composite CNTs-Ag-based coatings [111,112] and proper for application in implantology. Compared to our previous research [40] the CA value for the MWCNTs-based coatings was much higher, 133° vs. 68°. The present wettability of the coating is then improved in terms of biomedical applications, presumably because of plausible surface architecture, in which the presence of silver agglomerates only slightly decreases the hydrophilicity.

The results of corrosion tests are shown in Fig. 6. All the OCP values were positive due to surface passivation. The MWCNTs coatings exhibit higher j_{corr} and E_{corr} values than the MR sample, thus weakening the corrosion resistance of the Ti13Nb13Zr alloy (Table 2). The porous and fibrous structure lowers the corrosion resistance of titanium [113] and the presence of Ag NPs improves this behavior, likely by decreasing the porosity. On the other side, here the CNTs coatings decreased the corrosion current density, adversely to the substantial improvement in corrosion resistance reported in [114], attributed to their chemical inertness. Again, the architectural features such as porosity and components of coatings play an important role. As concerns the silver addition, its positive effect was already observed for polypyrrole coating on titanium [115] and is considered as the effect of better passivation. We think that the major cause of the corrosion behavior of CNTs-Ag coating is better than CNTs alone is followed by its sealing by nanoparticles of noble metal and decreasing porosity. Comparing this result to other coatings deposited on hydroxyapatite coatings on titanium, as recently strontium doped HAp [84,116], HAp coating is certainly more dense and less permeable for ions than HAp. Therefore, in future research, either anodic oxidation, or an elevation of Ag NPs amount, or including into the coating of the chemical compound sealing the pores research.

Summarizing the results it can be concluded that the addition of Ag NPs even in high amounts improves only some coating features. In particular, the increasing adhesion is still not quite enough and an addition of either a sub-layer or a component strongly coherent to both titanium and CNTs, or the mechanical/chemical preliminary surface treatment, or reinforcement of CNTs network with oxide particles, or EPD of silver at much higher voltage and time can be considered, investigated and developed. The small hardness and resistance to plastic deformation are acceptable or even desired taking into account the high loads carried on implants during their placement in the body. The advantages are high corrosion resistance and wettability of Ag-doped CNTs coatings.

5. Conclusions

The coating composed of the MWCNTs layer decorated with the Ag NPs layer demonstrates the surface roughness in a nanoscale range which can be accepted for medical applications. The relatively low mechanical properties of MWCNTs/Ag coating result from the loose MWCNTs layer structure and the penetration of the inner layer by Ag NPs only physically adsorbed on CNTs. The difference in adhesion of both coatings might be caused by the bare metal effect. The increased corrosion resistance compared to the MWCNTs base coating is likely produced by decreasing penetration of the layer by Ag NPs.

Funding

This research did not receive any specific grant from funding ncies in the public, commercial, or not-for-profit sectors.

CRediT authorship contribution statement

Dorota Rogala-Wielgus: Conceptualization, Methodology, Data curation, Visualization, Investigation, Formal analysis, Roles/Writing - original draft; **Beata Majkowska-Marzec:** Methodology, Visualization, Project administration; **Andrzej Zieliński:** Supervision, Writing - review & editing.

Declaration of Competing Interest

The authors declare that they have no known competing financial interests or personal relationships that could have appeared to influence the work reported in this paper.

Data availability

Data will be made available on request.

Acknowledgments

We are grateful to Dr. Grzegorz Gajowiec and Malwina Liszewska for their support in the evaluation of the results.

References

[1] P. Jiang, Y. Zhang, R. Hu, B. Shi, L. Zhang, Q. Huang, Y. Yang, P. Tang, C. Lin, Advanced surface engineering of titanium materials for biomedical applications: from static modification to dynamic responsive regulation, Bioact. Mater. 27 (2023) 15–57, https://doi.org/10.1016/j.bioactmat.2023.03.006.
[2] B. Makurat-Kasprolewicz, A. Ossowska, Recent advances in electrochemically surface treated titanium and its alloys for biomedical applications: a review of anodic and plasma electrolytic oxidation methods, Mater. Today Commun. 34 (2023), 105425, https://doi.org/10.1016/j.mtcomm.2023.105425.
[3] X. Han, J. Ma, A. Tian, Y. Wang, Y. Li, B. Dong, X. Tong, X. Ma, Surface modification techniques of titanium and titanium alloys for biomedical orthopaedics applications: a review, Colloids Surf. B Biointerfaces 227 (2023), 113339, https://doi.org/10.1016/j.colsurfb.2023.113339.
[4] S. Chowdhury, N. Arunachalam, Surface functionalization of additively manufactured titanium alloy for orthopaedic implant applications, J. Manuf. Process. 102 (2023) 387–405, https://doi.org/10.1016/j.jmapro.2023.07.015.
[5] J.C.M. Souza, M.B. Sordi, M. Kanazawa, S. Ravindran, B. Henriques, F.S. Silva, C. Aparicio, L.F. Cooper, Nano-scale modification of titanium implant surfaces to enhance osseointegration, Acta Biomater. 94 (2019) 112–131, https://doi.org/10.1016/j.actbio.2019.05.045.
[6] R.C. Costa, B.E. Nagay, C. Dini, M.H.R. Borges, L.F.B. Miranda, J.M. Cordeiro, J. G.S. Souza, C. Sukotjo, N.C. Cruz, V.A.R. Barão, The race for the optimal antimicrobial surface: perspectives and challenges related to plasma electrolytic oxidation coating for titanium-based implants, Adv. Colloid Interface Sci. 311 (2023), 102805, https://doi.org/10.1016/j.cis.2022.102805.
[7] Z. Yuan, Y. He, C. Lin, P. Liu, K. Cai, Antibacterial surface design of biomedical titanium materials for orthopedic applications, J. Mater. Sci. Technol. 78 (2021) 51–67, https://doi.org/10.1016/j.jmst.2020.10.066.
[8] H. Chouirfa, H. Bouloussa, V. Migonney, C. Falentin-Daudré, Review of titanium surface modification techniques and coatings for antibacterial applications, Acta Biomater. 83 (2019) 37–54, https://doi.org/10.1016/j.actbio.2018.10.036.
[9] J. Quinn, R. Mcfadden, C.-W. Chan, L. Carson, Titanium for Orthopedic Applications: an Overview of Surface Modification to Improve Biocompatibility and Prevent Bacterial Biofilm Formation, ISci 23 (2020) https://doi.org/10.1016/j.isci. 2020.101745.
[10] L.M. Pandey, Design of biocompatible and self-antibacterial titanium surfaces for biomedical applications, Curr. Opin. Biomed. Eng. 25 (2023), 100423, https://doi.org/10.1016/j.cobme.2022.100423.
[11] S. Wang, X. Zhao, Y. Hsu, Y. He, F. Wang, F. Yang, F. Yan, D. Xia, Y. Liu, Surface modification of titanium implants with Mg-containing coatings to promote osseointegration, Acta Biomater. 169 (2023) 19–44, https://doi.org/10.1016/j.actbio.2023.07.048.
[12] S. Malathi, I. Pakrudheen, S.N. Kalkura, T.J. Webster, S. Balasubramanian, Disposable biosensors based on metal nanoparticles, Sens. Int. 3 (2022), 100169, https://doi.org/10.1016/j.sintl.2022.100169.
[13] D.A. Ali, M.M. Mehanna, Role of lignin-based nanoparticles in anticancer drug delivery and bioimaging: an up-to-date review, Int. J. Biol. Macromol. 221 (2022) 934–953, https://doi.org/10.1016/j.ijbiomac.2022.09.007.
[14] Q. Xu, F. Xiao, H. Xu, Fluorescent detection of emerging virus based on nanoparticles: from synthesis to application, TrAC, Trends Anal. Chem. 161 (2023), 116999, https://doi.org/10.1016/j.trac.2023.116999.
[15] S. Zhang, J. Bai, W. Kong, H. Song, Y. Liu, G. Liu, L. Ma, L. Zhou, Y. Jiang, Dendritic mesoporous silica nanoparticles for enzyme immobilization (in press.), Green. Chem. Eng. (2023), https://doi.org/10.1016/j.gce.2023.07.002.

[16] N. Hossain, M.H. Mobarak, M.A. Mimona, M.A. Islam, A. Hossain, F.T. Zohura, M. A. Chowdhury, Advances and significances of nanoparticles in semiconductor applications – A review, Results Eng. 19 (2023), 101347, https://doi.org/10.1016/j.rineng.2023.101347.
[17] S. Shenoy, K. Sridharan, A robust photocatalyst using silver quantum clusters grafted in titanium dioxide nanotubes, Surf. Interfaces 30 (2022), 101941, https://doi.org/10.1016/j.surfin.2022.101941.
[18] W. Ma, X. Zhang, Study of the thermal, electrical and thermoelectric properties of metallic nanofilms, Int. J. Heat. Mass Transf. 58 (2013) 639–651, https://doi.org/10.1016/j.ijheatmasstransfer.2012.11.025.
[19] N.D. Hai, N.M. Dat, N.T.H. Nam, H. An, L.T. Tai, L.M. Huong, C.Q. Cong, N.T. H. Giang, N.T. Tinh, N.H. Hieu, A review on the chemical and biological synthesis of silver nanoparticles@graphene oxide nanocomposites: a comparison, Mater. Today Sustain. 24 (2023), 100544, https://doi.org/10.1016/j.mtsust.2023.100544.
[20] Z. Wang, S. Liang, Y. Kang, W. Zhao, Y. Xia, J. Yang, H. Wang, X. Zhang, Manipulating interfacial polymerization for polymeric nanofilms of composite separation membranes, Prog. Polym. Sci. 122 (2021), 101450, https://doi.org/10.1016/j.progpolymsci.2021.101450.
[21] S. Ali, X. Chen, S. Ahmad, W. Shah, M. Shafique, P. Chaubey, G. Mustafa, A. Alrashidi, S. Alharthi, Advancements and challenges in phytochemical-mediated silver nanoparticles for food packaging: recent review (2021–2023), Trends Food Sci. Technol. 141 (2023), 104197, https://doi.org/10.1016/j.tifs.2023.104197.
[22] R.H. Althomali, W.A. Adeosun, Wet chemically synthesized metal oxides nanoparticles, characterization and application in electrochemical energy storage: an updated review, Synth. Met. 298 (2023), 117424, https://doi.org/10.1016/j.synthmet.2023.117424.
[23] M. Rafiq, R.S. Khan, A.H. Rather, T.U. Wani, A. Qureashi, A.H. Pandith, S. Rather, F.A. Sheikh, Overview of printable nanoparticles through inkjet process: their application towards medical use, Microelectron. Eng. 266 (2022), 111889, https://doi.org/10.1016/j.mee.2022.111889.
[24] S. Rathinavel, K. Priyadharshini, D. Panda, A review on carbon nanotube: an overview of synthesis, properties, functionalization, characterization, and the application, Mater. Sci. Eng.:B. 268 (2021), 115095, https://doi.org/10.1016/j.mseb.2021.115095.
[25] N. Manikandan, V.P. Suresh Kumar, S. Siva Murugan, G. Rathis, K. Vishnu Saran, T.K. Shabariganesh, Carbon nanotubes and their properties-The review, Mater. Today Proc. 47 (2021) 4682–4685, https://doi.org/10.1016/j.matpr.2021.05.543.
[26] J.-E. Park, Y.-S. Jang, T.-S. Bae, M.-H. Lee, Biocompatibility Characteristics of Titanium Coated with Multi Walled Carbon Nanotubes—Hydroxyapatite Nanocomposites, Mater 12 (2019) 224, https://doi.org/10.3390/ma12020224.
[27] X. Ji, X. Li, H. Yu, W. Zhang, H. Dong, Study on the carbon nanotubes reinforced nanocomposite coatings, Diam. Relat. Mater. 91 (2019) 247–254, https://doi.org/10.1016/j.diamond.2018.11.027.
[28] N. Anzar, R. Hasan, M. Tyagi, N. Yadav, J. Narang, Carbon nanotube - A review on Synthesis, Properties and plethora of applications in the field of biomedical science, Sens. Int. 1 (2020), 100003, https://doi.org/10.1016/j.sintl.2020.100003.
[29] S.A. Mezzasalma, L. Grassi, M. Grassi, Physical and chemical properties of carbon nanotubes in view of mechanistic neuroscience investigations. Some outlook from condensed matter, materials science and physical chemistry, Mater. Sci. Eng. C. 131 (2021), 112480, https://doi.org/10.1016/j.msec.2021.112480.
[30] B.O. Murjani, P.S. Kadu, M. Bansod, S.S. Vaidya, M.D. Yadav, Carbon nanotubes in biomedical applications: current status, promises, and challenges, Carbon Lett. 32 (2022) 1207–1226, https://doi.org/10.1007/s42823-022-00364-4.
[31] C. Caoduro, E. Hervouet, C. Girard-Thernier, T. Gharbi, H. Boulahdour, R. Delage-Mourroux, M. Pudlo, Carbon nanotubes as gene carriers: focus on internalization pathways related to functionalization and properties, Acta Biomater. 49 (2017) 36–44, https://doi.org/10.1016/j.actbio.2016.11.013.
[32] M.M. Farag, Recent trends on biomaterials for tissue regeneration applications: review, J. Mater. Sci. 58 (2023) 527–558, https://doi.org/10.1007/s10853-022-08102-x.
[33] A. Zieliński, B. Majkowska-Marzec, Whether Carbon Nanotubes Are Capable, Promising, and Safe for Their Application in Nervous System Regeneration. Some Critical Remarks and Research Strategies, Coat 12 (2022) 1643, https://doi.org/10.3390/coatings12111643.
[34] K. Stenberg, S. Dittrick, S. Bose, A. Bandyopadhyay, Influence of simultaneous addition of carbon nanotubes and calcium phosphate on wear resistance of 3D-printed Ti6Al4V, J. Mater. Res. 33 (2018) 2077–2086, https://doi.org/10.1557/jmr.2018.234.
[35] A. Wesełucha-Birczyńska, E. Stodolak-Zych, W. Piś, E. Długoń, A. Benko, M. Błażewicz, A model of adsorption of albumin on the implant surface titanium and titanium modified carbon coatings (MWCNT-EPD). 2D correlation analysis, J. Mol. Struct. 1124 (2016) 61–70, https://doi.org/10.1016/j.molstruc.2016.04.050.
[36] J. Deng, S. Pang, C. Wang, T. Ren, Biotribological properties of Ti-6Al-4V alloy treated with self-assembly multi-walled carbon nanotube coating, Surf. Coat. Technol. 382 (2020), 125169, https://doi.org/10.1016/j.surfcoat.2019.125169.
[37] D. Gopi, E. Shinyjoy, M. Sekar, M. Surendiran, L. Kavitha, T.S. Sampath Kumar, Development of carbon nanotubes reinforced hydroxyapatite composite coatings on titanium by electrodeposition method, Corros. Sci. 73 (2013) 321–330, https://doi.org/10.1016/j.corsci.2013.04.021.
[38] X. Pei, Y. Zeng, R. He, Z. Li, L. Tian, J. Wang, Q. Wan, X. Li, H. Bao, Single-walled carbon nanotubes/hydroxyapatite coatings on titanium obtained by electrochemical deposition, Appl. Surf. Sci. 295 (2014) 71–80, https://doi.org/10.1016/j.apsusc.2014.01.009.
[39] S. Devgan, S.S. Sidhu, Surface modification of β-type titanium with multi-walled CNTs/ μ-HAp powder mixed Electro Discharge Treatment process, Mater. Chem. Phys. 239 (2020), 122005, https://doi.org/10.1016/j.matchemphys.2019.122005.
[40] Majkowska-Marzec, Rogala-Wielgus, Bartmański, Bartosewicz, Zieliński, Comparison of Properties of the Hybrid and Bilayer MWCNTs—Hydroxyapatite Coatings on Ti Alloy, Coat 9 (2019) 643, https://doi.org/10.3390/coatings9100643.
[41] B. Chen, X. Li, Y. Jia, L. Xu, H. Liang, X. Li, J. Yang, C. Li, F. Yan, Fabrication of ternary hybrid of carbon nanotubes/graphene oxide/MoS2 and its enhancement on the tribological properties of epoxy composite coatings, Compos. Part A Appl. Sci. Manuf. 115 (2018) 157–165, https://doi.org/10.1016/j.compositesa.2018.09.021.
[42] H. Maleki-Ghaleh, J. Khalil-Allafi, Characterization, mechanical and in vitro biological behavior of hydroxyapatite-titanium-carbon nanotube composite coatings deposited on NiTi alloy by electrophoretic deposition, Surf. Coat. Technol. 363 (2019) 179–190, https://doi.org/10.1016/j.surfcoat.2019.02.029.
[43] D. Rogala-Wielgus, B. Majkowska-Marzec, A. Zieliński, B.J. Jankiewicz, Mechanical Behavior of Bi-Layer and Dispersion Coatings Composed of Several Nanostructures on Ti Substrate, Appl. Sci. 11 (2021) 7862, https://doi.org/10.3390/app11177862.
[44] D. Rogala-Wielgus, B. Majkowska-Marzec, A. Zieliński, M. Bartmański, B. Bartosewicz, Mechanical Behavior of Bi-Layer and Dispersion Coatings Composed of Several Nanostructures on Ti13Nb13Zr Alloy, Mater 14 (2021) 2905, https://doi.org/10.3390/ma14112905.
[45] M.A. Gizawy, H.A. Shamsel-Din, I.M. Abdelmonem, M.I.A. Ibrahim, L. A. Mohamed, E. Metwally, Synthesis of chitosan-acrylic acid/multiwalled carbon nanotubes composite for theranostic 47Sc separation from neutron irradiated titanium target, Int. J. Biol. Macromol. 163 (2020) 79–86, https://doi.org/10.1016/j.ijbiomac.2020.06.249.
[46] J. Marchewka, P. Jeleń, E. Długoń, M. Sitarz, M. Błażewicz, Spectroscopic investigation of the carbon nanotubes and polysiloxane coatings on titanium surface, J. Mol. Struct. 1212 (2020), 128176, https://doi.org/10.1016/j.molstruc.2020.128176.
[47] Z. Ye, J. Li, L. Liu, F. Ma, B. Zhao, X. Wang, Microstructure and wear performance enhancement of carbon nanotubes reinforced composite coatings fabricated by laser cladding on titanium alloy, Opt. Laser Technol. 139 (2021), 106957, https://doi.org/10.1016/j.optlastec.2021.106957.
[48] S. Vahedi, R.M. Aghdam, M.H. Sohi, A.H. Rezayan, Characteristics of electrospun chitosan/carbon nanotube coatings deposited on AZ31 magnesium alloy, J. Mater. Sci. Mater. Med. 34 (2023), 8, https://doi.org/10.1007/s10856-022-06703-1.
[49] A. Dhaka, S. Chand Mali, S. Sharma, R. Trivedi, A review on biological synthesis of silver nanoparticles and their potential applications, Results Chem. 6 (2023), 101108, https://doi.org/10.1016/j.rechem.2023.101108.
[50] A. Peter, S. Sadanandan, E.S. Bindiya, N. Mohan, S.G. Bhat, K. Abhitha, Biofilm inhibition on natural rubber by hydrophilic modification using carboxymethyl chitosan stabilised high energy faceted silver nanoparticles, Carbohydr. Polym. Technol. Appl. 6 (2023), 100357, https://doi.org/10.1016/j.carpta.2023.100357.
[51] B. Wang, Z. Wu, J. Lan, Y. Li, L. Xie, X. Huang, A. Zhang, H. Qiao, X. Chang, H. Lin, H. Zhang, T. Li, Y. Huang, Surface modification of titanium implants by silk fibroin/Ag co-functionalized strontium titanate nanotubes for inhibition of bacterial-associated infection and enhancement of in vivo osseointegration, Surf. Coat. Technol. 405 (2021), 126700, https://doi.org/10.1016/j.surfcoat.2020.126700.
[52] A. Perumal, S. Kannan, R. Nallaiyan, Silver nanoparticles incorporated polyaniline on TiO_2 nanotube arrays: a nanocomposite platform to enhance the biocompatibility and antibiofilm, Surf. Interfaces 22 (2021), 100892, https://doi.org/10.1016/j.surfin.2020.100892.
[53] N.M. Mwenze, M. Juma, M. Maaza, Z. Birech, M.S. Dhlamini, Laser liquid ablation for silver nanoparticles synthesis and conjugation with hydroxychloroquine for Covid-19 treatment (in press.), Mater. Today Proc. (2023), https://doi.org/10.1016/j.matpr.2023.08.195.
[54] M. Stoian, A. Kuncser, F. Neatu, M. Florea, M. Popa, S.N. Voicu, M.C. Chifiriuc, A. Hanganu, M.E. Anghel, M. Tudose, Green synthesis of aminated hyaluronic acid-based silver nanoparticles on modified titanium dioxide surface: influence of size and chemical composition on their biological properties, Int. J. Biol. Macromol. 253 (2023), 127445, https://doi.org/10.1016/j.ijbiomac.2023.127445.
[55] G. Karabulut, N. Beköz Üllen, E. Akyüz, S. Karakuş, Surface modification of 316L stainless steel with multifunctional locust gum/polyethylene glycol-silver nanoparticles using different coating methods, Prog. Org. Coat. 174 (2023), 107291, https://doi.org/10.1016/j.porgcoat.2022.107291.
[56] Ł. Pawłowski, M. Bartmański, A. Mielewczyk-Gryń, A. Zieliński, Chitosan/poly(4-vinylpyridine) coatings formed on AgNPs-decorated titanium, Mater. Lett. 319 (2022), 132293, https://doi.org/10.1016/j.matlet.2022.132293.
[57] Ł. Pawłowski, M. Asim Akhtar, A. Zieliński, A.R. Boccaccini, Biological properties of chitosan/Eudragit E 100 and chitosan/poly(4-vinylpyridine) coatings electrophoretically deposited on AgNPs-decorated titanium substrate, Mater. Lett. 336 (2023), 133885, https://doi.org/10.1016/j.matlet.2023.133885.
[58] Ł. Pawłowski, J. Wawrzyniak, A. Banach-Kopeć, B.M. Cieślik, K. Jurak, J. Karczewski, R. Tylingo, K. Siuzdak, A. Zieliński, Antibacterial properties of laser-encapsulated titanium oxide nanotubes decorated with nanosilver and

covered with chitosan/Eudragit polymers, Biomater. Adv. 138 (2022), 212950, https://doi.org/10.1016/j.bioadv.2022.212950.
[59] M.S. Tawakal, A.M. Abdelghany Metwally, N.A. El-Wassefy, M.A. Tawfik, M. S. Shamaa, Static friction, surface roughness, and antibacterial activity of orthodontic brackets coated with silver and silver chitosan nanoparticles (in press.), J. World Fed. Orthod. (2023), https://doi.org/10.1016/j.ejwf.2023.08.002.
[60] H. Waqas, U. Farooq, D. Liu, M. Alghamdi, S. Noreen, T. Muhammad, Numerical investigation of nanofluid flow with gold and silver nanoparticles injected inside a stenotic artery, Mater. Des. 223 (2022), 111130, https://doi.org/10.1016/j.matdes.2022.111130.
[61] J. Gaviria, A. Alcudia, B. Begines, A.M. Beltrán, J. Villarraga, R. Moriche, J. A. Rodríguez-Ortiz, Y. Torres, Synthesis and deposition of silver nanoparticles on porous titanium substrates for biomedical applications, Surf. Coat. Technol. 406 (2021), 126667, https://doi.org/10.1016/j.surfcoat.2020.126667.
[62] A. Damle, R. Sundaresan, J.M. Rajwade, P. Srivastava, A. Naik, A concise review on implications of silver nanoparticles in bone tissue engineering, Biomater. Adv. 141 (2022), 213099, https://doi.org/10.1016/j.bioadv.2022.213099.
[63] N. Xu, T. Zhang, X. Wang, L. Wang, Cardioprotective effects of plant-based silver nanoparticles: describing a modern drug, Inorg. Chem. Commun. 158 (2023), 111525, https://doi.org/10.1016/j.inoche.2023.111525.
[64] B. Arul, R. Kothai, Biosynthesis, in-vitro antioxidant and cytotoxic potential of silver nanoparticles of Abutilon hirtum (Lamp) Sweet (in press.), Mater. Today Proc. (2023), https://doi.org/10.1016/j.matpr.2023.08.009.
[65] A. Zandvakili, M. Moradi, P. Ashoo, R. Pournejati, R. Yosefi, H.R. Karbalaei-Heidari, S. Behaein, Investigating cytotoxicity effect of Ag- deposited, doped and coated titanium dioxide nanotubes on breast cancer cells, Mater. Today Commun. 32 (2022), 103915, https://doi.org/10.1016/j.mtcomm.2022.103915.
[66] A. Balasubramanian, K. Ramalingam, In-vivo anticancer activity of biosynthetic silver nanoparticles of Cassia marginata Roxb against NMU-Induced mammary carcinoma (in press.), Mater. Today Proc. (2023), https://doi.org/10.1016/j.matpr.2023.07.011.
[67] K. Krishnamoorthy, S. Jayaraman, R. Krishnamoorthy, S. Manoharadas, M. A. Alshuniaber, B. Vikas, V.Priya Veeraraghavan, Green synthesis and evaluation of anti-microbial, antioxidant, anti-inflammatory, and anti-diabetic activities of silver nanoparticles from Argyreia nervosa leaf extract: an invitro study, J. King Saud. Univ. -Sci. 35 (2023), 102955, https://doi.org/10.1016/j.jksus.2023.102955.
[68] S. Maheshwari, Synergistic effects of Woodfordia fruticosa silver nanoparticles accelerating wound healing in Swiss mice in vivo (in press.), Intell. Pharm. (2023), https://doi.org/10.1016/j.ipha.2023.09.005.
[69] F. Qiu, H. Lu, X. Wang, Y. Yang, M. Ding, Evaluation of the nephroprotective properties of silver nanoparticles green-mediated by arabic gum on the lipopolysaccharide-induced acute kidney injury, Inorg. Chem. Commun. 155 (2023), 111043, https://doi.org/10.1016/j.inoche.2023.111043.
[70] R.S.A. Hameed, S. Obeidat, M.T. Qureshi, S.R. Al-Mhyawi, E.H. Aljuhani, M. Abdallah, Silver nanoparticles – Expired medicinal drugs waste accumulated at hail city for the local manufacturing of green corrosion inhibitor system for steel in acidic environment, J. Mater. Res. Technol. 21 (2022) 2743–2756, https://doi.org/10.1016/j.jmrt.2022.10.081.
[71] S.R. Al-Mhyawi, Green synthesis of silver nanoparticles and their inhibitory efficacy on corrosion of carbon steel in hydrochloric acid solution, Int. J. Electrochem. Sci. 18 (2023), 100210, https://doi.org/10.1016/j.ijoes.2023.100210.
[72] N. Raghavendra, R.T. Mahesh, B. Mahanthesh, J. Mackolil, Optimization of anti-corrosion performance of novel magnetic polyaniline-Chitosan nanocomposite decorated with silver nanoparticles on Al in simulated acidizing environment using RSM, Int. J. Biol. Macromol. 195 (2022) 329–345, https://doi.org/10.1016/j.ijbiomac.2021.11.207.
[73] E. Ituen, A. Singh, L. Yuanhua, O. Akaranta, Biomass-mediated synthesis of silver nanoparticles composite and application as green corrosion inhibitor in oilfield acidic cleaning fluid, Clean. Eng. Technol. 3 (2021), 100119, https://doi.org/10.1016/j.clet.2021.100119.
[74] M. Ali Asaad, P. Bothi Raja, G. Fahim Huseien, R. Fediuk, M. Ismail, R. Alyousef, Self-healing epoxy coating doped with Elaeis guineensis/silver nanoparticles: a robust corrosion inhibitor, Constr. Build. Mater. 312 (2021), 125396, https://doi.org/10.1016/j.conbuildmat.2021.125396.
[75] C. Chen, W. Li, X. Liu, J. Yu, S. Xing, J. Yang, Q. Han, Silver nanoparticles/graphene oxide arranged on polytetrafluoroethylene substrate hydrophilic modified with TiO2 to construct efficient air purification material, J. Environ. Chem. Eng. 11 (2023), 110848, https://doi.org/10.1016/j.jece.2023.110848.
[76] V.-D. Doan, V.T. Le, D.L. Tran, T.L.H. Nguyen, D.C. Nguyen, A.-T. Nguyen, V. T. Le, Catalytic reduction of nitrophenols using Gnetum montanum extract capped silver nanoparticles, Mol. Catal. 534 (2023), 112804, https://doi.org/10.1016/j.mcat.2022.112804.
[77] E. Naderi-Samani, R.S. Razavi, K. Nekouee, H. Naderi-Samani, Synthesis of silver nanoparticles for use in conductive inks by chemical reduction method, Heliyon 9 (2023), e20548, https://doi.org/10.1016/j.heliyon.2023.e20548.
[78] B.-J. Kim, J.-S. Park, Y.-J. Hwang, J.-S. Park, Characteristics of silver meshes coated with carbon nanotubes via spray-coating and electrophoretic deposition for touch screen panels, Thin Solid Films 596 (2015) 68–71, https://doi.org/10.1016/j.tsf.2015.07.084.
[79] Y. Shao, Y. Luan, C. Hao, J. Song, L. Li, F. Song, Antimicrobial protection of two controlled release silver nanoparticles on simulated silk cultural relic, J. Colloid Interface Sci. 652 (2023) 901–911, https://doi.org/10.1016/j.jcis.2023.08.116.
[80] X. Ji, X. Li, H. Yu, W. Zhang, H. Dong, Study on the carbon nanotubes reinforced nanocomposite coatings, Diam. Relat. Mater. 91 (2019) 247–254, https://doi.org/10.1016/j.diamond.2018.11.027.
[81] D.-E. Kim, C.-L. Kim, H.-J. Kim, A novel approach to wear reduction of micro-components by synthesis of carbon nanotube-silver composite coating, CIRP Ann. 60 (2011) 599–602, https://doi.org/10.1016/j.cirp.2011.03.014.
[82] N. Hintsho, L. Petrik, A. Nechaev, S. Titinchi, P. Ndungu, Photo-catalytic activity of titanium dioxide carbon nanotube nano-composites modified with silver and palladium nanoparticles, Appl. Catal. B 156–157 (2014) 273–283, https://doi.org/10.1016/j.apcatb.2014.03.021.
[83] B. Wang, J. Lan, H. Qiao, L. Xie, H. Yang, H. Lin, X. Li, Y. Huang, Porous surface with fusion peptides embedded in strontium titanate nanotubes elevates osteogenic and antibacterial activity of additively manufactured titanium alloy, Colloids Surf. B Biointerfaces 224 (2023), 113188, https://doi.org/10.1016/j.colsurfb.2023.113188.
[84] B. Wang, A. Bian, F. Jia, J. Lan, H. Yang, K. Yan, L. Xie, H. Qiao, X. Chang, H. Lin, H. Zhang, Y. Huang, Dual-functional" strontium titanate nanotubes designed based on fusion peptides simultaneously enhancing anti-infection and osseointegration, Biomater. Adv. 133 (2022), 112650, https://doi.org/10.1016/j.msec.2022.112650.
[85] B. Wang, Z. Wu, S. Wang, S. Wang, Q. Niu, Y. Wu, F. Jia, A. Bian, L. Xie, H. Qiao, X. Chang, H. Lin, H. Zhang, Y. Huang, Mg/Cu-doped TiO2 nanotube array: a novel dual-function system with self-antibacterial activity and excellent cell compatibility, Mater. Sci. Eng. C. 128 (2021), 112322, https://doi.org/10.1016/j.msec.2021.112322.
[86] N. Roy, A. Ejaz, S.W. Joo, S. Jeon, Aligned silver nanoparticles anchored on pyrrolic and pyridinic-nitrogen induced carbon nanotubes for enhanced oxygen reduction reaction, Thin Solid Films 769 (2023), 139710, https://doi.org/10.1016/j.tsf.2023.139710.
[87] D.U. Bahar, C. Topcu, D. Ozcimen, I. Isildak, A Novel Borate Ion Selective Electrode Based On Carbon Nanotube-Silver Borate, Int. J. Electrochem. Sci. 15 (2020) 899–914, https://doi.org/10.20964/2020.01.40.
[88] G. Yang, R. Wang, D. Fang, T. Hu, C. Bao, J. Yi, Nano-silver modified carbon nanotubes to reinforce the copper matrix composites and their mechanical properties, Adv. Powder Technol. 33 (2022), 103672, https://doi.org/10.1016/j.apt.2022.103672.
[89] M.S. Islam, A.N. Naz, M.N. Alam, A.K. Das, J.H. Yeum, Electrospun poly(vinyl alcohol)/silver nanoparticle/carbon nanotube multi-composite nanofiber mat: fabrication, characterization and evaluation of thermal, mechanical and antibacterial properties, Colloid Interface Sci. Commun. 35 (2020), 100247, https://doi.org/10.1016/j.colcom.2020.100247.
[90] T. Umair Wani, A. Hamid Rather, R. Saleem Khan, J. Macossay, A.H. Jadhav, P. M. Srinivasappa, A. Abdal-hay, S. Rather, F.A. Sheikh, Titanium dioxide functionalized multi-walled carbon nanotubes, and silver nanoparticles reinforced polyurethane nanofibers as a novel scaffold for tissue engineering applications, J. Ind. Eng. Chem. 121 (2023) 200–214, https://doi.org/10.1016/j.jiec.2023.01.024.
[91] B. Şimşek, T. Uygunoğlu, Ö.F. Dilmaç, Comparative evaluation of the effectiveness of PTFE nanoparticles on cement pastes properties with multi-wall carbon nanotubes, graphene oxide and silver nanoparticles, Constr. Build. Mater. 319 (2022), 126077, https://doi.org/10.1016/j.conbuildmat.2021.126077.
[92] L. Hu, Z. Kang, Enhanced flexible polypropylene fabric with silver/magnetic carbon nanotubes coatings for electromagnetic interference shielding, Appl. Surf. Sci. 568 (2021), 150845, https://doi.org/10.1016/j.apsusc.2021.150845.
[93] F. Taherkhani, Hydrogen storage via silver–aluminum bimetallic nanoparticle supported on different shapes defect on carbon nanotube, Int. J. Hydrog. Energy 47 (2022) 5380–5392, https://doi.org/10.1016/j.ijhydene.2021.11.142.
[94] D. Park, M. Kim, J. Kim, Preparation and structure dependent thermoelectric properties of flexible N-type nanostructured silver(I) selenide/multi-walled carbon nanotube composite film, Appl. Surf. Sci. 613 (2023), 156150, https://doi.org/10.1016/j.apsusc.2022.156150.
[95] O.K. Abudayyeh, A. Chavez, S.M. Han, B. Rounsaville, V. Upadhyaya, A. Rohatgi, Silver-carbon-nanotube composite metallization for increased durability of silicon solar cells against cell cracks, Sol. Energy Mater. Sol. Cells 225 (2021), 111017, https://doi.org/10.1016/j.solmat.2021.111017.
[96] N.M. Deghiedy, N.M. Yousif, H.M. Hosni, M.R. Balboul, Silver-modified electrodes based on amorphous MnO_2/ carbon nanotube: Multicomponent approach to enhance the performance of supercapacitors, J. Phys. Chem. Solids 161 (2022), 110445, https://doi.org/10.1016/j.jpcs.2021.110445.
[97] X. Huang, D. Wang, L. Hu, J. Song, Y. Chen, Preparation of a novel antibacterial coating precursor and its antibacterial mechanism, Appl. Surf. Sci. 465 (2019) 478–485, https://doi.org/10.1016/j.apsusc.2018.09.160.
[98] S.K. Yadav, H.E. Atyia, S.S. Fouad, A. Sharma, N. Mehta, Study of linear and non-linear optoelectronic properties of thermally grown thin films of amorphous selenium doped with graphene, multiwalled carbon nanotubes, and silver nanoparticles, Diam. Relat. Mater. 136 (2023), 110030, https://doi.org/10.1016/j.diamond.2023.110030.
[99] W. Lv, J. Hu, J. Liu, C. Xiong, F. Zhu, Porosity effect on the mechanical properties of nano-silver solder, Nanotechnol 34 (2023), 165701, https://doi.org/10.1088/1361-6528/ACB4F3.
[100] R.K. Goyal, A.N. Tiwari, Y.S. Negi, Microhardness of PEEK/ceramic micro- and nanocomposites: correlation with Halpin–Tsai model, Mater. Sci. Eng. A. 491 (2008) 230–236, https://doi.org/10.1016/j.msea.2008.01.091.
[101] A.O. Adegbenjo, B.A. Obadele, P.A. Olubambi, Densification, hardness and tribological characteristics of MWCNTs reinforced Ti6Al4V compacts

consolidated by spark plasma sintering, J. Alloy. Compd. 749 (2018) 818–833, https://doi.org/10.1016/j.jallcom.2018.03.373.
[102] J.D. Kim, H. Yun, G.C. Kim, C.W. Lee, H.C. Choi, Antibacterial activity and reusability of CNT-Ag and GO-Ag nanocomposites, Appl. Surf. Sci. 283 (2013) 227–233, https://doi.org/10.1016/j.apsusc.2013.06.086.
[103] M.A.L. Dos Reis, N.M. Barbosa Neto, M.E.S. De Sousa, P.T. Araujo, S. Simões, M. F. Vieira, F. Viana, C.R.L. Loayza, D.J.A. Borges, D.C.S. Cardoso, P.D.C. Assunção, E.M. Braga, Raman spectroscopy fingerprint of stainless steel-MWCNTs nanocomposite processed by ball-milling, AIP Adv. 8 (2018), 015323, https://doi.org/10.1063/1.5018745.
[104] M.E. David, R.-M. Ion, R.M. Grigorescu, L. Iancu, A.M. Holban, A.I. Nicoara, E. Alexandrescu, R. Somoghi, M. Ganciarov, G. Vasilievici, A.I. Gheboianu, Hybrid materials based on multi-walled carbon nanotubes and nanoparticles with antimicrobial properties, Nanomater 11 (2021) 1415, https://doi.org/10.3390/nano11061415.
[105] S.-G. Kim, O.-K. Park, J.H. Lee, B.-C. Ku, Layer-by-layer assembled graphene oxide films and barrier properties of thermally reduced graphene oxide membranes, Carbon Lett. 14 (2013) 247–250, https://doi.org/10.5714/cl.2013.14.4.247.
[106] A.T.S.C. Brandão, S. Rosoiu, R. Costa, O.A. Lazar, A.F. Silva, L. Anicai, C. M. Pereira, M. Enachescu, Characterization and electrochemical studies of MWCNTs decorated with Ag nanoparticles through pulse reversed current electrodeposition using a deep eutectic solvent for energy storage applications, J. Mater. Res. Technol. 15 (2021) 342–359, https://doi.org/10.1016/j.jmrt.2021.08.031.
[107] J. Dias Corpa Tardelli, A.C. Duarte Firmino, I. Ferreira, A. Cândido dos Reis, Influence of the roughness of dental implants obtained by additive manufacturing on osteoblastic adhesion and proliferation: a systematic review, Heliyon 8 (2022), e12505, https://doi.org/10.1016/j.heliyon.2022.e12505.
[108] B. Ren, Y. Wan, C. Liu, H. Wang, M. Yu, X. Zhang, Y. Huang, Improved osseointegration of 3D printed Ti-6Al-4V implant with a hierarchical micro/nano surface topography: an in vitro and in vivo study, Mater. Sci. Eng. C. 118 (2021), 111505, https://doi.org/10.1016/j.msec.2020.111505.
[109] N. Walter, T. Stich, D. Docheva, V. Alt, M. Rupp, Evolution of implants and advancements for osseointegration: a narrative review, Inj 53 (2022) S69–S73, https://doi.org/10.1016/j.injury.2022.05.057.
[110] C.A. Isaza M, B. Zuluaga D, J.S. Rudas, H.A. Estupiñán D, J.M. Herrera R, J. M. Meza, Mechanical and Corrosion Behavior of Plasma Electrolytic Oxidation Coatings on AZ31B Mg Alloy Reinforced with Multiwalled Carbon Nanotubes, J. Mater. Eng. Perform. 29 (2020) 1135–1145, https://doi.org/10.1007/s11665-020-04633-z.
[111] M.L. Masheane, L.N. Nthunya, S.P. Malinga, E.N. Nxumalo, B.B. Mamba, S. D. Mhlanga, Synthesis of Fe-Ag/f-MWCNT/PES nanostructured-hybrid membranes for removal of Cr(VI) from water, Sep. Purif. Technol. 184 (2017) 79–87, https://doi.org/10.1016/j.seppur.2017.04.018.
[112] L. Macevele, K. Moganedi, T. Magadzu, Investigation of antibacterial and fouling resistance of silver and multi-walled Carbon Nanotubes Doped Poly(Vinylidene Fluoride-co-Hexafluoropropylene) Composite Membrane, Membr. (Basel 7 (2017) 35, https://doi.org/10.3390/membranes7030035.
[113] E. Długoń, W. Simka, A. Fraczek-Szczypta, W. Niemiec, J. Markowski, M. Szymanska, M. Blazewicz, Carbon nanotube-based coatings on titanium, Bull. Mater. Sci. 38 (2015) 1339–1344, https://doi.org/10.1007/s12034-015-1019-4.
[114] S. Singh, C. Srivastava, Effect of carbon nanotube incorporation on the evolution of morphology, phase and compositional homogeneity, surface oxide chemistry and corrosion behaviour of electrodeposited FeCuMnNiCo-carbon nanotube composite coatings, Electrochim. Acta 439 (2023), 141639, https://doi.org/10.1016/j.electacta.2022.141639.
[115] C. García-Cabezón, V. Godinho, C. Pérez-González, Y. Torres, F. Martín-Pedrosa, Electropolymerized polypyrrole silver nanocomposite coatings on porous Ti substrates with enhanced corrosion and antibacterial behavior for biomedical applications, Mater. Today Chem. 29 (2023), https://doi.org/10.1016/j.mtchem.2023.101433.
[116] B. Wang, Y. Li, S. Wang, F. Jia, A. Bian, K. Wang, L. Xie, K. Yan, H. Qiao, H. Lin, J. Lan, Y. Huang, Electrodeposited dopamine/strontium-doped hydroxyapatite composite coating on pure zinc for anti-corrosion, antimicrobial and osteogenesis, Mater. Sci. Eng. C. 129 (2021), 112387, https://doi.org/10.1016/j.msec.2021.112387.

6.5 [A5]

POLITECHNIKA GDAŃSKA | WYDZIAŁ INŻYNIERII MECHANICZNEJ I OKRĘTOWNICTWA

RESEARCH UNIVERSITY

OŚWIADCZENIE

Dotyczy publikacji w czasopiśmie naukowym:

Rogala-Wielgus D., Majkowska-Marzec B. Zieliński A., Roszek K., Liszewska M.: *Evaluation of adhesion strength, corrosion, and biological properties of the MWCNTs/TiO_2 coating intended for medical applications*, RSC Advances. 13 (2023) 30108-30117. https://doi.org/10.1039/d3ra05331h

Impact Factor: 3,9
Punkty wg MNiSW: 100 pkt.

Oświadczamy, że wkład autorów w powstanie powyższej publikacji kształtuje się następująco:

L.p.	Współautor	Wkład, %	Wkład merytoryczny
1.	**Dorota Rogala-Wielgus**	**60**	**realizacja przeglądu literaturowego; opracowanie koncepcji badań; przygotowanie powłok; przeprowadzenie badań, analiza wyników; przygotowanie manuskryptu; korekta końcowa; edycja manuskryptu; przygotowanie odpowiedzi na recenzje; rola autora korespondencyjnego**
2.	Beata Majkowska-Marzec	25	opracowanie koncepcji badań; przeprowadzenie badań, analiza wyników
3.	Andrzej Zieliński	5	nadzór merytoryczny; korekta końcowa, edycja manuskryptu; przygotowanie odpowiedzi na recenzje
4.	Katarzyna Roszek	5	przeprowadzenie badań biologicznych; korekta opisu wyników badań biologicznych; korekta końcowa
5.	Malwina Liszewska	5	przeprowadzenie spektroskopii Raman'a; korekta opisu wyników spektroskopii Raman'a; korekta końcowa

Podpisy współautorów:

Dorota Rogala-Wielgus
mgr inż. Dorota Rogala-Wielgus

Majkowska-Marzec Beata
dr inż. Beata Majkowska-Marzec

prof. dr hab. inż. Andrzej Zieliński

K Roszek
dr hab. Katarzyna Roszek

Malwina Liszewska
mgr inż. Malwina Liszewska

POLITECHNIKA GDAŃSKA **pg.edu.pl**
Ul. Gabriela Narutowicza 11/12
80-233 Gdańsk

RSC Advances

PAPER

Cite this: *RSC Adv.*, 2023, **13**, 30108

Evaluation of adhesion strength, corrosion, and biological properties of the MWCNT/TiO_2 coating intended for medical applications

Dorota Rogala-Wielgus, *[a] Beata Majkowska-Marzec, [a] Andrzej Zieliński, [a] Katarzyna Roszek [b] and Malwina Liszewska [c]

Multi-wall carbon nanotube (MWCNT) coatings are gaining increasing interest because of their special properties used in many science fields. The titania coatings are known for their improvement of osteoblast adhesion, thus changing the surface architecture. Bi-layer coatings comprising 0.25 wt% of the MWCNTs and 0.30 wt% of titania (anatase structure) were synthesized in a two-stage procedure using the electrophoretic deposition method (EPD). The MWCNT and TiO_2 coatings were deposited with voltage and time parameters, respectively, of 20 V and 0.5 min, and 50 V and 4 min. EDS, AFM, SEM, Raman spectroscopy, nano-scratch test, potentiodynamic corrosion tests, wettability studies, and cytotoxicity determined with MTT (3-(4,5-dimethylthiazol-2-yl)-2,5-diphenyltetrazolium bromide) test on human dermal fibroblasts (HDF) and mouse osteoblast precursors (MC3T3), and lactate dehydrogenase (LDH) activity test were carried out on examined surfaces. The prepared MWCNT/TiO_2 coating is uniformly distributed by MWCNTs and agglomerated by TiO_2 particles of size ranging from 0.1 to 3 μm. Raman spectroscopy confirmed the anatase structure of the TiO_2 addition and showed typical peaks of the MWCNTs. The MWCNT/TiO_2 coating had higher roughness, higher adhesion strength, and improved corrosion resistance compared to the MWCNT basic coating. The results of biological tests proved that physicochemical properties of the surface, such as high porosity and wettability of MWCNT/TiO_2-coated material, would support cell adhesion, but toxic species could be released to the culture medium, thus resulting in a decrease in proliferation.

Received 6th August 2023
Accepted 18th September 2023

DOI: 10.1039/d3ra05331h

rsc.li/rsc-advances

1 Introduction

Among nanomaterials, carbon allotropes of carbon nanotubes (CNTs) have gained significant attention owing to their unique properties: chemical inertness, exceptionally high mechanical strength, significant electrical conductivity, and often content-related optical properties. Therefore, construction and functional materials containing CNTs have been developed in various fields of interest. The last reviews on such materials have shown the great potential of CNTs, in medicine as reinforced polymer-based composites,[1] in tissue engineering,[2] and as optical contrast agents for cell imaging,[3] in electronics for the construction of CNT-based nanogenerators,[4] supercapacitors, and high-performance batteries,[5] in industry for the development of construction reinforced polymers[6] and reinforcement of cement concrete,[7,8] and in chemistry for adsorptive removal of metal ions,[9] and as catalysts in hydrogenation processes.[10]

CNTs have seldom been proposed as coating components and exceptionally as single layers. Recently, such implementations have resulted in abrasion-resistant, photothermal, and superhydrophobic anti-icing coatings,[11–14] anticorrosion and mechanically resistant coatings,[15–18] antifouling coating,[19] and coatings designed especially for heat exchangers and microwaves.[20,21]

CNT-based coatings deposited on titanium and its alloys, including NiTi, are infrequent and highly diversified. The carboxylic multi-wall carbon nanotube (MWCNT) coating on Ti alloy with CNT content from 0.05 to 0.2 wt% was designed to decrease friction and wear rates.[14] The most popular ones are hydroxyapatite (HAp) coatings reinforced with CNTs in amounts of up to 2 wt%[22] or 0.01 to 0.1 wt%,[23] which are expected to increase hardness and adhesion strength. The HAp–Ti coatings doped with 1 wt% of MWCNTs on NiTi alloy[24] and (Ce, Sr)HAp–agar–chitosan–MWCNTs (an amount unknown) on Ti[25] were proposed for their better hardness, adhesion, and biological behavior. The tantalum oxide and CNTs were obtained by

[a]*Division of Biomaterials Technology, Institute of Manufacturing and Materials Technology, Faculty of Mechanical Engineering and Ship Technology, Gdansk University of Technology, 11 Narutowicza Str., 80-233 Gdańsk, Poland. E-mail: dorota.wielgus@pg.edu.pl*

[b]*Faculty of Biological and Veterinary Sciences, Nicolaus Copernicus University in Toruń, Lwowska 1 Str., 87-100 Toruń, Poland*

[c]*Institute of Optoelectronics, Military University of Technology, Kaliskiego 2 Str., 00-908 Warsaw, Poland*

applying the sol–gel method to increase corrosion resistance, adhesion, and bioactivity.[26,27] MWCNTs deposited on Ti in amounts of 5, 10, and 20 μg cm^{-2} were planned to enhance osseointegration.[28] All these coatings were specially designed and investigated as potential candidates for surface modifications of titanium implants. Moreover, the self-lubricating coatings Al3Ti–3CNTs–3Cu–7SiC were produced by laser melting for light material processing.[29] The CNT–polysiloxane coating was proposed as chemically resistant, durable, and highly hydrophobic,[30] and epoxy resin vapor-deposited with CNT coatings for aircraft applications[31] was developed.

The coatings are prepared by employing different techniques. They include mostly plasma spraying,[32–34] electrophoretic deposition method (EPD),[35–37] laser cladding,[38] and electrostatic spraying.[39] However, electrophoretic deposition (EPD) is also widely used to prepare CNT coatings[40,41] because it enables the manipulation of the CNTs to deposit on surfaces with variable shapes, including flat or balk, gives control over coating parameters, is low-cost and time-saving.[42]

The addition of CNTs to the coatings deposited on titanium and its alloys can improve several properties important for implants. However, CNTs can form agglomerates because of the significant van der Waals chemical force, which adversely affects the properties of the coatings. The proposed techniques include covalent or non-covalent functionalization in a liquid rather than in a solid.[43] Recently, modification of MWNCT surfaces by ZrO_2 nanoparticles was shown to enhance the dispersion of MWCNTs and increase their adhesion to the epoxy matrix and its mechanical and fracture behavior.[44] Among them are mechanical properties enhanced by CNTs present as the adhesion strength from 18.5 to 24.2 MPa at 1 wt%,[22] from 17.2 MPa to 32.1 MPa at 1 wt%,[24] from 21 to 29 MPa,[25] and from 17.5 to 32.1 MPa[37] and observed only qualitatively by the homogenous dispersion of CNTs in the matrix for CNT content in the range of 2–6 wt%.[34] The hardness was elevated from 6.12 to 7.22 GPa at 2 wt%[22] and from 72 HV to 405 HV at 1 wt%.[24] Young's modulus increased from 115 to 135 MPa at 2 wt%,[22] and also from 70 to 400 MPa.[37] The deposition of MWNCTs on titanium caused about a 10% decrease under dry conditions, but even a 90% decrease in SBF (simulated body fluid),[14] and a moderate change in wear volume from 14.14×10^6 to 10.6×10^6 mm^3 was found after adding CNTs to TiO_2 in the sprayed-made coating.[32] A decreasing current density was noticed for the CNT–Hap coating from 0.54 to 0.05 μA cm^{-2} at 1 wt% CNTs.[22] On the contrary, after adding MWCNTs to HAp–Ta_2O coating, corrosion current density increased from 0.011 to 0.021 μA cm^{-2}.[27] The contact angle changed from 40° for Ti to 31° for Ti–Ta_2O_5.[27]

Biological behavior has often been reported to be positively affected by the addition of CNTs. The coating composed of tantalum oxide and CNTs modified with phosphonic acid[26,27] improved bioactivity, and the titanium substrate electrochemically anodized and coated with CNTs increased the proliferation of MC3T3 cells and induced the formation of hydroxyapatite, making the surface proper for application in dental implants.[45] The HAp–Ti–MWCNT composite coating was claimed to improve cellular proliferation and growth on the surface of NiTi alloy.[37] For Ti and its alloys as substrates, in hydroxyapatite coatings, the addition of CNTs increased cell viability.[22] In more complex carrageenan–chitosan–(Ce, Sr)HAp coatings, the MWCNTs also positively affected cell adsorption in *in vivo* tests,[25] for collagen–CNTs, enhanced cell proliferation was observed,[28] and for HAp–SCNTs, improved bioactivity determined by MTT and ALP essays, cell morphology and proliferation appeared.[23]

The basic mechanical properties of the multi-wall carbon nanotube coating with titania (MWCNT/TiO_2), which is the object of this research, were examined and discussed in our previous work.[36] Herein, the presented results include adhesion strength, corrosion resistance, and biological behavior, which together strongly justify the potential application of the developed coating for implantology, particularly endoprosthesis and dental implants. The literature shows that a mixture of TiO_2 polymorphs at a concentration of 80% in anatase and 20% in rutile is the most effective in biomedical applications.[46,47] Thus, TiO_2 in crystalline anatase form is more active than TiO_2 in rutile form, and at the same time, it is more effective for antimicrobial purposes.[47] However, the anatase TiO_2 polymorph shows worse corrosion resistance[48] and cytotoxicity properties[47] compared to the rutile form. In this study, we used the anatase; it has a large Young's modulus of 177.24 GPa[49] and a small share modulus of 42.69 GPa,[49] which are properties demanded by coatings intended for the endoprosthesis.

2 Experimental

2.1 Preparation of the substrate surface

The round-shaped specimens of 20 mm diameter and 4 mm thick were prepared from Ti13Nb13Zr alloy (Xi'an SATE Metal Materials Development Co., Ltd., Xi'an, China) of the following composition: 13.18 wt% Nb, 13.49 wt% Zr, 0.085 wt% Fe, 0.035 wt% C, 0.004 wt% H, 0.078 wt% O, <0.001 wt% S, 0.055 wt% Hf and remaining Ti. The surface preparation was further described in ref. 35 and included surface grounding with SiC paper of up to #800 grit; cleaning in acetone (Chempur, Piekary Śląskie, Poland) for 2 min; distilled water for 2 min; etching in 5% solution of hydrofluoric acid (Chempur, Piekary Śląskie, Poland); and rinsing in distilled water. This prepared substrate was assigned an MR value (native material).

2.2 Preparation of CNT coatings

The MWCNT (–COOH modified, 3D-Nano, Krakow, Poland) coatings were prepared using EPD with parameters and bath composition, as shown in Table 1.

The MWCNT EPD bath was composed of 0.25 wt% of MWCNTs suspended in distilled water. Before the deposition process, the suspension was ultrasonically dispersed for 1 h in an ultrasonic bath (MKD-8, MKD Ultrasonic, Warsaw, Poland), with power and frequency of 300 W and 25 kHz, respectively. The MWCNT/TiO_2 coating was prepared in a two-stage process. First, the MWCNT layer was formed by EPD in the bath of the composition described above. Then, the second, TiO_2 (3D-Nano, Krakow, Poland) layer was created by EPD in the bath

Table 1 EPD process parameters for the examined coatings

Material	Substrate	Deposited materials	Content of component in a bath (wt%)	EPD time (min)	EPD voltage (V)
MR	Ti13Nb13Zr	—	—	—	—
MWCNTs[36]	Ti13Nb13Zr	MWCNTs	0.25	0.5	20
MWCNT/TiO_2 [36]	Ti13Nb13Zr	(I) MWCNTs	0.25	0.5	20
		(II) TiO_2	0.30	4	50

comprising 0.30 wt% of TiO_2, isopropyl alcohol as a solvent, and 1 wt% of polysorbate 20 (Tween 20, Sigma-Aldrich, Poznan, Poland). The suspension was then ultrasonically dispersed for 6 h, and the power and frequency were set the same as those observed during the dispersion of the MWCNT suspension.

The EPD for the MWCNT coating was conducted with Ti13Nb13Zr as a positive electrode and stainless steel as a negative electrode, while for the MWCNT/TiO_2 coating, the electrodes were converted. The distance between the electrodes was about 0.5 cm.

2.3 Chemical composition and topography

The surface topography was evaluated using an atomic force microscope (AFM NaniteAFM, Nanosurf, Bracknell, Great Britain) in non-contact mode at 20 mN force. The average roughness index S_a values were estimated based on 512 lines made in the area of 80.4 × 80.4 μm.

A high-resolution scanning electron microscope (SEM JEOL JSM-7800F, Tokyo, Japan) with an LED detector was used at a 5 kV acceleration voltage to observe the surface morphology.

An X-ray energy dispersive spectrometer (EDS) (Octane Elite 25, EDAX Ametek, Berwyn, PA, USA) was used to evaluate the chemical composition of the MWCNT/TiO_2 coating.

2.4 Chemical structure and crystallography

The measurements were carried out using a Raman microscope (Renishaw InVia Plc., Wotton-under-Edge, UK) equipped with an EMCCD detector (Andor Technology Ltd., Oxford Instruments, Belfast, UK) and the objective lens set at 20×. The wavelength of the laser radiation during Raman spectroscopy tests was 532 nm; the measurement time, the measurement counts at significant points, and the laser radiation power of the MWCNT sample were 1 s, 5, and *ca.* 0.2 mW, respectively, and those of the MWCNT/TiO_2 coating were 0.5 s, 10, and *ca.* 1 mW, respectively. Raman spectra measurements were prepared as maps consisting of the mean values of 100 points and the standard deviation of the signal sample. The collected Raman spectra were processed in WiRE 5.5 software and then averaged using CasaXPS software.

2.5 Adhesion determination

Nano-scratch tests were carried out using the NanoTest™ Vantage (Micro Materials, Wrexham, Great Britain) in increasing load mode from 0 to 200 mN at a distance of 500 μm, with a loading rate of 1.3 mN s^{-1}. The adhesion strength was evaluated based on the critical load (L_c), which was determined by the abrupt change in critical friction (F_t) in the F_t to critical force (F_n) relation graph. In the end, the scratches were investigated using a light microscope (BX51, OLYMPUS, Tokyo, Japan), and the results were shown as mean ± SD ($n = 5$).

2.6 Corrosion behavior

Corrosion tests were carried out using a potentiostat (Atlas 0531, Atlas Sollich, Gdańsk, Poland), with the AtlasCorr05 software, by calculating the corrosion potential (E_{corr}) and corrosion current density (j_{corr}) based on Tafel extrapolation. The sample served as the working electrode, a platinum rod as the counter electrode, and a saturated calomel electrode as the reference electrode, immersed in Ringer's solution (composition: NaCl, 8.6; $CaCl_2$, 0.33; KCl, 0.30 g L^{-1}) at a temperature of 37 °C. The open circuit potential (OCP) was stabilized for 1 h, and potentiodynamic measurements were performed from −1.0 V to 1.0 V at a scan rate of 1 mV s^{-1}.

2.7 Wettability

The water contact angle (CA) was evaluated using a goniometer (Contact Angle Goniometer, Zeiss, Oberkochen, Germany) with the pendant drop mode. Wettability was measured for 10 s after the drop fell down the surface, and the CA result for each surface, shown as a mean ± SD ($n = 3$), was red after 5 s.

2.8 Biological characterization

Cytotoxicity studies were conducted using a human dermal fibroblast (HDF, Biokom, Poland) cell line and mouse osteoblast precursors (MC3T3, Sigma-Aldrich, Germany). The HDF cells were grown in DMEM-LG (Dulbecco's Modified Eagle's Medium, Low Glucose) and MC3T3 in EMEM (Eagle's Minimum Essential Medium), both supplemented with 10% Fetal Bovine Serum (FBS) according to ref. 50. Before the experiment, the approximately 1×10^4 cells in culture media of 5 μL were seeded on the tested materials, different specimens in separate wells of a 12-well plate, and left for 3 h for adhesion. Then, the culture medium was added and incubated for 24 h and 72 h in a direct test. In an indirect test, the examined specimens were immersed in culture media for 72 h, and then as prepared suspension was used to HDF and MC3T3 cell culture seeded 24 h before in a 12-well plate. Cell viability was assessed based on an MTT (3-(4,5-dimethylthiazol-2-yl)-2,5-diphenyltetrazolium bromide) (Sigma-Aldrich, Germany) assay, which showed cell ability to reduce MTT. The absorbance of the reduced formazan was measured at 570 nm using

a Synergy HT Multi-detection reader (BioTek Instruments, Winooski, VT, USA).

To check the integrity of the cell membranes, a lactate dehydrogenase (LDH) activity test was performed. The decrease in NADH (nicotinamide adenine dinucleotide, reduced disodium salt) (Sigma-Aldrich, Germany), indicating an increase in the number of damaged cells in the culture medium, was measured after 24 h and 72 h. To 150 μL of culture media, 25 μL of NADH (2.5 mg mL^{-1}) and 25 μL of sodium pyruvate (2.5 mg mL^{-1}) (Sigma-Aldrich, Germany) were added. The LDH activity was assessed spectrophotometrically (Synergy HT Multi-detection Reader, BioTek Instruments, Winooski, VT, USA) by measuring absorbance at 340 nm. The result for each sample was shown as a percentage of positive control samples treated with 1% Triton X-100 and labeled as 100% damaged cells.

2.9 Statistical data

The experimental values were provided as mean ± standard deviation (SD), and the statistical significance of differences between each specimen was evaluated utilizing Origin 8 by one-way analysis of variance (ANOVA), as depicted in figures (*).

3 Results and discussion

3.1 Chemical composition and topography

A chemical EDS-based analysis of the MWCNT/TiO_2 coating, shown in Fig. 1, was conducted to detect the elements present in the coating. Titanium, zirconium, and niobium are the elements that originate from the substrate material, and carbon, titanium, and oxygen originate from the coating. Additionally, some elements, Cl and K, are impurities that appear in the deposition process. The presence of high peaks of carbon and titanium proves the deposition of the MWCNT/TiO_2 layer.

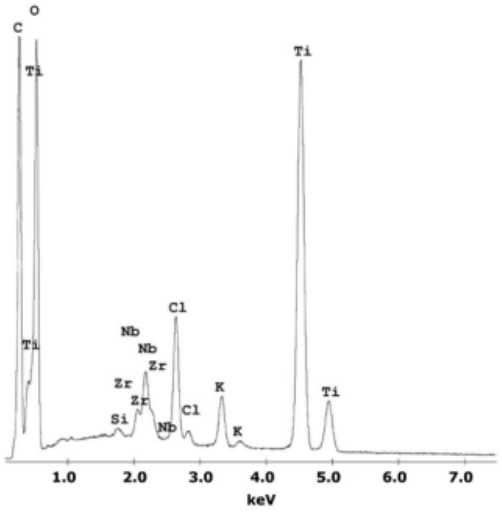

Fig. 1 The EDS spectra of the MWCNT/TiO_2 coating.

Table 2 Roughness S_a parameter for the examined surfaces

Material	Roughness S_a parameter (μm)
MR	0.069[a]
MWCNTs	0.159[a]
MWCNT/TiO_2	0.901

[a] Results are shown before in ref. 64.

Table 2 shows the surface roughness S_a values for all examined surfaces estimated with an experimental error of less than 0.05 μm.

The roughness of the MWCNT coating increased more than 5.5-fold with the addition of titania nanoparticles. A similar effect was observed in our previous work.[36] This is caused by the small TiO_2 nanoparticles agglomerating on the MWCNT surface, as observed in Fig. 2, showing the SEM topography of the MWCNT and MWCNT/TiO_2 coatings.

The MWCNT coating (Fig. 2A–C) is uniformly distributed. The difference in thickness in particular areas of the coatings was previously estimated at 0.55 μm.[36] Fig. 2D–F demonstrates the SEM topography of the MWCNT/TiO_2 coating. The MWCNT coating is transparent and thoroughly covered by titania agglomerates of different shapes and sizes ranging from 0.1 to 3 μm. In our previous study, the average TiO_2 aggregate surface area was approximately 1.5 μm^2.[36] The lamellar structure of each agglomerate can be observed, probably resulting from the coating's synthesis method, where coatings are built layer by layer during the EPD deposition process. The coating thickness measured earlier was 2.016 μm.[36]

3.2 Chemical structure and crystallography

The chemical characterization of the coatings was based on Raman spectroscopy. The Raman spectra for the MWCNT and the MWCNT/TiO_2 coating are shown in Fig. 3. The values of the bands, with appropriate assignments for the characteristics of the bands, are listed in Tables 3 and 4, for MWCNT and MWCNT/TiO_2 coatings, respectively.

For the MWCNT coating, the values of each band (Fig. 3A) are similar to those shown in the literature, except for an extra Raman shift at 2942 cm^{-1} (second 2D (G′) band). The MWCNT coating exhibits three characteristic bands: disordered mode (D band), tangential mode (G band), and G′ band. The D mode, which appears for the MWCNTs coating at 1350 cm^{-1}, represents the disorder in sp^2-hybridized carbon atoms (graphene, which creates carbon nanotubes), the extent of sidewall defects or applied functionalization.[51] The G band appears at 1588 cm^{-1} and the G′ band, called the first overtone of the D band, at 2699 cm^{-1}, which are called the two modes representing graphitic materials. The G mode is related to the stretching of the C–C bond, and the G′ mode can be distinguished for non-defect sp^2 carbon materials.[51] The second shift for the G′ band is found at 2942 cm^{-1}, as observed several times for single-wall

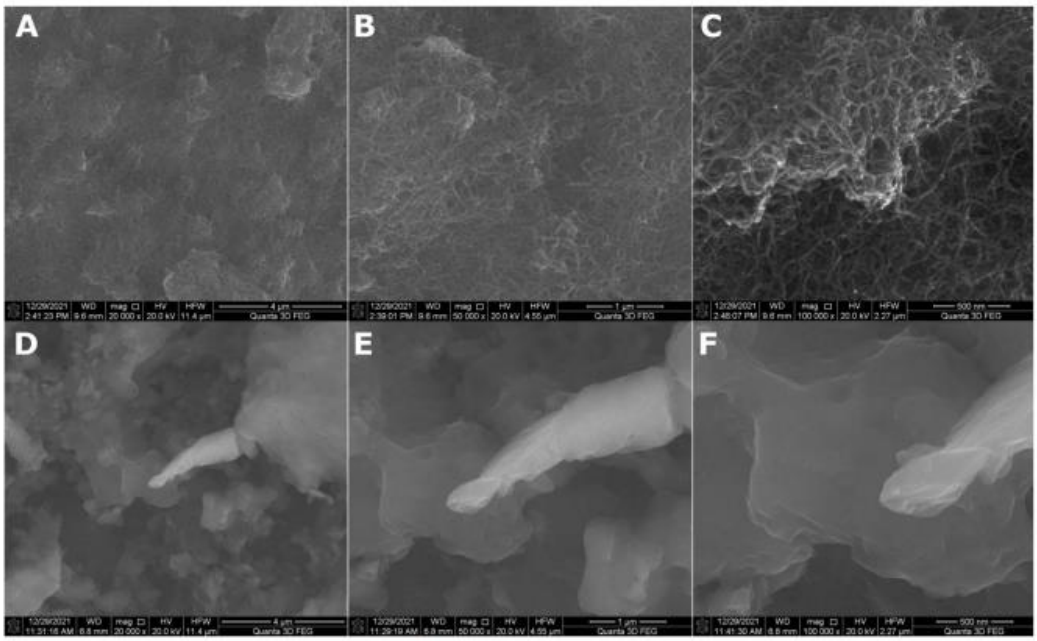

Fig. 2 SEM surface topography of the MWCNT coating (A–C) and the MWCNT/TiO_2 coating (D–F) demonstrated in different resolutions.

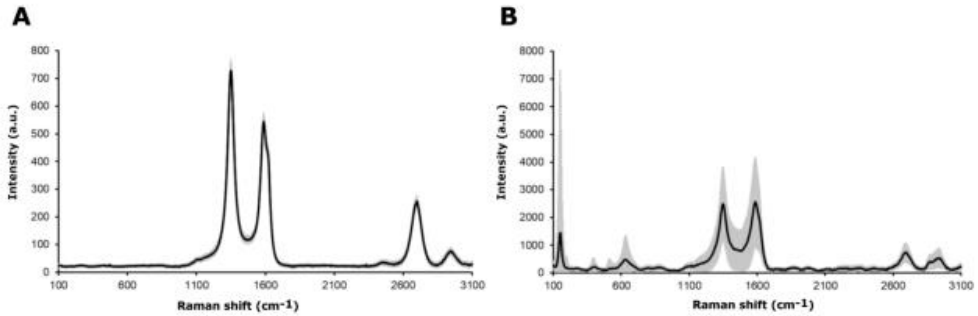

Fig. 3 Raman spectra of (A) the MWCNT coating and (B) the MWCNT/TiO_2 coating, where the black line presents an average Raman spectrum and the gray area is a standard deviation of the signal.

carbon nanotubes (SWCNTs) and double-wall carbon nanotubes (DWCNTs), and assigned to the tubes inside CNTs, whose diameter is smaller than the outer ones or resonance with the incident and scattered light or presence of structural defects, which might be eliminated after thermal treatment.[52] The D and G band intensity (I_D/I_G) ratios are used to identify the degree of structural defects or the level of functionalization of MWCNTs.[51,53] The lowest I_D/I_G ratio occurs when more structural defects appear, which are the characteristics of the MWCNTs compared to those of SWCNTs and DWCNTs. The I_D/I_G ratio for the MWCNT coating is about 1.34. The literature reports an I_D/I_G ratio of 1.1437 (ref. 51) or 1.46 (ref. 54), according to our results.

The values of Raman shifts of the MWCNT/TiO_2 coating (Fig. 3B) are close to those shown in the literature for the anatase phase of the titania, as illustrated in Table 4. Five optical phonon modes can be distinguished, and the assignment of the bands indicated is based on ref. 55 and 56. All of them represent five modes in the range of 150–630 cm^{-1} in accordance with Kamil *et al.* results,[51] as shown in Table 4. Fig. 3B also demonstrates the mode characteristics of the MWCNT coating, which shifted and broadened and possessed

Table 3 Raman active optical phonon modes for the MWCNT coating compared with MWCNT powder and literature results for MWCNT coating

	D band (cm^{-1})	G band (cm^{-1})	G′ band (2D band) (cm^{-1})	G′ band (2D band) (cm^{-1})	Ref.
MWCNTs	1350	1588	2699	2942	—
MWCNT coating on Ti13Nb13Zr substrate	1345	1580	2690	—	61
MWCNT powder	1346	1583	2694	—	62
MWCNT composite (prepared by evaporation and drying process)	1340	1574	2694	—	51

Table 4 Raman active optical phonon modes for the MWCNT/TiO_2 coating compared with rutile and anatase TiO_2 structures

	$E_{g(1)}$ (cm^{-1})	$E_{g(2)}$ (cm^{-1})	$B_{1g(1)}$ (cm^{-1})	$A_{1g(1)} + B_{1g(2)}$ (cm^{-1})	$E_{g(3)}$ (cm^{-1})	D band (cm^{-1})	G band (cm^{-1})	G′ band (2D band) (cm^{-1})	G′ band (2D band) (cm^{-1})	Ref.
MWCNT/TiO_2	150	200	401	519	630	1348	1587	2687	2938	—
MWCNT/TiO_2 composite	144	195.5	397	514	637	1356	1598.5	Doesn't indicated	—	51
TiO_2 (anatase)	146	194	395	514	636	—	—	—	—	55

a lower I_D/I_G ratio of 0.97. It is evident that the addition of titania to the MWCNT coating resulted in more structural defects than the bare MWCNT coating. The shift of the D and G bands is due to the interaction between the TiO_2 nanoparticles and the MWCNT coatings,[51,57] with the I_D/I_G ratio slightly higher than that shown by David *et al.* for the MWCNT/TiO_2 film, which is 0.842.[57] The archived values of the modes for both the MWCNTs and the MWCNT/TiO_2 coating are slightly different from those reported in the literature, presumably owing to the effect of some impurities or a substrate.

3.3 Adhesion determination

Fig. 4 shows the adhesion nano-scratch test result for the MWCNT/TiO_2 coating, with the indicated L_c value demonstrating the moment of the coating delamination, where F_n is the normal force and F_t is the friction force.

Table 5 shows the estimated values of L_c and critical friction F_c for the examined coatings. The MWCNT/TiO_2 coating demonstrates an almost 3.5-fold higher L_c value than the MWCNT coating, showing an improved adhesion strength. The adhesion strength measured by the shear strength test (according to ASTM standard F1044-99) for the MWCNT/TiO_2/HAp coating demonstrated the adhesion strength for the coating EPD-deposited at 50 V for 1 min as 11.9 ± 3.3 MPa.[58] The literature values of adhesion strength are then comparable to our results, within the limits of an experimental error. The adhesion can depend on mechanical properties, such as hardness, Young's modulus, and coating thickness, thus not only the coating composition determines the interface between a coating and a substrate. Therefore, the hardness of the tough TiO_2 agglomerates on the surface of the MWCNT coating, together with its good fit to the substrate material, allows the coating to adhere better to the Ti13Nb13Zr substrate. The hardness of TiO_2 can be taken as 1 GPa and that of the MWCNTs as 0.204 GPa.[59,60] Owing to the higher hardness of TiO_2 nanoparticles, the indenter tip encountered the titania particles on its way during the nano-scratch test and passed through the MWCNT/TiO_2 coating at a higher L_c than in the MWCNT coating.

The adhesion strength also depends on coating thickness, coating structure, substrate architecture (evaluated using surface preparation), and method of synthesis.[63] As regards the MWCNT/TiO_2 coating thickness, it was assessed previously at 2.016 μm,[36] while the thickness of the TiO_2 coatings below 3 μm

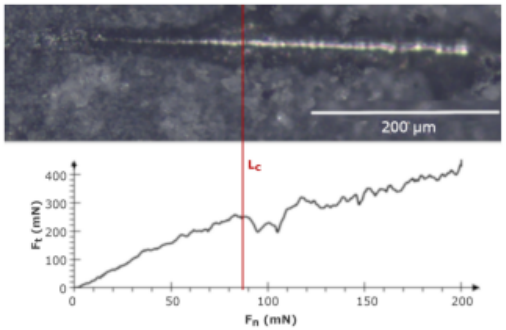

Fig. 4 The nano-scratch test result for the MWCNT/TiO_2 coating, with an indicated L_c.

Table 5 The results of critical parameters after the nano-scratch test, where the result is presented as mean ± SD (n = 5)

Material	Critical load (L_c) (mN)	Critical friction (F_c) (mN)
MWCNTs	25.3 ± 1.9	41.2 ± 2.1
MWCNTs/TiO_2	88.3 ± 1.8	248.5 ± 3.7

was reported to promote the loss of adhesion originating from the presence of titania agglomerates.[63]

There is one more parameter describing the adhesion strength of the coating, which is the ratio of hardness to reduced Young's modulus (H/E_r), reported previously in ref. 36, which describes the coating endurance for substrate deflections under load. The results of the H/E_r ratio for the MWCNT and MWCNT/TiO_2 coatings were 0.005 and 0.013, respectively,[36] which agree with the present results of the nano-scratch test, demonstrating the positive effect of the use of titania.

3.4 Corrosion behavior

The corrosion resistance test's results are shown in Table 6. The MR and MWCNT corrosion resistance parameters have been discussed previously.[64]

The addition of TiO_2 to MWCNT coatings lowers the j_{corr} and E_{corr} of the MWCNT coating, thus improving its corrosion resistance. The same result was reported for CNT/TiO_2 coating deposited on other substrates, such as Mg–Zn–Ca alloy,[65] MgZn alloy,[66] and HA–Ti–MWCNTs on TiNi alloy.[37] Compared to the MR material's corrosion parameters, the application of MWCNT/TiO_2 coating weakens the corrosion resistance of the substrate Ti13Nb13Zr alloy. For composite material comprising MWCNTs and TiO_2, excellent corrosion resistance was observed,[67] but the MWCNT coating had a porous structure that enhanced the transport of aggressive ions into the substrate and localized corrosion. Moreover, adding TiO_2 into the coating decreases its porosity by filling pores and voids, thus increasing the corrosion resistance of the MWCNT coating, as observed in other reports.[65,66]

3.5 Wettability

Fig. 5 and Table 7 show the wettability measurement results for the examined surfaces. All of the surfaces are hydrophilic and both the MWCNTs and the MWCNT/TiO_2 coatings demonstrate a contact angle between 50 and 60°, which is required for biomedical applications. The achieved results for the MWCNT coating are in accordance with our previous data shown in ref. 68. For the MWCNT/TiO_2 materials, the literature demonstrates different results. For the MgZn/5TiO_2–0.5MWCNT composite (composed of 5 wt% TiO_2 and 0.5 wt% MWCNTs), the CA was reported as 87.0 ± 2.1°.[66] Here, the difference might result in the effect of MgZn in the composite.

Ho *et al.* reported the CA for the MWCNT/TiO_2 membrane of 45.55 ± 1.13°,[69] which is slightly lower than the CA of our MWCNT/TiO_2 coating.

Table 6 Corrosion test results for examined surfaces

Material	E_{corr} (V (SCE))	j_{corr} (nA cm^{-2})
MR[a]	−0.019 ± 0.007	38.66 ± 5.92
MWCNTs[a]	−0.109 ± 0.002	325.61 ± 33.61
MWCNT/TiO_2	−0.206 ± 0.003	97.42 ± 9.39

[a] Results previously discussed in ref. 64.

Fig. 5 Results of water contact angle measurements for MR (A), the MWCNT coating (B), the MWCNT/TiO_2 coating (C), where the results are presented as mean ± SD (n = 3).

Table 7 Results of water contact angle measurements for the examined surfaces

Material	CA left (°)	CA right (°)	Mean CA (°)
MR	74.22 ± 4.96	73.09 ± 8.46	73.65 ± 6.58
MWCNTs	55.02 ± 1.02	55.84 ± 1.63	55.43 ± 1.29
MWCNTs/TiO_2	57.16 ± 2.01	59.46 ± 1.29	58.31 ± 1.60

3.6 Biological characterization

The results of the *in vitro* cytotoxicity studies are shown in Fig. 6 and 7. The viability of the HDF and MC3T3 cells was assayed using the MTT test. The highest cell viability for both HDF and MC3T3, and in both the direct and indirect tests, was observed for the MWCNT coating.

The MWCNT coating in the direct test demonstrated a slight decrease in HDF cell viability after 24 h, followed by an increase from 83.62% to 119.27% of the control after 72 h of incubation (Fig. 6A). It can be underpinned by the topography of the MWCNT coating, which promotes cell adhesion on a porous structure during the first 24 h; then, it also supports cell proliferation. There are reports on the carboxylated MWCNT–chitosan material's ability to achieve a porous microstructure, improving cell adhesion.[70] However, the HDF cell viability of the MWCNT/TiO_2 coating in the direct test after 24 h of incubation was negligibly lower than that for the MWCNT coating, while after 72 h, the HDF cell viability for the MWCNT/TiO_2 coating considerably decreased to 67.02% of the control but was still higher than that of the pure substrate material. Herein, we can conclude that the topography of the MWCNT/TiO_2 coating is as desirable as that of the MWCNT coating for cell adhesion, while after 72 h, the TiO_2 nanoparticles started to have a stronger toxic effect on HDF cells and decreased their proliferation rate. According to the literature, the cytotoxicity of MWCNT/TiO_2 films is dose-dependent, but there are also reports about the non-toxic effect of MWCNTs decorated with TiO_2 after 24 h and 72 h, where the HDF cell viability was similar to that of the control, and the MWCNT_TiO_2 composite concentrations were 0.02 and 0.05%.[37] However, the strong toxic influence of crystal phase TiO_2 and a decrease in A549 and MCF-7 cell viability have also been reported in the literature.[71]

The HDF and MC3T3 cell viability in an indirect test (Fig. 6B) was surprisingly low, suggesting that the tested specimens may have a toxic effect on the cells. In the case of the MWCNT coating, HDF cell viability in an indirect test is the highest and reaches

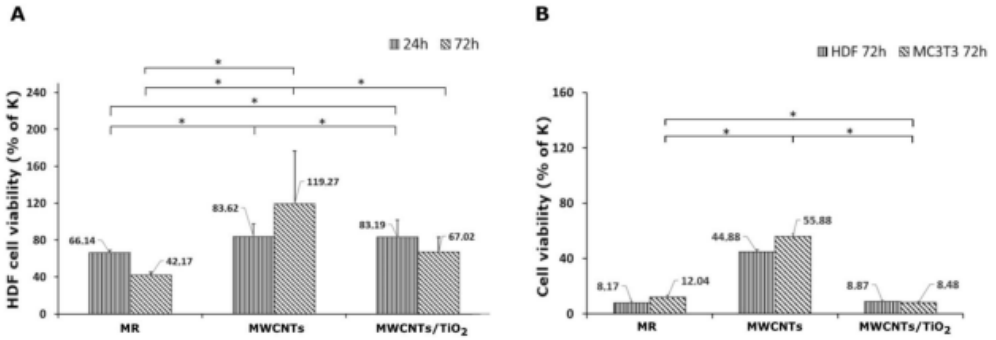

Fig. 6 Viability of HDF cells after 24 and 72 h in direct test (A) and of HDF and MC3T3 cells after 72 h in indirect test (B), assayed with the MTT test ($n = 3$, * at a 0.05 level all the data was significantly drawn from a normally distributed population according to the Shapiro–Wilk normality test and according to one-way ANOVA the data are significantly different). The control values (100% cell viability) were assayed for untreated cells.

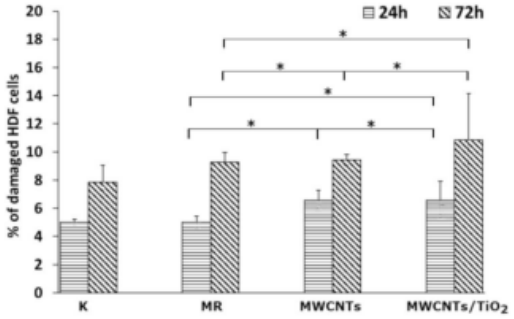

Fig. 7 LDH activity in the culture media of HDF cells for 24 and 72 h ($n = 3$, * at a 0.05 level all the data was significantly drawn from a normally distributed population according to the Shapiro–Wilk normality test and according to one-way ANOVA the data are significantly different).

44.88% of the control but is still too low for successful application in biomedicine. The MC3T3 cells in the indirect test exhibited a viability of 55.88% of the control, but it is still unsatisfactory. These observations can be explained by toxic substances (*e.g.* some impurities) released from the material surface or with nutrients and growth factor depletion through their adsorption on the coating surface. Undoubtedly, the processes underlying this phenomenon deserve further elucidation. According to the literature, a carboxylated MWCNT–chitosan composite sol–gel material with osteogenic growth peptide (OGP(10–14)) showed potential for use in bone regeneration.[70] Additionally, MWCNT scaffolds showed higher MC3T3 cell viability contrary to poly(lactic-*co*-glycolic) acid (PLGA),[72] and the MWCNT layer on collagen-coated titanium plates supported cell proliferation.[73] The anodized TiO_2 nanoparticles (NPs) on titanium EPD coated with CNTs showed higher MC3T3 proliferation than TiO_2 NPs,[74] whereas a similar MWCNT coating reported by Park *et al.* demonstrated approximately 25% lower cell proliferation after 5 days than pure titanium.[75]

The LDH activity in the culture media (Fig. 7) was determined to check whether the MWCNT and MWCNT/TiO_2 coatings (or substances released by them) have the ability to damage cell membranes and induce necrosis of HDF cells. After 24 h, both the MWCNT and the MWCNT/TiO_2 coatings demonstrated a higher percentage of damaged HDF cells than the substrate material, but these values did not exceed 11% of the cells. However, after 72 h, the amount of damaged HDF cells was almost the same for the MWCNT coating (9.43%) and substrate material (9.29%), while the MWCNT/TiO_2 coating achieved 10.86% of the damaged cells. The literature shows that LDH release from MWCNTs is dose- and time-dependent. The MWCNT dose of 40 μg mL^{-1} and the longer exposure time of HDF cells to carbon nanotubes induced cell death. However, we can see that the percentage of damaged cells exposed to MWCNTs is time dependent and much lower than that reported in the literature.[76,77]

4 Conclusions

In this study, employing the EPD method, we obtained a uniformly distributed MWCNT coating agglomerated with titania particles (of anatase structure, confirmed by Raman spectroscopy) deposited on the Ti13Nb13Zr substrate material to check its adhesion strength, corrosion resistance, wettability and biocompatibility with HDF and MC3T3 cells.

The adhesion strength of the MWCNT/TiO_2 coating was 3.5-fold improved compared to that of the MWCNT coating owing to the tough and good fitting of titania to the substrate material, which was confirmed by calculating the H/E_r nanoindentation test parameter, reported previously in ref. 36.

The addition of titanium dioxide to the MWCNT coating resulted in more than 3-fold higher corrosion resistance than the basic MWCNT coating. TiO_2 particles fill the inside of the MWCNT coating pores, making them denser. The MWCNT/TiO_2 coating still exhibited worse corrosion resistance compared to the substrate material owing to its relatively high porosity, which is, however, the advantage of coatings intended for medical applications.

The results of biological tests confirmed that the improved mechanical and physicochemical properties of the surface, such as high porosity and wettability, in MWCNTs alone and MWCNT/TiO_2-coated material support cell adhesion. The modified coatings may also release toxic substances into the culture medium, thus resulting in a decrease in proliferation.

The characterized coatings may be promising for biomedical applications, but they undoubtedly require further research and improvement, for example by reduction of the TiO_2 content in the coating.

Author contributions

D. Rogala-Wielgus: conceptualization, methodology, visualization, investigation, formal analysis, resources, writing – original draft, writing – review & editing; B. Majkowska-Marzec: conceptualization, visualization, project administration; A. Zieliński: conceptualization, investigation, supervision, writing – review & editing; K. Roszek: investigation, resources, validation; M. Liszewska: investigation, resources, validation. All authors have approved the final version of the manuscript.

Conflicts of interest

There are no conflicts to declare.

Acknowledgements

We would like to show our sincere gratitude to Dr Grzegorz Gajowiec for his support in the evaluation of the results.

References

1 O. K. Abubakre, R. O. Medupin, I. B. Akintunde, O. T. Jimoh, A. S. Abdulkareem, R. A. Muriana, J. A. James, K. O. Ukoba, T.-C. Jen and K. O. Yoro, *J. Sci.: Adv. Mater. Devices*, 2023, **8**, 100557.
2 L. Bao, X. Cui, M. Mortimer, X. Wang, J. Wu and C. Chen, *Nano Today*, 2023, **49**, 101784.
3 H. Ijaz, A. Mahmood, M. M. Abdel-Daim, R. M. Sarfraz, M. Zaman, N. Zafar, S. Alshehery, M. M. Salem-Bekhit, M. A. Ali, L. B. Eltayeb and Y. Benguerba, *Inorg. Chem. Commun.*, 2023, **155**, 111020.
4 N. Afsarimanesh, A. Nag, M. Eshrat e Alahi, S. Sarkar, S. Mukhopadhyay, G. S. Sabet and M. E. Altinsoy, *Sens. Actuators, A*, 2022, **344**, 113743.
5 M. R. Zakaria, M. F. Omar, M. S. Z. Abidin, H. M. Akil and M. M. A. B. Abdullah, *Composites, Part A*, 2022, **154**, 106756.
6 A. Ali, S. S. R. Koloor, A. H. Alshehri and A. Arockiarajan, *J. Mater. Res. Technol.*, 2023, **24**, 6495–6521.
7 B. Y. Jayakumari, E. N. Swaminathan and P. Partheeban, *Constr. Build. Mater.*, 2023, **367**, 130344.
8 X. Zhang, Z. Mo, R. Arenal, W. Li and C. Wang, *Appl. Surf. Sci.*, 2023, **609**, 155208.
9 R. H. Krishna, M. N. Chandraprabha, K. Samrat, T. P. K. Murthy, C. Manjunatha and S. G. Kumar, *Appl. Surf. Sci. Adv.*, 2023, **16**, 100431.
10 M. D. Yadav, H. M. Joshi, S. V. Sawant, K. Dasgupta, A. W. Patwardhan and J. B. Joshi, *Chem. Eng. Sci.*, 2023, **272**, 118586.
11 Y. Liu, Y. Shao, Y. Wang and J. Wang, *Colloids Surf., A*, 2022, **648**, 129335.
12 T. Mao, C. Li, F. Mao, Z. Xue, G. Xu and A. Amirfazli, *Diamond Relat. Mater.*, 2022, **129**, 109370.
13 Z. Zhu, S. Kang, H. Chen, Q. Zhao, Z. Huo, P. Li, J. Kang and Y. Yin, *Diamond Relat. Mater.*, 2022, **129**, 109351.
14 H. Cao, P. Tian, J. Deng, Y. Li, C. Wang, S. Han and X. Zhao, *J. Mech. Behav. Biomed. Mater.*, 2023, **142**, 105825.
15 S. Singh and C. Srivastava, *Electrochim. Acta*, 2023, **439**, 141639.
16 S. P. Vinodhini and J. R. Xavier, *Mater. Sci. Eng., B*, 2023, **295**, 116621.
17 S. Yan, J. Li, J. Shi, X. Gao and K. Yu, *Mater. Chem. Phys.*, 2023, **307**, 128133.
18 X. Li, L. Li, W. Zhang, Y. Li, D. Ma, Q. Lei, S. Yu, J. Wang, Z. Wang and G. Wei, *Colloids Surf., A*, 2023, **670**, 131548.
19 K. Shaikh, S. N. Kazi, M. N. M. Zubir, K. Wong, S. A. B. M. Yusoff, W. A. Khan, M. S. Alam, S. Abdullah and M. H. B. M. Shukri, *Therm. Sci. Eng. Prog.*, 2023, **42**, 101878.
20 H. Sun, S.-Q. Yi, N. Li, K.-K. Zou, J. Li, L. Xu, Y.-Y. Wang, D.-X. Yan and Z.-M. Li, *J. Colloid Interface Sci.*, 2023, **649**, 501–509.
21 H. Seok, C. Han, D. Lee and Y. Kim, *Appl. Therm. Eng.*, 2023, **231**, 120938.
22 D. Gopi, E. Shinyjoy, M. Sekar, M. Surendiran, L. Kavitha and T. S. S. Kumar, *Corros. Sci.*, 2013, **73**, 321–330.
23 X. Pei, Y. Zeng, R. He, Z. Li, L. Tian, J. Wang, Q. Wan, X. Li and H. Bao, *Appl. Surf. Sci.*, 2014, **295**, 71–80.
24 H. Maleki-Ghaleh and J. Khalil-Allafi, *Surf. Coat. Technol.*, 2019, **363**, 179–190.
25 M. Chen, H. Zhang, S. Shan, Y. Li, X. Li and D. Peng, *J. King Saud Univ., Sci.*, 2020, **32**, 1175–1181.
26 A. Maho, S. Detriche, J. Delhalle and Z. Mekhalif, *Mater. Sci. Eng., C*, 2013, **33**, 2686–2697.
27 A. Maho, S. Linden, C. Arnould, S. Detriche, J. Delhalle and Z. Mekhalif, *J. Colloid Interface Sci.*, 2012, **371**, 150–158.
28 J. E. Park, I.-S. Park, M. P. Neupane, T.-S. Bae and M.-H. Lee, *Appl. Surf. Sci.*, 2014, **292**, 828–836.
29 Z. Ye, J. Li, L. Liu, F. Ma, B. Zhao and X. Wang, *Opt Laser. Technol.*, 2021, **139**, 106957.
30 J. Marchewka, P. Jeleń, E. Długoń, M. Sitarz and M. Błażewicz, *J. Mol. Struct.*, 2020, **1212**, 128176.
31 F. Cheng, Y. Xu, J. Zhang, L. Wang, H. Zhang, Q. Wan, W. Li, L. Wang and Z. Lv, *Surf. Coat. Technol.*, 2023, **457**, 129296.
32 P. He, H. Wang, S. Chen, G. Ma, M. Liu, Z. Xing, Y. Wang, S. Ding, D. He and X. Chen, *J. Alloys Compd.*, 2020, **819**, 153009.
33 P. Daram, C. Banjongprasert, W. Thongsuwan and S. Jiansirisomboon, *Surf. Coat. Technol.*, 2016, **306**, 290–294.
34 G. M. T. Basha, A. Srikanth and B. Venkateshwarlu, *Mater. Today: Proc.*, 2020, **20**, 191–194.
35 D. Rogala-Wielgus, B. Majkowska-Marzec, A. Zieliński and B. J. Jankiewicz, *Appl. Sci.*, 2021, **11**, 7862.

36 D. Rogala-Wielgus, B. Majkowska-Marzec, A. Zieliński, M. Bartmański and B. Bartosewicz, *Materials*, 2021, **14**, 2905.
37 H. Maleki-Ghaleh and J. Khalil-Allafi, *Mater. Corros.*, 2019, **70**, 2128–2138.
38 Q. H. Li, M. M. Savalani, Q. M. Zhang and L. Huo, *Surf. Coat. Technol.*, 2014, **239**, 206–211.
39 E. J. T. Pialago, J. Yoo, X. Zheng, B. R. Kim, S. J. Hong, O. K. Kwon and C. W. Park, *Int. J. Heat Mass Transfer*, 2020, **147**, 118958.
40 A. Wesełucha-Birczyńska, E. Stodolak-Zych, W. Piś, E. Długoń, A. Benko and M. Błażewicz, *J. Mol. Struct.*, 2016, **1124**, 61–70.
41 A. Frączek-Szczypta, E. Dlugon, A. Wesełucha-Birczyńska, M. Nocun and M. Blazewicz, *J. Mol. Struct.*, 2013, **1040**, 238–245.
42 M. Atiq Ur Rehman, Q. Chen, A. Braem, M. S. P. Shaffer and A. R. Boccaccini, *Int. Mater. Rev.*, 2021, **66**, 533–562.
43 C. Gao, M. Guo, Y. Liu, D. Zhang, F. Gao, L. Sun, J. Li, X. Chen, M. Terrones and Y. Wang, *Carbon*, 2023, **212**, 118233.
44 A. Rathi and S. I. Kundalwal, *Polym. Compos.*, 2020, **41**, 2491–2507.
45 Y. Bai, I. Park, T. Bae, K. Kim, F. Watari, M. Uo and M. Lee, *J. Wuhan Univ. Technol., Mater. Sci. Ed.*, 2011, **26**, 867–871.
46 H. N. Pantaroto, J. M. Cordeiro, L. T. Pereira, A. B. de Almeida, F. H. Nociti Junior, E. C. Rangel, N. F. A. Neto, J. H. D. da Silva and V. A. R. Barão, *Mater. Sci. Eng., C*, 2021, **119**, 111638.
47 S. Jafari, B. Mahyad, H. Hashemzadeh, S. Janfaza, T. Gholikhani and L. Tayebi, *Int. J. Nanomed.*, 2020, **15**, 3447–3470.
48 M. T. Acar, H. Kovacı and A. Çelik, *Mater. Today Commun.*, 2022, **33**, 104396.
49 X. Liu and J. Fu, *Optik*, 2020, **206**, 164342.
50 M. Fandzloch, W. Bodylska, K. Roszek, K. Halubek-Gluchowska, A. Jaromin, Y. Gerasymchuk and A. Lukowiak, *Nanoscale*, 2022, **14**, 5514–5528.
51 A. M. Kamil, F. H. Hussein, A. F. Halbus and D. W. Bahnemann, *Int. J. Photoenergy*, 2014, **2014**, 1–8.
52 I. O. Maciel, M. A. Pimenta, M. Terrones, H. Terrones, J. Campos-Delgado and A. Jorio, *Phys. Status Solidi B*, 2008, **245**, 2197–2200.
53 S. Costa, E. Borowiak-Palen, M. Kruszyńska, A. Bachmatiuk and R. J. Kaleńczuk, *Mater. Sci.*, 2008, **26**, 433–441.
54 M. S. Tehrani, P. A. Azar, P. Ehsaninamin and S. M. Dehaghi, *J. Appl. Environ. Biol. Sci.*, 2014, **4**, 316–326.
55 L. Kernazhitsky, V. Shymanovska, T. Gavrilko, V. Naumov, L. Fedorenko, V. Kshnyakin and J. Baran, *Ukr. J. Phys.*, 2014, **59**, 246–253.
56 R. Palomino-Merino, P. Trejo-Garcia, O. Portillo-Moreno, S. Jiménez-Sandoval, S. A. Tomás, O. Zelaya-Angel, R. Lozada-Morales and V. M. Castaño, *Opt. Mater.*, 2015, **46**, 345–349.
57 M. E. David, R. M. Ion, R. M. Grigorescu, L. Iancu, A. M. Holban, F. Iordache, A. I. Nicoara, E. Alexandrescu, R. Somoghi, S. Teodorescu and A. I. Gheboianu, *Nanomaterials*, 2022, **12**, 239.
58 O. Albayrak, O. El-Atwani and S. Altintas, *Surf. Coat. Technol.*, 2008, **202**, 2482–2487.
59 Å. K. Jämting, J. M. Bell, M. V. Swain, L. S. Wielunski and R. Clissold, *Thin Solid Films*, 1998, **332**, 189–194.
60 C. Zheng, W. Chen and X. Ye, *Opt. Mater.*, 2012, **34**, 1042–1047.
61 B. Majkowska-Marzec, P. Tęczar, M. Bartmański, B. Bartosewicz and B. J. Jankiewicz, *Materials*, 2020, **13**, 3991.
62 M. Daavari, M. Atapour, M. Mohedano, R. Arrabal, E. Matykina and A. Taherizadeh, *Surf. Interfaces*, 2021, **22**, 100850.
63 J. Ramier, N. Da Costa, C. J. G. Plummer, Y. Leterrier, J. A. E. Månson, R. Eckert and R. Gaudiana, *Thin Solid Films*, 2008, **516**, 1913–1919.
64 D. Rogala-Wielgus, B. Majkowska-Marzec and A. Zieliński, *Mater. Today Commun.*, 2023, under review.
65 H. R. Bakhsheshi-Rad, M. Abdellahi, E. Hamzah, M. Daroonparvar and M. Rafiei, *RSC Adv.*, 2016, **6**, 108498–108512.
66 M. T. Amirzade-Iranaq, M. Omidi, H. R. Bakhsheshi-Rad, A. Saberi, S. Abazari, N. Teymouri, F. Naeimi, C. Sergi, A. F. Ismail, S. Sharif and F. Berto, *Materials*, 2023, **16**, 1919.
67 E. J. Kim, K. h. Kim, J. Bak, K. Lee and E. Cho, *RSC Adv.*, 2022, **12**, 35943–35949.
68 B. Majkowska-Marzec, D. Rogala-Wielgus, M. Bartmański, B. Bartosewicz and A. Zieliński, *Coatings*, 2019, **9**, 643.
69 K. C. Ho, S. M. Raffi and Y. H. Teow, *Int. J. Nanoelectron. Mater.*, 2022, **15**, 207–222.
70 J. Zhong, J. Huang, L. Chen and J. Duan, *RSC Adv.*, 2022, **12**, 31663–31670.
71 V. De Matteis, M. Cascione, V. Brunetti, C. C. Toma and R. Rinaldi, *Toxicol. In Vitro*, 2016, **37**, 201–210.
72 G. Lalwani, A. Gopalan, M. D'Agati, J. S. Sankaran, S. Judex, Y.-X. Qin and B. Sitharaman, *J. Biomed. Mater. Res., Part A*, 2015, **103**, 3212–3225.
73 M. Terada, S. Abe, T. Akasaka, M. Uo, Y. Kitagawa and F. Watari, *Bio-Med. Mater. Eng.*, 2009, **19**, 45–52.
74 J. E. Park, I. S. Park, T. S. Bae and M. H. Lee, *Bioinorg. Chem. Appl.*, 2014, **2014**, 1–7.
75 J.-E. Park, Y.-S. Jang, T.-S. Bae and M.-H. Lee, *Coatings*, 2018, **8**, 159.
76 A. Patlolla, B. Patlolla and P. Tchounwou, *Mol. Cell. Biochem.*, 2010, **338**, 225–232.
77 C. L. Ursini, D. Cavallo, A. M. Fresegna, A. Ciervo, R. Maiello, G. Buresti, S. Casciardi, F. Tombolini, S. Bellucci and S. Iavicoli, *Toxicol. In Vitro*, 2012, **26**, 831–840.

7. DOROBEK NAUKOWY

7.1 Wskaźniki bibliometryczne na dzień 09.12.2023 r.

Dane zgodnie z Web of Science	**Dane zgodnie z Scopus**	**Dane zgodnie z Google Scholar**
Index Hirscha: 3	Index Hirscha: 3	Index Hirscha: 3
Liczba cytowań: 30	Liczba cytowań: 28	Liczba cytowań: 46

7.2 Publikacje

1. Rogala Wielgus D., Majkowska-Marzec B., Bartmański M.: *The influence of laser alloying with carbon nanotubes of Ti13Nb13Zr on some of its mechanical properties in biomedical application,* Welding Technology Review. 90 (2018) 18-23. https://doi.org/10.26628/wtr.v90i7.935

2. Rogala Wielgus D., Majkowska-Marzec B.: *Wpływ metody trawienia i spiekania na właściwości mechaniczne powłok z nanorurek węglowych osadzonych elektroforetycznie na podłożu Ti13Nb13Zr*, Inżynier i Fizyk Medyczny 8 (2019) 417-420.

3. Majkowska-Marzec B., Rogala-Wielgus D., Bartmański M., Bartosewicz B., Zieliński A.: *Comparison of properties of the hybrid and bilayer MWCNTs-hydroxyapatite coatings on Ti alloy*. Coatings 9 (2019) 1-13. https://doi:10.3390/coatings9100643.

4. Rogala-Wielgus D., Majkowska-Marzec B., Zieliński A., Bartmański M., Bartosewicz B.: *Mechanical behavior of bi-layer and dispersion coatings composed of several nanostructures on Ti13Nb13Zr alloy*. Materials 14 (2021) 2905. https://doi.org/10.3390/ma14112905.

5. Rogala-Wielgus D., Majkowska-Marzec B., Zieliński A., Jankiewicz B. J.: *Mechanical behavior of bi-layer and dispersion coatings composed of several nanostructures on Ti substrate*. Applied Science-Basel 11 (2021) 7862. https://doi.org/10.3390/app11177862.

6. Rogala-Wielgus D., Majkowska-Marzec B. Zieliński A., Roszek K., Liszewska M.: *Evaluation of adhesion strength, corrosion, and biological properties of the MWCNTs/TiO_2 coating intended for medical applications*. RSC Advances. 13 (2023) 30108-30117. https://doi.org/10.1039/d3ra05331h

7. Rogala-Wielgus D., Majkowska-Marzec B., Zieliński A.: *Characteristics of silver-dopped carbon nanotube coating destined for medical applications.*

Materials Today Communications. 38 (2023) 107712. https://doi.org/10.1016/j.mtcomm.2023.107712

8. Rogala-Wielgus D., Zieliński A.: *Preparation and properties of composite coatings, based on carbon nanotubes, for medical applications*, Carbon Letters. (2023). https://doi.org/10.1007/s42823-023-00626-9

7.3 Wystąpienia konferencyjne

1. VIRTUAL EVENT- Global Summit on Future of Materials Science and Research (29-30 czerwiec 2021), wystąpienie ustne "*Mechanical properties of bi-layer and dispersion coatings composed of several nanostructure*"

2. 5th Edition of World Nanotechnology Conference (21-22 września 2022), wystąpienie ustne "*Mechanical properties of coatings composed of several nanostructures deposited on Ti and Ti13Nb13Zr alloy*"

3. 2nd International Meet on Biomaterials And Tissue Engineering (BIOMATMEET2023) (17 kwietnia 2023), wystąpienie ustne: "*Mechanical and corrosion properties of MWCNTs coatings with nanosilver addition intended for biomedical application*"

4. II Ogólnopolska Konferencja Naukowa „Implanty 2019- Nowoczesna implantologia- dylematy i nadzieje" (28-29 czerwca 2019), plakat „*Powłoki z nanorurek węglowych na stopie Ti13Nb13Zr przeznaczone do zastosowań biomedycznych*".

5. III Ogólnopolska Konferencja Naukowa „Implanty 2021- koncepcja a realia we współczesnej implantologii" (18 czerwca 2021), plakat „*Właściwości mechaniczne kompozytowych powłok z nanorurek węglowych z dodatkami*"